THE EVOLUTIONARY HISTORY OF THE FELIFORMIA: CONTINGENCY,

CONSTRAINT, DISPARITY

by

PAUL ZACHARY BARRETT

A DISSERTATION

Presented to the Department of Earth Sciences
and the Division of Graduate Studies of the University of Oregon
in partial fulfillment of the requirements
for the degree of
Doctor of Philosophy

June 2022

DISSERTATION APPROVAL PAGE

Student: Paul Zachary Barrett

Title: The Evolutionary History of the Feliformia: Contingency, Constraint, Disparity

This dissertation has been accepted and approved in partial fulfillment of the requirements for the Doctor of Philosophy degree in the Department of Earth Sciences by:

Prof. Samantha S. B. Hopkins	Chairperson/Advisor
Prof. Edward B. Davis	Core Member
Prof. Thomas Giachetti	Core Member
Prof. Stephen Frost	Institutional Representative

and

Krista Chronister	Vice Provost for Graduate Studies

Original approval signatures are on file with the University of Oregon Division of Graduate Studies.

Degree awarded June 2022

DISSERTATION ABSTRACT

Paul Zachary Barrett

Doctor of Philosophy

Department of Earth Sciences

June 2022

Title: The Evolutionary History of the Feliformia: Contingency, Constraint, Disparity

Constraint is a fundamental concept in evolutionary theory. The possibilities are not endless for what shape an organism can take, nor ecology of one generation to the next. Cat-like carnivorans (Feliformia) offer a unique opportunity in investigating aspects of evolutionary constraint, given several of their constituent clades are purported to experience this phenomenon in terms of limited evolutionary potential, but also in the presence of some clades with extreme durophagous (bone-crushing) and sabertooth morphology. I investigated the evolutionary history of feliforms by considering their phylogeny, ecology and cranial morphology. I recover results that suggest there are three distinct ecospaces within which feliforms reside. The first is occupied by those small in overall size, covering a wide dietary and ecological spectrum, up to but not including hypercarnviory. These broad ecologies are facilitated by a narrow band of similar cranial shapes, evocative of "one to many mapping". The second ecospace is occupied by soft-flesh specialists, such as felids (cats) and nimravids. These hypercarnivores possess distinct (non-overlapping) crania from the first ecospace, optimized for bite force and large gape angles. The evolutionary end member of this ecospace are those taxa possessing sabertooth morphology and the most disparate cranial shapes of all. The third ecospace is that of hyaenids, with a diverse ecological breadth optimized for dental toolkit and body mass, channeled by postcranial cursorial adaptations. The evolutionary end member of this ecospace are those taxa possessing

durophagous morphology. In all three ecospaces, constraint exists in what cranial morphology and ecological transitions are possible. Large size nor hypercarnivory are achievable within the small feliform ecospace, and thus require transitions into the other two zones. Soft-flesh specialization is a road of no return that does not facilitate ecospace transitions. The hyaenid ecospace does not facilitate transitions into the 'soft flesh' ecospace, nor by extension sabertooth morphology. These limitations are a result of phylogenetic baggage and functional challenges, but fruitfully channel extreme cranial shapes (soft-flesh specialist) and diverse ecologies (hyaenids) that couldn't exist without these constraints.

CURRICULUM VITAE

NAME OF AUTHOR: Paul Zachary Barrett

GRADUATE AND UNDERGRADUATE SCHOOLS ATTENDED:

     University of Oregon, Eugene, Oregon, USA
     South Dakota School of Mines & Technology, Rapid City, South Dakota, USA
     Idaho State University, Pocatello, Idaho, USA

DEGREES AWARDED:

     Doctor of Philosophy, Earth Sciences, 2022, University of Oregon
     Master of Science, Paleontology, 2015, South Dakota School of Mines &
         Technology
     Bachelor of Science, Geology, 2010, Idaho State University

AREAS OF SPECIAL INTEREST:

     Paleontology
     Phylogenetic Systematics
     Paleoecology
     Morphology

PROFESSIONAL EXPERIENCE:

     Graduate Employee, University of Oregon, 2016-2022

     Staff Research Associate I, University of California, Davis, 2017

     Field Paleontologist/Preparator/Curator, Geoscientists-in-the-Parks, Wind Cave
         National Park, 2015

     Paleontology Monitor, United States Bureau of Reclamation, 2010

     Curatorial Assistant, Idaho Museum of Natural History, 2009-2011

GRANTS, AWARDS, AND HONORS:

Department of Earth Sciences Research Excellence Award, University of Oregon, 2022

Open Access Article Processing Charge Award Fund, University of Oregon, 2021

Baldwin Scholarship, University of Oregon Department of Earth Sciences 2017,
2018, 2019, 2020

Annual Meeting Grant, European Association of Vertebrate Palaeontology, 2019

Special "Opps" Travel and Research Award, University of Oregon, 2019

Graduate Student Research Award, Geological Society of America, 2018

J.P. and Virginia Gries Memorial Fellowship, South Dakota School of Mines &
Technology, 2013

Idaho Promise Scholarship, Idaho State University, 2006, 2007

PUBLICATIONS:

Barrett, P. Z. 2021. The largest hoplophonine and a complex new hypothesis of nimravid evolution. Scientific Reports 11:1–9.

Barrett, P. Z., S. S. B. Hopkins, and S. A. Price. 2021. How many sabretooths? Reevaluating the number of carnivoran sabretooth lineages with total-evidence Bayesian techniques and a novel origin of the Miocene Nimravidae. Journal of Vertebrate Paleontology 41(1): e1923523.

Miller, S. A., P. Z. Barrett, W. N. F. McLaughlin, and S. S. B. Hopkins. 2020. Endemism and migration in the Kochkor Basin? Identification and description of *Adcrocuta eximia* (Mammalia: Carnivora: Hyaenidae) and c.f. *Paramachaerodus* (Mammalia: Carnivora: Felidae) fossils at the Miocene locality of Ortok, Kyrgyzstan. Palaeontologia Electronica 23(3): a45.

Barrett, P. Z., L. Finkelman, G. Perdue, W. N. F. McLaughlin, D. M. Reuter and S. S. B. Hopkins. 2020. Small carnivoran fauna of the Mascall Formation, Crooked River Basin, central Oregon. Journal of Vertebrate Paleontology 39(5): e1717506.

Retallack, G. J., J. M. Theodor, E. B. Davis, S. S. B. Hopkins and P. Z. Barrett. 2018. First dinosaur (Ornithopoda) from Early Cretaceous (Albian) of Oregon, USA. Journal of Vertebrate Paleontology 38(4): (1)-(5).

Barrett, P. Z. 2016. Taxonomic and systematic revisions to the North American Nimravidae (Mammalia, Carnivora). PeerJ 4:e1658.

E. Welsh, C. A. Boyd, K. D. Spearing, and P. Z. Barrett. 2015. Stratigraphic and taxonomic revision of a North American false saber-toothed cat cub. Proceedings of the South Dakota Academy of Science 94:141-153.

ACKNOWLEDGMENTS

I wish to thank my parents who fostered my interest in paleontology since I was four years old. To my committee, who provided countless hours of engagement and discourse that brought this project to fruition. Of special thanks, my advisor Dr. Samantha Hopkins, who facilitated my growth on evolutionary theory leading up to my comprehensive exams, and supplied much of the funds and connections to collect the data for this dissertation once I passed. Dr. Stephan Frost, who shaped the way I view the evolution of morphology, the dark arts of imputation and rigor in my science. I also thank the many curators and collection managers that steward the natural history of the world. Through them I engaged with the evolutionary history of our planet and learned the best places to get a bite to eat and things to do on the weekend. Dr. Suzanne Gascoyne, who helped me become a better human. You immeasurably aided me in navigating the emotional trials of a Ph.D., resulting in a more confident, objective and hopefully, introspective person. To my partner, Sophie Miller, you showed me the path to my PhD was more than the research it contains, the transformative experience which outshines the paper on the wall or any occupation that paper may bring. Thank you for being patient, listening to me drone on about exciting as well as drab ideas. You are my most aggressive cheerleader. Finally, to my future self, you should be proud. This journey was worth it.

For those of whom the old bones come alive and join the pageant of the living.

TABLE OF CONTENTS

LIST OF FIGURES

LIST OF TABLES

Chapter I

Introduction

Variation supplies the raw material by which natural selection operates, "variation supposes, while selection disposes." However, numerous studies have acknowledged the importance of understanding that, unlike Darwin's original formulation, variation generated by organisms is not isotropic (Olson and Miller, 1958; Vermeij, 1973; Gould, 2002; Goswami et al., 2011). Possibilities are not limitless, as evident by the non-equal occupation of morphospace and ecology of all lineages. What obstructs the opportunities for some lineages and perhaps facilitates diversity and disparity for others remain central questions in biology and evolutionary theory (Dobzhansky, 1951; Hutchinson, 1959; Gould, 2002).

Hypotheses have existed since Galton (1869) that there may be minimally stable states or positions in both morphology and ecology, where evolution proceeds less like a rolling billiard ball of isotropic generational variation, and more analogous to a polyhedron that flips facets of stable ecomorphology. In other words, maybe a reasonable amount of isotropic variation is created in each generation, but only a limited amount is tenable in being a successful organism. From these proposals rose ideas of channelized evolution (Haeckel, 1866; Eimer, 1890; Hyatt, 1897; Goldschmidt, 1940) that held promise in predicting the course of shape and niche change if the framework could be understood. Evolutionary history or deep homology may play a truly integral part in determining what shapes and occupations an organism can achieve, either through lack of genetic raw material or variation, or developmental correlation of parts that will not allow certain changes to happen. However, these same correlations may also provide an axis of exploitation, where a greater magnitude of change may be possible within a certain trajectory

compared to equally probable random change in any direction (Goswami et al., 2014). This fruitful channeling could then be viewed as a positive aspect of constraint leading to more extreme shapes and, by extension, ecologies than would be possible under Darwin's initial hypothesis.

Areas of limited variation are often ascribed to specialists. With the concept of one-to-one mapping of ecology to shape, one would expect that fewer niches or a more limited ecology would correlate with less morphological variation. Among the carnivoran clades, low amounts of cranial-dental variation have been described in literature for "cat-like" feliform carnivores such as felids and nimravids (Radinsky, 1981a, 1982; Van Valkenburgh, 1991; Holliday and Steppan, 2004). This reduced raw material is argued to relate to increased specialization towards a hypercarnivorous diet, one dominated by a predominance of vertebrate prey. Felids and nimravids both exhibit simplified dentition that efficiently slices soft flesh but lacks the grinding surfaces found in more omnivorous carnivores (Evans and Pineda-Munoz, 2018). The loss of grinding surfaces on teeth seems to be an evolutionary road of no return, resulting in an ecomorphological constraint that did not allow these specialists to evolve additional ecologies (Solé and Ladevèze, 2017; Brocklehurst, 2019).

Consequently, feliforms offer a unique opportunity to investigate aspects of evolutionary constraint, not only for the perceived lack of variation inherent to their specialist clades, but also the extreme morphologies acquired by extinct sabertooth and bone-crushing members. Was constraint an aspect of feliform evolution that limited possibilities for certain lineages, or did that same constraint fruitfully channel the extreme morphologies that did evolve? Additionally, since all clades did not enter into the hypercarnivorous and presumably specialized realms of cats, nimravids and hyenas, what gave these latter groups the push to get there in the first place?

2

I investigated the evolutionary history of feliforms by considering their phylogeny, ecology and cranial morphology across the following chapters. In Chapter II, I construct a hypothesis of feliform evolutionary relationships using total-evidence Bayesian techniques. This methodology allowed me to incorporate molecular (nuclear and mitochondrial genome), dental and osteological morphology and stratigraphic occurrence data in a single analysis. This phylogeny serves as a framework for all following analyses, while also assessing relationships of several purported feliform taxa for the first time, e.g., percrocutids, and holistically estimating major clade originations and relative speciation and extinction rates by combining the fossil and living record.

Chapter III assesses ecological evolution of feliforms in terms of their diet, dental toolkit and body mass. I used hypotheses of adaptive radiation, as facilitated by tectonic and climatic events, as a framework to assess different clades' ecological trajectory. However, I compared models of adaptive radiation to other potential processes to best explain the patterns observed in feliform natural history. These models included random walk, trended evolution, optimal body mass and toolkit per dietary category, and clade-based regime shifts. Using the results of Chapter II, I was also able to incorporate phylogenetic uncertainty for all analyses by virtue of sampled trees over the course of the Bayesian analysis tree search.

Chapter IV explores the generating forces of feliform cranial shape through 3D geometric morphometric analysis. I assessed which feliform clades possess the greatest cranial disparity, such do clades with broad ecological occupation have greater variance compared to specialists? I consider multiple plausible sources of cranial disparity such as allometry as a line of least evolutionary resistance, integration of the developmental units of the cranium, the geologic time a clade has existed to evolve disparate shapes, and dietary ecology.

Chapter V synthesizes the above analyses into a narrative of feliform evolution and offers predictions for all terrestrial carnivorans. This narrative finds support for constraint in the evolutionary history of feliforms with a finite number of possible ecospaces. Certain transitions are not possible from one ecospace to another, but these same constraints fruitfully channel the extreme endmembers of cranial evolution and ecology that otherwise are inaccessible to other groups, i.e., sabertooth and durophagous morphology. Similar patterns are further observed for caniforms and suggestive of a general process at work in the evolution of terrestrial carnivores.

Chapter II

Phylogeny of the Feliformia

Introduction

Current hypotheses of feliform relationships are derived from primarily molecular- or morphological-only datasets (though see Barrett et al., 2021). Molecular hypotheses (e.g. Nyakatura and Bininda-Emonds, 2012; Paijmans et al., 2017; Zhou et al., 2017; Slater and Friscia, 2019; Hassanin et al., 2021) differ extensively from morphological ones (e.g. Wesley-Hunt and Flynn, 2005; Spaulding and Flynn, 2012), such as the placement of the Hyaenidae (hyenas) as distantly related to the Felidae (cats) in molecular phylogenies, while most closely related to the Felidae in morphological phylogenies. An additional issue is the cited morphological studies, including the preliminary total-evidence analysis of Barrett et al. (2021), sample extinct taxa from across the Feliformia, but contain typically one representative operational taxonomic unit (OTU) per family, usually extant. These living OTUs are commonly derived members of their respective families and thus may generate long-branch attraction in phylogenetic hypotheses (Bergsten, 2005). Another explanation for this discrepancy is that differing topologies in molecular trees result from the inability to include most extinct taxa, while all multifamily morphological trees are depauperate in the extant and fossil taxa that they do contain. Furthermore, several extinct clades of feliform (e.g., Percrocutidae, Lophocyonidae, Machairodontinae) have rarely been included in broad feliform phylogenetic analyses, so their placement is poorly known. Combined, these challenges have resulted in uneven knowledge of feliform relationships. Extant or recently extinct clades with molecular data have returned

consistent relationships, but necessarily devoid of the diversity of extinct clades, while taxa known only from morphology suffer from lack of analyses, limited taxon sampling or both.

Is there a contradiction in the evolutionary relationships of feliforms depending on what datasets one employs, or is this an artifact of methodology and taxon sampling? Here I present a broad investigation of the phylogenetic relationships of feliform taxa by examining the relationships of all major families, and numerous OTUs within each family, with extensive morphological and molecular datasets. I address the conflict of past analyses by employing total-evidence techniques (Lee et al., 2009; Pyron, 2011; Ronquist et al., 2012) which use a Bayesian framework to create a probabilistic model of evolution, inclusive of molecular data, fossil data, and stratigraphic information in a single analysis. Specifically, I implement a total-evidence analysis with a Sampled Ancestor, Birth-Death Skyline with Serial Sampling (SABDSKY) model (Stadler et al., 2013; Gavryushkina et al., 2014) which allows the identification of direct ancestors and changing speciation, extinction and sampling rates through time. This analysis yields a dated phylogeny of extinct and living taxa combining data previously studied in separate morphology-only and molecular-only analyses. Furthermore, this analysis places several taxa/clades in novel arrangements allowing de novo assessment of historical patterns of morphological and ecological evolution.

Methods

Taxa Selection

I chose feliform taxa that captured the cranial disparity and ecological diversity of their given clade, while providing even taxonomic coverage. All feliform taxa with published aDNA (n=7)

were also incorporated into this analysis to provide greater resolution on phylogenetic relationships along with molecular data from all extant taxa. The fossil record of feliform carnivorans is not symmetric across clades, with collections and literature favoring large-bodied taxa, e.g. felids, hyaenids and nimravids. However, I included well-preserved small-bodied fossil viverrids, herpestids and stem feloids/viverroids whenever possible. The final phylogenetic analysis includes 124 taxa, plus five caniform outgroups, with approximately two-thirds of all taxa being extinct.

Molecular Data

I downloaded three nuclear loci and complete mitochondrial genomes from Genbank for the forty-five extant and seven extinct (aDNA) taxa of the analysis (Appendix A). However, where complete mitochondrial genomes were unavailable, I used individual mitochondrial genes. I aligned Nucleotide sequences one gene at a time using MAFFT v.7 online server (Katoh et al., 2019), with the G-INS-I and 'Leave gappy regions' parameters selected. All sites containing missing data were removed. This necessitated the loss of codon-position information for all save one mitochondrial gene (ND4L). I deleted the stop codons and manually optimized these aligned sequences in UGENE v. 35.1 (Okonechnikov et al., 2012) to maintain codon positions when possible and trimmed excess bases of tail data that had no comparative sequences. I then concatenated the aligned sequences in SequenceMatrix (Vaidya et al., 2011) and analyzed them for partitioning schemes utilizing PartitionFinder version 2.1.1 (Lanfear et al., 2016) on XSEDE (Towns et al., 2014) through the CIPRES Science Gateway v. 3.3 (Miller et al., 2011). I designated twenty data blocks for the dataset, such that only genes IRBP and ND4L were separated into three blocks based on codon positions. The remainder I gave a single block per

molecular sequence. I defined linked branch lengths and investigated all evolutionary models available to BEAST 2 (40 models) using a 'greedy' partitioning strategy to compare partitions and differential substitution models under the Bayesian information criterion (BIC). A 10-partition scheme was best supported (Appendix B, Table 1).

Table 1. Best supported substitution models recovered in PartitionFinder2 using the Bayesian information criterion (BIC).

No. of partitions	Partition	Model
1	*ND4L_1stpos, COX3, ATP6, COX2, COX1*	HKY+I+G+X
2	*ND4, CYB, ND1, ATP8, ND5, ND3*	GTR+I+G+X
3	*TTR, CHRNA_1*	SYM+G
4	*IRBP_1stpos*	TRN+G+X
5	*IRBP_2ndpos*	TRNEF+I
6	*IRBP_3rdpos*	HKY+G+X
7	*ND2*	HKY+I+G+X
8	*ND4L_2ndpos*	HKY+I+G+X
9	*ND4L_3rdpos*	HKY+I+G+X
10	*ND6*	HKY+G+X

Morphology Data

I scored all taxa from personal observation of specimens or literature as listed in Appendix C for 325 morphological characters derived from prior carnivoran/feliform phylogenetic analyses (Van Valkenburgh et al., 1990; Werdelin and Solounias, 1991; Salles, 1992; Bryant, 1996; Peigné, 2003; Rothwell, 2003; Gaubert et al., 2005; Wesley-Hunt and Flynn, 2005; Tseng and Wang, 2007; Christiansen, 2008a; Salesa et al., 2010; Sakamoto and Ruta, 2012; Salesa et al., 2012; Spaulding and Flynn, 2012; Christiansen, 2013; Robles et al., 2013a; Barrett, 2016; Morales et al., 2019; Barrett, 2021; Barrett et al., 2021) and several novel characters. When possible, multiple individuals of a given taxon were scored to assess polymorphic conditions. Characters and their associated descriptions can be found in Appendix D, while the resultant morphology character matrix is Appendix E. I assessed six competing schemes of morphological character partitioning and evolution by Bayes Factor via a Generalized Stepping Stone (GSS; Fan et al., 2011) analysis (Table 2). These schemes partitioned characters based upon anatomical association (cranial/post-cranial), number of states a character contains (n-states), or a combination of the two. I additionally wrote custom evolutionary rate matrices for specific multistate characters (Appendix F) that included ordered, multipath and Dollo (irreversible) characters to compare to null unordered character evolution. Each scheme was assessed by GSS with 10 steps, a chain length of five million and 50% burnin.

Table 2. Summary of marginal log-likelihoods and Bayes factor (BF) support for differential substitution models and partitioning schemes of the morphology data. Log BF values are reported as the support of the best model (model 6) over the inline model. P=partition used, * = best supported model.

Scheme	n-state partition	Cranial/Post-cranial part.	Complex Evo. models	Marginal log-likelihood	Log BF vs Best Model
1		P		-16804.22	4058.26
2		P	P	-14672.40	1926.44
3	P	P		-12984.09	238.13
4	P			-12974.56	228.60
5	P	P	P	-12752.54	6.58
6*	P		P	-12745.96	-

Total-evidence Analysis

I jointly estimated tree topology, branch lengths and evolutionary parameters in a Bayesian framework using BEAST2, version 2.6.3 (Bouckaert et al., 2014) with a Sampled Ancestor, Birth-Death Skyline with Serial Sampling (SABDSKY) model as a tree prior (Stadler et al., 2013; Gavryushkina et al., 2014). A SABDSKY model allows analyzed taxa to be direct ancestors (zero length branches) to other taxa, while serial skyline models facilitate changes in extinction, speciation or sampling rates through time, factors which are likely non-trivial to the approximately 50 million year history of feliform evolution (Liow and Finarelli, 2014; Pires et al., 2017). I assessed the number of speciation and extinction rate shifts (sampling standard deviation was found to approximately zero, thus rejecting the presence of rate variation and justifying the use of a single sampling parameter) by first arbitrarily testing ten evenly spaced

shifts at 5 Ma increments. I visualized/assessed the proposed shifts in Tracer version 1.7.1

(Rambaut et al., 2018) and the 'bdskytools' R package (Plessis, 2016). From these results, I

reduced the number of shifts to six with boundaries correlating to the rate inflection points in

Figure 1. Speciation (R_e) and extinction (δ) were given uniform priors [0,10], while sampling

was given a uniform [0,1]. The origin parameter was given a lognormal distribution, offset of

47.4 Ma (being the FAD of the oldest taxon in the analysis), mean=1.0, standard deviation=1.25

and 'mean in real space' parameter selected.
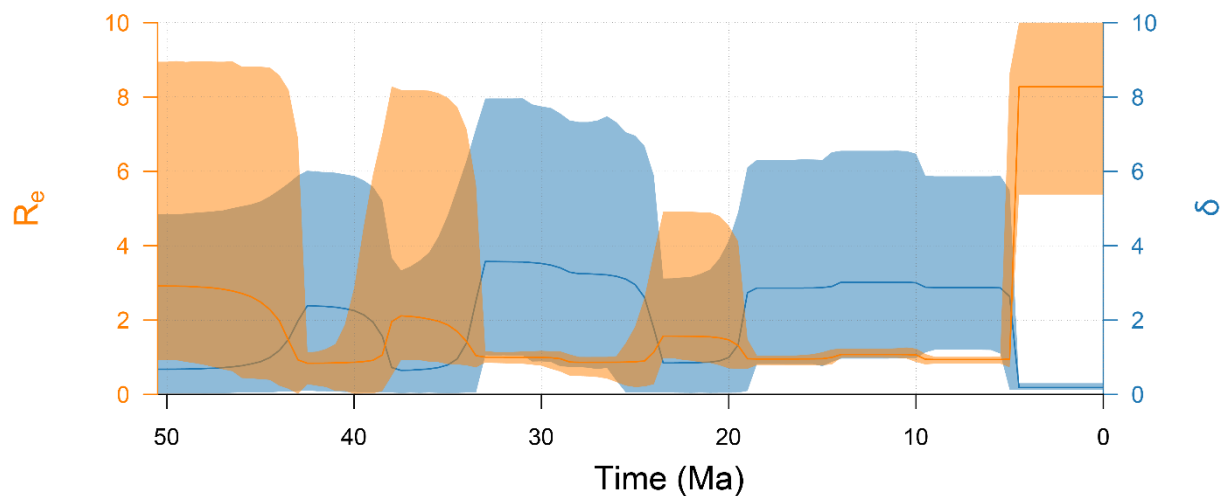
Figure 1. Skyline plot of assessed changes in speciation (Re) and extinction (δ) rates through
time of the Feliformia.

I set each morphological partition to evolve under the Lewis Mkv model, or those best supported

by the GSS analysis, scheme 6. All partitions were set to accommodate ascertainment bias and

ambiguities in the character matrix with a substitution rate that varied across characters

according to a Gamma distribution shared by all partitions. I modelled the shared morphological clock with an uncorrelated relaxed clock model with log-normal distributed rates. For molecular data, I applied a single lognormal relaxed clock model with partitions and evolutionary models following the results of the PartitionFinder2 analysis. I derived the distributions (with provided justifications) of tip dates from the information in Appendix G.

Early runs of the analysis displayed a lack of convergence between the morphological and molecular data, thus I constructed a reasonable time-scaled starting tree in R version 4.0.3 (R Core Team, 2020) using the 'DatePhylo' function in the 'strap' package (Bell and Lloyd, 2014). I set a relatively uninformed "equal" set of branch lengths, calculated across a feliform tree derived from relationships in literature (e.g. Turner et al., 2008; Christiansen, 2013; Slater, 2015; Slater and Friscia, 2019; Barrett, 2021; Barrett et al., 2021) using the First Appearance Data (FAD) as described in Appendix G. These branches I further scaled using the 'minBranchLength' function in 'paleotree' (Bapst, 2012) with a setting of 1.5 to approximate divergence dates of major clades following molecular hypotheses as listed in the aforementioned literature. I finally specified a minimal set of topology constraints separating the ingroup from the outgroup taxa, as well as relationships within the outgroup Caniformia as ascertained from phylogenetic analyses in the prior listed literature.

I ran Markov Chain Monte Carlo (MCMC) chains for 100 million generations, sampling trees and parameters every 10,000 generations, until satisfactory sampling of parameters had been reached as assessed by Tracer v. 1.7.1. Thus, I discarded 10% burn-in and estimated topology and posterior probabilities from the remaining generations in the form of a maximum clade credibility (MCC) tree with median node heights.

I assessed morphological synapomorphies via TNT v. 1.5 (Goloboff and Catalano, 2016) on the MCC tree of the above analysis. TNT only reports synapomorphies supported by both ACCTRAN and DELTRAN optimization and thus forms a conservative assessment of shared derived character states.

Results

The MCC tree is presented in Figure 2. Overall, broad (family-level) relationships are consistent to those recovered in molecular analyses, with felids and prionodontids sister to the viverroids (e.g. Zhou et al., 2017; Slater and Friscia, 2019; Hassanin et al., 2021). Similarly, relationships within families containing extant taxa largely follow those of molecular analyses, though differences do exist. Euplerids follow relationships of Hassanin et al. (2021), but differ in the placement of the fossa, *Cryptoprocta ferox,* relative to previously referenced studies. The Herpestinae (solitary mongooses) lineage differs amongst all cited studies, while the clade Mungotinae (eusocial mongooses) is recovered in the same arrangement amongst all cited studies. The poor resolution of the Herpestinae is reflected in the relatively poor support metrics amongst these studies and the present one, indicating need for future work with this clade. Similarly, certain feline relationships differ amongst all studies, while pantherine felids were recovered in the same arrangement. The recovered internal relationships of the remaining extant clades were identical to those of the literature previously cited.

Figure 2. Maximum clade credibility tree of Feliformia. Values adjacent to nodes are posterior probability support ≥0.5. Extinct taxa with analyzed aDNA are indicated by the double-helix symbol. Silhouettes are taken from phylopic.org.

I recovered extinct taxa in several novel arrangements, though the overall pattern of nimravids as sister to the feloids with *Tapocyon* as a stem-feliform was recovered in recent analyses (Tomiya and Tseng, 2016; Barrett et al., 2021) and in the present analysis with 1.0 posterior probability

(PP) for each clade. The Nimravidae exhibits a basal split consisting of the Hoplophoninae and Nimravinae of Barrett (2021), though the taxa *Dinictis* and *Pogonodon* are recovered as basal members of the Hoplophoninae (0.74 PP), while *Maofelis* and unnamed specimen MA-PHQ 348 as basal members of the Nimravinae (0.12 PP). The remaining differences in relationships of the Nimravidae are to regions of the tree where both the present study and Barrett (2021) recovered poor resolution.

The African palm civet, *Nandinia binotata*, is recovered in a novel relationship nested amongst the Stenoplesictidae (0.53 PP), late Oligocene stem feloids. This clade further includes *Proailurus*, *Stenogale* and *Palaeoprionodon*, similar to previous morphology only studies, minus the inclusion of *Nandinia* (Wesley-Hunt and Flynn, 2005; Spaulding and Flynn, 2012; Solé et al., 2014, 2016).

The felids are split amongst the Machairodontinae (0.94 PP, seven synapomorphies) and Felinae + Pantherinae (1.0 PP, eight synapomorphies) with *Pseudaelurus validus* as stem to both (1.0 PP). The Machairodontinae contains the Smilodontini, Homotherini and a series of stem "Metailurini" taxa which diverged from the remaining living felids at approximately 15.17 Ma, comparable to other molecular-only analyses, ranging from 14-22 Ma (Paijmans et al., 2017; Slater and Friscia, 2019; Barnett et al., 2020). The Homotherini of the present study contains *Homotherium*, *Xenosmilus* and *Amphimachairodus* taxa (0.54 PP, three synapomorphies) diverging from the Smilodontini at 10.78 Ma, much shallower than the molecular aDNA analysis of Paijmans et al. (2017) at ~18 Ma, though comparable to Slater and Friscia (2019), 11.78 Ma. The *Homotherium* species *H. latidens* and *H. serum* were also assessed to have an extremely shallow divergence (~0.46 Ma), supporting a conspecific relationship previously hypothesized in analyses with narrower taxonomic scope (Antón et al., 2014; Paijmans et al., 2017). The

Smilodontini of the present study contain *Smilodon* and *Megantereon* (0.99 PP, seven synapomorphies). As previously mentioned the remaining machairodontines form a grade of stem "metailurins", resembling the relationships presented in Christiansen (2013) most closely. However, the taxa *Nimravides* and *Machairodus* were recovered as well supported (0.72-0.86 PP) stem members of Smilodontini + Homotherini clade, while the remainder recovered poorer support at the base of the Machairodontinae.

Extinct lions, *Panthera atrox* and *Panthera leo spelaea*, are recovered in the same relationships of previous molecular studies, with the Eurasian cave lion sister to the North American lion and the living African lion stem to both, but at slightly deeper divergence dates, 1.58-2.31 Ma (Barnett et al., 2009, 2016). The North American cheetah-like cat, *Miracinonyx*, was recovered as sister to *Puma concolor* (1.0 PP), diverging approximately 3.63 Ma, comparable to past molecular analyses (Barnett et al., 2005; Slater and Friscia, 2019).

Hyaenids experienced perhaps the most disparate changes in relationships compared to past analyses which generally described an evolutionary trajectory of 'civet-like' to extremely durophagous forms (Werdelin and Solounias, 1991; Turner et al., 2008; Coca-Ortega and Pérez-Claros, 2019). The present study recovers up to three independent lineages evolving durophagous morphology. However, similar to Werdelin and Solounias (1991), the civet- and mongoose-like *Proteletitherium*, *Plioviverrops* and *Tungurictis* were recovered in basal positions. Tip ward of these taxa, the first durophagous clade is recovered of *Tongxinictis* and *Allohyaena* (0.5 PP). This is followed by the divergence of the 'ictithere', Hyaenotheriini + Ictitheriinae of Semenov (2008), taxa including *Ictitherium viverrinum*, *Hyaenictitherium hyaenoides* and *Hyaenotherium wongii* (0.96 PP, four synapomorphies). Subsequently to diverge is the second clade of durophagous morphs, including *Belbus*, *Palinhyaena*, and *Lycyaena* (0.58 PP).

However, this clade's precise position within the greater Hyaenidae is not robustly supported with adjacent nodes yielding only 0.37-0.54 PP values. The final major clade (0.58 PP) of the Hyaenidae contains the crown group plus a sister-group of cursorial meat and bone specialists and durophagous taxa (*sensu* Coca-Ortega and Pérez-Claros, 2019). The non-crown clade contains the taxa *Chasmaporthetes*, and a novel *Adcrocuta + Pachycrocuta* clade (0.94 PP, five synapomorphies). *Pachycrocuta* has been closely connected to the *Hyaena* genus, both taxonomically and cladistically (see Liu et al., 2021), but the present study finds a more distant relationship. The crown clade contains the living and recently extinct taxa (i.e. *Crocuta crocuta spelaea*) in the relationship of molecular hypotheses (Koepfli et al., 2006; Slater and Friscia, 2019; Westbury et al., 2020; Hassanin et al., 2021), diverging from a common ancestor at ~7.7 Ma. Basal to these taxa lie the entirety of the 'percrocutid' (sensu Werdelin and Solounias, 1991) species of this study. Percrocutids have long been attributed to a separate family (Schmidt-Kittler, 1976; Chen and Schmidt-Kittler, 1983; Werdelin and Solounias, 1991), based upon derived dentition and their early geologic occurrence. However, the present study recovers them nested far within the Hyaenidae, immediately basal to the living taxa (0.68 PP, nine synapomorphies). The taxa *Dinocrocuta gigantea* and *Percrocuta carnifex* are recovered in a sister-group relationship (0.97 PP), while the remaining *Percrocuta* taxa form a grade below the extant species.

The last feliform family assessed was the Lophocyonidae, whose highly supported internal relationships (0.96-1.0 PP, seven synapomorphies) are found to be identical to those of Morales et al. (2019). However, placement of this clade within the Viverroidea was not well resolved by the present analysis. The aforementioned analysis of Morales et al. (2019) hypothesized a relationship sister to the hyaenids, to the exclusion of viverrids, but did not include herpestid

taxa. The present study recovered lophocyonids between viverrids and the hyaneid + euplerid + herpestid clade, but posterior probability of placement only ranged from 0.09-0.27 PP for adjacent nodes. This high uncertainty is likely related to the equally uncertain placement of other historically enigmatic feliform taxa: *Herpestides antiquus*, *Kichechia zamanae* and *Kanuites lewisae* (0.05-0.25 PP) in this analysis.

Discussion

The recovered feliform phylogeny presents new insights into relationships of several clades, as well as aspects of overall diversification and rates of speciation for the clade. Compared to the most recent Nimravidae analysis (Barrett, 2021), *Maofelis* and MA-PHQ 348 were recovered as stem Nimravines, sister to the European taxa *Dinailurictis*, *Quercylurus* and *Eofelis*. This is not unreasonable, given all these Eurasian taxa share an apomorphic triple rooted P3, though the support for this clade is low, 0.25 PP. Likewise, the clade of *Dinictis* and *Pogonodon* was also recovered in a different part of the tree, as stem hoplophonines, but in contrast, this relationship had substantial support, 0.74 PP. These differences in topology to Barrett (2021) may relate to the differential model choice (FBD versus BDSKY) of the two analyses, given the morphology character matrices contain identical scorings for the shared characters. Of course, the present analysis also contains one hundred more characters than Barrett (2021), which may have reconstructed different models of character evolution even when most of these characters were non-parsimony informative for nimravids. Regardless, the results of this analysis suggest that the stem members of each nimravid subfamily are somewhat unstable, needing additional characters and/or newly discovered taxa to aid in their resolution. However, the current phylogeny is informative on the oldest occurrences of purported nimravids. These specimens are from the

Irdinmanhan Asian land mammal age of China, and represented by fragmentary upper canines (Chow, 1958; Ding et al., 1977; Zheng et al., 1978). Problematically, these canine fragments are referred to *Eusmilus* (a genus otherwise not known until the late Eocene), based upon their degree of compression and presence of serrations. These teeth are more derived than the geologically younger (late Eocene) *Maofelis cantonensis* (Averianov et al., 2016) for which a whole cranium is known. The present phylogenetic analysis suggests that an Irdinmanhan or older age (i.e., ≳43 Ma) for the basal nimravid node is highly improbable (Median = 41.33 Ma; 95% credible interval = [38.76, 43.94] Ma). Combined, these early records are more likely those of machaeroidine oxyaenodonts, another group of sabertooth carnivores known more securely from the Irdinmanhan of China (Zack, 2019a; Zack et al., 2022).

A notable long branch of this study's phylogeny is located on the stem of the Feloidea. This region of the tree has received little phylogenetic work in literature, with groups such as the palaeogalids and stenoplesictids rarely incorporated in evolutionary trees. Palaeogalids are small viverroid-like feliforms first known from the late Eocene of North America, whereby they achieve a Holarctic distribution in the Oligocene and early Miocene (Wang and Zhang, 2015). The exact phylogenetic placement of this family has long been disputed, but the only analysis thus far places the clade at the base of the Feliformia (Wang and Zhang, 2015). However, given the geologic age of the earliest nimravids and lack of temporal context in the aforementioned analysis, a future Bayesian tip-dated phylogeny may shed light on the placement of this clade. Furthermore, a recently described *Palaeogale* specimen (JODA 13221) from the Turtle Cove Member of the John Day Formation features a complete cranium with intact and fully ossified auditory bullae (Famoso and Orcutt, 2022). Basal nimravids and all stenoplesictids lack a fully ossified auditory bulla, which implies that palaeogalids independently acquired this condition, as

seen in Miocene nimravids, or may nest higher within crown Feliformia. Inclusion of the John

Day specimen in any subsequent phylogenetic analysis will go far in unraveling the evolutionary

history of this group. Stenoplesictids also offer a fruitful avenue of investigation given numerous

publications describing their anatomy, but lacking in phylogenetic analysis (e.g. Hunt, 1989,

1998a; Peigné, 1999; Peigné and De Bonis, 1999; Hunt, 2001a; Hans-Volker et al., 2007). A

sample of stenoplesictids was analyzed in the presented phylogeny, suggesting that the living

African palm civet *Nandinia* may represent the last surviving descendant of this once hypo- to

hypercarnivorous clade. *Nandinia* has been found has the most-basal member of the extant

Feliformia in several molecular analyses (Flynn et al., 2005; Nyakatura and Bininda-Emonds,

2012; Paijmans et al., 2017; Zhou et al., 2017; Slater and Friscia, 2019; Hassanin et al., 2021),

with frequent commentary on its apparently plesiomorphic partially-ossified auditory bullae in

morphological analyses (Hunt, 1987, 1989, 1998a; Wible and Spaulding, 2013). The inclusion of

Nandinia in the Stenoplesictidae fits well with the molecular divergence estimates of the current

and prior studies, as well as the bullar condition of representative stenoplesictids of the latest

Oligocene (Hunt, 1998a; Peigné and De Bonis, 1999). Thus, the evolution of an ossified bulla

amongst feliforms may have occurred on three independent occasions: nimravids, palaeogalids

and crown Feliformia minus stenoplesictids.

Machairodontines were recovered with two, not three, well-supported tribes. However, it is

probably no coincidence that the purported third tribe, Metailurini, was also the only tribe

lacking aDNA data. Felids are generally believed to be conservative in their hypercarnivourous

morphology (Holliday and Steppan, 2004; Van Valkenburgh, 2007; Chamoli and Wroe, 2011),

creating challenges in the available diversity of morphological characters when the identified

fossil material is limited in most taxa to craniodental remains. The most recent machairodontine

analysis (Werdelin and Flink, 2018) was also unable to recover these traditional tribes, even with a slightly expanded ingroup compared to this study's phylogeny (18 versus 14). However, the presented phylogeny did provide support for some disputed machairodontine hypotheses. The genus *Nimravides* has been suggested to be a taxon stem to Pantherinae + Felinae which convergently became sabertoothed given its relatively less derived dental morphology, geologic age and geographic context (Werdelin et al., 2010; Piras et al., 2018). This hypothesis cannot be ruled out by the tree of Werdelin and Flink (2018), given its unstable position as a stem feline or machairodontine depending on the settings of that study. However, this analysis supports the taxon as a machairodontine (0.94 PP) located near the base of the subfamily, before the split of smilodontins and homotherins. *Nimravides* is a New World taxon, with at least one species (*Nimravides catocopis*) suggested to be a member of the Old World homotherin *Machairodus* lineage (Antón et al., 2013). The presented results cast doubt on that hypothesis. However, no Old World *Machairodus* taxa were included in this analysis, so assessment of immigration events and tribe allocation for *Machairodus* taxa will require an expanded taxa set, though recent phylogenetic analyses suggest Old World *Machairodus* may not be a homotherin either (Christiansen, 2013; Werdelin and Flink, 2018). Additionally, *Promegantereon* was not recovered as a stem smilodontin, a relationship historically hypothesized, but not demonstrated via phylogenetic analysis (Christiansen, 2013; Werdelin and Flink, 2018). Instead, this taxon was recovered in a poorly supported clade (0.24 PP) at the base of the machairodontines reminiscent of hypothesized metailurins (see Christiansen, 2013). Much like *Nimravides*, this region of the machairodontine tree would benefit from the addition of further taxa. Recent revisions and anatomical descriptions offer abundant content to include a potential clade or grade of taxa thought to be convergent on felines and pantherines (Werdelin and Lewis, 2001; Spassov and

Geraads, 2015; Li and Spassov, 2017; de Bonis et al., 2018; Piras et al., 2018). One final area of the felid tree that would benefit from increased scrutiny, is the ancestry and descendant relationships of *Pseudaelurus* and *Hyperailurictis* with other felids. Numerous stem felids have historically been lumped into the *Pseudaelurus* genus, but renewed interest in a hypothesis of differential lineages of felid evolution has gained ground in recent years. Old World *Pseudaelurus* has been hypothesized to be a stem member of the Machairodontinae, while New World *Hyperailurictis* stem to all felids, or even a basal felid offshoot that gave rise to an endemic *Nimravides* (Kretzoi, 1929; Werdelin et al., 2010; Browne and Reynolds, 2015; Piras et al., 2018). However, even with the wealth of fossil material and publications on these early felids (e.g. Hunt, 1998a; Rothwell, 2001, 2003; Robles et al., 2013b), no analysis has given them broad context to support the splitting of these stem taxa into distinct lineages. Future work will go a long way towards our understanding of the evolution of the felids, how many lineages converged upon sabertooth, feline and pantherine morphologies, and biogeographic history of the entire family.

Perhaps the most novel result of this phylogeny is the recovery of percrocutids as derived hyaenids (1.0 PP). As previously mentioned, the derived dentition of these taxa has been the main evidence for their exclusion from the hyaenids. Specifically, in the dp4 a metaconid that is medially located within the trigonid complex and clearly separated from the talonid has been argued to be synapomorphic for hyaenids, while an inline, posteriorly placed metaconid connected with the talonid is the pattern among percrocutids (Schmidt-Kittler, 1976; Chen and Schmidt-Kittler, 1983; Werdelin and Solounias, 1991). However, in the work of Schmidt-Kittler (1976) it is suggested that this percrocutid condition could be the result of rapid evolution towards a hypercarnivorous morphology, losing the crushing talonid in favor of the slicing

trigonid. In the same work, the author describes the percrocutid condition in a variety of other feloids and nimravids (see Xiong, 2019 for a more detailed discussion) suggesting that it may have evolved multiple times. In fact, this morphology is present in the aardwolf, *Proteles*, and formed the basis for its removal to a separate Protelidae, inclusive of *Percrocuta* and *Dinocrocuta* (Baryshnikov and Averianov, 1993; Averyanov and Baryshnikov, 1996). The presented phylogeny used this character as part of its analysis, but still recovered all percrocutids as derived hyaenids, a hypothesis proposed, but untested in Xiong (2019) based upon basicranial morphology in *Dinocrocuta*. Furthermore, these taxa were recovered basal to the living hyaenids, but this relationship is challenged by the well-supported hypothesis that *Proteles* is the most basal living hyaenid (Zhou et al., 2017; Slater and Friscia, 2019; Westbury et al., 2020; Hassanin et al., 2021). Thus, any phylogenetic analysis relying on morphology (especially dental characters) to connect extinct taxa to the extant will be hampered by *Proteles*' near total lack of postcanine dentition and derived insectivorous lifestyle. This is reflected in the nodal support of the extant taxa to the most closely related "percrocutid" (0.46 PP). However, support does increase through progressive root-ward nodes (0.58-0.75 PP). This resolution of relationships does suggest rapid evolution of the aardwolf worlds insectivory given its most recent common ancestors were well adapted for a durophagous lifestyle.

Several internal nodes of the Hyaenidae were recovered with low to moderate support. For example, the relationship between the civet- and mongoose-like taxa *Protictitherium* and *Plioviverrops* only received 0.36 PP. This may be related to the species chosen if these genera are well represented in the fossil record, but later occurring than other congeners (Turner et al., 2008; Gracia, 2015). Addition of more of the currently thirteen recognized species of these genera (Turner et al., 2008) will likely increase support and resolution of this region of the

hyaenid tree by reducing long branch attraction and maximizing inclusion of transitional morphology. This general suggestion of increased taxon sampling will likely benefit all poorly or moderately supported nodes of the presented phylogeny, especially given the large diversity of extinct hyaenids, approximately one-third of which was sampled for this study (Werdelin and Solounias, 1991; Turner et al., 2008). One of these regions that still contains several evolutionary and taxonomic questions is that of the 'ictitheres'. Representing a diverse group (~13 taxa) of jackal or wolf-like taxa, 'ictitheres' may represent a unique clade characterized by a combination of five synapomorphies: a more anteriorly located bullar partition, the presence of second molars in both upper and lower dentition, enlarged m1 talonid and m2 surface area, an alisphenoid canal, and the lack of an enlarged frontal sinus (Semenov, 1989, 2008). However, all of the above features are ancestral for viverroids (save the bullar partition character) and thus unable to diagnose a clade with a recent common ancestor distinct from living hyaenids. Indeed, *Ictitherium viverrinum*, namesake of the 'ictitheres', was recovered in a position within typical 'hyaenotheres' (sensu Semenov, 1989), casting doubt within this analysis of a monophyletic clade for these canid-like taxa.

Finally, the last region of the recovered phylogeny that would benefit from increased sampling and investigation is that of stem viverroids. Of those analyzed, the lophocyonids formed the most cohesive group with highly supported internal relationships, but poorly constrained broader placement within Viverroidea. Lophocyonids are feliforms that evolved to be herbivorous browsers with highly complex lophate dentition (Morales et al., 2019). This dental complexity provides numerous morphological characters to resolve intraclade relationships, but basicranial morphology is unknown, creating challenges in determining the most recent common ancestor within the viverroids. Additional taxa such as *Lophocyon paraskevaidisi* (Koufos et al., 1995)

with known rostrum and near complete dentaries may help refine these relationships, but knowledge of the bullar condition from future specimens would likely contribute much more in broader relationships given the synapomorphic disparity of viverroid families for this feature (Hunt, 1987, 1989, 1991). Conversely, a taxon which does present known bullar morphology, could not be confidently resolved. *Kanuites lewisae* has a mosaic of basicranial features found in both herpestids and viverrids. *K. lewisae* possesses the viverrid oblique bullar partition, but herpestid + euplerid carotid artery caudal entotympanic posterior entrance (Werdelin, 2019). Furthermore, the temporal occurrence of *K. lewisae* (14.0-13.4 Ma) is as expected for both stem herpestids and viverrids. However, one illuminating feature that may be determined from CT scanning is the condition of the fossa for the tensor tympani in the petrosal, character 34. In both herpestids and euplerids this fossa forms a delicate tube, compared to a general depression or absence in all other feliforms. This feature may then help resolve the placement of this relatively well-known taxon and inform on greater mosaic evolution of a set of families known for their convergence (Gaubert et al., 2005).

Kichechia zamanae was also tentatively placed in the viverroids. Despite substantial fossil material, this hypothesized basal paradoxurine resolved outside both the Viverridae and Herpestidae. Without known basicranial morphology, clade allocation relies upon dental morphology. However, the prominent bunodont cusps of this taxon are known from other viverrid and herpestid taxa such as *Hemigalus*, *Bdeogale* and possibly *Atilax*, while the prominent cusps of the m1 trigonid and talonid including hypoconid and entoconid is ancestral for all viverroids. Additionally, the temporal occurrence of 20.0-17.0 Ma for this taxon is deeper than the inferred split of the Paradoxurinae and Viverrinae (sensu Gaubert and Veron, 2003) at 15.7 Ma. As already discussed, the main issue with placement of all of this study's stem

viverroids is lack of information on non-convergent morphological features (i.e., basicranial anatomy). Unfortunately, what remains is homoplastic or ancestral dental morphology that creates uncertainty in the precise placement of *Kichechia zamanae* and likely the other stem viverroids such as *Herpestides* and *Kanuites*.

The phylogenetic history of the Feliformia is relatively recent compared to the deeper Eocene roots of many Caniformia clades (e.g. Hunt, 1996; Nyakatura and Bininda-Emonds, 2012; Paterson et al., 2020) with diversification receiving three main pulses, the end Eocene, end Oligocene, and possibly a third within the last five million years (Figure 1). Even so, feliforms acquired broad morphology and ecology, from likely folivores, to durophages, and sabertooth morphs, the latter of which is not found within caniforms. Furthermore, feliforms, in contrast to caniforms, can be recognized by a distinctive auditory bulla morphology (often distinct per family) and a pattern of ontogenetic development that remains stable over a significant time interval in the middle and late Cenozoic. This basicranial morphology is fruitful ground for assessment of phylogenetic relationships as in the present study, even in the face of rapid evolution and dentognathic convergence of many clades. The present phylogeny used this information to generate a novel set of relationships among extinct taxa, while combining advances in molecular phylogenetic methods to produce the most expansive hypothesis to date. While not comprehensive, this phylogeny does inform on the relationships of "percrocutids" as derived hyaenids, the ancestry of the living African palm civet, *Nandinia* within the stenoplesictids, the origin of the earliest nimravids, and details of machairodontine tribal evolution. From these inferences, a benchmark for subsequent analyses is possible, but perhaps more importantly, a framework within which to assess aspects of the timing and rates of feliform trait evolution across a time-scaled phylogeny, one that includes thousands of posterior sampled

trees to incorporate phylogenetic uncertainty. To put it simply, we have barely begun to scratch the cat tree.

Chapter III

Ecological Evolution in the Feliformia

Introduction

The uneven distribution of niche occupation across the tree of life has been a central question of evolutionary biologists (Dobzhansky, 1951; Hutchinson, 1959). Adaptive radiations, in which a key adaptive feature allows a clade to speciate rapidly, have often been used to explain the dominance of members of a single lineage in a particular ecological role (Simpson, 1944, 1953; Schluter, 2000). Opportune events are thought to create high rates of evolution for a clade early in its history, evolutionary rates that quickly diminish as an ecospace is saturated. This pattern is typified by "early burst" models of evolution (Harmon et al., 2010), one among many growing analytical tools to assess evolutionary patterns. However, recent literature suggests early burst evolution is primarily observed within higher taxonomic levels while other forces operate upon lower ones, such as selection towards optimal phenotypic values or Brownian motion over geologic time (Slater, 2015; Law et al., 2018a; Slater and Friscia, 2019).

Yet, even within an adaptive radiation there appears to be limitations on what niches are filled/created. For example, why are there not more grazing ecologies amongst bovids and cervids following their late Miocene radiations, particularly with the spread of C4 grasslands (Cantalapiedra et al., 2013)? Horses famously developed traits that facilitated their grazing ecology through the Cenozoic (Matthew, 1926), including tall-crowned teeth (hypsodonty) with complex grinding surfaces, and a single toe (monodactyly) on an elongate limb. Though these traits may not be directly caused by expanding Cenozoic grasslands (Hansen, 1997; McHorse et

al., 2019), the comparative dearth of bovids and cervids with similar morphology and grazing ecology raises the question of why these clades did not radiate into this ecospace.

One possible explanation for biased ecospace exploitation relates to diet. It has been shown that there is a dietary transition bias associated with mammals, likely related to physiological challenges of switching to certain food types and energetic constraints of a given diet and body mass (Carbone et al., 1999; Price et al., 2012; Pineda-Munoz et al., 2016; Reuter, 2021). For example, the transition from herbivore to omnivore is far more common than omnivore to carnivore, and non-specialized insectivory is only feasible for an organism up to approximately 21 kg (Carbone et al., 2007). This latter point relates to a general decrease in dietary breadth at larger body size, where energetic constraints prevent exploitation of certain resources beyond a given size (McNab, 1986). Furthermore, phylogenetic baggage may not allow specific morphologies to efficiently utilize a given portion of ecospace, or at all. Even if a hypothetical phenotype can be produced it may not be actualized through functional restrictions, such as non-overlapping whorls in the shells of bivalves to produce a working hinge between the valves (Raup, 1966).

Amongst carnivorans, Law (2021) found patterns in head-body elongation ratios showed best-support for clade-based optimality shifts, and not models grounded in ecological traits, such as diet, locomotion or hunting behavior. Overall, living carnivorans have similar values in body shape, but certain clades possess clade-based radiations into stout (hyaenids and ursids) or elongate forms (weasels, genets and seals). This is suggestive of contingent opportunities leading to access of new ecospace with its own optimal trait value, and not that of rapid/broad occupation of ecospace that quickly decelerates. Conversely, Slater and Friscia (2019) found support for early burst patterns across living Carnivora for certain dental traits associated with

food processing, but not for body mass nor metrics of mechanical advantage in craniodental morphology. Together, this supports a decoupling, or differential selection, of size and shape evolution across Carnivora, and the importance of phylogenetic history

In this study, I test for the presence of adaptive radiations in body size and dental toolkit amongst living and fossil feliforms. The carnivoran clade Feliformia is an example of a group that has experienced a presumed bias in ecospace exploitation (Van Valkenburgh, 2007). Specifically, felids and nimravids seem to acquire their characteristic 'cat-like' morphology (e.g. foreshortened face, reduced dentition specializing in soft-flesh, retention of supinating/pronating forelimbs) in the earliest fossil forms and remain relatively unchanged until the present, or until their extinction, in the case of nimravids (Werdelin et al., 2010; Barrett, 2021). Why felids and nimravids did not come to occupy additional ecospace (save sabertooth ecomorphology), such as omnivory or even durophagy (bone-cracking as in hyenas) has remained a question many evolutionary biologists and paleontologists have asked (Radinsky, 1982; Holliday and Steppan, 2004; Van Valkenburgh, 2007; Chamoli and Wroe, 2011). The present study seeks to assess the evolutionary patterns of the Feliformia, and well-represented fossil clades. Were felids and nimravids examples of adaptive radiations that quickly occupied their adaptive zones, and if so, how did this differ from other feliform groups, such as hyenas, which occupied a far greater set of dietary and morphological ecologies? Furthermore, do small feliforms exhibit constraint in their evolution or facilitation because of the metabolic and functional discussion above? Below, I assess the patterns of living and extinct feliform ecological evolution with comparisons to differential evolutionary models. These include adaptive radiation, stabilizing selection, clade-based shifts and stochastic evolution. Finally, I offer a process-based framework for these patterns as a narrative of feliform evolutionary history.

Methods

Data Collection

I collected morphological measurements from fossil and living feliform specimens, as well as published values, from museums and literature as listed in Appendix C. Measurements were taken using Mitutoyo digital calipers to 0.01mm precision. Where possible, only wild-caught specimens were measured, though dental measurements were taken from some zoo animals for certain taxa to increase sample sizes. From these measurements, I calculated four ecomorphological traits (Figure 3, Table 3) that have been shown to describe morphology associated with food acquisition and processing in previous studies (Friscia et al., 2007; Meachen-Samuels and Van Valkenburgh, 2009; Slater, 2015; Slater and Friscia, 2019). Body masses (in grams) for living taxa were taken from the panTHERIA database (Jones et al., 2009), while I estimated body masses for fossil taxa from lower m1 lengths, using Van Valkenburgh's (1990) family-specific regression equations. Fossil hyenas posed their own unique problems, for the small number of living taxa do not express the entire ecological or morphological diversity of extinct members of the family (Werdelin and Solounias, 1991). For these extinct ecomorphs I used the ecological classification of Coca-Ortega and Pérez-Claros (2019) and analogous family-specific regression equations (e.g. canid, viverrid, bone-crushing hyaenid) of Van Valkenburgh (1990). Finally, for certain extinct taxa, robust reconstructions of body mass are available (Christiansen and Harris, 2005; Wheeler and Jefferson, 2009; Palmqvist et al., 2011), in which case, I used these values with source cited in Appendix C. I then converted mass estimates to a linear scale by taking their cube roots and subsequently natural log-transformed them for analysis. This was done to avoid negative values and conflict with R functions throughout the analysis.
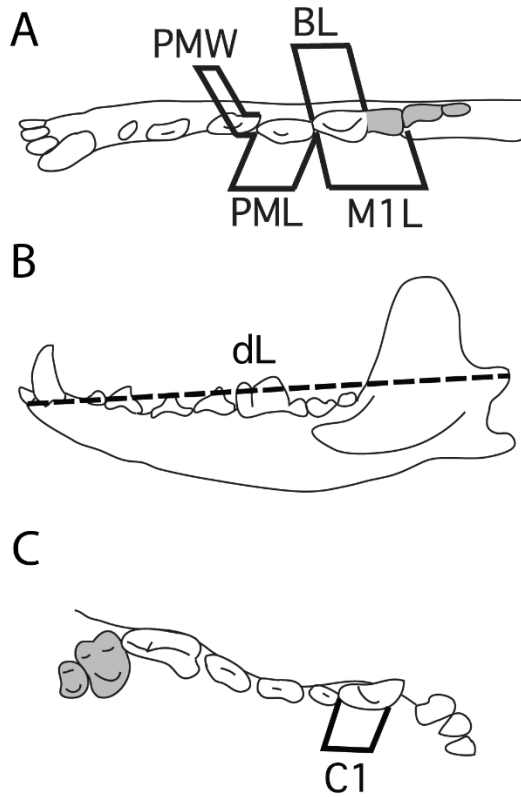
Figure 3. Measurements taken for ecomorphological traits. A: occlusal view of dentary and teeth. B: lateral view of dentary. C: occlusal view of upper dentition. PMW, lower fourth premolar width; PML, lower fourth premolar length; BL, blade length of lower first molar (trigonid); M1L, lower first molar length; dL, dentary length; C1, upper canine length. Modified from Slater and Friscia (2019: Fig. 1).

Table 3. Ecomorphological traits of analysis with abbreviations and constituent measurements.

Abbreviation	Meaning
C1	Compression of the upper canine, measured at the dentine-enamel junction as the mediolateral width divided by anteroposterior length
P4S	Robustness of the lower fourth premolar, measured as the maximum mediolateral width divided by maximum anteroposterior length
RBL	Relative blade length of the lower carnassial, measured as the anteroposterior ratio of trigonid length to overall m1 length
M1BS	m1 blade size relative to jaw length, measured as m1 trigonid length divided by length of dentary from anterior symphysis to posterior most portion of articular process
$ln\sqrt[3]{mass}$	The natural logarithm of the cube root of mass, in grams

I classified each feliform species to one of five dietary/ecological categories (hypocarnivore, mesocarnivore, hypercarnivore, durophage, or sabertooth) using linear discriminant analysis (LDA) implemented in the 'MASS' (Venables and Ripley, 2002) package for R v. 4.0.3 (R Core Team, 2020). The training set consisted of the four ecomorphological traits listed in Table 3 (C1, P4S, RBL, M1BS) measured for 134 extant taxa (Appendix H). Non-feliform species were included because fossil feliforms exhibit more extreme adaptions to hypo- and mesocarnivory than is realized in the extant radiation. Extant caniform data was supplemented with extinct species from Slater and Friscia (Slater and Friscia, 2019). The first three dietary categories were

assigned to extant taxa using the cutoffs of Van Valkenburgh (Van Valkenburgh, 2007) and the

Elton Traits dataset (Wilman et al., 2014) checked against the recent carnivoran ecological

analysis of Hopkins et al. (2021). Hypercarnivorous feliforms were considered as having ≥70%

vertebrate material in the diet, mesocarnivore = 50-69% and hypocarnivore ≤40% vertebrate

material, modified from ≤30% vert. of Van Valkenburgh (2007). *Crocuta*, *Hyaena*, and

Dinocrocuta were assigned to durophages, as were "transitional and fully developed bone-

crackers" from Coca-Ortega and Pérez-Claros (2019). *Dinocrocuta* has much literature justifying

a durophagous ecology (Tseng, 2009; Tseng and Binder, 2010), while the *Percrocuta* taxa of this

study do not and were thus classified using the canonical variates analysis of Coca-Ortega and

Pérez-Claros (2019). Scimitar- and dirk-tooth taxa were assigned as sabertooth in the training

set, while transitional scimitar- or dirk-tooth taxa were assigned by the LDA. Due to the

fragmentary nature of much fossil material, I performed a series of discriminant analyses,

iteratively reducing the number of variables to maximize species coverage. Classifications for

highly fragmentary taxa were consistent with expectations based on congeners. The predicted

categories for extinct taxa are available in Appendix H.

Analytical Methods

To understand the dynamics of body mass and carnassial evolution, I fit models of continuous

trait evolution to a random sample of 500 trees from the post-burnin posterior distribution of the

phylogenetic analysis of Chapter II. Constant-rate Brownian motion, temporally

accelerating/decelerating rate (early burst), and trended random walk models were fitted using

the 'fitContinuous' function in geiger (Pennell et al., 2014). I additionally fit two multipeak

Ornstein-Uhlenbeck (OU) models. The first was an ecological OU model using the mvMORPH

package (Clavel et al., 2015), while the second was a phylogenetic regime shift model using the

bayou package (Uyeda and Harmon, 2014). I limited the assessed OU evolutionary models to those possessing constant α (strength of pull) and σ^2 (evolutionary rate) terms; even though variable rate models do exist, simulations have shown unreliable inference for these models with phylogenies with a limited number of tips (Beaulieu et al., 2012). Measurement error was accounted for by including trait standard error in all evolutionary models. Because sample sizes were small for some species, I supplemented values for living taxa from Slater and Friscia (2019), while for poorly sampled extinct taxa I assigned each species a standard error of 0.0345, following Harmon et al. (2010). This was also the case for body mass standard error for all species, given that information is not included in the panTHERIA database. Relative model fit was assessed by computing small sample corrected Akaike Weights, AICcW. This was done for the entirety of the Feliformia, and subset analyses for the Felidae, Nimravidae, Hyaenidae and small feliforms.

Bayou uses a reversible-jump Markov chain Monte Carlo (MCMC) to fit multipeak OU models to estimate the placement and magnitude of regime shifts along lineages. This differs from the mvMORPH OU model by not assessing convergent evolution, but each shift is considered a unique adaptive regime (Uyeda and Harmon, 2014). Priors (Table 4) differed amongst the clades analyzed given the morphological breadth observed for body mass and RBL values.

Table 4. Priors for bayou analyses. Model parameter α = strength of pull, σ^2 = evolutionary rate, θ = optimal value. *= Calculated

using 'cdpois' option in bayou. RBL = relative blade length of the lower m1.

Model Parameter	Feliformia body mass	Feliformia RBL	Felidae body mass	Felidae RBL	Nimravidae body mass	Nimravidae RBL
α	Half-cauchy with scale factor 1	Half-cauchy with scale factor 1	Half-cauchy with scale factor 1	Half-cauchy with scale factor 1	Half-cauchy with scale factor 1	Half-cauchy with scale factor 1
σ^2	Half-cauchy with scale factor 0.1	Half-cauchy with scale factor 0.1	Half-cauchy with scale factor 0.1	Half-cauchy with scale factor 0.1	Half-cauchy with scale factor 0.1	Half-cauchy with scale factor 0.1
θ	Normal distribution with standard deviation = 1.3*sd of mass data, mean = mean of mass data	Beta distribution with shape 1 = 5 and shape 2 = 1	Normal distribution with standard deviation = 0.75*sd of mass data, mean = mean of mass data	Beta distribution with shape 1 = 5 and shape 2 = 1	Normal distribution with standard deviation = 0.5, mean = mean of mass data	Beta distribution with shape 1 = 5 and shape 2 = 1

Table 4. Continued for Feliformia, Felidae and Nimravidae.

Model Parameter	Feliformia body mass	Feliformia RBL	Felidae body mass	Felidae RBL	Nimravidae body mass	Nimravidae RBL
Number of shifts per branch	Fixed at one	Fixed at one	Fixed at one	Fixed at one	Fixed at one	Fixed at one
Branch-wise shift probability	Uniform	Uniform	Uniform	Uniform	Uniform	Uniform
Number of shifts	Conditional Poisson distribution* with mean = 0.1*number of edges on phylogeny and maximum = number of tips of phylogeny	Conditional Poisson distribution* with mean = 0.1*number of edges on phylogeny and maximum = 2*number of edges of phylogeny -2	Conditional Poisson distribution* with mean = 0.1*number of edges on phylogeny and maximum = number of tips of phylogeny	Conditional Poisson distribution* with mean = 0.1*number of edges on phylogeny and maximum = 2*number of edges of phylogeny -2	Conditional Poisson distribution* with mean = 0.1*number of edges on phylogeny and maximum = number of tips of phylogeny	Conditional Poisson distribution* with mean = 0.1*number of edges on phylogeny and maximum = number of tips of phylogeny
Location of shift along branch	Uniform	Uniform	Uniform	Uniform	Uniform	Uniform

Table 4. Continued for Hyaenidae and small feliforms.

Model Parameter	Hyaenidae body mass	Hyaenidae RBL	Small feliform body mass	Small feliform RBL
α	Half-cauchy with scale factor 1	Half-cauchy with scale factor 1	Half-cauchy with scale factor 1	Half-cauchy with scale factor 1
σ^2	Half-cauchy with scale factor 0.1	Half-cauchy with scale factor 0.1	Half-cauchy with scale factor 0.1	Half-cauchy with scale factor 0.1
θ	Normal distribution with standard deviation = 0.3, mean = mean of mass data	Beta distribution with shape 1 = 5 and shape 2 = 1.5	Normal distribution with standard deviation = 0.75*sd of mass data, mean = mean of mass data	Normal distribution with standard deviation = 0.75*sd of RBL data, mean = mean of RBL data
Number of shifts per branch	Fixed at one	Fixed at one	Fixed at one	Fixed at one
Branch-wise shift probability	Uniform	Uniform	Uniform	Uniform
Number of shifts	Conditional Poisson distribution* with mean = 0.1*number of edges on phylogeny and maximum = number of tips of phylogeny.	Conditional Poisson distribution* with mean = 0.1*number of edges on phylogeny and maximum = 2*number of edges of phylogeny -2.	Conditional Poisson distribution* with mean = 6 and maximum = number of tips of phylogeny.	Conditional Poisson distribution* with mean = 0.1*number of edges on phylogeny and maximum = 2*number of edges of phylogeny -2.
Location of shift along branch	Uniform	Uniform	Uniform	Uniform

I ran two independent MCMC chains with 1.5 million generations, each sampled every 1,000 generations for the full Feliformia phylogeny. These family-level phylogenies ran for 500,000 generations, with sampling at every 500. Convergence was assessed using Gelman and Rubin's R statistic via the 'gelman.R' function in bayou (Uyeda and Harmon, 2014). R values <1.1 were considered to have reached convergence, and samples prior to this were discarded as burn-in. Effective sample sizes were greater than 200 for all analyses, and frequently over 1,000. Only evolutionary shifts with a posterior probability (PP) above 0.5 using parameters averaged from the two chains were considered in subsequent analyses. To compare the results of the bayou model to that of the likelihood-based geiger and mvMORPH models, I converted the bayou output using the 'bayou2OUwie' function (Uyeda and Harmon, 2014). Clades identified via bayou for adaptive shifts were then assessed by a comparable OUM model in mvMORPH. The relative AICc weights of all models were then compared for best fit.

Results

Feliformia

The distribution of ecological variables can be seen in Figure 4. An Ornstein–Uhlenbeck (OU) for multiple dietary optima is the best-fitting evolutionary model for both body mass and RBL for the Feliformia, (Table 5, median AICcW = 0.49 for body mass and 1.0 for RBL). Body mass sees a general increase in optimal value progressing from hypocarnivore to sabertooth ecology, with the largest jump between hypercarnivore and durophagous. Carnivores are predicted to switch to hunting of large vertebrate prey at around 14.5-21 kg (Carbone et al., 2007), with prey of equal or larger mass than their own at a subsequent 21.5-25 kg (Carbone et al., 1999). The

hypercarnivore optimum is here inferred to be 11.32 kg. This was smaller than that observed by Slater (Slater, 2015) for living and extinct canids (median = 20.7 kg). A smaller optimal mass of 1.28 kg was estimated for hypocarnivory, but a larger mass of 16.55 kg for mesocarnivory (Table 5). However, both durophagous and sabertooth ecologies returned comparable and very large optimal body masses, with 173.62 kg for the former, and 179.11 kg for the latter.

The α-parameter of OU models describes the strength of attraction to the associated optima, with higher values indicating a stronger pull. This value can be reparametrized in terms of phylogenetic half-life, $t_{1/2}= \ln(2)/\alpha$, which describes the time required for adaptation to a new selective regime to outpace implied constraints of an ancestral regime (Hansen, 1997). The phylogenetic half-life of the median estimated α-parameter for body mass is approximately 10 million years (My). This implies strong and rapid selective pressure towards an optimal body mass given a dietary category.

Relative blade length of the m1 is also best explained by an adaptive peak model (median AICcW = 1.0, Table 5). This model predicts a median optimal relative blade length of 0.50 for hypocarnivorous feliforms, while mesocarnivorous feliforms are attracted to a slightly greater relative blade lengths of 0.54. Hypercarnivorous, durophagous, and sabertooth feliforms are all attracted to relative blade lengths of approximately 1.0. These latter two dietary ecologies in fact returned optimal values greater than 1.0. Though biologically impossible, the assessed OUM model could not be constrained for possible optimal ranges, and thus suggests even stronger attraction to total slicing component of the m1 than is observed in hypercarnivorous feliforms that do not have durophagous or sabertooth morphology.
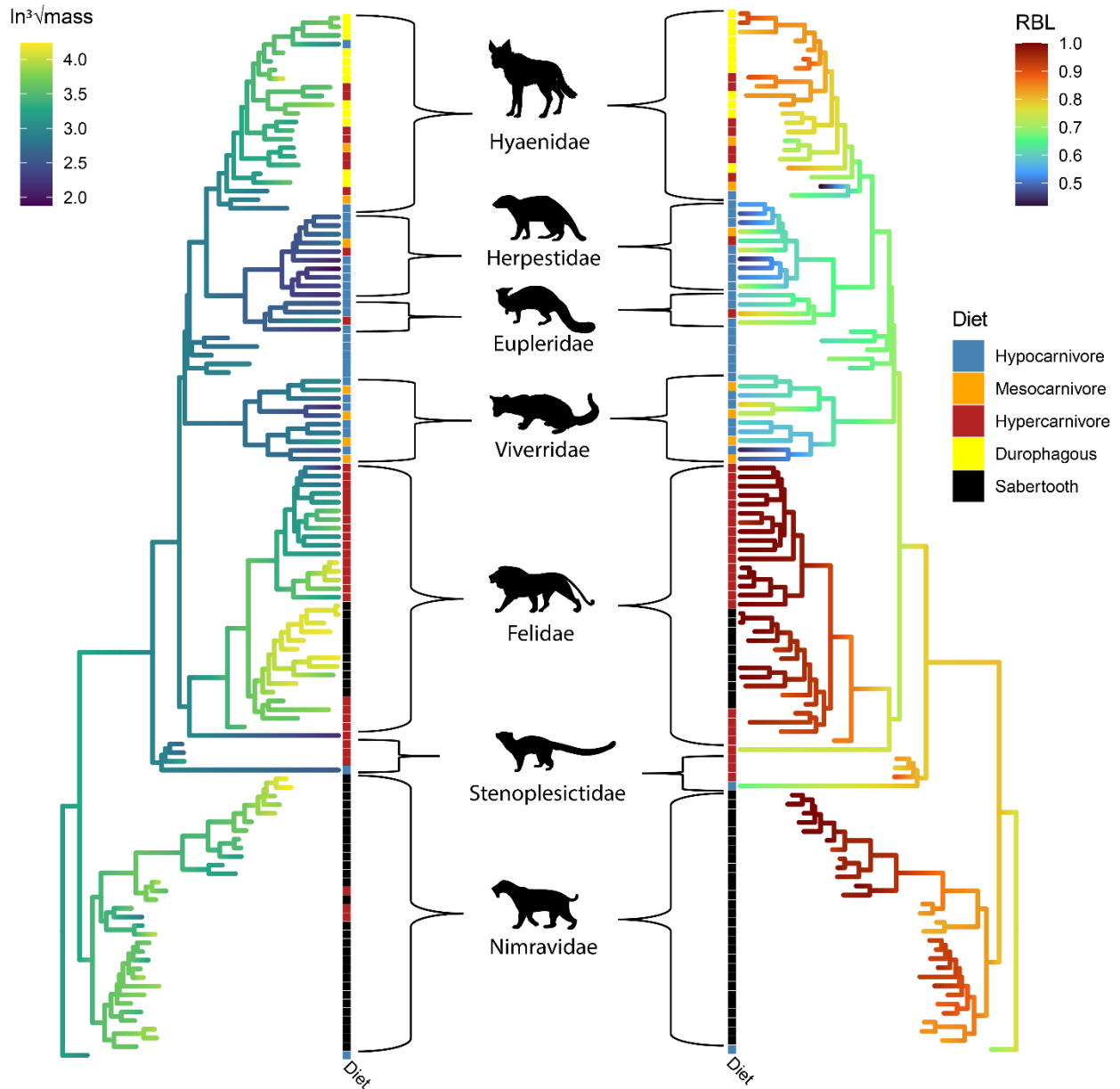
Figure 4. Distribution of ecological proxy variables used in the presented analysis, natural log of the cube root of body mass in grams, left, and the relative blade length of the lower m1, right. Ancestral states for both body mass and relative m1 blade length were estimated using the 'fastANC' function found in 'phytools' (Revell, 2012) on the MCC tree of Chapter II. Silhouettes taken from phylopic.org or created by the author.

Likewise, to optimal body mass values, the median estimated α-parameter (0.040) for relative

m1 blade length implies strong selection for these values, but not as strong as bodymass, $t_{1/2}=$

17.3 My. However, this value does approximate the divergence of major feloid clades, 15-31

Ma, suggesting the primary pull of RBL selection began at the clade's appearance and has been

sustained since.

Felidae

In contrast to overall feliform evolution, felid body mass was best explained by a model of

Brownian motion (AICcW = 0.62). This was approximately three times higher in weight than the

next best supported model, trended evolution, AICcW = 0.20, while an early burst model

received only slightly less support than this, AICcW = 0.18. Both OUM models were the poorest

supported with no node returned 0.5 or greater PP for the bayou analysis.

RBL evolution was best explained by an early burst model (AICcW = 1.0). This suggests that

initial high rates of evolution for a clade exponentially decay over time as a new niche becomes

available, but then is quickly saturated (Blomberg et al., 2003; Harmon et al., 2010). The scalar

value for this model (r = -13.98) describes the deceleration of evolution, as expected by a

hypothesis of adaptive radiation. The very large and negative value gives a feel for the rapidity

of this burst, one that is several orders of magnitude greater than found in estimates of overall

feliform RBL evolution under an early burst model, and indeed in large clades of other analyses

(Harmon et al., 2010).

Table 5. Median results from macroevolutionary model fits to 500 random trees from the stable Bayesian posterior of the phylogenetic analysis in Chapter II. Mass has been converted to kgs. OUM_{bayou} did not recover a shift at any location with over 0.5 PP for RBL.

Trait	Model	lnLk	AICc	AICcW	σ^2	Scalar	Hypo-carnivore	Meso-carnivore	Hyper-carnivore	Durophagous	Sabertooth
$ln\sqrt[3]{mass}$	BM	-33.76	71.62	0.02	0.013	-	-	-	-	-	-
	ACDC	-33.32	72.85	0.13	0.019	-0.012	-	-	-	-	-
	Trend	-33.98	74.16	0.01	0.013	0.002	-	-	-	-	-
	OUM_{diet}	-22.80	62.89	**0.49**	0.018	0.067	1.28	16.55	11.32	173.62	179.11
	OUM_{bayou}	-31.96	76.66	0.34	0.014	0.018	-	-	-	-	-
RBL	BM	-33.76	71.62	<0.01	0.013	-	-	-	-	-	-
	ACDC	145.17	-284.12	<0.01	7.5^{-4}	-0.013	-	-	-	-	-
	Trend	145.79	-285.37	<0.01	5.2^{-4}	0.002	-	-	-	-	-
	OUM_{diet}	159.32	-301.29	**1.0**	0.018	0.040	0.50	0.54	0.97	1.02	1.09
	OUM_{bayou}	-	-	-	-	-	-	-	-	-	-

Table 6. Median Felidae results from macroevolutionary model fits to 500 random trees from the stable Bayesian posterior of the phylogenetic analysis in Chapter II. Mass has been converted to kgs. OUM$_{bayou}$ did not recover a shift at any location with over 0.5 PP for body mass.

Trait	Model	lnLk	AICc	AICcW	σ^2	Scalar	Hypercarnivore	Sabertooth
$ln\sqrt[3]{mass}$	BM	-8.00	20.43	**0.62**	0.014	-	-	-
	ACDC	-8.05	22.98	0.18	0.011	0.016	-	-
	Trend	-8.06	23.00	0.20	0.014	-0.002	-	-
	OUM$_{diet}$	-8.21	38.97	<0.01	0.017	0.030	5.63	1788.15
	OUM$_{bayou}$	-	-	-	-	-	-	-
RBL	BM	-7.98	20.39	<0.01	0.014	-	-	-
	ACDC	6808.59	-13610.30	**1.0**	7.6^{-218}	-13.98	-	-
	Trend	5213.70	-10420.50	<0.01	7.1^{-218}	-2.5^{-18}	-	-
	OUM$_{diet}$	297.69	-572.83	<0.01	0.016	0.112	1.0	1.0
	OUM$_{bayou}$	462.74	-913.09	<0.01	1.8^{-33}	0.112	-	-

Nimravidae

Similar to felids, the best supported evolutionary models for nimravid body mass and RBL was Brownian motion and early burst respectively, Table 7. However, the relative support of a Brownian motion model for body mass over the next best supported model was not as great as in the Felidae, BM AICcW = 0.52, ACDC = 0.32. Additionally, the sigma squared parameter, which can be interpreted as the net rate of evolution (Harmon et al., 2010) was the same as in both nimravid and felid analyses. This suggests similar overall rates of body mass evolution even over different persistence times for each clade (Nimravidae = 34.3 Ma, Felidae = 18.9 Ma). RBL evolution for nimravids is also best explained by an early burst model (AICcW = 1.0). The rate parameter for this model is even greater than that inferred for felid evolution (r = -16.68), implying a very rapid decrease in evolutionary rates beyond an initial adaptive radiation.

Hyaenidae

Hyaenid ecological evolution returned similar results to the overall Feliformia, such that body mass and RBL evolution was best supported by an OU model for multiple dietary optima (Table 8), median AICcW = 0.95 for body mass and 0.48 for RBL). Body mass also sees an increase in optimal value progressing from hypocarnivore to durophagous ecology compared to overall Feliformia. The hypercarnivore optimum for hyaenids is inferred to be 25.46 kg. This is quite similar to that observed by Slater (Slater, 2015) for canids as mentioned previously, but the additional optimal values for hypo- and mesocarnivorous hyaenids (median optima = 3.19 kg, 16.11 kg respectively) are also quite similar to that observed by Slater for living and fossil canids, (hypo. = 3.2 kg and meso. = 4.7 kg). Durophagous hyaenids returned the largest optimal mass at 64.98 kg, similar to living *Crocuta* but less than that estimated in the overall feliform analysis. The phylogenetic half-life of the α-parameter for body mass returned the shortest value

of all analyses at 1.96 My. This implies extremely strong selective pressure towards an optimal body mass given a hyaenid dietary category.

Relative blade length of the m1 is also best explained by an adaptive peak model (median AICcW = 0.48, Table 8), but only moderately better supported than the next best model, early burst (AICcW = 0.27). The adaptive peak model predicts a median optimal relative blade length of 0.69 for hypocarnivorous hyaenids, while mesocarnivorous hyaenids are attracted to substantially smaller relative blade lengths of 0.44. Hypercarnivorous and durophagous hyaenids are all attracted to relative blade lengths closer to 1.0 (hyper. = 0.78, duro. = 0.86), but substantially less in value than seen in all other analyses. The α-parameter for RBL values also displayed a high attractive force (median = 0.348), $t_{1/2}$= 1.99 My compared to body mass estimates, but slightly smaller.

Small feliforms

Unique amongst all analyses, small feliforms found best support for Brownian motion in both RBL and body mass evolution, Table 9. The relative support of these models was about twice as great as the next best models, ACDC for the former and trended evolution for the latter. The sigma squared parameter for body mass evolution (0.008) was less than that in both nimravid and felid analyses, about half as large. This suggests that body mass evolution occurs at a slower pace amongst small feliforms, though expected given their overall amount of variance in this variable. The sigma squared value for RBL evolution (0.008) is about half of that inferred for other analyzed clades, also implying relatively slower rates of evolution for the dental toolkit.

Table 7. Median Nimravidae results from macroevolutionary model fits to 500 random pruned trees from the stable Bayesian posterior of the phylogenetic analysis in Chapter II. Mass has been converted to kgs. OUM$_{bayou}$ did not recover a shift at any location with over 0.5 PP for body mass or RBL.

Trait	Model	lnLk	AICc	AICcW	σ^2	Scalar	Hypercarnivore	Sabertooth
$ln\sqrt[3]{mass}$	BM	-3.82	12.06	**0.52**	0.014	-	-	-
	ACDC	-3.76	14.37	0.32	0.018	-0.023	-	-
	Trend	-3.64	14.14	0.15	0.014	0.013	-	-
	OUM$_{diet}$	-1.19	24.64	<0.01	0.023	0.139	3.89	61.44
	OUM$_{bayou}$	-	-	-	-	-	-	-
RBL	BM	-3.82	12.06	<0.01	0.014	-	-	-
	ACDC	938.19	-1869.38	**1.0**	2.0^{-71}	-16.677	-	-
	Trend	55.36	-103.73	<0.01	1.3^{-4}	0.005	-	-
	OUM$_{diet}$	54.22	-98.71	<0.01	0.023	0.034	-	1.0
	OUM$_{bayou}$	-	-	-	-	-	-	-

Table 8. Median Hyaenidae results from macroevolutionary model fits to 500 random trees from the stable Bayesian posterior of the phylogenetic analysis in Chapter 2. Mass has been converted to kgs. OUM_{bayou} did not recover a shift at any location with over 0.5 PP for body mass or RBL.

Trait	Model	lnLk	AICc	AICcW	σ^2	Scalar	Hypo-carnivore	Meso-carnivore	Hyper-carnivore	Durophagous
$ln\sqrt[3]{mass}$	BM	-3.38	11.36	0.03	0.012	-	-	-	-	-
	ACDC	-3.52	14.29	0.01	0.017	-0.041	-	-	-	-
	Trend	-2.79	12.85	0.01	0.011	0.021	-	-	-	-
	OUM_{diet}	7.06	12.16	**0.95**	0.023	0.353	3.19	16.11	25.46	64.98
	OUM_{bayou}	-	-	-	-	-	-	-	-	-
RBL	BM	-3.38	11.36	0.25	0.012	-	-	-	-	-
	ACDC	24.41	-41.41	0.27	0.003	-0.135	-	-	-	-
	Trend	23.03	-38.66	<0.01	0.001	0.006	-	-	-	-
	OUM_{diet}	34.36	-40.73	**0.48**	0.023	0.348	0.69	0.44	0.78	0.86
	OUM_{bayou}	-	-	-	-	-	-	-	-	-

Table 9. Median small feliform results from macroevolutionary model fits to 500 random trees from the stable Bayesian posterior of the phylogenetic analysis in Chapter 2. Mass has been converted to kgs. OUM_{bayou} did not recover a shift at any location with over 0.5 PP for body mass or RBL.

Trait	Model	lnLk	AICc	AICcW	σ^2	Scalar	Hypo-carnivore	Meso-carnivore	Hyper-carnivore
$ln\sqrt[3]{mass}$	BM	-8.29	20.96	**0.51**	0.008	-	-	-	-
	ACDC	-8.39	23.58	0.29	0.008	-3.0^{-4}	-	-	-
	Trend	-7.52	21.84	0.18	0.008	-0.011	-	-	-
	OUM_{diet}	-4.18	30.13	0.01	0.015	0.094	1.73	19.85	1.83
	OUM_{bayou}	-	-	-	-	-	-	-	-
RBL	BM	-8.29	20.96	**0.46**	0.008	-	-	-	-
	ACDC	30.23	-53.66	0.22	0.001	0.0134	-	-	-
	Trend	31.02	-55.25	0.30	0.001	-0.004	-	-	-
	OUM_{diet}	35.62	-49.48	0.03	0.015	0.142	0.59	0.65	0.79
	OUM_{bayou}	-	-	-	-	-	-	-	-

Discussion

Overall, feliform ecological evolution is pulled towards optima related to dietary category. However, clade-specific patterns suggest far more nuance in evolutionary history. Both nimravids and felids experienced an adaptive radiation (early burst) with entrance into hypercarnivore and sabertooth ecologies, while body mass evolution of these clades is best supported by a random walk over geologic time. The processes behind adaptive radiations are often hypothesized to relate to the development of 'key innovations' or contingent historical events that facilitate diversification by creating new ecological opportunities (Schaeffer, 1948; Van Valen, 1971; Gould, 1989; Sanderson and Donoghue, 1994; Hunter and Jernvall, 1995; Slater, 2015). Though it may be more straightforward to correlate the acquisition of a given morphologic feature with an adaptive radiation, the nature of contingent events implies chance opportunities such as sweepstakes dispersals or climatic change that generates a land bridge due to falling sea levels. These are events that if we were to "rewind the tape" (Gould, 1989) may not happen again. However, there are theoretical frameworks that, although unable to predict a given climatic or tectonic event, offer utility in predicting the biotic response to such a perturbation. For example, under Habitat Theory (Vrba, 1992) most speciation and extinction events are correlated to global tectonic and/or climatic changes, while common climatic fluctuations typically drive geographic habitat tracking as species move with their biome if possible. Furthermore, at times of global warming with a strong latitudinal thermal gradient, Habitat Theory predicts higher speciation rates at lower latitudes and higher extinction rates at higher latitudes. This principle is related to the habitat preference of specialist clades where resources would tend to disappear during recurrent environmental extremes. Though challenged for certain African Pliocene taxa (Bobe et al., 2002; Werdelin and Lewis, 2005; Frost, 2007; Faith and

50

Behrensmeyer, 2013), Habitat Theory may still provide a useful framework for global dynamics of the Cenozoic.

One assumption in the application of Habitat Theory to the fossil record is that clades, generally speaking, have maintained habit preference, or in other words, that the fundamental habit of a clade has changed minimally over geologic time. Most living feliforms, including felids, hyenas, mongooses, civets, and genets are found in tropical regions, while most terrestrial caniforms reside within temperate or seasonal climatic regions (Pickford and Morales, 1994; Hunt, 1996). This differential climatic signal is even found in the cranial shape of feliforms versus caniforms, where mean precipitation and temperature are significant predictors of cranial shape in feliforms, but not caniforms (Tseng and Flynn, 2018). The divergence time of the most recent common ancestor (MRCA) of nimravids for the phylogeny presented in Chapter II is suggested to be at approximately 41.3 Ma. Even the earliest nimravids are known to possess hypercarnivorous dentition, but based on phylogenetic analysis, and the results of the presented chapter, quickly derived this dental condition from more generalist feliforms present in the middle to early Eocene (Solé, 2014; Tomiya and Tseng, 2016; Barrett et al., 2021). The above MRCA date occurs slightly after the Middle Eocene Climatic Optimum (Zachos et al., 2001). This period of global warming is associated with an increase in hypercarnivory amongst mammals in North America (Tomiya et al., 2021), but also in the earliest Asian nimravid material (Chow, 1958; Peigné et al., 2000; Averianov et al., 2016). Nimravids likely originated in Asia, as did the earliest feliforms (Hunt, 1996, 1998a). If nimravids were also tropical specialists, the spread of this clade into North America would be predicted by Habitat Theory. As the thermal gradient extended northward during the Middle Eocene Climatic Optimum (Figure 5), nimravids would have found dispersal easier via northern passages into North America. Tropical specialists would

also benefit from increased speciation rates during this time, as seen in Figure 1, though it is unclear if this provided the impetus for the rapid development of hypercarnivory within this clade and non-carnivorans. Hypercarnivory amongst mammals appears to have experienced a process of slow assembly within the Cenozoic. One that didn't develop the familiar secant dentition and reduced tooth count until the Early to Middle Eocene in oxyaenodontan, hyaenodontan and carnivoramorphan taxa (Borths et al., 2016; Solé and Ladevèze, 2017). However, hypercarnivorous members of the above clades all seem to have rapidly acquired this dental toolkit during this epoch. Nimravids arrival in North America is also associated with rapid acquisition of sabertooth morphology compared to Asian ancestors, e.g., *Maofelis*. Compressed and serrated canines are known from the Hancock mammal quarry of Oregon (~40 Ma, Hanson, 1996), and a c.f. *Hoplophoneus* maxilla (San Diego Natural History Museum 60554) from the Pomerado conglomerate of San Diego (ca. 38-37 Ma). These first nimravids would have encountered large hyaenodont and mesonychid hypercarnivores (e.g. *Hyaenodon*, *Hemipsalodon*, *Harpagolestes*). Perhaps the rapid acquisition of sabertooth morphology allowed nimravids a way to access a greater variety of prey resources while staying relatively small in the presence of potentially competing non-carnivoramorphan hypercarnivores. What's more, following the loss of sabertooth machaeroidines prior to the Middle Eocene Climatic Optimum (Zack et al., 2022), an opportunity may have presented itself for a new lineage to create or occupy a similar ecology in North America.
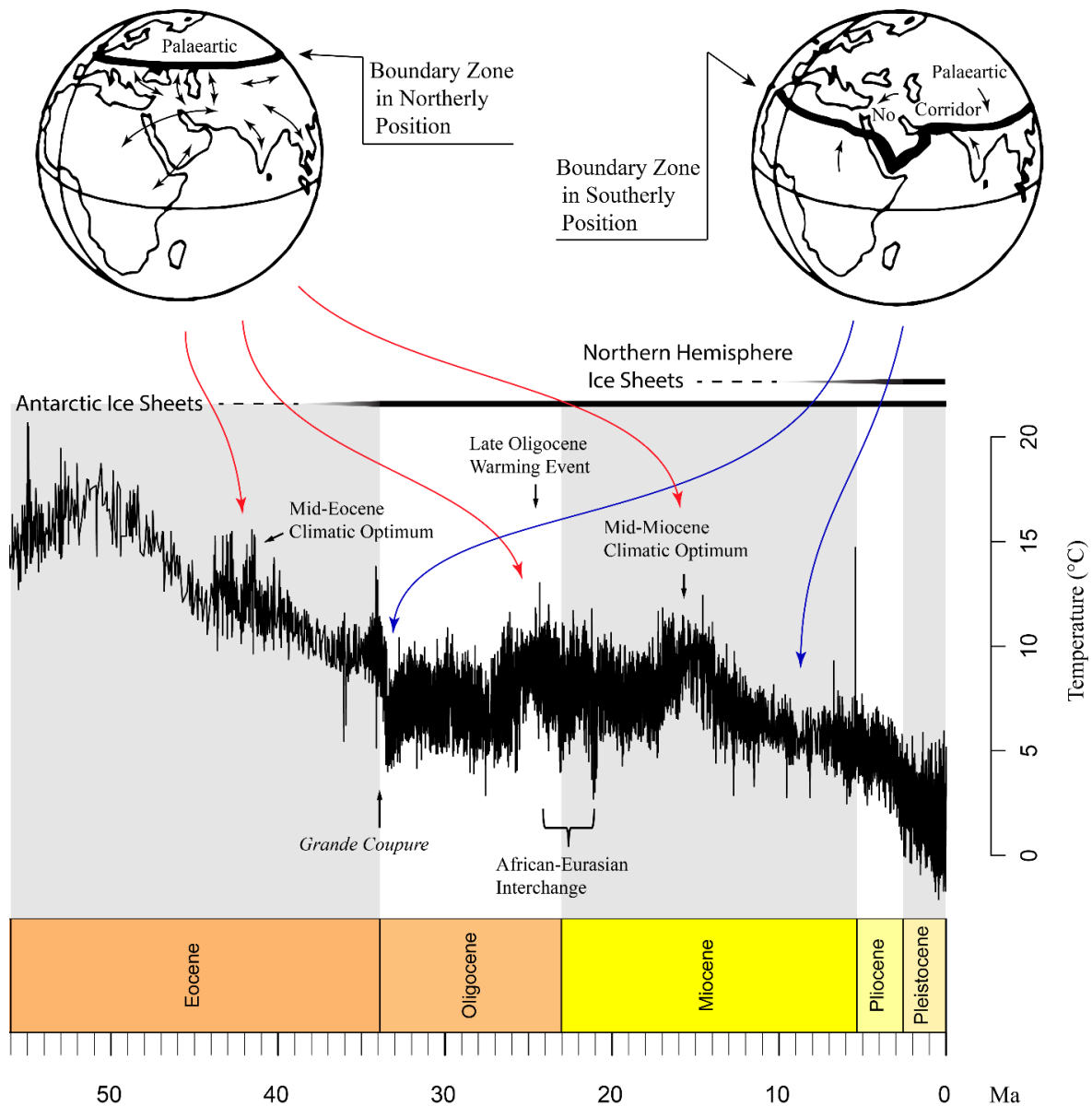
Figure 5. Latitudinal boundary shift of tropical and boreal climate zones from the Eocene to the present. Climate gradient modified from Pickford and Morales (1994), Fig. 5. Global climate data from Zachos et al. (2008), where absolute temperatures were converted from δ18O using the equation of Epstein et al. (1953). Climatic events are annotated above temperature curve while biogeographic events below curve. Note global geography depicts the modern arrangement, approximately Miocene to present.

Though unanalyzed at the clade level for ecological evolution, stenoplesictids are the earliest known feloids (save perhaps palaeogalids with a Chadronian occurence, Famoso and Orcutt, 2022) with a Late Eocene occurrence in Mongolia (Dashzeveg, 1996; Hunt, 1998a). The diversity and morphology of this clade is poorly known until the start of the Oligocene when a diversity of forms arise and spread into Europe. In fact, the earliest known feloids of the Oligocene are found at Quercy (France) at the Eo-Oligocene transition along with nimravids (Hunt, 1998a). This sudden European appearance is likely related to the *Grande Coupure*, an event with substantial faunal turnover and associated immigration of Asian taxa into Europe. The *Grande Coupure* was during a time of global cooling associated with Antarctic ice sheet formation (Zachos et al., 2001). Costa et al. (2011) summarize several theories for this event and the replacement of European taxa, but sea level drop with the formation of the Antarctic icesheet likely facilitated a land bridge to Europe to aid the dispersal of Asian taxa. Stenoplesictids are also known in Mongolia post-*Grande Coupure*, along with palaeogalids and nimravids, though there is a distinct lag (~2 Ma) between the first Oligocene geographic radiation and following feloid diversification (Dashzeveg, 1996; Hunt, 1998a). The latitude of both France and Mongolia are approximately at 45 degrees north, being substantially outside the tropics of today, combined with the rapid global cooling at the formation of Antarctic ice sheets, it would be expected under Habitat Theory to see a retraction of tropical specialists to the equator during this time, while biome generalists would be relatively unaffected. However, recent data suggests that high-latitude temperatures may have been almost as warm as those pre-Antarctic glaciation (O'Brien et al., 2020). This is hypothesized to be in part related to the lack of a northern ice sheet. Additionally, the East Asian record of mid-late Eocene and early Oligocene carnivoramorpha is quite poor (Ducrocq et al., 1995; Wang et al., 2007; Böhme et al., 2013). This suggests the taxa

that did immigrate into Europe during the *Grande Coupure* were relatively unencumbered by the global cooling at this period, either to being biome generalists or being in a high-latitude climate warmer than previously hypothesized but did not experience the boost in speciation rates associated with a warming climate as predicated under habitat theory. In fact, an increase in overall feloid diversity isn't seen for two million years after the event which does follow a rapid warm excursion immediately after the initial cold excursion of the Eo-Oligocene transition (Zachos et al., 2001).

The Oligocene saw rapid diversification of nimravid species (Barrett, 2021), but also in those of stenoplesictids and palaeogalids (Hunt, 1998a; Peigné, 1999; Peigné and De Bonis, 1999; Hunt, 2001a; Welsh, 2021; Famoso and Orcutt, 2022). Ecologically, save the living African Palm Civet (*Nandinia*), all analyzed stenoplesictids are hypothesized to be hypercarnivorous feliforms, though not derived to the degree seen in contemporary nimravids, nor in later hyaenids or felids. This suggests that the global faunal turnover of the Eo-Oligocene transition may have provided a large opportunity (contingent event) for Feliform diversification, as supported by the nimravid-specific RBL analysis of this chapter, though not yet assessed at the clade level for stenoplesictids nor palaeogalids.

The end of the Oligocene saw rapid global warming that was sustained into the early Miocene. Much like the *Grande Coupure* before it, another mass immigration event occurred, the African-Eurasian interchange. This event saw the immigration of African endemic species out of Arica, such as proboscideans, while Eurasian taxa including carnivorans and ungulates into Africa. However, there is a bias in what species immigrated and subsequently diversified. For example, feliforms were the dominant carnivorans to immigrate into Africa, while caniforms are only represented by two species (Pickford and Morales, 1994). For African immigrants,

proboscideans, hyracoids and aardvarks were the only groups to find substantial success when leaving Africa, likely beginning in the latest Oligocene (Lucas and Bendukidze, 1997; Antoine et al., 2003; Sen, 2013).

Habitat Theory would predict large-scale immigration of tropical biome specialists (i.e., most feliforms) to the newly accessible landmass with the same fundamental habitat within which they currently reside, especially during a period of global warming (Figure 5). It would also predict the exclusion of boreal, or Palearctic in this case, species from Africa, possibly related to differential reproductive strategies as influenced by seasonality and day length changes. At high latitudes, temperature and day length fluctuations are the greatest signals of seasonality, while at low latitudes these same fluctuations are minor and humidity changes dominate, lending the tropics to wet/dry seasonality (Pickford and Morales, 1994). Nimravids were perhaps the first carnivorans that arrived in Africa, presumably from Asia, given the lack of known European nimravid material of this age (Friscia et al., 2020; Barrett et al., 2021; Werdelin, 2021). However, a diversity of stenoplesictid, and stem feloid taxa also immigrated to Africa around the same time (Pickford and Morales, 1994; Morales and Pickford, 2021). This period (~25-20 Ma) correlates with an increase in speciation rate in the skyline plot of Figure 1; the divergence of hyaenids from herpestid/euplerid ancestors, the origin of felids, the origin and diversification of lophocyonids, and initial diversification of the Barbourofelini. In short, a great diversification of feliform taxa occurred resulting in the origin of most living families.

By 16 Ma, the earth would enter the Middle Miocene Climatic Optimum (Figure 5), the last excursion into a warming planet before a steady decline into the cooler and more familiar northern and southern icesheet driven system of the present (Zachos et al., 2001). With the rise in global temperatures, one would expect a correlated rise in feliform diversity under Habitat

theory. In fact, the phylogeny of Chapter II (Figure 2), recovers this as the MRCA for the extant radiation of viverrids and herpestids + euplerids, and the divergence of machairodontine felids from felines + pantherines. These values are further supported by the analysis of Slater and Friscia (2019) on a more inclusive taxon set of extant species. Globally, there is also a large increase in Mammalian diversity during the middle Miocene, including that of feliform taxa (Alroy, 1992; Pickford and Morales, 1994; Morales and Pickford, 2011; Grohé et al., 2020; Wang et al., 2020; Morales and Pickford, 2021). The present analysis found felid dietary evolution was best supported by an early burst model (Table 6); this was also the case for RBL evolution of viverrids and euplerids in Slater and Friscia (2019), inclusive of almost all living species. The latter finding for euplerids is perhaps no surprise as they are one of the most exemplary clades for contingency, with a highly supported sweepstakes dispersal to Madagascar from the African mainland (Yoder et al., 2003). Thus, it is no additional surprise that nearly all variables analyzed by Slater and Friscia (2019) found an early burst model as the best supported for euplerid evolution.

The remaining feliform clades, herpestids and hyaenids, show patterns of ecological evolution better explained by other processes. Herpestids have the most recent origin among the feliform clades, likely in Africa with a single Asian immigration event (Wesley-Hunt et al., 2010; Zhou et al., 2017). Slater and Friscia (2019) found both RBL and body mass evolution in herpestids was best supported by an OU model of evolution, suggesting there is an optimal value the clade was either constrained to, or pulled towards, and not an adaptive radiation. Furthermore, there appears to be no obvious correlation in global temperature at the extant herpestid origin (Zachos et al., 2001). Similarly, hyaenids seem drawn towards optimal body mass and dental toolkits, though the present analysis finds these values are correlated to a given dietary category. This is

the same result that was found by Slater (2015) for canid evolution, though a durophagous

category was not included in that study. The analogy between canid and hyaenid evolution has

been made before, where hyaenids are the Old World ecological analogs to the New World

canids (Hunt, 1996; Van Valkenburgh, 2007; Tseng and Wang, 2011), and thus the results of this

work offer a new line of inference on convergent evolution between these clades.

Both hyaenids and canids found remarkably similar optimal body mass (save mesocarnivory) per

dietary category (Table 10). However, the inferred phylogenetic half-life for these optima

differed by two orders of magnitude for hyaenids and canids, 1.96 Ma to 936 Ma respectively.

For hyaenids this suggests an incredibly strong pull towards optimal values within a given

category, but for canids, such weak attraction was better interpreted as a slow, sustained trend in

increased body mass across all three dietary categories, an assessment supported by the next best

supported model of Slater (2015), trended random walk. Relative blade length of m1 was not

assessed by Slater (2015), but relative lower grinding area (RLGA) was, being another proxy for

dental toolkit, and by extension diet. Higher values for this proxy indicate a greater grinding

proportion (compared to slicing), and unsurprisingly optimal values from hypo- to

hypercarnivory show a progressive decline in RLGA. Hyaenids show a similar pattern in

reducing the grinding component with increased hypercarnivory. However, values for hypo- and

mesocarnivory in hyaenids seemed backwards, such that hypocarnivory had greater optimal RBL

values than mesocarnivory. This may be explained by the trigonid not necessarily being

dedicated to a slicing function amongst carnivorans and instead being modified to a grinding or

puncturing (in the case of arthropod food items) component like the talonid behind it. Thus,

retaining a large trigonid, as in *Plioviverrops*, would be functionally advantageous. Closer

inspection of the total grinding versus slicing component of the dental toolkit in hyaenids and

canids shows distinct differences. Specifically, there is a substantially greater grinding

component retained in hypercarnivorous canids than hyaenids, even though the pull towards each

clade's optimal dietary value was comparably strong, $t_{1/2}$= 1.99 Ma for hyaenids and 3.85 Ma for

canids. This distinction may result from phylogenetic constraint unique to each clade, especially

in the context of dental morphology and diet (Hopkins et al., 2021). This constraint has been

hypothesized for durophagy in the two clades where the retention of posterior molars may have

resulted in the shift of bone-crushing teeth/cusps in borophagine canids to the anterior P4 and

lower m1 compared to that of non-carnassial premolars in hyaenids whom otherwise lose the

posterior molars (Tseng and Wang, 2011).

Table 10. Median optimal body mass (in kg) values from model fits of 500 random trees from

the stable Bayesian posterior of the phylogenetic analysis for hyaenids of the present analysis

and that of canids in Slater (2015).

	Hypocarnivore	Mesocarnivore	Hypercarnivore
Hyaenidae	3.19	16.11	25.46
Canidae	3.19	4.71	20.70

A core concept of adaptive radiations has been an initial rapid diversification and phenotypic

evolution that "...fit the divergent environments they exploit" (Schluter, 2000). I subsequently

assessed this evolutionary pattern via early burst models of decelerating rates of phenotypic

evolution. The underlying process behind these patterns is primarily explained by the work of

Simpson (1944, 1953) where high rates of evolution are required to move through nonadaptive

realms of the adaptive landscape to new stable realms. This view that evolution precedes through

'quantum' (Simpson, 1944), 'punctuated' (Eldredge and Gould, 1972) or only minimally stable states has existed since at least the work of Francis Galton (1869), who analogized evolution proceeding as a polyhedron flipping from one stable facet to another. Within each adaptive zone, Simpson suggested the existence of adaptive subzones giving opportunities for fine-scale ecological diversification. For example, felids and canids occupy their own unique subzones which can be grouped into a more inclusive 'fissiped' subzone as opposed to one of pinnipeds, and even more inclusively, all of the aforementioned can be grouped into carnivores as opposed to herbivores. Slater (2015) suggests that canids can be subdivided into canid hypo-, meso- and hypercarnivore subzones within which have their own optimal state. OU models can be viewed as evolutionary constraint, which in this context could be interpreted as a constraint in the dental morphology required to occupy a given dietary niche or subzone. The lack of an early burst signal for canids was suggested by Slater to be a result of early burst or adaptive radiations only existing at more inclusive clades. In fact, Slater and Friscia (2019) found that among extant Carnivora there was a preponderance of early burst dynamics, but primarily in only diet/dental related traits. At the family level this falls apart into far greater nuance of Brownian motion or OU models as best supported, a hierarchical distinction previously suggested in theoretical literature (Osborn, 1902; Simpson, 1944, 1953; Gould, 2002; Humphreys and Barraclough, 2014). The presented results suggest that feliform ecological evolution may best be explained as a pull towards optimal dental toolkits, and to a lesser extent body mass, per dietary category. However, these optima are filtered through contingent events, likely correlated to global climatic and/or tectonic dynamics.

Nimravids and felids explosively entered a nimravid/cat-like zone that ecologically may have prevented these clades from escaping (i.e., evolutionary ratchet, Van Valkenburgh et al., 2004)

related to phylogenetic constraints inherent to the clade. These constraints, much like tooth count in canids versus hyaenids, may have been contingent in themselves, such that the path to hypercarnivory from a hypo- or mesocarnivorous ancestor has several routes, e.g., cat/nimravid versus dog/hyaenid, and that one path may be more restrictive than the other. Canid and hyaenid hypercarnivores utilize more of the carcass than felids based on observation of living taxa (Van Valkenburgh, 1996) and dental microwear and enamel structure in fossil forms (Tseng, 2012; Desantis et al., 2015). The consumption of bone or otherwise resilient vertebrate material in addition to soft flesh may have facilitated the retention or development of robust molars in canids and bone-cracking premolars in hyaenids. Thus, the difference in what parts of vertebrate prey are consumed may be a more important distinction than how much vertebrate prey is consumed and the resulting evolutionary patterns. For canids, this could provide an escape to a more omnivorous diet and the ability to specialize in a given dietary subzone. For felids and nimravids, explosive entry into soft flesh hypercarnivory may have been irreversible, a potential generalization for mammals (Brocklehurst, 2019). Even with findings that mammal cusp number and placement are under the control of relatively limited genetic pathways allowing potentially a diverse array of dental complexity from early crown developmental (Jernvall and Jung, 2000; Kangas et al., 2004; Kavanagh et al., 2007; Harjunmaa et al., 2014), the loss of talon(ids) is seemingly inflexible to recovery (Solé and Ladevèze, 2017). Rapid felid and nimravid hypercarnivorous shifts seem to be tied to global climatic/tectonic dynamics, in turn associated with faunal turnover. These turnover events may provide contingent opportunities for soft-flesh specialist hypercarnivores to quickly exploit new resources by rapid dental toolkit specialization, but ones that constrain descendant taxa to remain within this ecospace.

The ecological evolution of hyaenids and canids saw exploration of multiple subzones, one of which was hypercarnivory. This path was still rapid given the estimated phylogenetic half-life values of the present study and that of Slater (2015), but it does not seem correlated with the type of global events that habitat theory would predict. Hyaenids may occupy a common canid-like subzone of the Neogene where optima from a hypo- or mesocarnivorous ancestor mediated the pull towards each dietary category, compared to a singular pull to extreme hypercarnivory. A possible explanation for this may lie in the postcranial *bauplän* of felids/nimravids versus canids and hyaenids. Early members of both the Canidae and Hyaneidae exhibit incipient cursorial morphology, including reduced ability to retract the distal phalanges and supinate/pronate the forelimb (Hunt Jr. and Solounias, 1991; Wang, 1993; Figueirido et al., 2015). These changes likely enhanced efficiency in covering large distances (Janis and Wilhelm, 1993), but also reduced the ability to grapple with prey, as do modern felids. Becoming increasingly face-orientated in predation, canids and hyaenids may have relied more upon the integration and optimization of body size and dental tool kit than do soft-flesh specialists and thus set them down a distinct ecospace trajectory.

A third situation is seemingly possible in the case of small feliforms, where body mass and dental toolkit evolve via random walk. This third subzone of small carnivorans and associated dietary subzones, achieves broad dietary ecologies, possibly related to their small size (Pineda-Munoz et al., 2016). Evolutionary patterns of small feliforms may correlate to the morphological refuge discussed for canids and hyaenids, in that a hypocarnivorous (and specifically insectivorous) ancestor may better facilitate evolution into varied dietary categories at small size. This bias in dietary shifts across mammalian evolution has been recovered in the work of Price et al. (Price et al., 2012) and Reuter (2021), where far greater dietary transitions occur from diets

that feature invertivory than any other. This malleability in ecology is likely facilitated by being small, where metabolic and structural burdens have minimal impact compared to mammals of larger size (Carbone et al., 1999, 2007).

The current study suggests that the hypothesis of early burst evolution being only observable at higher taxonomic levels, while stabilizing selection or Brownian motion dominates lower levels is overly simplistic. Instead, there appears to be a story of contingent opportunity mediated by global tectonic and climatic factors, but these too are filtered through phylogenetic baggage accrued through entrance into different ecological zones. Soft-flesh specialists rapidly appear at times of massive faunal turnover, from lineages with plesiomorphic carnivoramorphan postcranial morphology. However, the descendants of these lineages are constrained to remain within this ecospace with the loss of dental hardware lending itself to different diets. Climatic/tectonic events also facilitate the diversification and appearance of other feliform clades, but the evolutionary patterns expressed differ from those of felids and nimravids. Hyaenids experienced vast ecological diversity optimized for body mass and dental toolkit. This ecospace trajectory may have been necessitated by the early postcranial modifications to cursoriality in the clade and correlated face-centric predation. With the loss of this ancestral postcranial morphology, both hyaenids and canids may have been excluded from soft-flesh specialization, even if the opportunity existed, such as the "cat-gap" in the early Miocene of North America. However, retention of more generalized dentition combined with cursorial adaptations may channel body size and dental tool kit optimization per dietary category. Finally, small feliforms experience apparent random evolution in both body size and dentition. These clades' appearance and diversification can also be correlated with global tectonic and climatic events, but given the absolute size of their members, are free to drift across a range of ecological

options, being freed of the constraints of large size. However, once opportunities do present themselves the above ecospace trajectories come into play with growing body size and postcranial adaptations. For example, the fossa (*Cryptoprocta ferox*) acquired familiar felid ecomorphology in Madagascar after a sweepstakes dispersal of a herpestid-like ancestor from Africa. Further analysis within a paleoecological framework may find more similarities than differences in subzone occupation of additional Carnivoran clades. The caniform groups of Mustelidae, Mephitidae, Ailuridae and Procyonidae may occupy the small ecospace of sister group small feliforms, while certain subfamilies of ursids and amphicyonids may fall within that of canids and hyaenids. Regardless, contingent opportunity from global events seems to drive the evolution of feliform carnivorans, but the path they take is mediated by ecological pathways previously taken and consequent phylogenetic baggage.

Chapter IV

Evolution of feliform cranial shape

Introduction

The processes that govern the evolution of shape amongst the pageant of life, are central

questions in biology (Dobzhansky, 1951; Hutchinson, 1959; Gould, 2002). Studies suggest that

there is a variable degree of connection between morphology and ecology (Marroig and

Cheverud, 2005; Hunt, 2007; Harmon et al., 2010; Santana and Cheung, 2016; Slater and Friscia,

2019). For example, mammals have a strong association between dental and gnathic morphology

and their diet (Evans et al., 2007; Boyer, 2008; Christensen, 2014; Pineda-Munoz et al., 2016;

Grossnickle, 2020; Wang et al., 2021). Taxa that consume large amounts of vertebrate material

possess reduced dentary lengths and enhanced shearing surfaces to maximize power and

efficiency in processing animal tissue, while folivorous mammals lengthen the dentary and

increase tooth occlusal area and complexity to aid in grinding of tough floral material. However,

how this form and function correlation extends to overall cranial shape has remained less clear

(Figueirido et al., 2011; Tseng, 2013; Tseng and Flynn, 2018). While some authors have found a

connection between diet and cranial shape (Sacco and Van Valkenburgh, 2004; Wroe and Milne,

2007), others recover only a predictive connection for bite force (Christiansen, 2008b; Maestri et

al., 2016; Law et al., 2018b), which when tied to diet, only discriminates between

hypercarnivores and generalists in terrestrial carnivorans (Radinsky, 1981b; Rovinsky et al.,

2021).

For the latter studies, the lack of predictive power for a broad swath of diet (0-70% vertebrate

material = hypo-mesocarnivores) may relate to constraint in phylogeny, which, by limiting

possible morphologies, creates stochastic variation that disrupts expected mapping of form to function (Raup and Gould, 1974). However, ecomorphological categories have been assessed in the fossil and living record (Martin, 1989; Werdelin, 1996; Van Valkenburgh, 2007; Turner et al., 2008; Coca-Ortega and Pérez-Claros, 2019; Barrett, 2021) by the iterative appearance of certain morphologies over geologic time, and presumably comparable ecologies to which they belong. This observation can be extended to the conclusion that a lineage that entered many dietary ecologies should be more morphologically disparate than one that did not, and by some metrics, more successful (Guillerme et al., 2020). Of the carnivoran clades, low amounts of cranial-dental variation have been historically presented in literature for "cat-like" carnivores such as felids and nimravids (Radinsky, 1981a, 1982; Van Valkenburgh, 1991). Foreshortened faces and reduced tooth counts optimize forces in slicing meat at the scissor-like carnassials and prey seizing with the canines. This reduced raw material for selection is argued to relate to increased specialization and narrow morphological disparity amongst hypercarnivores with concomitant increased extinction risk (Holliday and Steppan, 2004; Van Valkenburgh et al., 2004; Van Valkenburgh, 2007). Specifically, loss of posterior grinding molars in soft-flesh specialist hypercarnivores may have put them on an evolutionary road of no return (evolutionary ratchet), resulting in an ecomorphological constraint that did not allow them to evolve additional ecologies. However, recent 3D Geometric Morphometric (3DGM) analyses suggest that cranial disparity for hypercarnivores may be greater than that of generalists among living carnivorans, particularly amongst feliforms (Michaud et al., 2018, 2020). This disparity may in turn be an underestimate, for living carnivores do not occupy the entire range of morphologies, and presumably ecologies, of extinct lineages. Sabertooth and bone-cracking carnivores were once species-rich components of past ecosystems, and it has been suggested that their cranial

morphology may have operated under different rules than their extant relatives in terms of disparity and cranial modularity (Holliday and Steppan, 2004; Goswami et al., 2015).

Even with the seeming inability to recover molar crushing basins (Solé and Ladevèze, 2017), there may be another reason for aberrant disparity patterns in the crania of soft-flesh hypercarnivores (i.e. felids and nimravids). Recent literature has shown that morphology is often integrated from developmental genetic sequences (Gehring, 1996; Shubin et al., 1997; Tomarev et al., 1997) to gross anatomy (Goswami, 2006; Goswami and Polly, 2010a; Goswami et al., 2014, 2015) in such ways that structures can covary, generating morphology that changes in sync. Do felids and nimravids present limited evolutionary potential resulting from overly integrated cranial development compared to other clades, or does developmental integration provide a fruitful channel to more extreme morphologies (Goswami et al., 2015)? In this study, I use 3DGM analyses to assess feliform cranial allometry and morphology within and among 73 species spanning approximately 34 million years of evolution. Specifically, I ask the following questions:

(1) Are there distinct cranial morphologies for each ecological category?

(2) Does disparity differ among these categories?

(3) What is the source of disparity in more morphologically diverse clades?

(3a) Does morphological disparity increase in clades that have had more time to evolve, or

(3b) Does greater variance in size allow a line of least evolutionary resistance for morphological variation via allometry?

(3c) If allometry is important, is there a common allometric trajectory amongst feliforms?

(4) Does integration (an indicator of developmental constraints), enable or limit potential in the evolution of feliform cranial shape?

Methods

Materials

The morphological dataset is composed of 157 cranial specimens, representing 73 extinct and

extant feliform species (Appendix I). When possible, I sampled one male and female individual

of a species to approximate the range of sexual dimorphism for that species, while I chose

species to sample the cranial disparity of a given clade, including an "average" shape and more

outlying morphologies as well. I then sorted these species into ten monophyletic clades as

recovered in Chapter II: Felinae/Pantherinae (FP), Machairodontinae, Felidae, Stenoplesictidae,

Nimravidae, Viverridae, Hyaenidae, Herpestidae, Eupleridae, and Prionodontidae. I digitized 69

three-dimensional (3D) landmarks (Figure 6, Table 11) using a Microscribe G2LX digitizer

(Immersion Corp., San Jose, CA). During data collection I stabilized individual crania with clay

supports and digitized landmarks in two sets, one in dorsal view and the other in ventral view. I

used a set of four reference landmarks in both views to facilitate alignment of the dorsal and

ventral datasets. The two sets were then stitched together using the 'unifyLandmarks' function of

the 'StereoMorph' package (Olsen and Westneat, 2015) in R v. 4.1.2 (R Core Team, 2020). I

considered alignments sufficient when alignment error was less than or equal to the manufacturer

stated accuracy of the Microscribe G2LX digitizer (0.3mm). I supplemented the Microscribe-

generated data set with a few rare taxa/specimens landmarked from published CT scans or

photogrammetry-generated 3D models. These latter specimens were digitized in Landmark

Editor v. 3.0 (Institute for Data Analysis and Visualization, University of California, Davis).
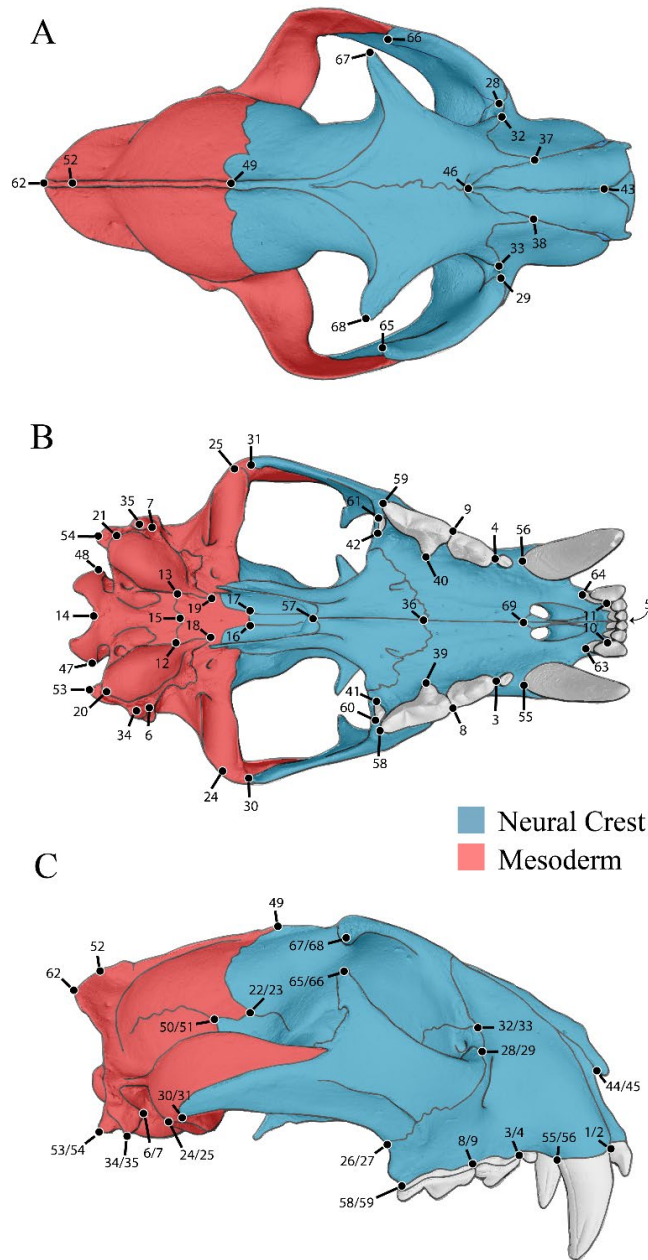
Figure 6. Position of the landmarks taken on the cranium for 3DGM analyses (69 landmarks) to quantify variation in shape of feliform crania. A, dorsal view. B, ventral view. C, right lateral view. Landmarks are subset into two modules, Neural Crest (NC, blue) and Mesoderm (MD, red), based on tissue origin of cranial elements. The skull used for this representation is a leopard (Panthera pardus, Felidae).

Table 11. Definition of anatomical landmarks used in the three-dimensional geometric

morphometric analyses.

Landmark	Definition
1	Anterior border of canine at alveolus-left
2	Anterior border of canine at alveolus-right
3	Anterior border of P3 at alveolus-left
4	Anterior border of P3 at alveolus-right
5	Anterior midline suture of premaxilla
6	Anteromedial point of mastoid process-left
7	Anteromedial point of mastoid process-right
8	Anterolateral border of P4 alveolus-left
9	Anterolateral border of P4 alveolus-right
10	Anteromesial border of I3 at alveolus-left
11	Anteromesial border of I3 at alveolus-right
12	Basioccipital basisphenoid bulla suture-left
13	Basioccipital basisphenoid bulla suture-right
14	Basion
15	Basisphenoid basioccipital midline suture
16	Basisphenoid presphenoid suture-left
17	Basisphenoid presphenoid suture-right
18	Bulla anterior medial extreme-left
19	Bulla anterior medial extreme-right
20	Bulla posterior lateral extreme-left
21	Bulla posterior lateral extreme-right
22	Frontal parietal alisphenoid suture-left
23	Frontal parietal alisphenoid suture-right
24	Glenoid fossa lateral extreme-left
25	Glenoid fossa lateral extreme-right

Table 12 continued.

Landmark	Definition
26	Jugal maxilla ventral suture-left
27	Jugal maxilla ventral suture-right
28	Jugal maxilla lacrimal suture-left
29	Jugal maxilla lacrimal suture-right
30	Jugal squamosal ventral suture-left
31	Jugal squamosal ventral suture-right
32	Lacrimal frontal maxilla suture-left
33	Lacrimal frontal maxilla suture-right
34	Mastoid process ventral tip-left
35	Mastoid process ventral tip-right
36	Maxilla-palatine midline suture
37	Maxilla frontal nasal suture-left
38	Maxilla frontal nasal suture-right
39	Medial border of P4 at widest point of alveolus-left
40	Medial border of P4 at widest point of alveolus-right
41	Medial M1 alveolus-left
42	Medial M1 alveolus-right
43	Nasal-anterior midline suture
44	Nasal-premaxilla suture anterior-left
45	Nasal-premaxilla suture anterior-right
46	Nasals frontal midline suture
47	Occipital condyle lateral extreme-left
48	Occipital condyle lateral extreme-right
49	Parietal-Frontal midline suture
50	Parietal-squamosal-alisphenoid suture-left
51	Parietal-squamosal-alisphenoid suture-right
52	Parietals occipital midline suture
53	Paroccipital process tip-left

Table 13 continued.

Landmark	Definition
54	Paroccipital process tip-right
55	Posterior border of canine at alveolus-left
56	Posterior border of canine at alveolus-right
57	Posterior border of palatine at midline
58	Posterior of carnassial at alveolus-left
59	Posterior of carnassial at alveolus-right
60	Posterolateral border alveolus M1-left
61	Posterolateral border alveolus M1-right
62	Posterodorsal tip of occiput at midline
63	Posterolateral border of I3 at alveolus-left
64	Posterolateral border of I3 at alveolus-right
65	Postorbital process base (jugal)-right
66	Postorbital process base (jugal)-left
67	Postorbital process tip (frontal)-left
68	Postorbital process tip (frontal)-right
69	Premaxilla maxilla ventral midline suture

Because the crania of extinct taxa were often incompletely preserved, I imputed missing landmarks to maximize the size of the dataset. Two additional fossil specimens, TMM 933-3444 (*Homotherium serum*) and CB 07 (*Eusmilus sicarius*) were retrodeformed to correct for postdepositional shape changes using the 'symmetrize' function of the 'Morpho' R package (Schlager, 2017). I first performed imputation via reflection across the plane of symmetry using the 'mirrorfill' function in the 'paleomorph' package (Lucas and Goswami, 2017). These mirrored models I then used to impute absent landmarks by the 'estimate.missing' function in the 'geomorph' package (Adams et al., 2021) with the thin-plate spline method. Imputation

proceeded in three iterations to maximize accuracy, given the 'estimate missing' function interpolates landmarks using a reference specimen within the analyzed dataset. Thus, felids and nimravids were grouped for imputation, with a second group composed of durophagous hyaenids, and a final group containing the remaining taxa (i.e., viverroids). This final group included the hyaenid genera: *Ictitherium*, *Hyaenotherium* and *Tungurictis*. While paraphyletic, these hyaenids and other viverroid families exhibit similar dolichocephalic cranial shapes.

The digitized landmarks for all crania I then subjected to Generalized Procrustes Analysis (GPA) superimposition which translates the specimens to a common origin, scales each specimen to unit centroid size, and rotates each specimen to minimize landmark distances using a least-squares calculation. The resulting Procrustes coordinates I projected into tangent space with a principal components analysis (PCA) using the 'gm.prcomp' geomorph function to identify the major axes of cranial shape among all the crania in the analysis. I identified morphological changes associated with the major PC axes by calculating a series of indices of individual crania and then examined their Pearson's correlation to said axes.

Disparity and Integration

I calculated disparity as the Procrustes variance (trace of the group covariance matrix, divided by group *n*) of each clade of interest using the 'morphol.disparity' function in geomorph v. 4.0.1 (Adams et al., 2021; Baken et al., 2021) with 1000 randomized residual permutations (Collyer et al., 2015). I performed this calculation while assessing the impact of allometry and clade age on disparity, because certain feliform clades span orders of magnitude in body mass while others do not. Thus, strong allometric trends may provide a line of least evolutionary resistance towards generating disparity in clades with large size variance. Similarly, morphological disparity for a clade may simply be the result of having more time to accrue within relatively ancient lineages

compared to recently diverging ones. I further calculated disparity per dietary category (Table 12) as determined in Chapter III, while adding extant invertebrate specialists as those with ≥70% invertebrate material in their diet as determined by the Elton Trait dataset (Wilman et al., 2014), checked against the recent carnivoran ecological analysis of Hopkins et al. (2021). I compared ecological cranial disparity by using the 'morphol.disparity' function and model coords ~ log(Csize) with 1000 randomized residual permutations. Randomization of residuals allows assessment of model effects and summary statistics, especially important for the high dimensionality of trait data versus sample size of 3DGM analyses (Adams, 2014a; Adams and Collyer, 2015). The Bonferroni correction accounted for multiple comparisons (Bonferroni, 1936).

Table 14. Definitions of dietary categories for analysis of cranial shape.

Dietary Category	Definition
Invertivore	≥70% invertebrate material
Hypocarnivore	≤40% vertebrate material
Mesocarnivore	50-69% vertebrate material
Hypercarnivore	≥70% vertebrate material
Durophagous	Hypercarnivore with bone-cracking morphology
Sabertooth	Hypercarnivore with sabertooth morphology

I calculated cranial integration two ways. The first measure used was eigenvalue dispersion (equations 7&8, Goswami and Polly, 2010b), equal to the standard deviation of eigenvalues from the correlation matrix of the PCA. With high values of eigenvalue dispersion, variance will be concentrated in the first few eigenvectors resulting from high covariance between landmarks.

The second measure calculated the integration of the mesoderm (MD) and neural crest (NC) developmental modules. I determined module assignment for each landmark by the tissue origin of the bone on which a given landmark was located (Figure 6). The origins of cranial bones, as neural crest or mesoderm derived, were assigned following Ferguson and Atit (2019) for the face and vault elements, and McBratney-Owen et al. (2008) for the cranial base. The squamosal is derived from both Neural crest and Mesoderm tissues (Ferguson and Atit, 2019), thus landmarks 30-31 were treated as NC, while 24-25 were assigned to MD. Landmark 49 was located on the sutural boundary between the NC and MD modules and was assigned to the MD module, as the coronal suture is of mesoderm origin (Mishina and Snider, 2014). I assessed integration of these two developmental modules with the 'integration.test' function geomorph. This is a two-block partial least squares analysis (PLS, Rohlf and Corti, 2000), also referred to as a singular warps analysis (Bookstein et al., 2003). The z-scores were used for clade comparisons while significance was derived from 1000 random permutations of individuals in one partition to those in the other.

I tested the relationship between morphological disparity and integration by performing two sets of regressions using the base R function lm(). I regressed morphological disparity against both eigenvalue dispersion values and against between-module integration (z-scores) of the MD and NC regions.

Allometric Variation

I assessed the impact of allometry on clade evolution in two ways. The first looked at per-clade influence of allometry on shape variation by using the geomorph function 'procD.lm' and the equation (Procrustes coordinates) ~ log(centroid size)+RCS. Relative canine size (RCS) was

included in particular to assess its role in predicting cranial shape in sabertooth carnivorans (Slater and Van Valkenburgh, 2008). Significance was evaluated with Goodall's (1991) F-test with 1,000 permutations for this and the subsequent analyses.

For the second set of analyses, variation in evolutionary (among-clades) allometries was tested using an ANCOVA model where Procrustes shape coordinates were regressed against log centroid size and clade membership with the model coords ~ log(Csize) * clade. A post hoc test using the package RRPP (ver. 1.1.2; Collyer and Adams, 2018, 2019) function pairwise evaluated whether the evolutionary allometric slopes of clades (n =10) significantly differ from one another. Multiple comparisons were accounted for by reducing α to .01. The model was visualized by plotting the regression scores of shape on size versus log centroid size (Drake and Klingenberg, 2008). I also compared these results with a phylogenetic ANCOVA (pANCOVA) using geomorph's procD.pgls (Adams, 2014a), which executes the ANCOVA model in a phylogenetic framework. This pANCOVA used mean averaged crania from all 73 species and a pruned version of the phylogenetic tree of Chapter 2 (Figure 7) that only included taxa sampled for this analysis.

Phylogenetic Signal and Evolutionary Rates

I calculated the phylogenetic signal of the cranial landmark dataset with a multivariate K-value (K_{mult}) (Adams, 2014b) using the 'physignal' function in geomorph. K_{mult} uses 1000 random permutations to assess how well the morphometric data fit a phylogenetic tree. A K_{mult} value of zero corresponds to absence of phylogenetic signal, whereas a K_{mult} value greater than one indicates a strong phylogenetic signal, implying that morphological traits are conserved within the phylogeny.
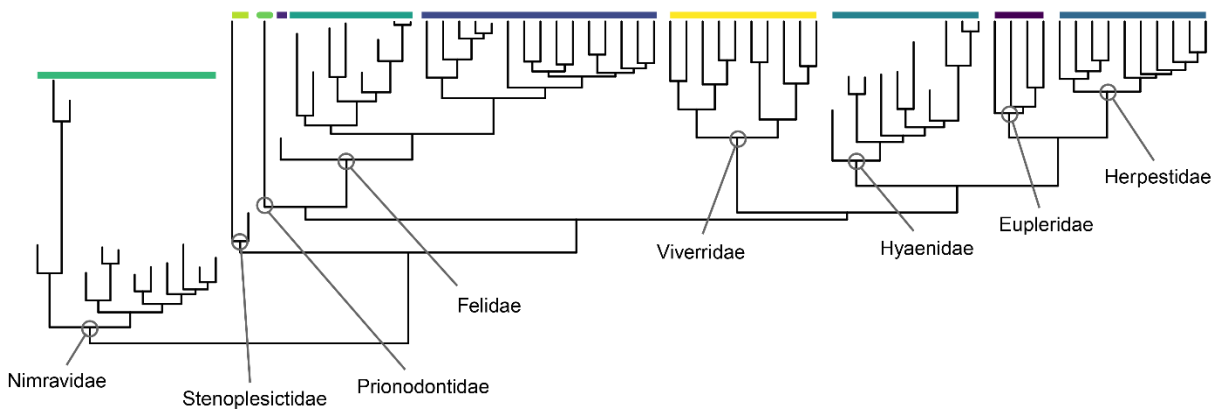
Figure 7. Pruned MCC phylogeny of Chapter II to include only those feliforms analyzed in the present cranial morphology chapter.

I calculated the morphological rates of evolution for each clade of interest by using the geomorph function 'compare.evol.rates' on the same pruned tree. I performed 1000 simulations of Brownian motion trait evolution which were summarized with the net evolutionary rate of each clade obtained from the sum of squared distances between taxa and the origin of their clade (O'Meara et al., 2006; Adams, 2014c). This procedure was also performed on mean natural log centroid sizes for species crania to estimate rates of cranial size evolution. I compared the clade-wise rates of size and shape evolution and morphological disparity with ordinary least squares regression analysis in the base R function lm(). I further compared rates of evolution per dietary category making pairwise comparisons (over 1000 iterations) of shape evolution rates between all dietary categories. The Bonferroni correction accounted for multiple comparisons (Bonferroni, 1936).

Dietary Impact

I tested the effect of diet on feliform cranial shape by first calculating the degree of carnivory (proportion of vertebrate material in the diet) for extant taxa, taken from the Elton Traits (Wilman et al., 2014) database and checked against Hopkins et al. (2021). I then regressed this value against relative blade length (RBL) of the lower first molar (taken from the dataset in Appendix H) and estimated the degree of carnivory for extinct taxa using the base lm() and predict() functions in R. Degree of carnivory for all taxa was then regressed against mean cranial shape for feliforms using the geomorph procD.pgls function within a phylogenetic framework.

Results

PC1 (Figure 8) accounts for 44.68% of feliform shape variation and describes morphological changes associated with sabertooth morphology, with progressively more derived sabertooth taxa towards the negative side of the axis. This is echoed by the correlation of relative canine size (distance from landmark 1 to 55 divided by centroid size) to the PC1 axis, ($r = -0.87$, $p = 2.2 \times 10^{-16}$). PC2 (14.57% of variation) describes changes from brachycephalic to dolichocephalic morphology, reflected in the correlation of relative palate length (distance from landmark 5 to 57 divided by centroid size) to the PC2 axis, ($r = 0.70$, $p = 2.2 \times 10^{-16}$). Every other PC axis describes less than 10% of remaining cranial shape variation. Within the PC 1 and 2 morphospace, all viverroids save hyaenids overlap each other with positive scores on the PC1 axis and positive to slightly negatives scores on the PC2. Hyaenids occupy an area near the origin, but primarily extend into positive PC2 morphospace. Felines and pantherines extend the furthest into negative PC2, with the largest members also having the most negative PC1 scores. The aforementioned

taxa generally occupy an upper right to lower left orientation in the PC1 and 2 morphospace while extending perpendicular to them lie the entirety of the sabertooth machairodontine and nimravid taxa. This is a similar pattern to that recovered in the 2D GM analysis of Slater and Van Valkenburgh (2008).
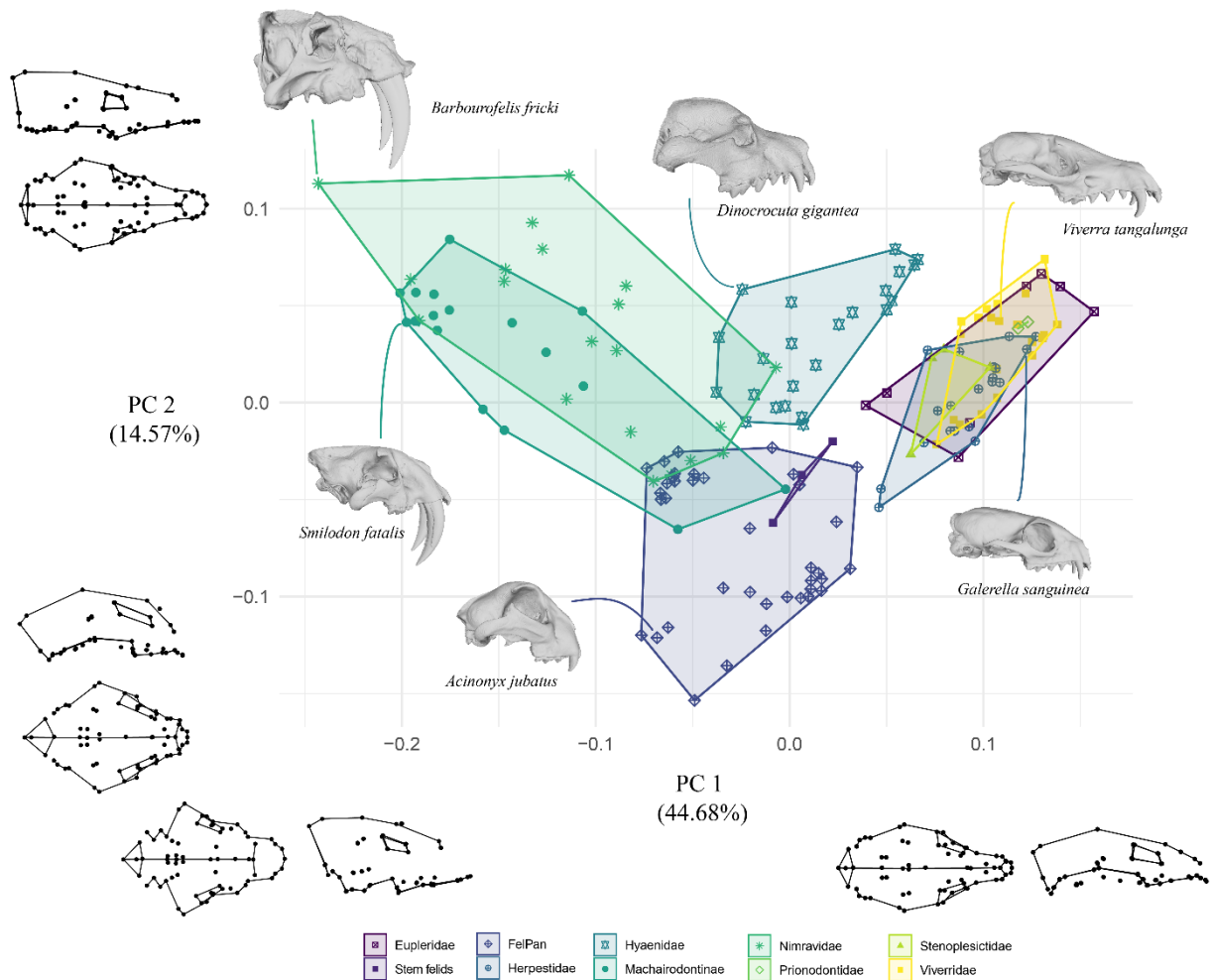
Figure 8. PCA of all cranial feliform specimens. Convex hulls surround clades of interest while individual taxa are indicated by a surface scan of their place in morphospace. Below and to the left side of PC1 and 2 are wire frame models of the change in landmarks at the extreme of each principal component from a right lateral and dorsal perspective.

Procrustes ANOVA Results

Clade membership, log centroid size, and relative canine size are significant predictors of cranial

shape, though the influence on each clade of the latter two variables differs, Table 13 and Table

14. Felines and pantherines had by far the greatest allometric signal (49%) while nimravids had

the least (9%) and almost all other clades (save herpestids) had an intermediate signal between

20 and 26%. Relative canine size was minimally explanatory for cranial variation in most clades

(3-7%) except for the euplerids (47%) and sabertooth machairodontines (19%) and nimravids

(24%).

Table 15. Allometry and effect of relative canine size (RCS) on cranial shape as determined by

ANOVA of shape (Procrustes coordinates) ~ log(centroid size)+RCS for each clade. Disparity

was calculated by Procrustes variance adjusted for allometry and clade age. Statistically

significant (p <0.05) values are in bold. Eigenvalue dispersion does not include a significance

assessment.

	ln Centroid Size	RCS	Disparity	Eigenvalue dispersion	Developmental module integration
Eupleridae	0.204	**0.466**	0.012	0.408	**1.909**
Felinae/Pantherinae	**0.487**	**0.035**	0.013	0.167	**4.708**
Herpestidae	**0.119**	0.070	0.008	0.236	**3.522**
Hyaenidae	**0.246**	0.043	0.016	0.218	**3.013**
Machairodontinae	**0.259**	**0.185**	0.020	0.250	**3.763**
Nimravidae	0.090	**0.238**	0.017	0.236	**3.411**
Viverridae	**0.256**	**0.071**	0.011	0.229	**2.459**

Table 16. Evolutionary allometry ANCOVA. Evolutionary allometry (among clades) uses the mean shapes and mean centroid sizes of the 73 species, which were then grouped into ten clades (including the one monospecific lineage). Df = degrees of freedom, SS = sum of squares, MS = mean square, R2 = coefficient of determination, F= F statistic, Z= effect sizes, Pr(>F) = significance value.

	Df	SS	MS	R^2	F	Z	Pr(>F)
log(Csize)	1	0.871	0.871	0.271	120.64	5.158	<0.001
clade	9	1.159	0.129	0.361	17.842	12.253	<0.001
log(Csize):clade	9	0.193	0.021	0.06	2.968	5.48	<0.001
Residuals	137	0.989	0.007	0.308			
Total	156	3.21					

Levels of Morphological Disparity and Integration

Age of lineage had a significant correlation with allometrically adjusted disparity (Figure 9). Adjusting Procrustes variance for both allometry and lineage age found machairodontines with the highest level of morphological cranial disparity (Table 13), followed by nimravids and hyaenids. Felines/pantherines, euplerids and viverrids possessed moderate levels of disparity, while herpestids had the least overall. Disparity per dietary category (Table 15) recovered sabertooth taxa having the greatest amount of size-adjusted variance. This is followed by durophagous taxa in second; mesocarnivores, hypercarnivores and invertivores with comparable intermediate values, and hypocarnivores with the least. However, Bonferroni-corrected significance values only recover sabertooth and hypocarnivores as significantly different in disparity.

Table 17. Cranial disparity (Procrustes variance adjusted for size) per dietary category. Upper triangle is absolute difference between dietary categories while lower triangle contains p-values.

	Hypocarn.	Mesocarn.	Hypercarn.	Durophag.	Sabertooth	Invertivor.
Hypocarn.	-	0.0062	0.0058	0.0086	0.0136	0.0044
Mesocarn.	1	-	3.00E-04	0.0024	0.0074	0.0018
Hypercarn.	1	1	-	0.0028	0.0077	0.0014
Durophag.	1	1	1	-	0.0049	0.0042
Sabertooth	**0.015**	1	0.105	1	-	0.0091
Invertivor.	1	1	1	1	0.495	-

Integration, as determined by both eigenvalue dispersion and developmental module integration, has no significant correlation to allometric and lineage age adjusted disparity (Figure 10 and Figure 11). Eigenvalue dispersion was similar for all clades save euplerids, which possessed a value almost twice as great as other feliforms. However, felines/pantherines had the greatest between-module integration value. There was also a greater spread of this integration metric for other clades, with the sabertooth clades, hyaenids, and herpestids having moderate values, and viverrids and euplerids the least overall.

Phylogenetic Signal and Evolutionary Rates

The phylogenetic signal of feliform cranial shape is K = 0.59 ($p < 0.001$). This is substantially greater than that observed across extant Carnivora in Michaud et al. (K = 0.38: 2018), though less than that of extant feliforms in Michaud et al. (K= 0.78: 2020), implying that feliforms have a more conserved ancestral cranial morphology than carnivorans overall, and that fossil taxa may have a disproportionate impact on this calculation. Clade-wise rates of size evolution (Figure 12)

Feliformia Clade Age and Disparity (Allometry Adjusted)

Adjusted $R^2 = 0.67$
$p < 0.02$

Nimravidae

Machairodontinae

Felinae + Pantherinae

Hyaenidae

Eupleridae

Viverridae

Herpestidae

Disparity

Clade Age (mya)
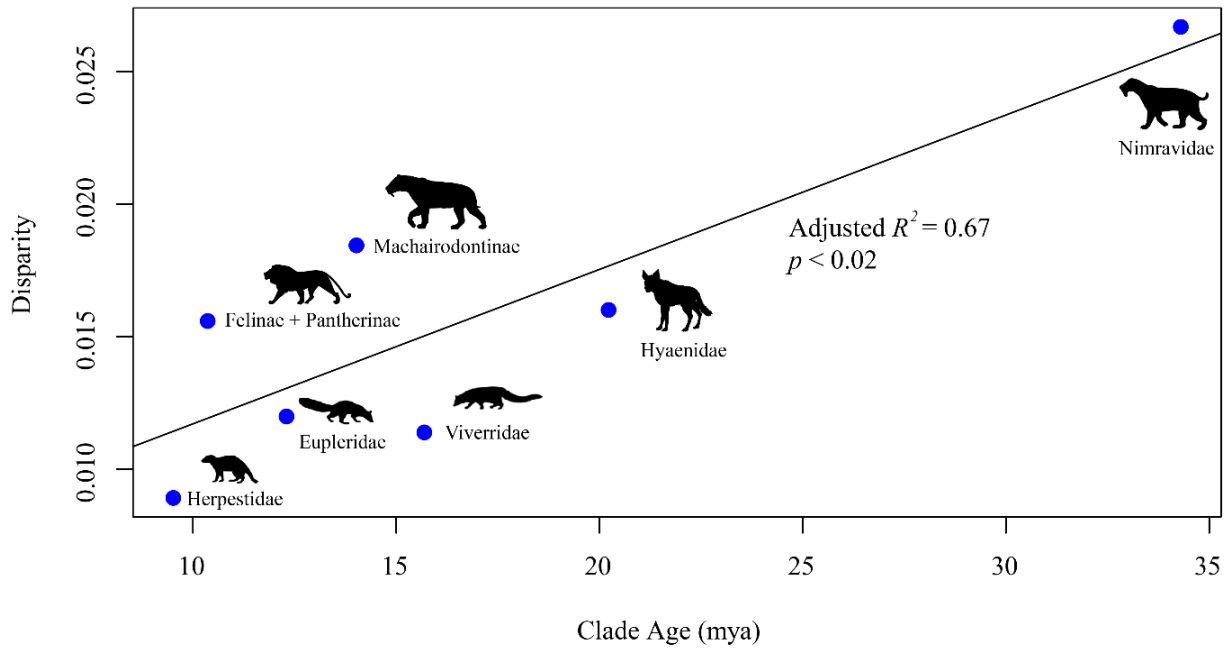
Figure 9. Relationship between feliform lineage age and disparity (Procrustes variance).

Disparity has been adjusted for allometry.

Figure 10. Relationship between feliform cranial integration (Eigenvalue dispersion) and disparity (Procrustes variance). Disparity has been adjusted for allometry and age of lineage.

Feliformia Integration and Disparity (Allometry & Age Adjusted)

Adjusted $R^2 = -0.11$
$p < 0.56$
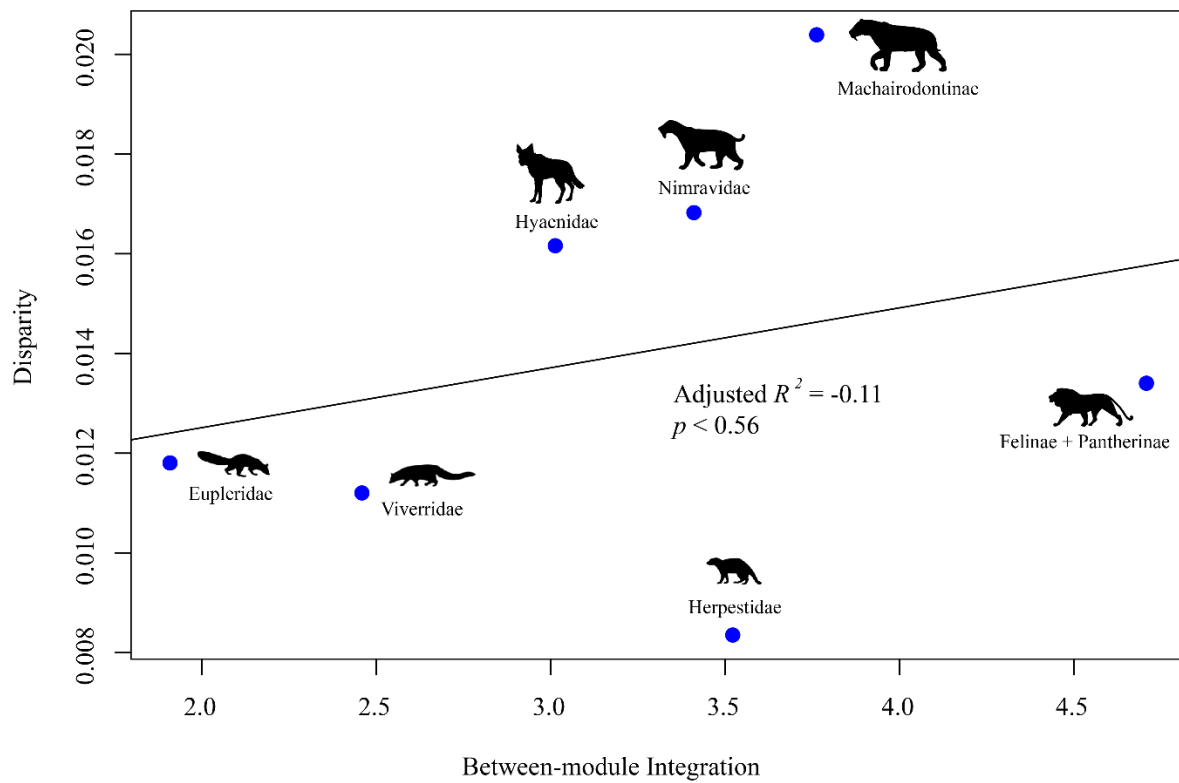
Figure 11. Relationship between feliform cranial integration (between developmental module) and disparity (Procrustes variance). Disparity has been adjusted for allometry and age of lineage.

poorly predicted rates of morphological shape evolution ($R^2 = -0.08$, $p < 0.52$). Of note, machairodontines and nimravids appear as outliers, having the greatest rates of shape evolution, but even with their removal the fit is non-significant ($R^2 = 0.46$, $p < 0.08$). For the rates of size and shape evolution, only that of shape evolution significantly predicted cranial disparity (Figure 12).

Pairwise analysis of shape evolution rates amongst dietary categories revealed that crania of sabertooth carnivores evolved 2.2-5.1 times faster than those of non-sabertooths (Table 16; $p <$

0.02). A similar result was found for durophagous and hypercarnivorous carnivores relative to hypocarnivorous ones, with a value 1.9 times ($p < 0.02$) faster for the former, and 1.74 times ($p < 0.02$) faster for the latter. All other pairwise comparisons were nonsignificant.

Allometric Variation

Feliform cranial morphology exhibits substantial evolutionary (among-clades) allometry ($R^2 = 0.27$, $p<0.001$). This is less than that of clade membership ($R^2 = 0.36$, $p<0.001$) indicating strength in phylogenetic signal over a common allometric trajectory (Table 14). The ANCOVA of the interaction between clade membership and log centroid size further shows very little support for distinct allometric trends per clade ($R^2 = 0.06$, $p<0.001$). However, the pANCOVA (Table 17) of mean shapes against size returned contradictory results with size being the only significant variable accounting for 7% of variation. All other variables were insignificant within this phylogenetic framework. Figure 13B shows the similarity in evolutionary trajectories for each clade, which when taken with the post hoc test for homogeneity of slopes found that, out of 55 pairwise comparisons, only two had significant differences in slopes (Table 18). The significantly different comparisons are the felines/pantherines to the hyaenids ($p<0.002$) and nimravids as compared to the machairodontines ($p<0.004$).

Dietary Impact

The regression of RBL on degree of carnivory returned a significant correlation ($R^2 = 0.55$, $p< 2.2e^{-16}$). However, the phylogenetic ANOVA of cranial shape on diet was not significant $R^2= 0.02$, $p<0.12$). Figure 14 shows the relationship between these variables, where from 0 to 70% vertebrate material in the diet, feliforms possess a narrow range of cranial shapes, while at $\geq 80\%$ feliforms occupy a very diverse range. This pattern is reflected in the cranial disparity
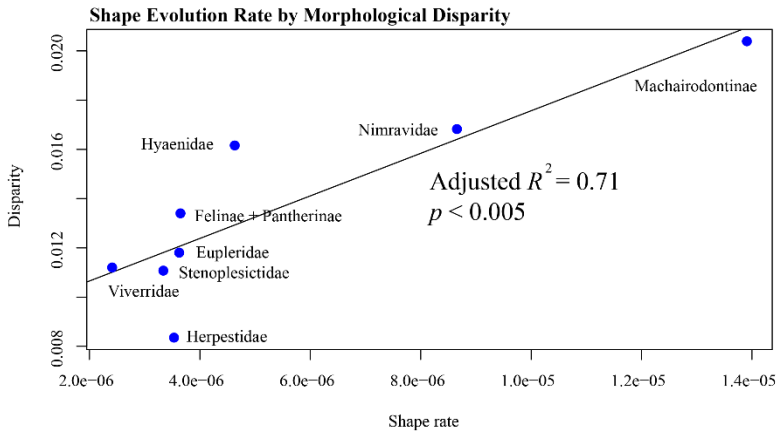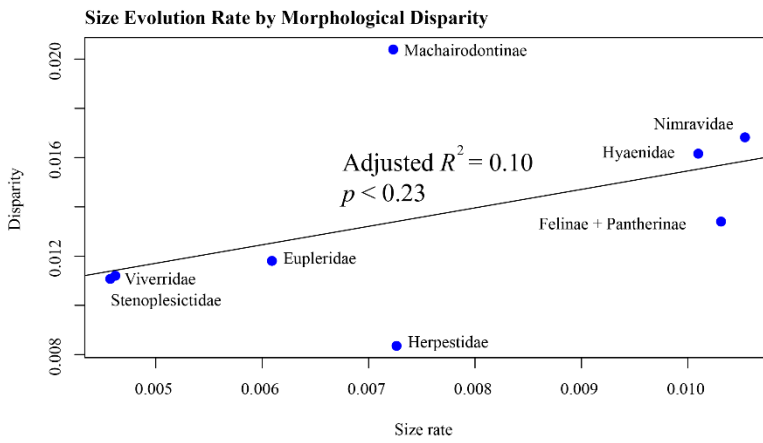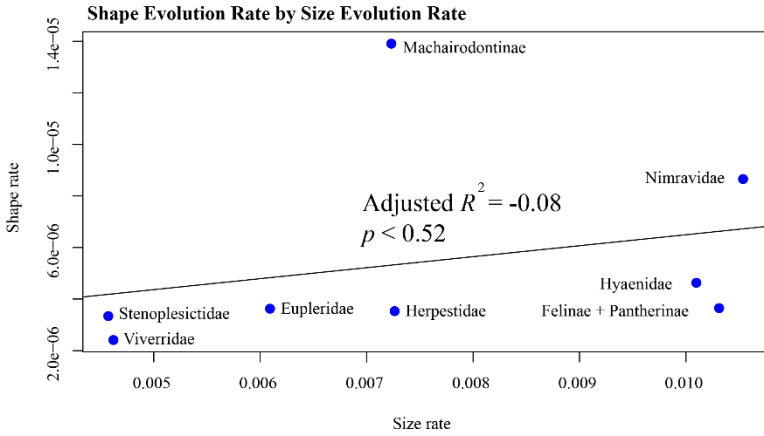
Figure 12. Relationship between feliform size and shape evolutionary rates, and morphological disparity (Procrustes variance). Disparity has been adjusted for allometry and age of lineage.

Table 18. Pairwise cranial shape evolution rates between dietary ecologies in upper triangle, with p-value significance in lower triangle.

	Hypocarn.	Mesocarn.	Hypercarn.	Durophag.	Sabertooth	Invertivor.
Hypocarn.	-	1.29	1.74	2.36	5.07	1.81
Mesocarn.	1	-	1.35	1.82	3.92	1.4
Hypercarn.	**0.015**	1	-	1.35	2.91	1.04
Durophag.	**0.015**	0.06	0.944	-	2.15	1.3
Sabertooth	**0.015**	**0.015**	**0.015**	**0.015**	-	2.8
Invertivor.	0.03	1	1	1	**0.015**	-

(Procrustes variance) of species with ≥80% vertebrate material in their diet being greater than that of those ≤ 70%, 0.014 versus 0.009. Furthermore, phylogenetic signal was greater for those species with ≤ 70% vertebrate material in their diet (K= 0.6587, $p<$ 0.001), while less for those with ≥80% (K= 0.4003, $p<$ 0.001).

Discussion

Ecological cranial shape and disparity

The PCA of cranial morphospace (Figure 8) and phylogenetic regression of degree of carnivory on cranial shape (Figure 14) found broad connections to ecology, but not the degree reported in some past analyses (Wroe and Milne, 2007; Goswami et al., 2011). There is a distinct region of morphospace occupied by sabertooth feliforms, but almost the entirety of hypo-mesocarnivores, i.e., herpestids, viverrids, euplerids, stenoplesictids, prionodontids overlap each other. What remains are two other distinct regions, occupied by hyaenids and felids respectively (with some overlap from sabertooth clades) indicating that phylogeny might have substantial input on morphospace occupation compared to dietary category in most cases among feliforms.
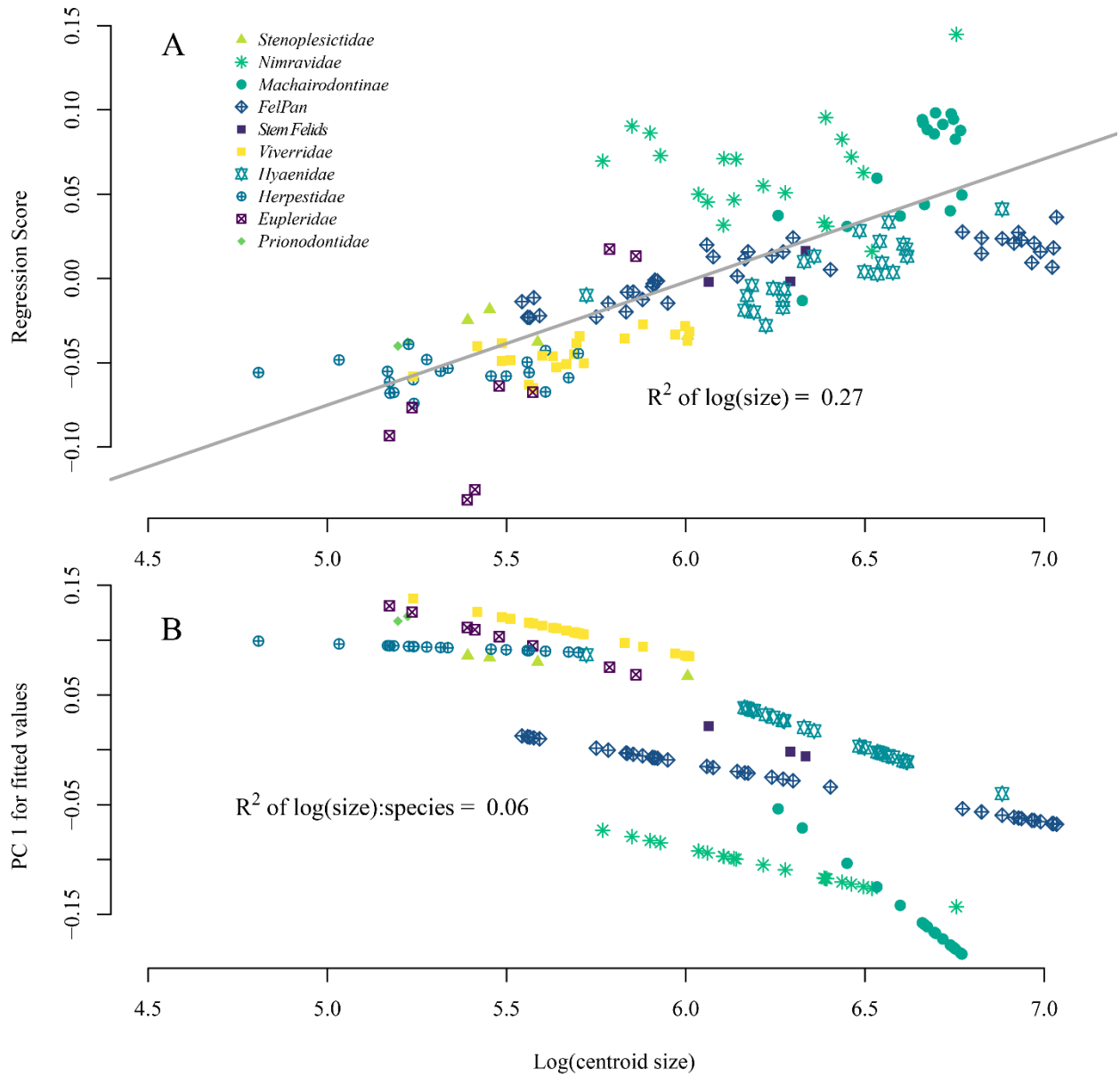
Figure 13. Log centroid size versus the regression scores of shape and size for each specimen (A). Idealized allometric trajectories predicted values for each clade, highlighting similarities in evolutionary allometric slopes (B).

Table 19. Evolutionary allometry pANCOVA. Csize = centroid size, Df = degrees of freedom, SS = sum of squares, MS = mean square, R2 = coefficient of determination, F= F statistic, Z= effect sizes, Pr(>F) = significance value.

	Df	SS	MS	Rsq	F	Z	Pr(>F)
log(Csize)	1	0.006	0.006	0.073	5.216	3.506	<0.001
clade	9	0.006	0.001	0.07	0.553	-2.666	<0.994
log(Csize):clade	8	0.009	0.001	0.102	0.91	-0.132	<0.55
Residuals	54	0.064	0.001	0.756			
Total	72	0.085					

This lack of convergence of skull shape on diet or ecology is reflected in the regression of degree of carnivory, where there exists a narrow range of cranial shapes for the vast majority of the dietary spectrum, and only within the realm of hypercarnivory do cranial shapes occupy new and more variable zones. This result is more aligned with recent studies that were unable to find significant correlation between cranial shape and diet among carnivorans (Law et al., 2018b; Rovinsky et al., 2021).

The present results support a decoupling of cranial shape and diet until hypercarnivory is reached. The vast majority of diets are served by a narrow cranial shape, or "one-to-many" ecological mapping. This dietary regime does coincide with changes in dental morphology, implying dentition is far more labile relative to a species' environment than what its skull looks like. Crania within this range are thus little altered (or subject to stabilizing selection) from ancestral morphology as indicated by the stronger phylogenetic signal (K=0.66), with observed variation likely the outcome of phylogenetic stochastic processes (Raup and Gould, 1974).

Table 20. Pair-wise homogeneity of slope test summary of p values for distinct evolutionary allometric trajectories. Significantly

different comparisons are in bold. Fel Pan = Felinae + Pantherinae, Machair. = Machairodontinae, Prionodont. = Prionodontidae,

Stenoples = Stenoplesictidae

	Eupleridae	Stem Felid	FelPan	Herpestidae	Hyaenidae	Machair.	Nimravidae	Prionodont.	Stenoples.	Viverridae
Eupleridae	1	0.94	0.745	0.383	0.982	0.97	0.926	0.95	0.473	0.257
Stem Felid	0.94	1	0.353	0.681	0.347	0.986	0.669	0.942	0.936	0.605
FelPan	0.745	0.353	1	0.311	0.002	1	0.515	0.9	0.854	0.663
Herpestidae	0.383	0.681	0.311	1	0.976	0.944	0.138	0.936	0.703	0.964
Hyaenidae	0.982	0.347	**0.002**	0.976	1	0.822	0.09	0.928	0.411	0.659
Machair.	0.97	0.986	1	0.944	0.822	1	0.004	0.948	0.998	0.99
Nimravidae	0.926	0.669	0.515	0.138	0.09	**0.004**	1	0.91	0.341	0.499
Prionodont.	0.95	0.942	0.9	0.936	0.928	0.948	0.91	1	0.95	0.936
Stenoples.	0.473	0.936	0.854	0.703	0.411	0.998	0.341	0.95	1	0.313
Viverridae	0.257	0.605	0.663	0.964	0.659	0.99	0.499	0.936	0.313	1
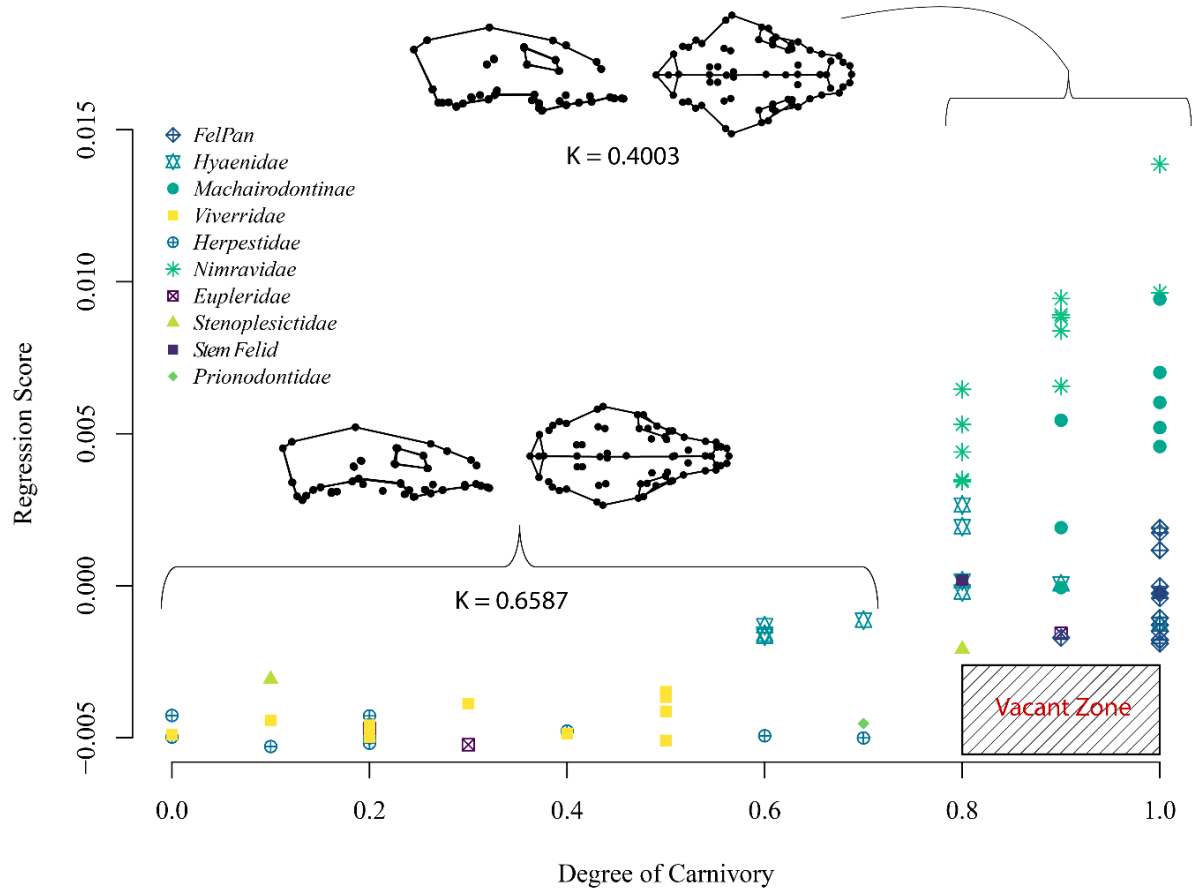
Figure 14. Relationship between degree of carnivory and feliform cranial shape (PGLS). Mean cranial shape (in right lateral and dorsal views) of species with ≤ 70% vertebrate material in their diet below and ≥80% above. Presented K values indicate associated phylogenetic signal for the cranial shapes of those species.

Hypercarnivores, on the other hand, occupy a diverse range of cranial shapes that likely are needed to subdue and consume a proportionally diverse set of prey or animal materials. This can be viewed as "many-to-one" mapping of morphology to ecology, with the "one" truly referring to the narrow band of almost exclusively vertebrate material in the diet. Within this zone there

are differential demands upon the feliform skull that are not met by the ancestral shape, and thus

no hypercarnivore taxon analyzed occupied that zone. Other studies have shown the demands of

bite force and its effect on cranial shape when it comes to hypercarnivory (Law et al., 2018b),

durophagy (Tseng and Wang, 2011; Figueirido et al., 2013; Tseng, 2013), or sabertooth

morphology (Figueirido et al., 2011; Christiansen, 2012). Taken together, these demands require

different optimization leading to distinct cranial shapes, such as the dissipation of compressive

force in durophagous hyaenids, the required increase in the gape of sabertooth feliforms, and

overall cranial rigidity and strength in bite force for hypercarnivores in subduing/consuming their

prey.

Surprisingly, only one of the analyzed pair-wise comparisons of ecological category and cranial

disparity found significance: sabertooth forms versus hypocarnivores. While each ecological

category has a distinct cranial morphology, the range of variance within each category is similar.

This feature of sabertooths was also observed in the osteometric analysis of Holliday and

Steppan (2004) where increasing specialization did not correlate with morphological diversity

except in the most specialized sabertooth taxa. The uniqueness of sabertooth taxa may relate to

niche partitioning of scimitar- and dirk-tooth forms occupying additional morphospace

(Lautenschlager et al., 2020). This greater disparity is reflected in extremely high rates of

morphological evolution (Table 16), greater than all other ecological categories (2.2-5.1 times

faster), suggesting high selective pressures for these cranial shapes. High rates were also

observed for durophagous and hypercarnivorous carnivores relative to hypocarnivorous ones, but

the associated disparity of these categories was not significantly different. The disparity of non-

sabertooth hypercarnivores compared to more generalized ecomorphs has been contradictory.

Holliday and Steppan (2004) recovered hypercarnivores with less disparity than non-

hypercarnivorous sister groups, while Michaud et al. (2020), found greater cranial disparity among hypercarnivorous feliforms than generalists (all other taxa) in their analysis. However, both may be accurate in describing certain patterns through respective methodological approach. Holliday and Steppan (2004)'s data primarily looked at dentognathic measurements, such as specific tooth lengths and widths and dentary output lever lengths. As previously stated, hypercarnivory showed trends in tooth loss and tooth row length reduction to accommodate higher bite forces, while dentition was often simplified in overall topography to facilitate slicing or bone-crushing mechanics. With the loss of posterior molars, overall variance would necessarily go down (no variance for these structures), leading to less overall disparity than taxa with broader diets. Michaud et al. (2020) and the present study suggest that from a cranial shape point of view, hypercarnivores are just as capable of occupying a range of shapes as other dietary categories with many pathways/shapes lending themselves to a hypercarnivorous ecology (many-to-one mapping). Conversely, dentognathic restrictions on a diet high in vertebrate material are limiting, especially in regard to evolvability of non-hypercarnivorous ecologies and broader diets.

Clade disparity and impact of lineage age

As questioned at the start of this study, the age of a lineage may play a substantial role in explaining disparity among clades, as an ancient lineage may have simply accrued substantial disparity by random walk dynamics over geologic time, disparity that younger clades may also achieve if provided with enough time. Indeed, there is a correlation of cranial disparity and age of lineage, where nimravids, as the oldest lineage, (34.3 Ma), have the greatest disparity. Similarly, herpestids have the least and are the youngest lineage (9.52 Ma), while all others are intermediate. Thus, adjusting for both allometry and age of lineage, where do we find the

greatest variance in cranial shapes amongst feliforms? In other words, on a more level playing field of size and time to evolve numerous and varied shapes, do certain clades still possess exceptional cranial disparity? Yes, with this adjustment machairodontines become the most diverse clade of cranial shapes, followed by similar values for nimravids and hyaenids. Felines/pantherines, euplerids and viverrids form a clump of similar values in third, while herpestids still remain the least disparate clade. In short, felids possess the greatest cranial disparity amongst feliforms. Setting aside sabertooth morphs for a moment, this great level of disparity is still observed in felines/pantherines, having comparable values to ecologically and taxonomically diverse euplerids and vivverids. Though perhaps not apparent in the outward appearance of many felids, derived cranial shapes have been the subject of several analyses, such as the unique skull of the cheetah (*Acinonyx jubatus*) that possesses resistance to compressive forces more analogous to a durophage and unlike the expectation for a cursorial specialist (Chamoli and Wroe, 2011; Tseng, 2013). The incipient sabertooth morphology of the clouded leopard (Christiansen, 2006, 2008c) also adds to the diverse morphological range of this clade, as does the primarily piscivorous flat-headed cat (*Prionailurus planiceps*), with a cranial shape consistent with its name. These relatively high cranial disparity values for felids were also observed by Michaud et al. (2018) and Figueiridoe et al. (2011) in their analyses, in spite of a different method of assessment and range of taxa.

Perhaps unsurprisingly, relative canine size had substantial impact on cranial shape for machairodontines (~19%) and nimravids (~24%), the clades containing sabertooth feliforms. However, euplerids saw the greatest impact of this variable (~47%), a result which may be correlated with the taxa sampled. Only four species of euplerid were included in this study, representing extremes and apparent average of cranial shape for the family. Most euplerids

appear similar to their African herpestid relatives (e.g., *Salanoia*), while others are ecomorphologically divergent towards invertebrate diets, such as *Eupleres*, or hypercarnivory in *Cryptoprocta*. This high cranial variance was found to be the greatest among living feliforms by Michaud et al. (2018), but with the narrow sample of this study, the hypercarnivorous outlier of *Cryptoprocta* may be driving an overrepresented relative canine size signal. Greater taxonomic inclusion may reduce the RCS signal for the clade and/or inform on the extent of modification that occurs in the euplerid skull to accommodate hypercarnivorous canines.

For the sabertooth clades, hypertrophied canines no doubt contribute to the greater range of cranial shapes not seen in other hypercarnivores. The required reorganization of the cranium to wield such hardware has been argued as a possible escape of soft-flesh specialists into new realms of disparity, when retreating back into omnivory or a more general diet is no longer possible (Holliday and Steppan, 2004). Nimravids' high disparity may be summarized across several ecomorphs that would later appear in machairodontines and maybe even felines (Barrett, 2021). The "cat-like" cranial morphology may represent the only way to exist as a soft flesh specialist unless sabertooth modifications are undertaken. However, once that evolutionary path is opened, differential niches in scimitar- or dirk-tooth morphology may allow renewed variation to exist as large canines (and associated behavioral adaptations) are incorporated into the hypercarnivore mold. What follows are high rates of morphological evolution, with rapid selection for these features, generating a relationship between rates of morphological evolution and disparity (Figure 12), not seen in other clades (Slater, 2013; Jones et al., 2015; Michaud et al., 2018; Simons et al., 2020).

Allometry

The relatively large predictive influence of size on cranial shape (27%) suggests that allometry is indeed important within Feliformia (for some clades such as felines and pantherines extremely so) such that there may be a common allometric trajectory for this clade. Furthermore, if size variation represents a line of least evolutionary resistance for morphological evolution, it would be expected that (1) rates of size evolution would be correlated with rates of cranial shape evolution, and (2) rates of size evolution would be predictive of cranial disparity. Taken at face value these connections do not exist within the results of the present study (Figure 12). However, when comparing size and shape rates of evolution, machairodontines and nimravids exist as outliers from what appears to be an otherwise linear relationship. Removal of these clades still results in a non-significant relationship ($R^2 = 0.46$, $p < 0.08$), but the reduced power of fewer observations may obfuscate a real correlation. As discussed throughout, sabertooth taxa exhibit anomalously high rates of evolution, and nimravids are recovered with the lowest levels of allometry of any feliform clade assessed, a non-statistically significant 9%. Part of this may relate to the existence of highly derived (e.g. dirk-tooth) nimravid taxa at either end of the size spectrum (Barrett, 2021), demonstrating that size is not required to generate these extreme morphologies. These low allometric values are not seen in machairodontines, but the even higher rates of morphological evolution within this clade fits into a narrative of high selective pressure and rapid evolution for this ecology.

Even with these deviations in morphological rates of evolution for sabertooth clades, support for some level of common allometry amongst feliforms was found in this study (Table 14, Figure 13). Save sabertooth taxa and the vermivore specialist *Eupleres*, most taxa present a linear relationship in shape with increasing size. Comparisons of idealized allometric trajectories

further found only two significantly different results, that of machairodontines and nimraivds; and hyaenids with felines/pantherines. Machairodontines and nimravids evolved similar cranial shapes but did so under apparently different allometric trajectories. Implying that size, once again, has a differential impact on cranial evolution for these clades. The other clades that differ significantly, hyaenids and non-sabertooth felids, perhaps demonstrate the uniqueness in size-correlated changes amongst soft-flesh specialists with reduced tooth counts and brachiocephalic crania compared to those of incipient to fully developed durophagy and comparatively dolichocephalic crania. Regardless, the deviants are all clades with large size ranges, and all contain hypercarnivores, with hyaneids the only of these clades containing taxa that are not solely hypercarnivorous. The lack of significance between other clades may thus relate to a lack of selective pressure to pull them off this common allometric trajectory of utility of mapping a narrow range of generalized cranial shapes onto a broad swath of dietary possibilities. The lack of significant differences in allometric trajectories between hypercarnivorous clades and more generalized ones may then simply be a result of lack of overlap in size ranges to robustly infer these differences, or small members of hypercarnivous clades are not that different from large members of generalist clades, as in hyaenids.

A variable connection in macroevolutionary size to shape is observed in several clades. For example, Simons et al. (2020) found no correlation in catarrhine primate morphological evolutionary rates (size or shape) and disparity, but did find a correlation for size and shape evolutionary rates, unlike the present study. However, their additional finding that most of the variation in within-clade allometries is best explained by a shared allometry model indicates that allometry is still an important factor in catarrhine cranial evolution. This hypothesis is supported by numerous other primate studies (Collard and O'Higgins, 2001; Singleton, 2002; Mitteroecker

et al., 2004; Schaefer et al., 2004), which found that allometric trends are apparent in interspecific cranial shape differences, but that species do not merely share allometric scaling trajectories. Instead, details of primate evolution are likely constrained by the necessity of maintaining the numerous functional roles of the cranium throughout an organism's life span preventing size from being the sole force in the production of morphological disparity (Simons et al., 2020).

Comparatively, Marcy et al. (2020) found strong support for conserved allometric slopes across Australian murids, save for carnivore and folivore specialists. The static (within-species) allometric trajectories were self-similar to evolutionary (among-species) Australian murid allometry. This pattern is more similar to that seen in non-mammalian vertebrate clades. Bird cranial evolution seems to possess strong allometric patterns; for example, the shape of bird of prey beaks is controlled almost entirely by size (~80%, Bright et al., 2016). In another example of this strong allometry in birds, most nightbird (Strisores) cranial shapes display changes associated with heterochrony (Navalón et al., 2021). Similarly, encephalization, or growth of the brain causes changes in the topology of its bony base inside the cranium leading to predictable effects on the shape of the whole skull (Marugán-Lobón et al., 2022).

Overall, mammals are thought to have a high degree of evolvability in cranial allometry (Tsuboi et al., 2018), such that specific or generic allometric slopes can be far more variable than seen at higher taxonomic levels. Taken together with the present study, it appears that feliforms share relatively similar allometric trajectories until ecological selection on some aspect of hypercarnivory pulls them off into new realms of shape space. Certain clades, such as hyaenids, appear to deviate less from generalized small feliform taxa, while soft-flesh specialists like felids

and nimravids possess the greatest shift in allometric intercepts and possibly slopes to accommodate their derived ecology.

Cranial integration

The idea that variation, or the raw material for evolution, may not be isotropic in nature, but instead has limitations that facilitate or constrain subsequent evolution, has been a prominent hypothesis within evolutionary theory for well over a century (Galton, 1869; Gould, 2002). Strong correlations between traits may limit or outright prevent certain traits from existing, while on the other hand, such correlations may funnel or fruitfully channel variation in extreme directions that increase the rate and/or magnitude of observed variation (Goswami et al., 2014). This idea of constraint may then be a fertile hypothesis for why certain feliform clades never achieved a given level of disparity in their evolutionary history, representing a "smoking gun" of underlying processes worthy of investigation. For the present study, magnitude of cranial integration was employed as a proxy of developmental constraint, one that has the additional benefit of being collected from the fossil record.

Amongst carnivorans, there have been contradictory results and arguments for the effect of integration on the generation of cranial disparity. For example, increasing integration has been used to explain increased disparity across the latest Pleistocene in *Smilodon* and dire wolves (Goswami et al., 2015), while that same integration may also be responsible for differential morphospace occupation of machairodontines compared to nimravids (Goswami et al., 2011). Conversely, in assessment of cranial module integration and disparity for living terrestrial carnivorans and primates, over half of comparisons found no significant correlation between these variables, but when significant results were found the effect of integration on disparity is in limitation of morphological variability (Goswami and Polly, 2010a). A similarly complicated

result was found for pinnipeds, wherein ecology may be driving integration values (Randau et al., 2019), while no correlation was found in levels of integration and disparity generated when comparing domesticated mammals with their wild ancestors (Wilson et al., 2021).

Like these latter studies, the predictive power of integration on disparity of this analysis returned insignificant results (Figure 10 and Figure 11). This was still the case when values of raw clade disparity were used for eigenvalue dispersion ($R^2 = -0.16$, $p<0.69$), while even poorer results for between-module integration ($R^2 = -0.20$, $p<0.90$). These results suggest that no connection exists between how tightly integrated (developmentally or otherwise) a feliform's cranium is and the range of morphological variation it can achieve. Instead, crania remain generally similar to each other, fulfilling a wide variety of dietary and ecological roles until the constraint of hypercarnivory comes into play. At this time, necessary considerations for subduing or processing non-compliant vertebrate prey overrides the ancestral cranial shape in feliforms generating new morphologies. Some of these shapes appear to fall on a common allometric trajectory of smaller clades (i.e., hyaenids), suggesting that the path to generating diverse prey material hypercarnivory and durophagy has a solution different than that of soft-flesh specialized hypercarnivores. Felids and nimravids occupy their own allometric and morphospace realms reflecting a presumed similar ecology and path into their varied cranial shapes, perhaps ending in sabertooth morphology. Regardless, feliform cranial shape seems to remain the same until it isn't. There is no underlying restriction (as assessed via integration) that prevents them from achieving disparate cranial forms; instead, a high dietary/ecological bar must be cleared before selection pressure directs cranial evolution into new realms.

Chapter V

Conclusion

Feliforms of small size exist within a realm of opportunity. This ecospace allows the exploitation of diverse resources including invertebrate-dominated diets, folivory, frugivory, hypocarnivory and mesocarnivory. A narrow range of cranial shapes accomplishes these diverse diets, while the dental toolkit is unencumbered to optimize for the challenges in processing each food material (Figure 15). This pattern is seen in the random walk small feliform body size and dental toolkit take as they evolve, the labile nature of convergent evolution of living small feliform species (Gaubert et al., 2005), and the challenges in resolving phylogenetic relationships amongst fossil taxa of this ecospace. However, there is a tipping point where extreme diet, and to a lesser extent body mass, take over, to shape the morphology and ecology of feliform evolution.

Hypercarnivory, as observed at ≥80% vertebrate material in the diet, forces selection for more robust cranial morphology to subdue and process prey items. This selection necessitates vacating the ancestral feliform cranial mold and occupying a distinct, broader area of shape space. However, what path a feliform takes into this realm depends upon its style of hypercarnivory and distinct ecospace. Soft-flesh specialists such as felids, nimravids, *Cryptoprocta* and *Proailurus* rapidly acquire their familiar cranial and dentognathic condition, with loss of posterior molars, enhancement of the shearing surfaces of the carnassials, robust canines and brachiocephalic crania. With the loss of grinding dentition and the associated capacity to process plant material, there appears to be no return to former ecospaces. This is not all bad, for soft-flesh hypercarnivory is tenable across multiple orders of magnitude in body size; one can be minute as in the black-footed cat (*Felis nigripes*), less than 2.5 kg (Renard et al., 2015), or enormous as in

the extinct North American Lion (*Panthera leo atrox*), up to possibly 457 kg (Wheeler and

Jefferson, 2009). Furthermore, allometry may offer a line of least evolutionary resistance for

these hypercarnivores, for access to new prey items may only require the cranial (and likely post-

cranial) changes associated with allometric scaling (Meachen-Samuels and Van Valkenburgh,

2009; Slater and Van Valkenburgh, 2009), scaling that differs compared to non-soft-flesh-

specialists. Though, a more extreme realm exists beyond these familiar cat-like shapes from this

ecospace, one of sabertooth morphology. Becoming sabertooth opens new doors into cranial

disparity, variance not seen within any other ecomorphology. An obvious source for this

increased variance is the reorganization of the cranium to facilitate wielding such hardware, but

two new ecologies appear to open up as well, that of scimitar- and dirk-tooth morphs. Scimitar-

tooth carnivores fall closer to the common allometric line of other feliforms (Fig. 13A), requiring

fewer modifications in terms of gape management than dirk-tooth morphs. Studies of

machairodontines find differentiation in their respective diets via isotopic analysis, which is also

reflected in their respective *baupläne* argued to favor pursuit or ambush predation (Feranec,

2004; DeSantis et al., 2021). Regardless, body mass doesn't appear to be that important as a

sabertooth carnivore. Some of the smallest nimravids were also the most derived dirk-tooth

morphs, such as *Eusmilus cerebralis*, but the inferred largest feliform of this entire study,

Barbourofelis fricki, was possibly the most derived dirk-tooth placental mammal to have ever

existed (Barrett, 2021). This range of extremes is not as complemented in equal extremes of

body mass in machairodontines, but bobcat sized members are known to have also existed (de

Bonis et al., 2018), though unable to be included in this study.

103
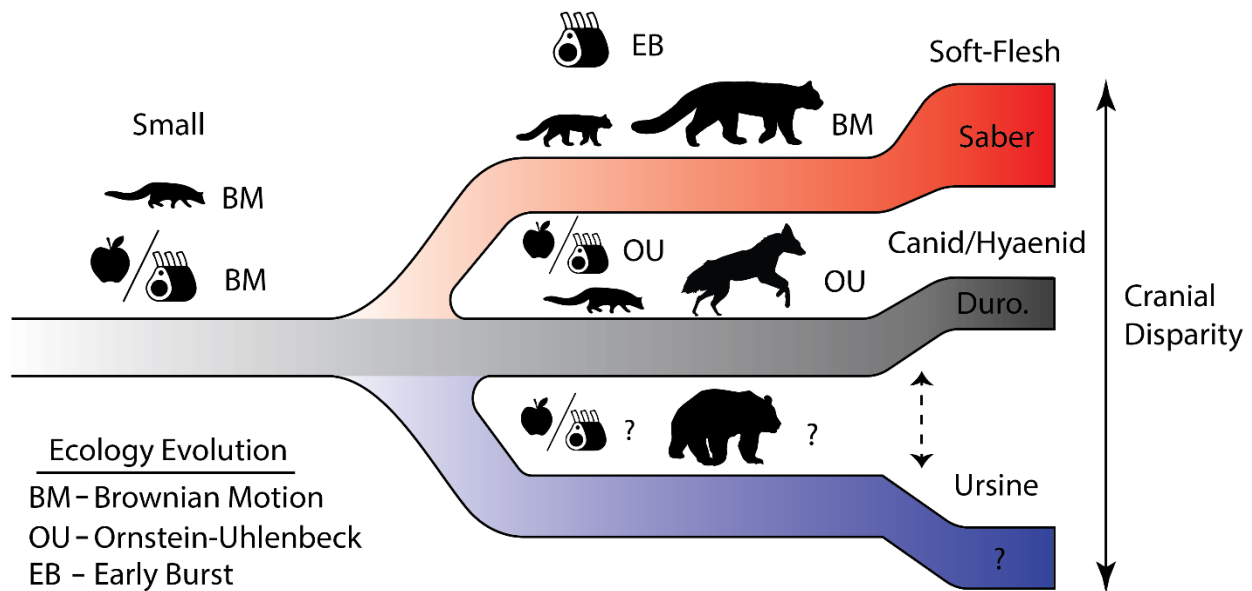
Figure 15. Hypothesis of terrestrial carnivoran evolution with regards to ecology and cranial morphology. Silhouettes reference relative body size possible within each ecospace (small to large), while food icons an approximation of dietary spectrum. Silhouettes taken from Phylopic.org.

The other feliform path into hypercarnivory is that occupied by hyaenids. Unlike soft-flesh specialists, hyaenids facilitate their cranial shape by use of the common allometric trajectory of most feliforms, those occupying the small-bodied ecospace. Hyaenids are notable in their ecological exploitation of nearly all dietary categories examined in this study, though with two exceptions, soft-flesh specialization as in living felids, and sabertooth morphology. Why didn't hyaenids evolve these ecomorphologies? As stated above, reduction or loss of posterior molars is associated with felid ecomorphology. This reduction is seen in *Hyaena*, and to a greater degree in *Crocuta*, where M1s are typically not present. However, all hypercarnivorous hyaenids

maintain robust premolar dentition, something not seen in felids nor nimravids. Indeed, the upper P3 and lower p3-4 are used for durophagy in many hyaenids, but not all, such as *Chasmaporthetes* (Coca-Ortega and Pérez-Claros, 2019). So again, why the difference? It is informative that canids and hyaenids returned similar results in the mode of their ecological evolution. Both clades found the best fit for an optimal body mass and dental toolkit per dietary category, and canids also did not converge on soft-flesh specialization in the same way as felids and nimravids. Amongst canids, hypercarnivory is a delayed acquisition of ecospace evolution (Slater, 2015). It forms a terminus of ecomorphology across all three subfamilies. Compare this to the paleoecology analyses of felids and nimravids, which saw greatest support for early burst dynamics directly into hypercarnivory. A clearer picture of the evolutionary trajectory for hyaenids will require a more comprehensive phylogeny, that better samples the 'ictitheres' and the more hypo- to mesocarnivorous lineages. However, current literature suggests that the evolution of hypercarnivory in hyaenids is similar to that of canids with delayed acquisition (Werdelin and Solounias, 1991; Turner et al., 2008). Hyaenids may be unable to access soft-flesh specialization, as were canids, from insurmountable phylogenetic inertia. The fossil record suggests that both lineages developed cursorial morphology, early on losing the ability to supinate and pronate the forelimbs, and to retract the distal phalanges (Hunt Jr. and Solounias, 1991; Wang, 1993; Figueirido et al., 2015; Gracia, 2015). Generally speaking, the felid postcranial condition is plesiomorphic among Carnivoramorpha (Spaulding and Flynn, 2009, 2012; Solé et al., 2014, 2016) and likely associated with arboreal adaptations to the dense canopy forests of the Eocene (Tomiya et al., 2021). Cursoriality favors face-orientated predation in canid-like hypercarnivores, compared to ambush and grappling strategies found in felids, and presumably nimravids (Ewer, 1973; Andersson, 2005). The cranium of soft-flesh specialists

maximizes gape capability while balancing bite force (even in non-sabertooths) to allow quick dispatch of prey, a benefit in solitary predators (Figueirido et al., 2011; Meloro et al., 2015). Thus, the early trajectory of hyaenids and canids into cursoriality with increasing body size may not have allowed them to switch tracks to the ecospace shared by felids and nimravids. Instead, the hyaenid/canid postcranial situation may have predisposed these lineages to communal hypercarnivory, necessitating a different strategy in capturing large prey (Van Valkenburgh and Koepfli, 1993; Van Valkenburgh et al., 2003). This hyaenid/canid ecospace and associated evolutionary trajectory may also be shared by the amphicyonid lineages, Daphoeninae and Temnocyoninae, and the ursid hemicyonines (Hunt, 1996, 1998b, 2001b). All experienced similar patterns of cursorial adaptations and dolichocephalic cranial shapes with broad dental tool kits capable of omnivory. Furthermore, all of these lineages produced members with adaptations to durophagy via hypercarnivory, save perhaps hemicyonines. Future paleoecological and cranial morphology analyses could assess the validity of the comparison, but sufficient phylogenies are also in need.

Interestingly, a fourth ecospace category may exist, encompassing extant ursines. Turning to the fossil record it appears that the Amphicyoninae lineage once occupied this ecospace, featuring large size, relative plantigrade posture, but a range of hypo-hypercarnivorous diets. Much like the above comparisons to other caniforms, future study may find a unique hypercarnivorous end member for this ecospace, one possibly occupied by taxa such as *Ysengrinia* and *Magericyon* (Viranta, 1996; Peigné et al., 2008; Soledad Domingo et al., 2013). Furthermore, unlike the previous ecospaces, both ursids and amphicyonids seemed capable of switching from canid/hyaenid ecospace to the ursine space during their evolutionary history and thus offer a

unique area of inquiry of why these clades where able to make the shift, while hyaenids and canids were not.

The above discussion offers potential pathways in carnivoran evolution, but not the process-based push that may get them moving or shifting to new zones. For that, contingency in natural history may be the best explanation. Small feliforms, and maybe even caniforms such as mustelids, procyonids, ailurids, mephitids, seem labile in their ability to shift rapidly in diet and associated dental toolkits. However, climatic and tectonic sourced opportunity may be required to facilitate rapid radiations into soft-flesh specialized hypercarnivory or the wide ecological occupation of canids and hyaenids. Nimravids gained purchase in North America, through circum-Pacific immigration from Asia, into an increasingly mosaic forested landscape after the Mid-Eocene climatic optimum. This was also shortly after the extinction of sabertooth machaeroidines (Zack et al., 2022), facilitating a potential contingent opportunity for nimravids. The Oligo-Miocene transition saw both global warming and the African-Eurasian interchange. This period correlates with the divergence of hyaenids from their common ancestors with herpestids and euplerids the origin of felids, the origin and diversification of lophocyonids, and initial diversification of the barbourofelins. In short, an immense diversification, in both taxonomic and ecological diversity of feliforms. The most recent example of such contingent global opportunities may be the Middle Miocene Climatic Optimum, which recovers this time as the appearance of the most recent common ancestor for the extant radiation of viverrids and herpestids + euplerids, and the divergence of machairodontine felids from felines + pantherines. The success of euplerids is itself a phenomenal example of contingent evolution with the sweepstakes dispersal of a herpestid-like ancestor rafting to Madagascar and diversifying into the

107

ecologically broad family known today. So, viewed in one light, feliforms have been capable of invading numerous ecologies around the globe; they just required the opportunity to do so.

Considering the original question: Is there evolutionary constraint in feliforms? Apparently yes, but not in the way typically framed. Herpestids, viverrids, euplerids, prionodontids, etc. are constrained in staying small to exploit the diverse range of ecologies they occupy, small size that frees them from metabolic and functional challenges of greater mass. Additionally, they can do all of this with relatively little change in cranial morphology. However, once a feliform enters one of the other ecospace pathways outlined above, new constraints come into play, such as retreating from soft-flesh specialist hypercarnivory into a broader dietary category or switching tracks from the canid/hyaenid ecospace into the aforementioned felid/nimravid space. These constraints fruitfully channel the extreme endmembers of cranial evolution and ecology that otherwise are inaccessible to other groups, i.e., sabertooth and durophagous morphology. An important distinction of this work is the lack of support for an inherent developmental or cranial disparity constraint on the variation observed for supposedly stymied specialists, such as felids. Quite the opposite in fact; felids possess the greatest range of cranial variety of any feliform. Though narrow in their vertebrate dominated diet, they seem to have explored a diverse set of options in cranial shape, options that do not exist for more generalist feliforms, or ones that maybe could not exist without the constraints that have affected their evolutionary trajectory.

In the end, it seems Galton was correct. Only certain channels or facets seem viable for the route of evolution. This is expressed in the irreversible loss of the cusps and teeth in hypercarnivores, or the "re-development" of grappling forelimbs with retractile claws in lineages with cursorial postcrania. These kinds of limitations shape the evolutionary landscape, generating channels down which variation can proceed. This in turn is seen as convergence in the fossil record, and

for this study, the smoking gun of channelized evolution among terrestrial mammalian carnivores. Indeed, the above discussion points out these patterns among carnivorans, but broader taxonomic inclusion finds similar ecospaces for Sparassodonts in South America (Prevosti et al., 2012; Forasiepi and Sánchez-Villagra, 2014), marsupials in Australia (Rovinsky et al., 2021) and hyaenodont and oxyaenid "creodonts" (Borths et al., 2016; Zack, 2019b), the latter of which also developed sabertooth morphology within the machaeroidines (Zack et al., 2022). These broad repeated patterns suggest that the interface of terrestrial mammalian carnivores with Cenozoic ecosystems has been consistent. That within this framework only certain trajectories are possible to be a successful carnivore. These channels do provide a limit on what ecology and morphology is feasible, but they also facilitate the fruitful possibilities of extreme carnivory, unique for each channel.

Appendix A

Genbank Accession numbers for molecular data in phylogenetic analysis

	Nuclear			Mitogenome												
	IRBP	CHRNA-1	TTR-intron1	*MT-ATP6*	*MT-ATP8*	*MT-CO1*	*MT-CO2*	*MT-CO3*	*MT-CYB*	*MT-ND1*	*MT-ND2*	*MT-ND3*	*MT-ND4*	*MT-ND4L*	*MT-ND5*	*MT-ND6*
Acinonyx jubatus	XM_027062497	DQ081826	DQ082517	AF344830.1	AF344830.1	AF344830.1	AF344830.1	AF344830.1	AF344830.1	AF344830.1	AF344830.1	AF344830.1	AF344830.1	AF344830.1	AF344830.1	AF344830.1
Arctictis binturong	DQ683125			KX449332.1	KX449332.1	KX449332.1	KX449332.1	KX449332.1	KX449332.1	KX449332.1	KX449332.1	KX449332.1	KX449332.1	KX449332.1	KX449332.1	KX449332.1
Atilax paludinosus			AY750604			JF444116.1			AF522324.1		AY750647.1					
Bdeogale nigripes			AY950643						AY950655.1		AY974022.1					
Canis latrans	KT447969			DQ480511	DQ480511	DQ480511	DQ480511	DQ480511	DQ480511	DQ480511	DQ480511	DQ480511	DQ480511	DQ480511	DQ480511	DQ480511
Caracal caracal		DQ081831	DQ082521	KP202272	KP202272	KP202272	KP202272	KP202272	KP202272	KP202272	KP202272	KP202272	KP202272	KP202272	KP202272	KP202272
Catopuma temminckii	AY525034	DQ081842	DQ082532	KP271500.1	KP271500.1	KP271500.1	KP271500.1	KP271500.1	KP271500.1	KP271500.1	KP271500.1	KP271500.1	KP271500.1	KP271500.1	KP271500.1	KP271500.1
Civettictis civetta	AY170078	GU931024	AY170023	NC_033378	NC_033378	NC_033378	NC_033378	NC_033378	NC_033378	NC_033378	NC_033378	NC_033378	NC_033378	NC_033378	NC_033378	NC_033378
Crocuta crocuta	AY170087	AY928700	DQ082540	JF894377.1	JF894377.1	JF894377.1	JF894377.1	JF894377.1	JF894377.1	JF894377.1	JF894377.1	JF894377.1	JF894377.1	JF894377.1	JF894377.1	JF894377.1
Crocuta crocuta spelaea				MN320462.1	MN320462.1	MN320462.1	MN320462.1	MN320462.1	MN320462.1	MN320462.1	MN320462.1	MN320462.1	MN320462.1	MN320462.1	MN320462.1	MN320462.1

Species																
Crossarchus obscurus	AY170071		AF039726			JF444131.1		AY170101.1		AY170041.1						
Cryptoprocta ferox	AY170066	AY928705	AY170018					MG452178.1		MG452299.1						
Cynogale bennettii								DQ683992.1		DQ683983						
Eupleres goudotii								KY305488.1		MG452300.1						
Felis lybica ornata		DQ081814	DQ082507	KP202275.1	KP202275.1	KP202275.1	KP202275.1	KP202275.1	KP202275.1	KP202275.1	KP202275.1	KP202275.1	KP202275.1	KP202275.1	KP202275.1	KP202275.1
Fossa fossana	AY170067	GU931022	AY170019					AF511062.1		AY170037.1						
Galerella sanguinea			AY950646					AF522331.1		AY974027.1						
Genetta maculata	DQ267562		AY232627			KJ192810.1		AF511055.1		DQ683986.1						
Helogale parvula		DQ081852	AY750605					AF522333.1		AY750649.1						
Hemigalus derbyanus	AY170082		AY170027					AY170109.1		AY170052.1						
Herpestes edwardsii	AY170080		AY170025					DQ519053		AY170050						
Homotherium latidens				MF871701	MF871701	MF871701	MF871701	MF871701	MF871701	MF871701	MF871701	MF871701	MF871701		MF871701	MF871701
Homotherium serum				MF871703	MF871703	MF871703	MF871703	MF871703	MF871703	MF871703	MF871703	MF871703	MF871703		MF871703	MF871703
Hyaena hyaena	DQ267570	AY928702	DQ267552	NC_020669	NC_020669	NC_020669	NC_020669	NC_020669	NC_020669	NC_020669	NC_020669	NC_020669	NC_020669	NC_020669	NC_020669	NC_020669

Species																
Ichneumia albicauda		GU931020	AY950651			MN326093.1			AF522341.1		AY974034.1					
Leopardus pardalis	AB109335	DQ08184	DQ082524	KP202284.1	KP202284.1	KP202284.1	KP202284.1	KP202284.1	KP202284.1	KP202284.1	KP202284.1	KP202284.1	KP202284.1	KP202284.1	KP202284.1	KP202284.1
Lynx canadensis	DQ205910	AY928695	DQ082520	KP202281.1	KP202281.1	KP202281.1	KP202281.1	KP202281.1	KP202281.1	KP202281.1	KP202281.1	KP202281.1	KP202281.1	KP202281.1	KP202281.1	KP202281.1
Miracinonyx trumani						DQ097168.1			DQ097175.1							DQ097170.1
Mungos mungo	AY170065	AY928698	AY170017						AF522347.1		AY170035.1					
Nandinia binotata	AY170083	AY928704	AF039729	NC_024567	NC_024567	NC_024567	NC_024567	NC_024567	NC_024567	NC_024567	NC_024567	NC_024567	NC_024567	NC_024567	NC_024567	NC_024567
Neofelis nebulosa	AY525032	DQ081849	DQ082539	DQ257669.1	DQ257669.1	DQ257669.1	DQ257669.1	DQ257669.1	DQ257669.1	DQ257669.1	DQ257669.1	DQ257669.1	DQ257669.1	DQ257669.1	DQ257669.1	DQ257669.1
Otocolobus manul	AY525039	DQ081819	DQ082511	MH978908.1	MH978908.1	MH978908.1	MH978908.1	MH978908.1	MH978908.1	MH978908.1	MH978908.1	MH978908.1	MH978908.1	MH978908.1	MH978908.1	MH978908.1
Paguma larvata intrudens	AY525040		AY525055	KT191130.1	KT191130.1	KT191130.1	KT191130.1	KT191130.1	KT191130.1	KT191130.1	KT191130.1	KT191130.1	KT191130.1	KT191130.1	KT191130.1	KT191130.1
Panthera atrox						DQ899945.1										
Panthera leo	AY525036	AY928694	AF039725	NC_028302	NC_028302	NC_028302	NC_028302	NC_028302	NC_028302	NC_028302	NC_028302	NC_028302	NC_028302	NC_028302	NC_028302	NC_028302
Panthera leo spelaea				KX258452	KX258452	KX258452	KX258452	KX258452	KX258452	KX258452	KX258452	KX258452	KX258452	KX258452	KX258452	KX258452
Panthera pardus	AY525041	DQ081845	DQ082535	KP001507.1	KP001507.1	KP001507.1	KP001507.1	KP001507.1	KP001507.1	KP001507.1	KP001507.1	KP001507.1	KP001507.1	KP001507.1	KP001507.1	KP001507.1
Paradoxurus hermaphroditus	AY170086	AY92869		MG200264	MG200264	MG200264	MG200264	MG200264	MG200264	MG200264	MG200264	MG200264	MG200264	MG200264	MG200264	MG200264

laotum	7			.1	.1	.1	.1	.1	.1	.1	.1	.1	.1	.1	.1	.1
Poiana richardsonii	DQ267559		AY23620						AF511049.1							
Prionailurus planiceps		DQ081823	DQ082515	KY682729.1	KY682729.1	KY682729.1	KY682729.1	KY682729.1	KY682729.1	KY682729.1	KY682729.1	KY682729.1	KY682729.1	KY682729.1	KY682729.1	KY682729.1
Prionodon linsang	JN414782	DQ081850	DQ267551	MT559410.1	MT559410.1	MT559410.1	MT559410.1		MT559410.1	MT559410.1	MT559410.1			MT559410.1	MT559410.1	MT559410.1
Profelis aurata		DQ081832	DQ082522	NC_028299.1	NC_028299.1	NC_028299.1	NC_028299.1	NC_028299.1	NC_028299.1	NC_028299.1	NC_028299.1	NC_028299.1	NC_028299.1	NC_028299.1	NC_028299.1	NC_028299.1
Proteles cristatus		AY928703		MH662445.1	MH662445.1	MH662445.1	MH662445.1	MH662445.1	MH662445.1	MH662445.1	MH662445.1	MH662445.1	MH662445.1	MH662445.1	MH662445.1	MH662445.1
Puma concolor	DQ205911	DQ081824		NC_016470	NC_016470	NC_016470	NC_016470	NC_016470	NC_016470	NC_016470	NC_016470	NC_016470	NC_016470	NC_016470	NC_016470	NC_016470
Rhynchogale melleri		GU931021	AY950653						AF522344.1		AY974036.1						
Salanoia concolor			AY750607						AY187007.1		MG452301.1						
Smilodon populator				MF871700	MF871700	MF871700	MF871700	MF871700	MF871700	MF871700	MF871700	MF871700	MF871700	MF871700	MF871700	MF871700
Suricata suricata	AY170084	DQ081853	DQ082542	NC_045900.1	NC_045900.1	NC_045900.1	NC_045900.1	NC_045900.1	NC_045900.1	NC_045900.1	NC_045900.1	NC_045900.1	NC_045900.1	NC_045900.1	NC_045900.1	NC_045900.1
Taxidea taxus jacksoni	AB285379	AF498148	AY750598	HM106330.1	HM106330.1	HM106330.1	HM106330.1	HM106330.1	HM106330.1	HM106330.1	HM106330.1	HM106330.1	HM106330.1	HM106330.1	HM106330.1	HM106330.1
Viverra tangalunga tangalunga	AY170085		AF039731						AF511045.1		AY170055.1						
Viverricula indica schlegelii	DQ267568		AY232618	KX891745.1	KX891745.1	KX891745.1	KX891745.1	KX891745.1	KX891745.1	KX891745.1	KX891745.1	KX891745.1	KX891745.1	KX891745.1	KX891745.1	KX891745.1

Vulpes vulpes fulva	GQ214077	AY928693	AF039733	KP342452.1	KP342452.1	KP342452.1	KP342452.1	KP342452.1	KP342452.1	KP342452.1	KP342452.1	KP342452.1	KP342452.1	KP342452.1	KP342452.1	KP342452.1

Appendix B

Highest supported partition and evolutionary model scheme of molecular data as

determined via PartitionFinder 2

Settings

alignment   : ./infile.phy

branchlengths   : linked

models   : JC, K80, TRNEF, SYM, HKY, TRN, GTR, HKY+X, TRN+X, GTR+X, JC+G, K80+G, TRNEF+G, SYM+G, HKY+G, TRN+G, GTR+G, HKY+G+X, TRN+G+X, GTR+G+X, JC+I, K80+I, TRNEF+I, SYM+I, HKY+I, TRN+I, GTR+I, HKY+I+X, TRN+I+X, GTR+I+X, JC+I+G, K80+I+G, TRNEF+I+G, SYM+I+G, HKY+I+G, TRN+I+G, GTR+I+G, HKY+I+G+X, TRN+I+G+X, GTR+I+G+X

model_selection   : bic

search   : greedy

Best partitioning scheme

Scheme Name   : step_10

Scheme lnL   : -85150.29748535156

Scheme BIC   : 171846.019025

Number of params   : 169

Number of sites   : 9363

Number of subsets : 10

Subset	Best Model	# sites	subset id	Partition names
1	HKY+I+G+X	1678	1810c769b8f916a03fd2a6c2d9373381	ND4L_1stpos, COX3, ATP6, COX2, COX1

115

2 | GTR+I+G+X | 3990 | 08696fe9fcedeb6bee35f068c3f81ae3 | ND4, CYB, ND1, ATP8, ND5, ND3

3 | SYM+G | 1521 | c9715b8586452f904d516ab02113b915 | TTR, CHRNA_1

4 | TRN+G+X | 421 | 87e5cb9ee47837231e1b3b3e8777f356 | IRBP_1stpos

5 | TRNEF+I | 421 | 8201d351e9239325f36dd35b4c61c9af | IRBP_2ndpos

6 | HKY+G+X | 421 | 785a339441a44dfd0e936358a6abde9b | IRBP_3rdpos

7 | HKY+I+G+X | 396 | c61fec9e72928c8aa7170ad04a8e6142 | ND2

8 | HKY+I+G+X | 98 | eeb82570db336fc244e80a4f45ebdce5 | ND4L_2ndpos

9 | HKY+I+G+X | 98 | 321271c4f6bceb00245ec5d843fdc285 | ND4L_3rdpos

10 | HKY+G+X | 319 | eaeee0a798be6d486926234462330d84 | ND6

Scheme Description in PartitionFinder format

Scheme_step_10 = (ND4L_1stpos, COX3, ATP6, COX2, COX1) (ND4, CYB, ND1, ATP8, ND5, ND3) (TTR, CHRNA_1) (IRBP_1stpos) (IRBP_2ndpos) (IRBP_3rdpos) (ND2) (ND4L_2ndpos) (ND4L_3rdpos) (ND6);

Nexus formatted character sets

begin sets;

    charset Subset1 = 5160-5453\3 1827-2164 1-125 1388-1826 710-1387;

    charset Subset2 = 5454-6268 2165-2846 4110-4644 126-321 6269-7911 5041-5159;

    charset Subset3 = 8231-9363 322-709;

    charset Subset4 = 2847-4109\3;

    charset Subset5 = 2848-4109\3;

    charset Subset6 = 2849-4109\3;

    charset Subset7 = 4645-5040;

    charset Subset8 = 5161-5453\3;

    charset Subset9 = 5162-5453\3;

    charset Subset10 = 7912-8230;

charpartition PartitionFinder = Group1:Subset1, Group2:Subset2, Group3:Subset3, Group4:Subset4, Group5:Subset5, Group6:Subset6, Group7:Subset7, Group8:Subset8, Group9:Subset9, Group10:Subset10;

end;

Appendix C

Source Material for Morphological Character Scoring and Continuous Variables

American Museum of Natural History, New York City, New York, USA (**AMNH**)

American Museum of Natural History – Frick Collection, New York City, New York, USA (**F:AM**)

American Museum of Natural History, Comparative Anatomy Collection, New York City, New York, USA (**AMNH C.A.**)

Field Museum of Natural History, Chicago, Illinois, USA (**FMNH**)

Smithsonian National Museum of Natural History, Washington D.C., USA (**USNM**)

John Day Fossil Beds National Monument, Kimberly, Oregon, USA (**JODA**)

Grand Canyon National Park, Grand Canyon, Arizona, USA (**GRCA**)

University of Nebraska Lincoln State Museum, Lincoln, Nebraska, USA (**UNSM**)

Florida Museum of Natural History, University of Florida, Gainesville, Florida, USA (**UF**)

Texas Memorial Museum, University of Texas at Austin, Austin, Texas, USA (**TMM**)

Museum of Evolution of Uppsala University, Uppsala, Sweden (**M**)

University of California Museum of Paleontology, Berkeley, California, USA (**UCMP**)

Yale Peabody Museum, New Haven, Connecticut, USA (**YPM**)

Yale Peabody Museum, Princeton University Collection, New Haven, Connecticut, USA (**YPM PU**)

University of Kansas, Natural History Museum, Lawrence, Kansas, USA (**KUVP**)

Raymond M. Alf Museum of Paleontology, Claremont, California, USA (**RAM**)

Museum of Geology, South Dakota School of Mines and Technology, Rapid City, South Dakota, USA (**SDSM**)

University of Oregon, Museum of Natural and Cultural History-Modern Collection, Eugene, Oregon, USA (**B**)

Los Angeles County Museum, George C. Page Museum (Hancock Collection), Los Angeles, California, USA (**LACMHC**)

Museo Nacional de Ciencias Naturales-CSIC, Madrid, Spain (**MNCN**)

Museum National d'Histoire Naturelle, Paris, France (**MNHN**)

Museum für Naturkunde, Berlin, Germany (**MFN MB. Ma.**)

Beijing Natural History Museum, Beijing, China (**BNHM**)

Institute of Vertebrate Paleontology and Paleoanthropology, Chinese Academy of Sciences Beijing, China (**IVPP**)

Collection du Quercy, Faculté des Sciences de Marseille, France (**FSM PQ**)

University of Florence, Florence, Italy (**IGF**)

University of Washington Burke Museum, Seattle, Washington, USA (**UWBM**)

Kenya National Museum, Nairobi, Kenya (**KNM**)

Uganda Museum, Kampala, Uganda (**UM**)

Taxa	Specimens	Literature
Tungurictis spocki	AMNH 26600, 26610, 99146	(Hunt Jr. and Solounias, 1991; Wang, 2004)
Ictitherium viverrinum	AMNH 20696, China 51-L437; F:AM 144906, 144905	(Coca-Ortega and Pérez-Claros, 2019)
Hyaenotherium wongii	AMNH 20555, 22878, 99082, 99088, 99084, 99091, 99081, 99093, 99080, 99095, 20554, 20586	(Coca-Ortega and Pérez-Claros, 2019)
Hyaenictitherium hyaenoides	AMNH 144883; F:AM 144892, 144889	(Coca-Ortega and Pérez-Claros, 2019)
Lycyaena chaeretis	F:AM 145002, 144899, 144902	-
Chasmaporthetes lunensis	AMNH 99789, 99786, 99781, 26955, 101261, 113847; F:AM 99787, 99783; MNCN 67100	(Baryshnikov and Averianov, 1993a; Antón et al., 2006; Coca-Ortega and Pérez-Claros, 2019)
Chasmaporthetes ossifragus	UF 18088, 18089, 27366	(Berta, 1981)
Palinhyaena reperta	F:AM 144897	-
Adcrocuta exima	China -41L-339; AMNH 22880, 140301, 140298, 140299, 140300; F:AM 144903	(Baryshnikov and Averianov, 1993a; Kovachev, 2012; Coca-Ortega and Pérez-Claros, 2019)
Pachycrocuta brevirostris	AMNH 27757, 27756	(Werdelin and Solounias, 1991; Baryshnikov and Averianov, 1993a; Mutter et al., 2001; Palmqvist et al., 2011; Liu et al., 2021)
Tongxinictis primordialis	-	(Qiu et al., 1988b)
Allohyaena kidici	-	(Howell and Petter, 1985; Werdelin and Kurten, 1999; Coca-Ortega and Pérez-Claros, 2019)
Dinocrocuta gigantea	-	(Qiu et al., 1988a; Koufos, 1995; Zhang, 2005; Tseng and Binder,

		2010; Xiong, 2019)
Percrocuta carnifex	-	(Howell and Petter, 1985; Morales and Pickford, 2006; Ghaffar et al., 2019)
Percrocuta algeriensis	-	(Howell and Petter, 1985)
Percrocuta tobieni	-	(Howell and Petter, 1985; Werdelin, 2019)
Proteles cristatus	FMNH 211365; AMNH 24219	(Baryshnikov and Averianov, 1993a)
Crocuta crocuta	FMNH 34582, 18855	(Baryshnikov and Averianov, 1993a)
Hyaena hyaena	FMNH 101982, 47416	(Baryshnikov and Averianov, 1993a)
Plioviverrops orbignyi	MFN MB. Ma. 29580	(de Beaumont, 1969; Koufos, 2006, 2009, 2012)
Crocuta crocuta spelaea	MFN MB. Ma. 43, 44381, 29593, 29940, 30359, 30360, 29945, 30357, 29730, 29744, 29735, 29733, 29745, 51190.9, 92	(Anyonge, 1993; Baryshnikov and Averianov, 1993a; Coca-Ortega and Pérez-Claros, 2019)
Protictitherium crassum	-	(Chen and Schmidt-Kittler, 1983; Gracia, 2015)
Belbus beaumonti	-	(de Beaumont, 1968; Werdelin and Solounias, 1991; Koufos, 2011)
Proailurus lemanensis	AMNH 101931 (cast of holotype MNHN S.G. 3509)	(Schmidt-Kittler, 1976)
Pseudaelurus validus	AMNH 62128, 62167; F:AM 61847	(Hunt, 1998; Rothwell, 2001, 2003)
Promegantereon ogygia	-	(Salesa, 2002; Salesa et al., 2005, 2010a, 2010b; Christiansen, 2013; Siliceo et al., 2014)
Metailurus major	AMNH 131854 (cast of IVPP 5679), AMNH 26379, China-57-L548, Bx45L399; M 3841	(Kovatchev, 2001)
Nimravides pedionomus	F:AM 61855, 61852, 25205, 25206, 62156-B, 62156-C, 62154, 62153-A, 62155, 62174, 62158, 62157-B	-

Machairodus catocopis	F:AM 104044; Hig. 315-2306, KAN-30-18, KAN-85 125	(Antón et al., 2013)
Megantereon cultridens	AMNH 105446, 113842 (cast of IGF 831), 113848 (cast of IGF 827), 101471, 105087	(Vekua, 1995; Antón and Werdelin, 1998; Qiu et al., 2004; Christiansen and Adolfssen, 2007; Palmqvist et al., 2007; Christiansen, 2013)
Amphimachairodus giganteus	F:AM 50478, 50476	(Koufos, 2016)
Amphimachairodus coloradoensis	F:AM 104726/104727, 104725, 69263; #1745 Bx 50 DKLA, GY-147-4995-H, #4142 Bx 117, #1066 Bx 34, #901 Bx 29, #3711 Bx 101, #368 Bx 16, #3492 Bx 99, RED 175-3262	(Antón et al., 2013)
Dinofelis diastemata	F:AM 50445, 50446	(Werdelin and Lewis, 2001)
Homotherium serum	F:AM 142497, 128069, 116841; TMM 933-3444	(Meade, 1961; Collins, 1981; Christiansen, 2013; Antón et al., 2014)
Homotherium latidens	AMNH 104641; F:AM 50461, 50462, 50469	(Anyonge, 1993; Sardella and Iurino, 2012; Antón et al., 2014)
Homotherium ischyrus	AMNH 95297, F:AM 131893, Chan.35-856, Chan-42-929	(Hearst et al., 2011)
Smilodon fatalis	AMNH 14349; LACMHC 2002-R-289, R10864, R10688, A-3708, K-65, K-876, K-1541, K-2281, Q-1609, Q-2965, 36960, 37415, 37873, 38504, 38731, 39221, U-3585, R-423, R-6739, 40416, K-3309, K-4507, K-4671, J-6083, T-5113, T-3068, Q-5192, Q-3903, 46699, K-2768, N-1219, N-1737, 133528, 60175	(Matthew, 1910; Merriam and Stock, 1932; Christiansen and Harris, 2005)
Smilodon populator	MFN MB. Ma. 48108 (cast of MNHN F.BRD21)	(Kurtén and Werdelin, 1990; Christiansen and Harris, 2005; Rincón, 2006; de Castro and Langer, 2008; Christiansen, 2013; Wallace and Hulbert, 2013; McDonald and Werdelin, 2018)
Xenosmilus hodsonae	UF 60000, 19400, 22907, 45340, 45428, 223829, 223830, 223831, 223832, 244471, 274280, 312700	(Martin et al., 2011; Christiansen, 2013)
Caracal caracal	FMNH 135042, 57220	-
Lynx canadensis	FMNH 129341	(Leche, 1915)

Felis silvestris	FMNH 97861	(Leche, 1915)
Octolobus manul	MNHN 2010-646, 2009-251	-
Prionailurus planiceps	MNHN CG 1873-228	-
Catopuma temminckii	MNHN 1941-293	-
Profelis aurata	MNHN 1932-5233	-
Leopardus pardalis	FMNH 88887, 68895, 93174	(Schmidt-Kittler, 1976; Christiansen, 2008)
Acinonyx jubatus	AMNH C.A. 145071; FMNH 34589, 29635	(Leche, 1915; Van Valkenburgh et al., 1990)
Miracinonyx trumani	GRCA 21734	(Orr, 1969; Adams, 1979; Van Valkenburgh et al., 1990; Wang and Martin, 1993)
Puma concolor	FMNH 15532	(Van Valkenburgh et al., 1990; Christiansen, 2008)
Neofelis nebulosa	FMNH 75831	-
Panthera pardus	MNHN C.G. 1962-2884, MNHN A7927, MNHN 1996-521	(Leche, 1915; Christiansen, 2008)
Panthera leo	FMNH 31121; B 8707	(Leche, 1915; Hunt, 1987; Salles, 1992; Hsieh and Takemura, 1994; Mattern and McLennan, 2000; Christiansen, 2008; Lueders et al., 2012; De Schepper, 2016)
Panthera leo spelaea	MFN MB. Ma. 0948, 1956, 2246, 1953, 1906, 30090, 30118, 30112a, 30114a, b; MFN MB. Ma. 14322, 14321, 14317, 14320, 30124, 3642, 3643, 1964	(Anyonge, 1993)
Panthera atrox	AMNH 14397; LACMHC 572, 575, 597, 1564, 2903-R-6, 14621, X-6716, 14661, 14844, 14926, 14696, 14905, X-5036, R6740, 16311, 2911-R-1, 2907-R-4, 14722, 2908-R-7, 15297, 15460, 15379, 15536, 15582, X-7067, X-5552, 2937-2, X-5642, X-6274, X-6405, X-7279, 16043, X-9759	(Merriam and Stock, 1932; Wheeler and Jefferson, 2009)
Barbourofelis morrisi	AMNH 79999; F:AM 61876, 61900, 80000, 61895, 25204, 69359, 61893,	-

	61976, 61898, 61970, 125665, 61882, Bx-5-Bx-69 #25138-B	
Oriensmilus liupanensis	AMNH 144755 (cast of an uncatalogued BNHM specimen)	(Wang et al., 2020)
Sansanosmilus palmidens	-	(Filhol, 1890; Ginsburg, 1961; Morlo et al., 2004; Peigné, 2012)
Barbourofelis fricki	AMNH 108193 (cast of UNSM 76000); F:AM 61986, 61994, 61997, 99258, 68234, 2672, 61984, 61983, 125670, 116854, 61991; UWBM 72291	(Schultz et al., 1970; Joeckel and Stavas, 1996)
Barbourofelis loveorum	UF 24447, 36855, 36871, 37000, 36867, 23796, 24432, 36867, 25081, 25103, 25156, 25191, 25228, 25249, 25267, 25283, 25294, 25302, 27258, 37939, 25054, 25034, 36800, 25013, 24429; AMNH 125125	(Baskin, 1981; Neff, 1983; Hunt, 1987; Bryant, 1988a, 1988b, 1991)
Albanosmilus whitfordi	AMNH 14308; F:AM 61856, 61858, 61861, 61864, 61849, 61680, 61885	-
Eusmilus cerebralis	AMNH 6941; F:AM 98189, 69377; UCMP 123180, 123181; JODA 7047	-
Hoplophoneus oharrai	SDSM 2417	-
Hoplophoneus primaevus	F:AM 62007, AMNH 5338, 82440, 38980; USNM 18184; YPM PU 10741	(Bryant, 1988a; Barrett, 2016)
Hoplophoneus occidentalis	F:AM 102387, 62025, 62022; AMNH 1407, 655; KUVP 2874, 2561; RAM 10356	-
Nimravus brachyops	UCMP 1681, 2556, 76111; AMNH 6930, 6993, 6940, 6933; F:AM 62020, 62151; JODA 1312	(Welsh et al., 2015; Barrett, 2016)
Nimravus intermedius	AMNH 137130 (cast of FSM PQ 327), 105390 (cast of CM 2587); MFN MB. Ma. 29987, 29988, 29986, 29991, 29993, 29994, 29995; YPM PU 11569	(Schmidt-Kittler, 1976; Peigné and De Bonis, 1999; Peigné, 2003; Egi et al., 2016)
Pogonodon platycopis	AMNH 6938, 6953	(Barrett, 2016)
Pogonodon davisi	UCMP 789; AMNH 102156; F:AM 62026, 62042, 62024, 62018; JODA 5841; YPM 10520; YPM PU 11430	(Barrett, 2016)

Dinictis felina	AMNH 6937, 8777, 38805; YPM PU 12551, 13625, 12577, 11431	(Barrett, 2016)
Nanosmilus kurteni	UNSM 25505	-
Ginsburgsmilus napakensis	KNM-SO-5670; UM-P67-13	(Morales et al., 2001, 2008; Morlo et al., 2004; Morales and Pickford, 2018)
Prosansanosmilus eggeri	-	(Morlo et al., 2004)
Prosansanosmilus peregrinus	-	(Heizmann et al., 1980; Morlo et al., 2004; Morlo, 2006)
Afrosmilus hispanicus	-	(Belinchón and Morales, 1989; Azanza et al., 1993; Morales et al., 2001)
Afrosmilus turkanae	KNM-MO-15929, KNM-RU-15984, KNM-RU-15986, KNM-SO15973	(Morales et al., 2001; Werdelin and Peigné, 2010; Morales and Pickford, 2018)
Afrosmilus africanus	-	(Andrews, 1914; Savage, 1965; Morales et al., 2001)
Albanosmilus jourdani	-	(Robles et al., 2013)
Maofelis cantonensis	-	(Averianov et al., 2016)
Quercylurus major	-	(Ginsburg, 1979; Peigné, 2003)
Dinailurictis bonali	MFN MB. Ma. 29985	(Ginsburg, 1979; Peigné, 2003)
Eofelis edwardsii	-	(Ginsburg, 1979; Peigné, 2000; de Bonis et al., 2019)
Dinaelurus crassus	-	(Eaton, 1922)
MA-PHQ 348	-	(Peigné, 2001)
Eusmilus dakotensis	YPM PU 11079; UNSM 1068	(Hatcher, 1895; Morea, 1975; Bryant, 1996)
Eusmilus sicarius	YPM PU 12953 A (cast of YPM PU 12953)	-
Eusmilus adelos	USNM 12820, 18214	-
Eusmilus bidentatus	MFN MB. Ma. 30154, 30151	(Piveteau, 1931; Ringeade and Michel, 1994; Peigné and Brunet, 2001; Joeckel et al., 2002)
Eusmilus villebramarensis	-	(Peigné and Brunet, 2001; Peigné,

		2003)
Prionodon linsang	FMNH 88606	(Leche, 1915)
Nandinia binotata	AMNH 2409 C.A.; FMNH 149361, 55758	(Wesley-Hunt and Flynn, 2005; Spaulding and Flynn, 2012; Wible and Spaulding, 2013)
Hemigalus derbyanus	AMNH C.A. 9; FMNH 68717	(Leche, 1915)
Arctictis binturong	AMNH C.A. 1182; FMNH 53747	(Leche, 1915)
Civettictis civetta	FMNH 108174	(Leche, 1915)
Viverra tangalunga	FMNH 85116	(Leche, 1915)
Genetta maculata	FMNH 73044, 85987	-
Paradoxurus hermaphroditus	FMNH 338000, 140476	(Leche, 1915)
Paguma larvata	MNHN CG 1988-163, 1962-2062, 1913-577	-
Cynogale bennettii	MNHN CG 1962-170; MNHN A-2094	(Leche, 1915)
Poiana richardsonii	MNHN CG 1976-389	-
Viverricula indica	MNHN CG 1962-2113	(Leche, 1915)
Atilax paludinosus	MNHN CG 1995-426, 1877-153; MNHN 1871-121	-
Herpestes edwardsii	FMNH 83097	(Spaulding and Flynn, 2012)
Ichneumia albicauda	FMNH 73024, 157991	(Leche, 1915)
Bdeogale nigripes	FMNH 167685	-
Mungos mungo	FMNH 149365	-
Suricata suricata	FMNH 38348, 180674	-
Crossarchus obscurus	FMNH 54410	-
Rhynchogale melleri	MNHN CG 1962-992	-
Galerella sanguinea	MNHN CG 2000-1054, 2001-2188	-
Helogale parvula	MNHN CG1962-1056, 1987-176	-
Fossa fossana	FMNH 85196	-
Cryptoprocta ferox	FMNH 33950, 5655	(Carlsson, 1911)

Eupleres goudotii	FMNH 30492, MNHN CG 1962-2105	-
Salanoia concolor	MNHN CG 1962-2111	-
Kanuites lewisae	-	(Dehghani and Werdelin, 2008; Werdelin, 2019)
Kichechia zamanae	-	(Savage, 1965; Schmidt-Kittler, 1987; Morales and Pickford, 2011; Adrian et al., 2018)
Herpestides antiquus	-	(Chen and Schmidt-Kittler, 1983; Hunt, 1991; Morlo, 1996; Wolsan and Morlo, 1997; Wesley-Hunt and Flynn, 2005; Spaulding and Flynn, 2012)
Euboictis aliverensis	-	(Schmidt-Kittler, 1983; Fejfar and Schmidt-Kittler, 1984)
Sivanasua viverroides	-	(Fejfar and Schmidt-Kittler, 1984; Fejfar et al., 1997; Ginsburg and Morales, 1999)
Izmirictis cani	-	(Morales et al., 2019)
Palaeoprionodon lamandini	-	(Hunt, 1998, 2001; Wesley-Hunt and Flynn, 2005; Hans-Volker et al., 2007; Spaulding and Flynn, 2012)
Stenogale julieni	-	(Hunt, 1998; Wesley-Hunt and Flynn, 2005; Spaulding and Flynn, 2012; Wang et al., 2019)
Tapocyon robustus	-	(Wesley and Flynn, 2003; Wesley-Hunt and Flynn, 2005; Spaulding and Flynn, 2012)
Procynodictis vulpiceps	AMNH 2514	(Wesley-Hunt and Flynn, 2005; Spaulding and Flynn, 2012)
Hesperocyon gregarius	AMNH 50276	(Bryant, 1992; Wang, 1993, 1994; Wesley-Hunt and Flynn, 2005; Spaulding and Flynn, 2012)
Canis latrans	FMNH 135222	(Baryshnikov and Averianov, 1993b)
Vulpes vulpes	FMNH 64610	(Baryshnikov and Averianov, 1993b)

Taxidea taxus	FMNH 47747	(Leche, 1915)

References

Adams, D. B. 1979. The cheetah:Native American. Science 205:1155–1158.

Adrian, B., L. Werdelin, and A. Grossman. 2018. New Miocene Carnivora (Mammalia) from Moruorot and Kalodirr, Kenya. Palaeontologia Electronica 21.

Andrews, C. W. 1914. On the Lower Miocene vertebrates from British East Africa, collected by Dr. Felix Oswald. Quarterly Journal of the Geological Society of London 70:163–186.

Antón, A. M., M. J. Salesa, and G. Siliceo. 2013. Machairodont Adaptations and Affinities of the Holarctic Late Miocene Homotherin Machairodus (Mammalia, Carnivora, Felidae): The Case of Machairodus Catocopis Cope, 1887. Journal of Vertebrate Paleontology 33:1202–1213.

Antón, M., and L. Werdelin. 1998. Too well restored? The case of the Megantereon skull from Seneze. Lethaia Seminar 31:158–160.

Antón, M., A. Turner, M. J. Salesa, and J. Morales. 2006. A complete skull of Chasmaporthetes lunensis (Carnivora, Hyaenidae) from the Spanish Pliocene site of la Puebla de Valverde (Teruel). Estudios Geologicos 62:375–388.

Antón, M., M. J. Salesa, A. Galobart, and Z. J. Tseng. 2014. The Plio-Pleistocene scimitar-toothed felid genus Homotherium Fabrini, 1890 (Machairodontinae, Homotherini): Diversity, palaeogeography and taxonomic implications. Quaternary Science Reviews 96:259–268.

Anyonge, W. 1993. Body mass in large extant and extinct carnivores. Journal of Zoology 231:339–350.

Averianov, A., E. Obraztsova, I. Danilov, P. Skutschas, and J. Jin. 2016. First nimravid skull from Asia. Scientific Reports 6:1–8.

Azanza, B., E. Cerdeno, L. Ginsburg, J. Van Der Made, J. Morales, and P. Tassy. 1993. Les grands mammifères du Miocène inférieur d'Artesilla, bassin de Calatayud-Teruel (province de Saragosse, Espagne). Bulletin Du Museum National d'Histoire Naturelle Section C Sciences de La Terre Paleontologie Geologie Mineralogie 15:105–153.

Barrett, P. Z. 2016. Taxonomic and systematic revisions to the North American Nimravidae (Mammalia, Carnivora). PeerJ 4:e1658.

Baryshnikov, G. F., and A. O. Averianov. 1993a. Deciduous teeth of carnivorous mammals (Order Carnivora) Part V. Families Protelidae and Hyaenidae. Russian Academy of Sciences Proceedings of the Zoological Institute St. Petersburg 263:46–84.

Baryshnikov, G. F., and A. O. Averianov. 1993b. Deciduous teeth of carnivorous mammals (Order Carnivora) Part IV. Families Amphicyonidae and Canidae. Russian Academy of Sciences Proceedings of the Zoological Institute St. Petersburg 249:158–196.

Baskin, J. A. 1981. Barbourofelis (Nimravidae) and Nimravides (Felidae), with a Description of Two New Species from the Late Miocene of Florida. Journal of Mammalogy 62:122–139.

de Beaumont, G. 1968. Une intéressante mandibule de Hyaenidae (Carnivora) du Pontien de Samos. Archives Des Sciences 21:21–26.

de Beaumont, G. 1969. Brèves remarques sur Plioviverrops Kretzoi (Carnivora). Bulletin de La Société Vaudoise Des Sciences Naturelles 70:1–7.

Belinchón, M., and J. Morales. 1989. Los carnívoros del Mioceno Inferior de Buñol (Valencia, España). Revista Española de Paleontología 4:3–8.

Berta, A. 1981. The Plio-Pleistocene hyaena Chasmaporthetes ossifragus from Florida. Journal of Vertebrate Paleontology 1:341–356.

de Bonis, L., A. Gardin, and C. Blondel. 2019. Carnivora form the early Oligocene of the "Phosphorites du Quercy" in southwestern France. Geodiversitas 41:601–621.

Bryant, H. N. 1988a. The anatomy, phylogenetic relationships and systematics of the Nimravidae (Mammalia: Carnivora). University of Toronto, 414 pp.

Bryant, H. N. 1988b. Delayed Eruption of the Deciduous Upper Canine in the Sabertoothed Carnivore Barbourofelis lovei (Carnivora, Nimravidae). Journal of Vertebrate Paleontology 8:298–306.

Bryant, H. N. 1991. Phylogenetic relationships and systematics of the Nimravidae (Carnivora). Journal of Mammalogy 72:56–78.

Bryant, H. N. 1992. The Carnivora of the Lac Pelletier Lower Fauna (Eocene: Duchesnean), Cypress Hills Formation, Saskatchewan. Journal of Paleontology 66:847–855.

Bryant, H. N. 1996. Nimravidae; pp. 453–475 in D. R. Prothero and R. J. Emry (eds.), The Terrestrial Eocene-Oligocene Transition in North America. Cambridge University Press, Cambridge [England]; New York.

Carlsson, A. 1911. Über Cryptoprocta ferox. Zoologische Jahrbücher Abteilung Für Systematik 30:419–470.

de Castro, M. C., and M. C. Langer. 2008. New postcranial remains of Smilodon populator Lund, 1842 from southeastern Brazil. Revista Brasileira de Paleontologia 11:199–206.

Chen, G. F., and N. Schmidt-Kittler. 1983. The deciduous dentition of Percrocuta Kretzoi and the diphyletic origin of the hyaenas (Carnivora, Mammalia). Paläontologische Zeitschrift 57:159–169.

Christiansen, P. 2008. Phylogeny of the great cats (Felidae: Pantherinae), and the influence of fossil taxa and missing characters. Cladistics 24:977–992.

Christiansen, P. 2013. Phylogeny of the sabertoothed felids (Carnivora: Felidae: Machairodontinae). Cladistics 29:543–559.

Christiansen, P., and J. M. Harris. 2005. Body size of Smilodon (Mammalia: Felidae). Journal of Morphology 266:369–384.

Christiansen, P., and J. S. Adolfssen. 2007. Osteology and ecology of Megantereon cultridens SE311 (Mammalia; Felidae; Machairodontinae), a sabrecat from the Late Pliocene – Early Pleistocene of Senéze, France. Zoological Journal of the Linnean Society 151:833–884.

Coca-Ortega, C., and J. A. Pérez-Claros. 2019. Characterizing ecomorphological patterns in hyenids: A multivariate approach using postcanine dentition. PeerJ 6:e6238.

Collins, R. L. 1981. Scimitar cats, Homotherium serum Cope from Gassaway Fissure, Cannon County, Tennessee and the North American distribution of Homotherium. Journal of the Tennessee Academy of Science 56:15–19.

Dehghani, R., and L. Werdelin. 2008. A new small carnivoran from the Middle Miocene of Fort Ternan, Kenya. Neues Jahrbuch Fur Geologie Und Palaontologie - Abhandlungen 248:233–244.

Eaton, G. F. 1922. John Day Felidae in the Marsh Collection. American Journal of Science 4:425–452.

Egi, N., T. Tsubamoto, M. Saneyoshi, K. Tsogtbaatar, M. Watabe, B. Mainbayar, T. Chinzorig, and P. Khatanbaatar. 2016. Taxonomic revisions on nimravids and small feliforms (Mammalia, Carnivora) from the Upper Eocene of Mongolia. Historical Biology 28:105–119.

Fejfar, O., and N. Schmidt-Kittler. 1984. Sivanasua und Euboictis n. gen. - zwei pflanzenfressende Schleichkatzenvorläufer (Viverridae, Carnivora, Mammalia) im europäischen Untermiozän. Mainzer Geowissenschaftliche Mitteilungen 13:49–72.

Fejfar, O., N. Schmidt-Kittler, and M. Rummel. 1997. Sivanasua viverroides (Schlosser, 1916) from the Lower Miocene fissure filling Rothenstein 1/13/. Münchner Geowissenschaftliche Abhandlungen Reihe A Geologie Und Paläontologie 34:93–110.

Filhol, H. 1890. Études sur les Mammifères Fossiles de Sansan. Bibliothèque Des Hautes Études Section Des Sciences Naturelles 37:1–319.

Ghaffar, A., M. Akhtar, M. A. Khan, and M. A. Babar. 2019. Comments on percrocuta carnifex (carnivora, percrocutidae) based on new fossil material from the nagri formation (middle siwaliks) of hasnot, pakistan. Geologica Acta 17:1–9.

Ginsburg, L. 1961. La faune des carnivores miocènes de Sansan (Gers). Mémoires Du Muséum National d'Histoire Naturelle, Sér. C - Sciences de La Terre 9:1–190.

Ginsburg, L. 1979. Révision taxonomique des Nimravini (Carnivora Felidae) de l'Oligocène des Phosphorites du Quercy. Bulletin Du Muséum National d'Histoire Naturelle Paris 4e série 1:35–49.

Ginsburg, L., and J. Morales. 1999. Le genre sivanasua (Lophocyoninae, Hyaenodontidae, Creodonta, Mammalia) dans le miocene de france. Estudios Geológicos 55:173–180.

Gracia, S. F. 2015. Estudio de Protictitherium crassum del Cerro de los Batallones (Torrejón de Velasco, Madrid): aportación a la filogenia y evolución de la familia hyaenidae. Universidad Complutense de Madrid, 365 pp.

Hans-Volker, K., E. Gröning, and C. Brauckmann. 2007. Comment on a fossil civet skull from the Lower Oligocene of the Weisselster Basin (Saxonia, Germany). Studia Geologica Salmanticensia 43:215–225.

Hatcher, J. B. 1895. Discovery, in the Oligocene of South Dakota, of Eusmilus, a genus of sabre-toothed cats new to North America. The American Naturalist 29:1091–1093.

Hearst, J. M., L. D. Martin, J. P. Babiarz, and V. L. Naples. 2011. Osteology and myology of Homotherium ischyrus from Idaho; pp. 123–186 in V. L. Naples, L. D. Martin, and J. P. Babiarz (eds.), The other saber-tooths: Scimitar-tooth cats of the Western Hemisphere. The John Hopkins University Press, Baltimore.

Heizmann, E. P. J., L. Ginsburg, and C. Bulot. 1980. Prosansanosmilus peregrinus, ein neuer machairodontider Felide aus dem Miocän Deutschlands und Frankreichs. Stuttgarter Beiträge Zur Naturkunde B 58:1–27.

Howell, F. C., and G. Petter. 1985. Comparative observations on some middle and upper Miocene hyaenids. Genera: Percrocuta Kretzoi, Allohyaena Kretzoi, Adcrocuta Kretzoi (Mammalia, Carnivora, Hyaenidae). Geobios 18:419–476.

Hsieh, H.-M., and A. Takemura. 1994. The Rete Mirabile of the Maxillary Artery in the Lion (Panthera leo). Okajimas Folia Anatomica Japonica 71:1–12.

Hunt Jr., R. M., and N. Solounias. 1991. Evolution of the aeluroid Carnivora: hyaenid affinities of the Miocene carnivoran Tungurictis spocki from Inner Mongolia. American Museum Novitates 1–25.

Hunt, R. M. 1987. Evolution of the aeluroid Carnivora: significance of auditory structure in the nimravid cat Dinictis. American Museum Novitates 2886:1–74.

Hunt, R. M. 1991. Evolution of the aeluroid Carnivora: viverrid affinities of the Miocene carnivoran Herpestides. American Museum Novitates 3023:1–34.

Hunt, R. M. 1998. Evolution of the aeluroid Carnivora. Diversity of the earliest aeluroids from Eurasia (Quercy, Hsanda-Gol) and the origin of felids. American Museum Novitates 3252.

Hunt, R. M. 2001. Basicranial anatomy of the living linsangs Prionodon and Poiana (Mammalia, Carnivora, Viverridae), with comments on the early evolution of aeluroid carnivorans. American Museum Novitates 3330.

Joeckel, R. M., and J. M. Stavas. 1996. New Insights into the Cranial Anatomy of Barbourofelis fricki (Mammalia, Carnivora). Journal of Vertebrate Paleontology 16:585–591.

Joeckel, R. M., S. Peigné, R. M. Hunt Jr., and R. I. Skolnick. 2002. The auditory region and nasal cavity of Oligocene Nimravidae (Mammalia: Carnivora). Journal of Vertebrate Paleontology 22:830–847.

Koufos, G. D. 1995. The late Miocene percrocutas of Macedonia (Greece). Palaeovertebrata 24:68–84.

Koufos, G. D. 2006. The late Miocene vertebrate locality of Perivolaki, Thessaly, Greece: 4. Carnivora. Palaeontographica, Abteilung A: Palaozoologie - Stratigraphie 276:39–74.

Koufos, G. D. 2009. The Late Miocene Mammal Faunas of the Mytilinii Basin, Samos Island, Greece: New Collection 5. Carnivora. Beiträge Zur Paläontologie 31:57–105.

Koufos, G. D. 2011. The Miocene carnivore assemblage of Greece. Estudios Geologicos 67:291–320.

Koufos, G. D. 2012. New material of Carnivora (Mammalia) from the Late Miocene of Axios Valley, Macedonia, Greece. Comptes Rendus Palevol 11:49–64.

Koufos, G. D. 2016. Palaeontology of the upper Miocene vertebrate localities of Nikiti (Chalkidiki Peninsula, Macedonia, Greece). Carnivora. Geobios 49:53–67.

Kovachev, D. 2012. A complete skeleton of Adcrocuta eximia (Roth and Wagner, 1854) from the Upper Maeotian (Turolian) of Hadzhidimovo, SW Bulgaria. Geologica Balcanica 41:77–95.

Kovatchev, D. 2001. Description d'un squelette complet de Metailurus (Felidae, Carnivora, Mammalia) du Miocène supérieur de Bulgarie. Geologica Balcanica 31:71–88.

Kurtén, B., and L. Werdelin. 1990. Relationships between North and South American Smilodon. Journal of Vertebrate Paleontology 10:158–169.

Leche, W. 1915. Zur Frage nach der stammesgeschichtlichen Bedeutung des Milchgebisses bei den Säugetieren. 11. Viverridae, Hyaenidae, Telidae, Mustelidae, Creodonta. Zoologische Jahrbücher. Abteilung Für Systematik, Geographie Und Biologie Der Tiere 38:275–370.

Liu, J., J. Liu, H. Zhang, J. Wagner, Q. Jiangzuo, Y. Song, S. Liu, Y. Wang, and C. Jin. 2021. The giant short-faced hyena Pachycrocuta brevirostris (Mammalia, Carnivora, Hyaenidae) from Northeast Asia: A reinterpretation of subspecies differentiation and intercontinental dispersal. Quaternary International.

Lueders, I., I. Luther, G. Scheepers, and G. van der Horst. 2012. Improved semen collection method for wild felids: Urethral catheterization yields high sperm quality in African lions (Panthera leo). Theriogenology 78:696–701.

Martin, L. D., J. P. Barbiarz, and V. L. Naples. 2011. The osteology of a cookie-cutter cat, Xenosmilus hodsonae; pp. 42–97 in V. L. Naples, L. D. Martin, and J. P. Babiarz (eds.), The other saber-tooths: scimitar-tooth cats of the Western Hemisphere. Johns Hopkins University Press, Baltimore.

Mattern, M. Y., and D. A. McLennan. 2000. Phylogeny and Speciation of Felids. Cladistics 16:232–253.

Matthew, W. D. 1910. The phylogeny of the Felidae. Bulletin of the American Museum of Natural History 28:289–316.

McDonald, H. G., and L. Werdelin. 2018. The Sabertooth Cat, Smilodon populator (Carnivora, Felidae), from Cueva del Milodón, Chile; pp. 53–75 in L. Werdelin, H. G. McDonald, and C. A. Shaw (eds.), Smilodon: The Iconic Sabertooth. Johns Hopkins University Press, Baltimore.

Meade, G. E. 1961. The Saber-toothed Cat Dinobastis serus. Bulletin of the Texas Memorial Museum 2:23–60.

Merriam, J. C., and C. Stock. 1932. The Felidae of Rancho La Brea. The Carnegie Institution, Washington, 231 pp.

Morales, J., and M. Pickford. 2006. A large Percrocutid Carnivore from the Late Miocene (ca. 10-9 Ma) of Nakali, Kenya. Annales de Paleontologie 92:359–366.

Morales, J., and M. Pickford. 2011. Un nouveau carnivore paradoxuriné du Miocène supérieur des Siwaliks (Inde) et une révision des viverridés bunodontes d'Afrique. Geobios 44:271–277.

Morales, J., and M. Pickford. 2018. A new barbourofelid mandible (Carnivora, Mammalia) from the Early Miocene of Grillental-6, Sperrgebiet, Namibia. Communications of the Geological Survey of Namibia 18:113–123.

Morales, J., M. Pickford, and M. J. Salesa. 2008. Creodonta and Carnivora from the Early Miocene of the Northern Sperrgebiet, Namibia. Memoirs of the Geological Survey of Namibia 20:291–310.

Morales, J., M. J. Salesa, M. Pickford, and D. Soria. 2001. A new tribe, new genus and two new species of Barbourofelinae (Felidae, Carnivora, Mammalia) from the early Miocene of East Africa and Spain. Transactions of the Royal Society of Edinburgh: Earth Sciences 92:97–102.

Morales, J., S. Mayda, A. Valenciano, D. DeMiguel, and T. Kaya. 2019. A new lophocyonid, Izmirictis cani gen. et sp. nov. (Carnivora: Mammalia), from the lower Miocene of Turkey. Journal of Systematic Palaeontology 17:1127–1138.

Morea, F. M. 1975. On the species of Hoplophoneus and Eusmilus (Carnivora, Felidae). South Dakota School of Mines and Technology, 74 pp.

Morlo, M. 1996. Carnivoren aus dem Unter-Miozän des Mainzer Beckens - 2. Mustelida, Pinnipedia, Feliformia, Palaeogale. Senckenbergiana Lethaea 76:193–249.

Morlo, M. 2006. New remains of Barbourofelidae (Mammalia, Carnivora) from the Miocene of Southern Germany: implications for the history of barbourofelid migrations. Beiträge Zur Paläontologie 30:339–349.

Morlo, M., S. Peigné, and D. Nagel. 2004. A new species of Prosansanosmilus: implications for the systematic relationships of the family Barbourofelidae new rank (Carnivora, Mammalia). Zoological Journal of the Linnean Society 140:43–61.

Mutter, R. J., L. R. Berger, and P. Schmid. 2001. New evidence of the giant hyaena, Pachycrocuta brevirostris (Carnivora, Hyaenidae), from the Gladysvale cave deposit (Plio-Pleistocene, John Nash Nature Reserve, Gauteng, South Africa). Palaeontologia Africana 113:103–113.

Neff, N. A. 1983. The basicranial anatomy of the Nimravidae (Mammalia: Carnivora) : character analyses and phylogenetic inferences. City University of New York, 642 pp.

Orr, P. C. 1969. Felis trumani a new radiocarbon dated cat skull from Crypt Cave, Nevada. Bulletin of Santa Barbara Museum of Natural History Department of Geology 2:1–8.

Palmqvist, P., V. Torregrosa, J. A. Pérez-Claros, B. Martínez-Navarro, and A. Turner. 2007. A re-evaluation of the diversity of Megantereon (Mammalia, Carnivora, Machairodontinae) and the problem of species identification in extinct carnivores. Journal of Vertebrate Paleontology 27:160–175.

Palmqvist, P., B. Martínez-Navarro, J. A. Pérez-Claros, V. Torregrosa, B. Figueirido, J. M. Jiménez-Arenas, M. Patrocinio Espigares, S. Ros-Montoya, and M. De Renzi. 2011. The giant hyena Pachycrocuta brevirostris: Modelling the bone-cracking behavior of an extinct carnivore. Quaternary International 243:61–79.

Peigné, S. 2000. A new species of Eofelis (Carnivora: Nimravidae) from the Phosphorites of Quercy, France. Comptes Rendus de l'Académie Des Sciences, Paris 330:653–658.

Peigné, S. 2001. A primitive nimravine skull from the Quercy fissures, France: implications for the origin and evolution of Nimravidae (Carnivora). Zoological Journal of the Linnean Society 132:401–410.

Peigné, S. 2003. Systematic review of European Nimravinae (Mammalia, Carnivora, Nimravidae) and the phylogenetic relationships of Palaeogene Nimravidae. Zoologica Scripta 32:199–229.

Peigné, S. 2012. Les Carnivora de Sansan; pp. 559–660 in S. E. N. S. (ed.), Mammifères de Sansan. Muséum national d'Histoire naturelle, Paris.

Peigné, S., and L. De Bonis. 1999. Le premier crane de Nimravus (Mammalia, Carnivora) d'Eurasie et ses relations avec N. brachyops d'Amerique du Nord. Revue De Paleobiolgie 18:57–67.

Peigné, S., and M. Brunet. 2001. Une Nouvelle Espèce Du Genre Eusmilus (Carnivora: Nimravidae) De L'Oligocène (MP 22) D'Europe. Geobios 34:657–672.

Piveteau, J. 1931. Les Chats des Phosphorites du Quercy. Annales de Paléontologie 20:107–163.

Qiu, Z.-X., J. Y. Xie, and D. F. Yan. 1988a. Discovery of the skull of Dinocrocuta gigantea. Vertebrata PalAsiatica 26:128–138.

Qiu, Z., J. Ye, and J. Cao. 1988b. A new species of Percrocuta from Tongxin, Ningxia. Vertebrata Palasiatica 26:116–127.

Qiu, Z. -x., T. Deng, and B. -y. Wang. 2004. Early Pleistocene mammalian fauna from Longdan, Dongxiang, Gansu, China. Palaeontologia Sinica, New Series C 191:1–198.

Rincón, A. D. 2006. A first record of the Pleistocene saber-toothed cat Smilodon populator Lund, 1842 (Carnivora: Felidae: Machairodontinae) from Venezuela. Ameghiniana 43:499–501.

Ringeade, M., and P. Michel. 1994. A propos de l'Eusmilus (Eusmilus bidentatus ringeadei Ringeade et Michel, 1994) de Soumailles, lieu-dit de la commune de Pardaillan, Canton de Duras (Lot et Garonne, France) : étude descriptive. Paléo 6:5–37.

Robles, J. M., D. M. Alba, J. Fortuny, S. De Esteban-Trivigno, C. Rotgers, J. Balaguer, R. Carmona, J. Galindo, S. Almecija, J. V Berto, and S. Moya-Sola. 2013. New craniodental remains of the barbourofelid Albanosmilus jourdani (Filhol, 1883) from the Miocene of the Valles-Penedes Basin (NE Iberian Peninsula) and the phylogeny of the Barbourofelini. Journal of Systematic Palaeontology 11:993–1022.

Rothwell, T. P. 2001. Phylogenetic systematics of North American Pseudaelurus (Carnivora: Felidae). Columbia University, 358 pp.

Rothwell, T. P. 2003. Phylogenetic systematics of North American Pseudaelurus (Carnivora, Felidae). American Museum Novitates 3403.

Salesa, M. J. 2002. Estudio anatómico, biomecánico, paleoecológico y filogenético de Paramachairodus ogygia (Kaup, 1832) Pilgrim, 1913 (Felidae, Machairodontinae) del yacimiento vallesiense (Mioceno superior) de Batallones-1 (Torrejón de Velasco, Madrid). Universidad Complutense de Madrid, Madrid, 370 pp.

Salesa, M. J., M. Antón, A. Turner, and J. Morales. 2005. Aspects of the functional morphology in the cranial and cervical skeleton of the sabre-toothed cat Paramachairodus ogygia (Kaup, 1832) (Felidae, Machairodontinae) from the Late Miocene of Spain: implications for the origins of the machairodont killing bit. Zoological Journal of the Linnean Society 144:363–377.

Salesa, M. J., M. Anton, A. Turner, and J. Morales. 2010a. Functional anatomy of the forelimb in Promegantereon* ogygia (Felidae, Machairodontinae, Smilodontini) from the Late Miocene of Spain and the origins of the sabre-toothed felid model. Journal of Anatomy 216:381–396.

Salesa, M. J., M. Antón, A. Turner, L. Alcalá, P. Montoya, and J. Morales. 2010b. Systematic revision of the late Miocene sabre-toothed felid Paramachaerodus in Spain. Palaeontolgy 53:1369–1391.

Salles, L. O. 1992. Felid Phylogenetics: Extant Taxa and Skull Morphology (Felidae, Aeluroidea). American Museum Novitates 3047:67.

Sardella, R., and D. A. Iurino. 2012. The latest Early Pleistocene sabertoothed cat Homotherium (Felidae, Mammalia) from Monte Peglia (Umbria, central Italy). Bollettino Della Societa Paleontologica Italiana 51:15–22.

Savage, R. J. G. 1965. Fossil Mammal of Africa: The Miocene Carnivora of East Africa. Bulletin of the British Museum (Natural History) 10:239–316.

De Schepper, M. 2016. A comparative study in morphological defects of semen from African Lions (Panthera leo) and Caracal (Caracal caracal): collected by urethral catheterization and electro-ejaculation. Ghent University, 31 pp.

Schmidt-Kittler, N. 1976. Raubtiere aus dem Jungtertiär Kleinasiens. Palaeontographica Abteilung A 155:1–131.

Schmidt-Kittler, N. 1983. The Mammals from the Lower Miocene of Aliveri (Island of Evia, Greece). III. On a new species of Sivanasua Pilgrim, 1931 (Feliformia, Carnivora) and the phylogenetic position of this genus. Proceedings of the Koninklijke Nederlandse Akademie van Wetenschappen, C 86:301–318.

Schmidt-Kittler, N. 1987. The Carnivora (Fissipeda) from the lower Miocene of East Africa. Palaeontographica A197:85–126.

Schultz, C. B., M. R. Schultz, and L. D. Martin. 1970. A new tribe of saber-toothed cats (Barbourofelini) from the Pliocene of North America. Bulletin of the University of Nebraska State Museum 9:1–31.

Siliceo, G., M. J. Salesa, M. Antón, M. F. G. Monescillo, and J. Morales. 2014. Promegantereon ogygia (Felidae, Machairodontinae, Smilodontini) from the Vallesian (late Miocene, MN 10) of Spain: morphological and functional differences in two noncontemporary populations. Journal of Vertebrate Paleontology 34:407–418.

Spaulding, M., and J. J. Flynn. 2012. Phylogeny of the Carnivoramorpha: The impact of postcranial characters. Journal of Systematic Palaeontology 10:653–677.

Tseng, Z. J., and W. J. Binder. 2010. Mandibular biomechanics of Crocuta crocuta, Canis lupus, and the late Miocene Dinocrocuta gigantea (Carnivora, Mammalia). Zoological Journal of the Linnean Society 158:683–696.

Van Valkenburgh, B., F. Grady, and B. Kurtén. 1990. The Plio-Pleistocene cheetah-like cat Miracinonyx inexpectatus of North America. Journal of Vertebrate Paleontology 10:434–454.

Vekua, A. 1995. Die Wirbeltierfauna des Villafranchium von Dmanisi und ihre biostratigraphische Bedeutung. Jahrbuch Des Romisch-Germanischen Zentralmuseums Mainz 42:77–180.

Wallace, S. C., and R. C. Hulbert. 2013. A New Machairodont from the Palmetto Fauna (Early Pliocene) of Florida, with Comments on the Origin of the Smilodontini (Mammalia, Carnivora, Felidae). PLoS ONE 8:e56173.

Wang, X. 1993. Transformation from plantigrady to digitigrady: functional morphology of locomotion in Hesperocyon (Canidae: Carnivora). American Museum Novitates 1–23.

Wang, X. 1994. Phylogenetic systematics of the Hesperocyoninae (Carnivora, Canidae). Bulletin of the American Museum of Natural History 221.

Wang, X. 2004. New materials of Tungurictis (Hyaenidae, Carnivora) from Tunggur Formation, Nei Mongol. Vertebrata PalAsiatica 42:145–153.

Wang, X., and L. D. Martin. 1993. Natural Trap Cave. National Geographic Research & Exploration 9:422–435.

Wang, X., S. C. White, and J. Guan. 2020. A new genus and species of sabretooth , Oriensmilus liupanensis (Barbourofelinae, Nimravidae, Carnivora), from the middle Miocene of China suggests barbourofelines are nimravids, not felids. Journal of Systematic Palaeontology 18:783–803.

Wang, X., Q. Li, L. Sun, C. Deng, Q. Li, and W. Dusu. 2019. Biostratigraphy, magnetostratigraphy, and geochronology of lower Miocene Aoerban strata in Central Inner Mongolia. Palaeogeography, Palaeoclimatology, Palaeoecology 518:187–205.

Welsh, E., C. A. Boyd, K. Spearing, and P. Z. Barrett. 2015. Stratigraphic and taxonomic revision of a North American False Saber-toothed Cat Cub. Proceedings of the South Dakota Academy of Science 94:141–153.

Werdelin, L. 2019. Middle miocene carnivora and hyaenodonta from fort Ternan, Western Kenya. Geodiversitas 41:267–283.

Werdelin, L., and N. Solounias. 1991. The Hyaenidae : taxonomy, systematics and evolution. Fossils and Strata 30:104.

Werdelin, L., and B. Kurten. 1999. Allohyaena (Mammalia: Carnivora): giant hyaenid from the Late Miocene of Hungary. Zoological Journal of the Linnean Society 126:319–334.

Werdelin, L., and M. E. Lewis. 2001. A revision of the genus Dinofelis (Mammalia, Felidae). Zoological Journal of the Linnean Society 132:147–258.

Werdelin, L., and S. Peigné. 2010. Carnivora; pp. 603–657 in L. Werdelin and W. J. Sanders (eds.), Cenozoic Mammals of Africa. University of California Press, Berkeley, Los Angeles, London.

Wesley-Hunt, G. D., and J. J. Flynn. 2005. Phylogeny of the Carnivora: basal relationships among the carnivoramorphans, and assessment of the position of "Miacoidea" relative to Carnivora. Journal of Systematic Palaeontology 3:1–28.

Wesley, G. D., and J. J. Flynn. 2003. a Revision of Tapocyon (Carnivoramorpha), Including Analysis of the First Cranial Specimens and Identification of a New Species. Journal of Paleontology 77:769–783.

Wheeler, H. T., and G. T. Jefferson. 2009. Panthera atrox: body proportions, size, sexual dimorphism, and behavior of the cursorial lion of the North American plains. Museum of Northern Arizona Bulletin 65:423–444.

Wible, J. R., and M. Spaulding. 2013. On the cranial osteology of the African palm civet, Nandinia Binotata (Gray, 1830) (Mammalia, Carnivora, Feliformia). Annals of Carnegie Museum 82:1–114.

Wolsan, M., and M. Morlo. 1997. The status of "Plesictis" croizeti, "Plesictis" gracilis and "Lutra" minor: synonyms of the early Miocene viverrid Herpestides antiquus (Mammalia, Carnivora). Bulletin of the Natural History Museum London (Geol) 53:1–9.

Xiong, W.-Y. 2019. Basicranial morphology of Late Miocene Dinocrocuta gigantea (Carnivora: Hyaenidae) from Fugu, Shaanxi. Vertebrata Palasiatica 57:274–307.

Zhang, Z. 2005. New materials of Dinocrocuta (Percrocutidae, Carnivora) from Lantian, Shaanxi Province, China, and remarks on Chinese Late Miocene biochronology. Geobios 38:685–689.

Appendix D

Morphological Character List

1. Lacrimal facial process: (0), broad rostral flange; (1), small, present on face; (2), not present on face; (3), orbital flange reduced to area around lacrimal foramen (Wesley-Hunt and Flynn, 2005: character 1).

2. Ventral exposure of premaxilla; posterior extent of premaxilla, lateral to palatal foramen: (0), lateral to canine; (1), anterior to canine (Wesley-Hunt and Flynn, 2005: character 2).

3. Shape of infraorbital foramen: (0), elongate; (1), round (Wesley-Hunt and Flynn, 2005: character 3).

4. Length of palate – position of the posterior edge of palatine midline relative to tooth row: (0) posterior to upper tooth row; (1) anterior or equal to upper tooth row (Wesley-Hunt and Flynn, 2005: character 5).

5. Palatine canal primary anterior opening: (0), opening through palatine; (1), at maxilla–palatine suture; (2) opening through maxilla (Wesley-Hunt and Flynn, 2005: character 6).

6. Relative length of frontal and parietal at midline: (0) parietal greater than frontal; (1) parietal equal or subequal to frontal; (2) frontal midline much longer than parietal (Wesley-Hunt and Flynn, 2005: character 7).

7. Postorbital process: (0) prominent; (1) small, reduced (Wesley-Hunt and Flynn, 2005: character 8).

8. Paroccipital process size: (0) well-developed; (1) reduced (Wesley-Hunt and Flynn, 2005: character 9).

9. Paroccipital process shape: (0) simple process; (1) laterally flattened, thin, but is distinct process; (2) cupped around bulla, process not distinct; (3) absent (Wesley-Hunt and Flynn, 2005: character 10).

10. Placement of postglenoid foramen: (0) medially placed; (1) more lateral, external, very near edge of skull (Wesley-Hunt and Flynn, 2005: character 11).

11. Postglenoid foramen: (0) present; (1) greatly reduced, or missing (Wesley-Hunt and Flynn, 2005: character 12).

12. Shape of mastoid process: (0) forming a distinct process, extending out farther than paroccipital process, or subequal; (1) blunt, rounded, does not protrude significantly, more a swelling of the mastoid; (2) thin plate, no distinct process; (3) large tabular process, anteriorly sloping, obscuring much, if not all, of the auditory bulla; (4) large tabular process, extremely anteriorly inclined, closing or nearly enclosing the external auditory meatus by its junction with the glenoid pedicle, medially encroaching and affixed to the ventral floor of the bulla in the

vicinity of the ectotympanic (modified from Wesley-Hunt and Flynn, 2005: character 13 to incorporate states of Christiansen (2013): character 35).

13. Direction of mastoid process extension: (0) lateral – ventral; (1) ventral; (2) lateral; (3) none, or only swelling (Wesley-Hunt and Flynn, 2005: character 14).

14. Condyloid (hypoglossal) foramen position relative to postlacerate foramen: (0) distant; (1) close (less than the diameter of the hypoglossal foramen away); (2) conjoined with posterior lacerate foramen (Wesley-Hunt and Flynn, 2005: character 15).

15. Condyloid (hypoglossal) foramen position relative to groove between the occipital condyle and the paroccipital process: (0) inline or within groove; (1) anterior to groove (Wesley-Hunt and Flynn, 2005: character 16).

16. Posterior lacerate foramen: (0), present as a vacuity between the promontorium and the basioccipital; (1), present as an individual foramen (Wesley-Hunt and Flynn, 2005: character 17).

17. Fenestra cochleae (rotunda) position relative to mastoid tubercle: (0) posterior to mastoid tubercle; (1) anterior, subequal to mastoid tubercle (Wesley-Hunt and Flynn, 2005: character 18).

18. Relative distance between the foramen ovale and the alisphenoid canal: (0) separated by at least the diameter of the alisphenoid canal; (1) separated only by a thin wall; (2) no alisphenoid canal present (Wesley-Hunt and Flynn, 2005: character 19).

19. Ossification of tegmen tympani: (0) facial nerve exposed ventrally; (1) facial nerve partially embedded within tegmen tympani and floored in anteromedial segment; (2) facial nerve beneath a bony sheath that defines the fossa for tensor tympani muscle (Wesley-Hunt and Flynn, 2005: character 20).

20. Composition of mastoid tubercle: (0) mastoid tubercle formed by petrosal; (1) mastoid tubercle formed by squamosal (Wesley-Hunt and Flynn, 2005: character 22).

21. Anterior loop of internal carotid artery: (0) lack of an anterior loop of the internal carotid artery; (1) presence of the loop – excavation in basisphenoid; (2) presence of loop – but extrabullar (Wesley-Hunt and Flynn, 2005: character 23).

22. Suprameatal fossa (fossa on squamosal anterior to mastoid: (0) absent; (1) small; (2) large, well developed (Wesley-Hunt and Flynn, 2005: character 24).

23. Position of internal carotid artery: (0) internal carotid artery laterally positioned, transpromontorial, runs close to margin of fenestra cochlea, presence of a promontory artery, groove for stapedial artery may or may not be present; (1) internal carotid artery transpromontorial but medially positioned, course far from fenestra cochlea; (2) internal carotid

artery medial, extrabullar, inside a bony canal formed by the caudal entotympanic (Wesley-Hunt and Flynn, 2005: character 25).

24. Apron shelf on promontorium posterior to fenestra cochleae for entotympanic attachment: (0) absent; (1) blunt – surface present posterior to fenestra cochleae, but no extensive attachment possible; (2) extended, large area for attachment, may roof posterior bullar chamber (Wesley-Hunt and Flynn, 2005: character 26).

25. Ventral process of promontorium: (0) absent; (1) present, medially positioned on promontorium (Wesley-Hunt and Flynn, 2005: character 27).

26. Shape of the promontorium, anterior extension: (0) elongate, apron extension tapers to a point anteriorly, almond like in appearance; (1) elongate, rounded anteriorly; (2) blunt, quickly truncating; (3) elongate, apron is broad, flat extension, not almond-shaped and not blunt (Wesley-Hunt and Flynn, 2005: character 28).

27. Facet on promontorium indicative of ectotympanic contact: 0, absent; 1, present (Wesley-Hunt and Flynn, 2005: character 29).

28. Inferior petrosal sinus: (0) inferior petrosal sinus small; (1) inferior petrosal sinus greatly enlarged (Wesley-Hunt and Flynn, 2005: character 31).

29. A deep, well developed fossa or pit on the squamosal/alisphenoid recording the contact with the anterior crus or anterior face of the ectotympanic: (0) absent, may have slight/shallow indentation; (1) present, well developed, or bulla present and fully ossified (Wesley-Hunt and Flynn, 2005: character 32).

30. Shelf between mastoid process and paroccipital process: (0) laterally wide, curved trough with smooth surface; (1) laterally wide, could have flat surface, rugose or bulbous, no smoothed out trough; (2) very thin, outside edge could be raised; (3) no shelf present (Wesley-Hunt and Flynn, 2005: character 33).

31. Extent of flange on basiocciptal lateral edge bordering auditory region: (0) absent; (1) small, nascent; (2) well developed when compared to basal 'miacids' (Wesley-Hunt and Flynn, 2005: character 34).

32. Evidence on basisphenoid and basioccipital for marked medial inflation of the entotympanic: (0) absent; (1) present – inflation of entotympanic pushing medially onto and over the basioccipital (Wesley-Hunt and Flynn, 2005: character 35).

33. Evidence of marked posterior inflation of the entotympanic; entotympanic attached during life to paroccipital process or to extensive area posterior to the petrosal: (0) absent; (1) present (Wesley-Hunt and Flynn, 2005: character 36).

34. Epitympanic wing of the petrosal forms ventral floor to the anterior medial corner of the fossa for the tensor tympani muscle: (0) absent; (1) present, but relatively flat and horizontal; (2) ventral floor present, but not horizontal, instead it forms a delicate 'tube', the bony floor is not an extension of the petrosal (Wesley-Hunt and Flynn, 2005: character 38).

35. Placement of middle lacerate foramen: (0) foramen a vacuity – not defined anteriorly nor posteriorly, positioned directly anterior to petrosal; (1) foramen anteriorly defined, posteriorly bordered by petrosal – positioned equal or posterior to basisphenoid/basioccipital suture; (2) foramen defined anteriorly, petrosal may be undefined posterior border, foramen positioned in basisphenoid (or edge of alisphenoid) just anterior to basisphenoid/basioccipital suture; (3) foramen defined anteriorly and posteriorly completely bordered by basisphenoid, foramen positioned far anterior to basisphenoid/basioccipital suture; (4) lack of a foramen (Wesley-Hunt and Flynn, 2005: character 40).

36. M1, a defined cingulum continuous around the lingual face of the protocone: (0) absent; (1) complete cingulum present; (2) anterior segment of cingulae absent or smaller than posterior cingulae (Wesley-Hunt and Flynn, 2005: character 41).

37. M1, protocone height relative to paracone: (0) protocone shorter than paracone; (1) protocone equal or subequal to height of paracone; (2) protocone absent or lacks a cusp associated with the root (modified from Wesley-Hunt and Flynn, 2005: character 42).

38. M1, parastyle projects farther labially than metastyle: (0) absent; (1) present (Wesley-Hunt and Flynn, 2005: character 44)

39. M1, parastyle direction: (0) buccally with anterior direction; (1) buccally (Wesley-Hunt and Flynn, 2005: character 45).

40. M1, size of posterior lingual cingular shelf at base of protocone: (0) posterior lingual cingular shelf equal or subequal to anterior cingulum; (1) posterior lingual cingular shelf more pronounced, larger than anterior cingulum (Wesley-Hunt and Flynn, 2005: character 47).

41. M1, relative height of paracone and metacone: (0) paracone equals metacone in height; (1) paracone greater than metacone; (2) metacone absent (modified from Wesley-Hunt and Flynn, 2005: character 48).

42. M1, relative height of paraconule and metaconule: (0) paraconule greater than metaconule; (1) paraconule equal or subequal to metaconule; (2) both absent (Wesley-Hunt and Flynn, 2005: character 49).

43. M1, presence of hypocone: (0) absent; (1) present (distinct cusp); (2) present, formed by swelling of entire cingulum ridge (Wesley-Hunt and Flynn, 2005: character 50).

44. M1, width of parastylar shelf: (0) lack of a shelf; (1) broad; (2) narrow, consisting mainly of ridge (Wesley-Hunt and Flynn, 2005: character 51).

45. Presence of M3: (0) present; (1) absent (Wesley-Hunt and Flynn, 2005: character 53).

46. P4 protocone: (0) large, well-developed; (1) reduced or absent (Wesley-Hunt and Flynn, 2005: character 56).

47. Posterior accessory cusps on P3: (0) one cusp present; (1) two cusps present; (2) absent (Wesley-Hunt and Flynn, 2005: character 58).

48. Palatine, relative size: (0) midline length of palatine less than midline length of maxilla; (1) midline length greater than midline length of maxilla (Wesley-Hunt and Flynn, 2005: character 60).

49. Turbinal bones: (0) simple development of maxilloturbinals in nasal cavity; (1) maxilloturbinals large and branching, excluding nasoturbinals from narial opening (Wesley-Hunt and Flynn, 2005: character 62).

50. Jugal: (0) jugal reaches lacrimal, or is separated from it by only thin sliver of maxilla; (1) jugal widely separated from lacrimal, maxilla broadly laps posteriorly over anterior orbital rim (Wesley-Hunt and Flynn, 2005: character 64).

51. Anterior extent of palatine in orbit: (0) broadly contacts lacrimal; (1) fails to contact lacrimal (Wesley-Hunt and Flynn, 2005: character 65).

52. Postorbital constriction: (0) just anterior of frontoparietal suture, near posterior margin of frontal; (1) braincase expanded, with frontals making much greater contribution; fronto–parietal suture located more anteriorly in frontal (Wesley-Hunt and Flynn, 2005: character 66).

53. Posterior entrance of carotid artery into auditory capsule: (0) posterior entry, artery not enclosed in osseous tube; (1) posterior entry, artery enclosed in tube; (2) anterior entry, artery not enclosed in tube; (3) anterior entry, artery not enclosed in tube (Wesley-Hunt and Flynn, 2005: character 67).

54. Entotympanic: (0) fails to ossify, or is only weakly attached to auditory capsule; (1) ossified at least partially, and firmly fused to the skull (Wesley-Hunt and Flynn, 2005: character 68).

55. Ectotympanic contributes to external auditory meatal tube: (0) no; (1) yes (Wesley-Hunt and Flynn, 2005: character 69).

56. Ectotympanic septum: (0) absent; (1) present (Wesley-Hunt and Flynn, 2005: character 70).

57. Entotympanic septum: (0) absent; (1) present (Wesley-Hunt and Flynn, 2005: character 71).

58. Fenestra cochleae: (0) approximately equal in size to fenestra ovalis, cochlear fossula not developed; (1) at least three times the area of oval window, cochlear fossula well developed (Wesley-Hunt and Flynn, 2005: character 72).

59. Major a2 arterial shunt: (0) small; (1) large, intracranial rete (Wesley-Hunt and Flynn, 2005: character 75).

60. Major a4 arterial shunt: (0) present; (1) present, intracranial rete (Wesley-Hunt and Flynn, 2005: character 76).

61. Major anastomosis x: (0) absent; (1) present (Wesley-Hunt and Flynn, 2005: character 77).

62. P1: (0) present: (1) absent (Wesley-Hunt and Flynn, 2005: character 79).

63. P3 lingual cusp: (0) absent; (1) present (Wesley-Hunt and Flynn, 2005: character 80).

64. P4 hypocone: (0) absent; (1) present (Wesley-Hunt and Flynn, 2005: character 83).

65. p1: (0) present; (1) absent (Wesley-Hunt and Flynn, 2005: character 84).

66. Lower molars: (0); subequal in size; (1); m1 much larger than m2–3 and progressive decrease in size from m1–3 (Wesley-Hunt and Flynn, 2005: character 86).

67. M2 hypocone: (0) absent; (1) present (Wesley-Hunt and Flynn, 2005: character 87).

68. m3: (0) present; (1) absent (Wesley-Hunt and Flynn, 2005: character 88).

69. Baculum: (0) small and simple or absent; (1) long, stylized (Wesley-Hunt and Flynn, 2005: character 89).

70. Scapula, postscapular fossa: (0) absent; (1) present (Wesley-Hunt and Flynn, 2005: character 90).

71. Tail: (0) long; (1) reduced (Wesley-Hunt and Flynn, 2005: character 91).

72. Femur, third trocanter: (0) present; (1) absent (Wesley-Hunt and Flynn, 2005: character 94).

73. Cowper's (bulbourethral) gland: (0) present; (1) absent (Wesley-Hunt and Flynn, 2005: character 95).

74. Prostate gland: (0) small/vestigial; (1) large, ampulla bilobed (Wesley-Hunt and Flynn, 2005: character 96).

75. Anal glands: (0) simple; (1) enlarged and having enlarged anal sac (Wesley-Hunt and Flynn, 2005: character 98).

76. Scapula – supraglenoid tubercle morphology: (0) expands out over the glenoid fossa (*Didymictis*); (1) blunt, does not extend over the glenoid fossa (*Vulpavus*) (Spaulding and Flynn, 2012: character 100).

77. Scapula – acromion process angle: Either a short or a long process can be dorsally directed at the acromion process apex, or remain in the same plane as the scapular spine: (0) process angles dorsally (*Vulpavus*); (1) process remains in same plane as the scapular spine (*Canis*) (Spaulding and Flynn, 2012: character 101).

78. Scapula – acromion process length: The acromion process can terminate far distally to the glenoid fossa or terminate at or before the border. A long acromion can be used as a proxy for the presence of clavicles in extinct taxa. (0) process extends past glenoid fossa (*Vulpavus*); 1– process terminates before or at glenoid fossa (*Gulo*) (Spaulding and Flynn, 2012: character 102).

79. Scapula – coracoid process: (0) present, as a large clearly projecting process (*Felis*); (1) extremely small or absent (*Canis*) (Spaulding and Flynn, 2012: character 103).

80. Scapula – scapular spine morphology: Coded while viewing the spine from a ventral view of the scapula. (0) spine forms one continuous, smooth, downward curve (*Öodectes*); (1) spine has a dip or embayment in the curve (*Herpestes*) (Spaulding and Flynn, 2012: character 104).

81. Scapula – metacromion process: (0) present and well developed (*Herpestes*); (1) weak or absent (Otariidae) (Spaulding and Flynn, 2012: character 105).

82. Humerus – indentation on the anterior surface of the capitulum: (0) present (*Hyeanodon*); (1) absent (*Vulpavus*) (Spaulding and Flynn, 2012: character 106).

83. Humerus – olecranon fossa shape: (0) shallow and round (*Vulpavus*); (1) deep and slot-like (*Miacis uintensis*); (2) perforated (*Didymictis*) (Spaulding and Flynn, 2012: character 107).

84. Humerus – medial edge of posterior trochlea: (0) vertical (*Vulpavus*); (1) slanted (*Öodectes*) (Spaulding and Flynn, 2012: character 108).

85. Humerus – delto-pectoral crest: (0) present (*Vulpavus*); (1) absent (*Didymictis*) (Spaulding and Flynn, 2012: character 109).

86. Humerus – medial epicondyle: (0) ends with a well rounded head (*Vulpavus*); (1) poorly defined, appearing more like a blunt tubercle (*Didymictis*) (Spaulding and Flynn, 2012: character 110).

87. Humerus – medial epicondyle orientation (new): (0) lacks curvature (is straight) (*Öodectes*); (1) curves posteriorly (*Didymictis*) (Spaulding and Flynn, 2012: character 111).

88. Humerus – greater tuberosity height: (0) extends past head (*Didymictis*); (1) flush with head in height (*Vulpavus*) (Spaulding and Flynn, 2012: character 112).

89. Humerus – posterior trochlea: (0) not bound by high ridges (*Öodectes*); (1) bound by high ridges (*Canis*) (Spaulding and Flynn, 2012: character 113).

90. Humerus – brachial flange: (0) present and large, extending out from the body of the bone as a flat surface (*Vulpavus*); (1) small, nothing but a small raised line of bone (*Didymictis*) (Spaulding and Flynn, 2012: character 114).

91. Humerus – lesser tuberosity with a crest or ridge of bone leading from this feature down the shaft: (0) present (*Didymictis*); (1) absent (*Canis*) (Spaulding and Flynn, 2012: character 115).

92. Humerus – trochlea extent: (0) extends distally past capitulum when viewed anteriorly (*Didymictis*); (1) two articular surfaces are more inline (*Vulpavus*) (Spaulding and Flynn, 2012: character 116).

93. Humerus – epicondylar foramen: (0) present and round (*Hyaenodon*); (1) present and elongated (*Vulpavus*) (Spaulding and Flynn, 2012: character 117).

94. Humerus – distal L-shaped ridge of bone on capitulum in distal view: (0) present (*Vulpavus*) (1) absent (*Felis*) (Spaulding and Flynn, 2012: character 118).

95. Humerus – orientation of bone on the lateral distal margin: (0) faces laterally (*Hyaenodon*); (1) faces posteriorly (*Vulpavus*) (Spaulding and Flynn, 2012: character 119).

96. Humerus – ulnar collateral ligament insertion site size: (0) very large, forming a distinct circular pit (*Didymictis*); (1) small, forming only a shallow depression (*Vulpavus*) (Spaulding and Flynn, 2012: character 120).

97. Humerus – greater tuberosity angle: (0) greater tuberosity angled away from head; smooth arch is not formed with lesser tuberosity (*Didymictis*); (1) greater tuberosity more flush with head (*Vulpavus*) (Spaulding and Flynn, 2012: character 121).

98. Humerus – prominence of bicipital groove: (0) groove is very noticeable and deep (*Nandinia*); (1) groove is very subtle if noticeable at all (*Civetticits*) (Spaulding and Flynn, 2012: character 122).

99. Humerus – capitulum shape: (0) flat for the whole length with a uniform distal margin (*Thinocyon*); (1) rounded (*Vulpavus*) (Spaulding and Flynn, 2012: character 123).

100. Humerus - tricipital line: (0) large and distinctive (*Didymictis*); (1) reduced (*Nandinia*) (Spaulding and Flynn, 2012: character 124).

101. Ulna – semi-lunar notch distal border morphology: (0) W-shaped distal border; an indentation occurs between the articular surface with the radius and the rest of the facet (*Öodectes*); (1) indentation lacking (*Canis*) (Spaulding and Flynn, 2012: character 125).

102. Ulna – semi-lunar notch proximal border extent: (0) proximal ridge extends far from shaft surface (*Hyeanodon*); (1) proximal ridge flush with shaft surface (*Öodectes*) (Spaulding and Flynn, 2012: character 126).

103. Ulna – *m. bracialis* insertion site: (0) present (*Vulpavus*); (1) absent (*Ailurus*) (Spaulding and Flynn, 2012: character 127).

104. Ulna – *m. bracialis* insertion site position: (0) on anterior surface of ulna (*Vulpavus*); (1) on the medial margin of the shaft (*Öodectes*) (Spaulding and Flynn, 2012: character 128).

105. Ulna – radial notch curvature: (0) absent (*Vulpavus*); (1) present (*Ailurus*) (Spaulding and Flynn, 2012: character 129).

106. Ulna – deep tendon groove on proximal end of ulna: (0) present (*Hyaenodon*); (1) absent (*Vulpavus*) (Spaulding and Flynn, 2012: character 130).

107. Ulna – deep tendon groove on proximal end of ulna (Heinrich and Rose, 1997): (0) present (*Hyaenodon*); (1) absent (*Vulpavus*) (Spaulding and Flynn, 2012: character 131).

108. Ulna – olecranon process shape: (0) mediolaterally robust, square in shape (*Vulpavus*); (1) mediolaterally compressed (*Felis*) (Spaulding and Flynn, 2012: character 132).

109. Ulna – anconeal process extent: (0) projecting from the shaft, shelf like (*Didymictis*); (1) flush with shaft (*Vulpavus*) (Spaulding and Flynn, 2012: character 133).

110. Ulna – proximal border of semi-lunar notch, position: (0) lateral to the shaft (*Hyaenodon*); (1) centered with respect to the shaft (*Öodectes*) (Spaulding and Flynn, 2012: character 134).

111. Ulna – anteriormedial protuberuance development (Taylor, 1974): (0) well developed (*Nandinia*); (1) small (*Canis*) (Spaulding and Flynn, 2012: character 135).

112. Ulna – groove on lateral side of shaft: (0) present (*Hyaenodon*); (1) absent (*Vulpavus*) (Spaulding and Flynn, 2012: character 136).

113. Ulna shape – sigmoidal; the ulna is used as a proxy for the curved nature of all forelimb bones noted by Matthew (1909): (0) sigmoidal (*Vulpavus*); (1) straight (*Canis*) (Spaulding and Flynn, 2012: character 137).

114. Ulna – radial notch orientation (Heinrich and Rose, 1997): (0) faces anteriorly (*Didymictis*); (1) faces more laterally (*Vulpavus*) (Spaulding and Flynn, 2012: character 138).

115. Radius – radial head shape: (0) round (*Vulpavus*); (1) oval (*Didymictis*) (Spaulding and Flynn, 2012: character 139).

116. Radius – large scaphoid articulation surface: (0) present (*Didymictis*); (1) surface small (*Vulpavus*) (Spaulding and Flynn, 2012: character 141).

117. Radius – capitular eminence of radial head development; (0) small (*Vulpavus*); (1) large, disrupts radial rim (*Canis*) (Spaulding and Flynn, 2012: character 142).

118. Radius – distal articulation surface shape: (0) with a deep sulcus (*Erinaceus*); (1) smooth, lacks a deep sulcus (*Vulpavus*) (Spaulding and Flynn, 2012: character 143).

119. Carpus – cuneiform shape in proximal view: (0) triangular (*Nandinia*); (1) rectangular (*Vulpavus*) (Spaulding and Flynn, 2012: character 144).

120. Carpus – proximal surface of scapholunar, curvature: (0) fully convex (*Nandinia*); (1) convex and concave (*Herpestes*) (Spaulding and Flynn, 2012: character 145).

121. Carpus – uniciform width (new): (0) as wide as trapezoid and magnum combined (*Canis*); (1) small, only as wide as magnum alone (*Nandinia*) (Spaulding and Flynn, 2012: character 146).

122. Carpus – trapezium position (Yalden, 1970): (0) on the posterior surface of the trapezoid (*Canis*); (1) on the radial surface of the trapezoid (*Felis*) (Spaulding and Flynn, 2012: character 147).

123. Carpus – metacarpal III overlaps IV proximally (Bryant, 1991): (0) absent (*Canis*); (1) present (*Vulpavus*) (Spaulding and Flynn, 2012: character 148).

124. Carpus – distal surface of scapholunar shape (Yalden, 1970): (0) relatively smooth/even (*Canis*); (1) a sharp projection exists between the magnum and trapezoid (*Ursus*) (Spaulding and Flynn, 2012: character 149).

125. Carpus – cuneiform articulation with ulna, position: (0) on medial (radial) margin (*Felis*); (1) on distal surface of ulna (*Ursus*) (Spaulding and Flynn, 2012: character 150).

126. Carpus –metacarpal II strongly overlaps III proximally: (0) overlap small or absent (*Canis*); (1) overlap present and substantial (*Felis*) (Spaulding and Flynn, 2012: character 151).

127. Carpus – metacarpal length: (0) metacarpal lengths are equivalent to sum of phalanges (*Vulpavus*); 1– phalanges are longer than metacarpals (Otariidae) (Spaulding and Flynn, 2012: character 152).

128. Carpus – medial phalanx distal articular surface symmetry: (0) symmetrical (*Vulpavus*); (1) asymmetrical (*Felis*) (Spaulding and Flynn, 2012: character 153).

129. Carpus – proximal phalanges compressed dorsoventrally: (0) absent (*Vulpavus*); (1) present (*Hoplophoneus*) (Spaulding and Flynn, 2012: character 154).

130. Carpus – lateral excavation of the medial phalanx; (0) absent (*Vulpavus*); (1) present (*Felis*) (Spaulding and Flynn, 2012: character 155).

131. Femur – lesser trochanter orientation: (0) projects posteriorly (*Didymictis*); (1) projects medially (*Vulpavus*) (Spaulding and Flynn, 2012: character 156).

132. Femur – intertrochanteric crest extent: (0) extends to lesser trochanter (*Didymictis*); (1) becomes flush with shaft before reaching the lesser trochanter (*Vulpavus*) (Spaulding and Flynn, 2012: character 157).

133. Femur – position of lesser trochanter relative to the third trochanter: (0) third trochanter is lower (*Vulpavus*); (1) third trochanter is roughly at the same level (*Didymictis*) (Spaulding and Flynn, 2012: character 158).

134. Femur – supracondylar tuberosities: (0) absent (*Vulpavus*); (1) presence of two or more raised tuberosities just proximal to the condyles of the femur on the posterior shaft (*Canis*) (Spaulding and Flynn, 2012: character 160).

135. Femur – height of greater trochanter relative to head of femur: (0) greater trochanter is higher or sub-equal (*Vulpavus*); (1) greater trochanter is lower than head of femur (*Ursus*) (Spaulding and Flynn, 2012: character 161).

136. Femur – medial condyle morphology: (0) proximal edge of the articular surface of condyles are flush with the shaft, due to the lack of development of a condylar neck (*Vulpavus*); (1) proximal edge of the articular surface of condyles are not flush with the shaft, due to the development of a condylar neck (*Canis*) (Spaulding and Flynn, 2012: character 162).

137. Femur – lesser trochanter development: (0) strong, prominently projecting feature (*Vulpavus*); (1) small, barely more than a small bump or ridge on the shaft (*Ursus*) (Spaulding and Flynn, 2012: character 163).

138. Femur – greater trochanter broadest surface, orientation: (0) faces laterally (*Vulpavus*); (1) faces posteriorly (*Canis*) (Spaulding and Flynn, 2012: character 164).

139. Femur – patellar groove shape: (0) deep and narrow (*Didymictis*); (1) wide and flat (*Vulpavus*) (Spaulding and Flynn, 2012: character 166).

140. Femur – position of greater trochanter relative to shaft: (0) greater trochanter over distal midline (*Erinaceus*); (1) greater trochanter lateral to midline (*Didymictis*) (Spaulding and Flynn, 2012: character 167).

141. Tibia – deep groove on the posterior surface of the tibia (Matthew, 1909): (0) present (*Vulpavus*); (1) absent (*Canis*) (Spaulding and Flynn, 2012: character 169).

142. Tibia – posterior bone spur on distal tibia: (0) presence of a prominent bone spur on the posterior margin (*Vulpavus*); (1) spur absent (*Nandinia*) (Spaulding and Flynn, 2012: character 170).

143. Tibia – contact of inner borders of condyles: (0) in contact (*Vulpavus*); (1) separate (*Canis*) (Spaulding and Flynn, 2012: character 171).

144. Tibia – internal (medial) malleolus morphology: (0) forms a clear and distinct well-defined point (*Vulpavus*); (1) indistinct, forming a general extension of the medial surface of the tibia (*Civettictis*) (Spaulding and Flynn, 2012: character 172).

145. Pes – dorsal surface of astragalus, shape (Matthew, 1909): (0) smooth (*Vulpavus*); (1) grooved (*Canis*) (Spaulding and Flynn, 2012: character 174).

146. Pes – astragalus – height of fibular facet: (0) height subequal to length, resulting in a roughly square shaped facet (*Vulpavus*); (1) height much less than length, resulting in a more crescent shaped feature (*Canis*) (Spaulding and Flynn, 2012: character 175).

147. Pes – astragalar head shape when viewed dorsally: (0) rounded (*Vulpavus*); (1) flattened (*Canis*) (Spaulding and Flynn, 2012: character 176).

148. Pes – astragalus fossa, on the lateral edge, posterior ventral quadrant: (0) present (*Didymictis*); (1) absent (*Vulpavus*) (Spaulding and Flynn, 2012: character 178).

149. Pes – astragalus lateral margin, anterior ventral edge expansion: (0) lateral expansion present (*Vulpavus*); (1) expansion absent, creating a much smoother margin (*Procyon*) (Spaulding and Flynn, 2012: character 179).

150. Pes – astragalar head medial articulation surface extent: (0) extends backwards a great distance, past the border of the sustentacular facet (*Hyaenodon*); (1) short, does not extend past the start of the neck (*Vulpavus*) (Spaulding and Flynn, 2012: character 180).

151. Pes – astragalus sustentacular facet shape: (0) has clear edges, is somewhat convex, and does not extend into gully (*Vulpavus*); (1) is more flat than convex and extends into gully (*Canis*) (Spaulding and Flynn, 2012: character 181).

152. Pes – astragalar foramen; (0) present and dorsally positioned (*Vulpavus*); (1) present and posteriorly positioned (*Hyaenodon*); (2) absent (*Canis*) (Spaulding and Flynn, 2012: character 182).

153. Pes – astragalus, posterior ridge for ligament attachments, presence: (0) present, high (*Vulpavus*); (1) low or absent (*Felis*) (Spaulding and Flynn, 2012: character 183).

154. Pes – astragalus, orientation of posterior ridge for ligament attachments: (0) orientated at an oblique angle relative to the long axis of the astragalar trochlea (*Vulpavus*); (1) orientated in line with the trochlea (*Canis*) (Spaulding and Flynn, 2012: character 184).

155. Pes – astragalus-tibia articulation surface, extent: (0) covers entire posterior dorsal surface (*Canis*); (1) restricted, fails to cover entire posterior dorsal surface, leaving a gap in the lateral posterior quadrant (*Vulpavus*) (Spaulding and Flynn, 2012: character 185).

156. Pes – astragalus, cotylar fossa presence: (0) present (*Didymictis*); (1) absent (*Vulpavus*) (Spaulding and Flynn, 2012: character 187).

157. Pes – Calcaneus, sustentaculum position (Heinrich and Rose, 1997): (0) far from anterior border, roughly in the middle of the calcaneus (*Didymictis*); (1) close to anterior border (*Vulpavus*) (Spaulding and Flynn, 2012: character 188).

158. Pes – Calcaneus, peroneal tubercle development: (0) weakly developed, little more than a ridge (*Didymictis*); (1) well developed (*Vulpavus*) (Spaulding and Flynn, 2012: character 189).

159. Pes – astragalus neck development: (0) absent (lacks a clearly defined neck of astragalus) (*Erinaceus*); (1) present (*Vulpavus*) (Spaulding and Flynn, 2012: character 190).

160. Pes – calcaneus, cuboid facet shape: (0) irregularly shaped (*Didymictis*); (1) round (*Vulpavus*) (Spaulding and Flynn, 2012: character 191).

161. Pes – calcaneus, cuboid facet orientation: (0) angled dorsally (*Vulpavus*); (1) in planes other than dorsal (*Didymictis*) (Spaulding and Flynn, 2012: character 192).

162. Pes – calcaneus, fibular facet (Flynn and Galiano, 1982): (0) present (*Didymictis*); (1) absent (*Vulpavus*) (Spaulding and Flynn, 2012: character 193).

163. Pes – calcaneus –dorsal facet morphology: (0) smooth (*Vulpavus*); (1) clearly defined, sharp corner (rather than a smooth curve) (*Canis*) (Spaulding and Flynn, 2012: character 194).

164. Pes – cuboid, contact with metatarsal V (Bryant, 1991): (0) small (less than 40%) articular surface for metatarsal V (*Dinictis*); (1) large, articular surface for metatarsal V at least 40% of distal surface (*Canis*) (Spaulding and Flynn, 2012: character 195).

165. Pes – cuboid shape: (0) relatively rectangular (*Didymictis*); (1) wider proximally than distally (*Vulpavus*) (Spaulding and Flynn, 2012: character 196).

166. Pes – cuboid, tubercle for the long plantar ligament, position (Heinrich and Rose, 1997): (0) distal to the ectocuneiform articulation facet (*Didymictis*); (1) even with the ectocuneiform articulation facet (*Vulpavus*) (Spaulding and Flynn, 2012: character 197).

167. Pes – cuboid/astragalus contact (Matthew, 1909): (0) present (*Thinocyon*); (1) absent (*Vulpavus*) (Spaulding and Flynn, 2012: character 198).

168. Pes – navicular height: (0) height less than width (*Vulpavus*); (1) height roughly equal to or greater than width (*Canis*) (Spaulding and Flynn, 2012: character 199).

169. Pelvis – ilium, anterior expansion: (0) not expanded (*Felis*); (1) expanded dorsoventrally (*Canis*) Primitively for Carnivoramorpha the anterior ilium is not dorsoventrally expanded;

however in *Canis*, *Ursus*, *Hyaena*, and *Civettictis* a clear expansion is seen (Spaulding and Flynn, 2012: character 200).

170. Pelvis – ischial spine position: (0) located just posterior of the border of the acetabulum (*Didymictis*); (1) far posterior from acetabulum (*Vulpavus*); (2) spine absent (*Erinaceus*) (Spaulding and Flynn, 2012: character 201).

171. Pelvis – dorsal margin of acetabulum, position: (0) even with or above dorsal surface of pelvis (*Vulpavus*); (1) ventral to dorsal surface of pelvis (*Canis*) (Spaulding and Flynn, 2012: character 202).

172. Pelvis – angle at pubic symphysis: (0) 'U-like' (*Canis*); (1) 'V-like' (*Felis*) (Spaulding and Flynn, 2012: character 203).

173. Pelvis – ilium, anterior region morphology: (0) broad and flat (*Canis*); (1) divided by a distinct ridge running antero-posteriorly (*Vulpavus*) (Spaulding and Flynn, 2012: character 204).

175. Pelvis – ilium, ventral surface morphology: (0) broad and flat (*Thinocyon*); (1) narrow (*Vulpavus*) (Spaulding and Flynn, 2012: character 205).

176. Atlas – alar foramen: (0) absent, only a notch is present (*Canis*); (1) present, confluent with lateral vertebral foramen (*Herpestes*); (2) present, separate from lateral vertebral foramen (*Procyon*) (Spaulding and Flynn, 2012: character 207).

177. Atlas – transverse processes, orientation: (0) projects at right angle from the body (*Canis*); (1) extends posteriorly at an acute angle to the body (*Nandinia*) (Spaulding and Flynn, 2012: character 208).

178. Atlas – ventral arch length (Gaubert et al., 2005): (0) equal to or shorter than dens of axis (*Canis*); (1) longer than dens of axis (*Civettictis*) (Spaulding and Flynn, 2012: character 209).

179. Axis – body length: (0) roughly as long as it is wide (*Vulpavus*); (1) elongated relative to its width (*Felis*) (Spaulding and Flynn, 2012: character 210).

180. Cervical vertebrae – keel: (0) large ventral keel present (*Nandinia*); (1) ventral keel absent (*Dinictis*) (Spaulding and Flynn, 2012: character 211).

181. Cervical vertebrae – spinous processes, size: (0) large (*Canis*); (1) small (*Felis*) (Spaulding and Flynn, 2012: character 212).

182. Cervical vertebrae – dorsal lateral margin shape: (0) concave (*Öodectes*); (1) convex (*Felis*) (Spaulding and Flynn, 2012: character 213).

183. Sacrum – size compared to pelvis: (0) small, does not reach border of acetabulum (*Canis*); (1) large, reaches border of acetabulum (*Felis*) (Spaulding and Flynn, 2012: character 215).

184. Sacrum – neural spines: (0) clear and distinct from one another (*Nandinia*); (1) fused to one another, appearing as one long keel (*Canis*) (Spaulding and Flynn, 2012: character 216).

185. Alisphenoid, foramen ovale (position): (0) anterior to glenoid fossa; (1) medial to glenoid fossa. Comparisons made to the posterior-most edge of the glenoid fossa, not the process. Serves for the passage of the trigeminal nerve (V), internal maxillary artery and the medial meningeal artery (modified from Gaubert et al., 2005: character 71).

186. Basisphenoid, medial lacerate foramen: (0) covered by bullae; (1) anteriomedial to bullae (e.g., *Herpestes*). [Serves for the passage of the ascending pharyngeal artery.] (Gaubert et al., 2005: character 79).

187. Ectotympanic/entotympanic division: (0) not externally visible; (1) externally visible with infolding at junction, without clear suture; (2) externally visible, with clear suture. [In the viverrids, the point of contact between the two elements is marked by an inbending of the plates of bone. In the other feliforms, although one can detect the point of contact, it is because of structural differences.] (Modified from Gaubert et al., 2005: character 85).

188. Entotympanic, ventral floor ossification: (0) ossified; (1) unossified (i.e. *Nandinia*) (modified from Gaubert et al., 2005: character 102).

189. Vagina processus hyoideus: (0) confluent with stylomastoid foramen (giving the appearance of one foramen); (1) slightly separate from stylomastoid foramen (Gaubert et al., 2005: character 129).

190. i1- i3 projection: (0) extends upward; (1) procumbent (less than 45 degrees) (Gaubert et al., 2005: character 151).

191. C1, flanges: (0) posterior flange present; (1) absent; (2) anterior and posterior flanges present (Gaubert et al., 2005: character 156).

192. P3 number or roots: (0) two roots; (1) one root; (2) three roots (Gaubert et al., 2005: character 164).

193. P3, posterolingual cingulum: (0) present, reduced; (1) present, broad; (2) vestigial/absent (Gaubert et al., 2005: character 165).

194. p3, talonid: (0) absent; (1) present (Gaubert et al., 2005: character 169).

195. P4, parastyle: (0) absent/vestigial; (1) present, small (less than size of protocone); (2) present, large (near equal to protocone); (3) present, larger than protocone (Gaubert et al., 2005: character 172).

196. P4 posterolingual cingulum: (0) present; (1) vestigial; (2) absent (Gaubert et al., 2005: character 177).

197. p4 talonid: (0) absent/vestigial; (1) present (Gaubert et al., 2005: character 178).

198. p4 posterior accessory cusps: (0) 2 cusps, linear; (1) 1 cusp; (2) no cusps; (3) 2 or more cusps, nonlinear (Gaubert et al., 2005: character 179).

199. P4-M1 carnassial embrasure pit: (0) present; (1) absent (Gaubert et al., 2005: character 181).

200. M1 roots: (0) three roots; (1) two roots; (2) one root (Gaubert et al., 2005: character 183).

201. m1, trigonid: (0) present, considerably higher than talonid; (1) present, near equal in height to talonid; (2) absent (modified from Gaubert et al., 2005: character 187).

202. m1, trigonid proportion: (0) length less than talonid; (1) length near equal length of talonid; (2) trigonid length is 60% to 73% of total length; (3) 77-87%; (4) 88% and higher; (5) no talonid (modified from Gaubert et al., 2005: character 188; Barrett, 2016: character 30).

203. m1 metaconid: (0) large; (1) considerably smaller than paraconid; (2) absent (Gaubert et al., 2005: character 189).

204. m1, protoconid : (0) present; (1) absent (Gaubert et al., 2005: character 190).

205. m1 entoconid: (0) present; (1) absent (Gaubert et al., 2005: character 191).

206. m1 hypoconid: (0) present; (1) absent (Gaubert et al., 2005: character 192).

207. m1, hypoconulid: (0) absent; (1) present (Gaubert et al., 2005: character 193).

208. m1, small cusp between hypoconid and protoconid: (0) absent; (1) present (Gaubert et al., 2005: character 194).

209. M2, paracone and metacone: (0) metacone and paracone present, paracone larger; (1) metacone absent; (2) tooth without distinguishable cusps; ? = tooth absent (Gaubert et al., 2005: character 195).

210. M2, roots: (0) three roots; (1) two roots; (2) one root; (3) tooth absent (modified from Gaubert et al., 2005: character 198).

211. m2, cusps: (0) high trigonid with extremely elongate talonid due to large hypoconulid, tooth elongate oval outline; (1) talonid not elongate, tooth oval outline, no enlarged hypoconulid; (2) low trigonid, extremely elongate with low, well developed talonid cusps; (3) low trigonid, well developed talonid cusps; (4) tooth with cusps but no clear trigonid or talonid; (5) tooth without clearly defined cusps; (6) absent (modified from Gaubert et al., 2005: character 202).

212. Buccal cingulum, upper molars: (0) small/not developed; (1) enlarged (Gaubert et al., 2005: character 206).

213. Mandible, mandibular symphysis: (0) strong (well fused); (1) weak (not well fused) (Gaubert et al., 2005: character 212).

214. Mandible, medial shelf of angular process: (0) present, small ridge; (1) present, wide shelf; (2) absent (Gaubert et al., 2005: character 214).

215. p4 anterior accessory cusp: (0) absent; (1) smaller than posterior; (2) about equal to posterior; (3) larger than posterior (Gaubert et al., 2005: character 221).

216. Volume contribution of the feloid auditory bulla: (0) caudal entotympanic envelopes ectotympanic chamber (e.g. Felidae); (1) both chambers meet over the petrosal and display an external 'infolding' at their juncture with a septum oblique to the long axis of the skull, such that the caudal entotympanic penetrates the anterointernal (rostromedial) corner of the auditory region (e.g. viverrids); (2) both chambers meet over the petrosal and display an external 'infolding' at their juncture with a septum orthogonal to the long axis of the skull (e.g. herpestids); (3) ectotympanic chamber dominates with caudal entotympanic chamber restricted to posterior third of bulla with the division separating anterior and posterior chambers rostral of the mastoid and paroccipital processes (e.g. Ictitheriines); (4) ectotympanic chamber dominates bulla, partially or totally overlaying caudal entotympanic chamber via ventral overgrowth,

recumbent septum concealing posterior chamber within mastoid and paroccipital process (e.g. *Crocuta*, *Hyaena*): (5) anterior chamber formed by rostral entotympanic or pseudoseptum.

217. Mastoid invasion by bulla: (0) absent; (1) present.

218. P4 nimravid "parastyle": (0) absent; (1) present (Barrett et al., 2021: character 222).

219. P2: (0) double-rooted; (1) single-rooted; (2) absent (Barrett et al., 2021: character 224).

220. p3 posterior cusps: (0) no cusps; (1) one cusp (posterior cingular cusp); (2) two cusps (posterior cingular cusp and posterior accessory cusp) (Barrett et al., 2021: character 229).

221. Basicranial foramina: (0) petrobasilar venous sinus and sigmoid sinus merge intracranially and exit the posterior lacerate (jugular) foramen; (1) veins merge extracranially, passing through the petrobasilar and posterior lacerate foramina respectively (Barrett et al., 2021: character 231).

222. P4 protocone: (0) medial or posterior to paracone; (1) anterior to paracone or paracone-parastyle juncture; (2) anterior face of protocone approximately level with anterior face of parastyle; (3) protocone extending anteriorly of parastyle (modified from Werdelin and Solounias, 1991: character 9).

223. Shape of dentary tooth row: (0), tooth row straight; (l), tooth row curved, or convex (Werdelin and Solounias, 1991: character 10).

224. P4 metacone/metastyle blade length to paracone length ratio: (0): 0.54 or less; (1): 0.6-0.99; (2): 1-1.3; (3): 1.4 and greater (modified from Werdelin and Solounias, 1991: character 11).

225. Placement of camassials in tooth row: (0) carnassials in line with tooth row, i.e. at an angle relative to the sagittal plane); (l) carnassials parallel to sagittal plane (Werdelin and Solounias, 1991: character 14).

226. Placement of anterior accessory cusp of p4: (0) free of main cusp; (l) appressed to main cusp (Werdelin and Solounias, 1991: character 14).

227. Shape of anterior face of p3: (0) concave/straight; (l) convex (Werdelin and Solounias, 1991: character 15).

228. Position of infraorbital foramen: (0) positioned anterior to middle of P3; (1) positioned above middle to posterior of P3; (2) positioned above anterior edge of P4; (3) positioned above mid-posterior portion of P4 (modified from Werdelin and Solounias, 1991: character 22).
229. Position of anterior margin of orbit: (0) above or behind metastylar blade of P4; (1) above the anterior end of P4; (2) above P3 (modified from Werdelin and Solounias, 1991: character 23).

230. Suture between premaxillary and frontal on snout: (0) absent; (l) present (Werdelin and Solounias, 1991: character 24).

231. Size of inferior oblique muscle fossa at maxillary-lacrimal suture postero-dorsal to infra-orbital foramen: (0) small; (l) large; (2) absent (modified from Werdelin and Solounias, 1991: character 25).

232. Inferior oblique muscle Fossa II at juncture between maxillary, lacrimal, and Frontal: (0) absent; (l) present (Werdelin and Solounias, 1991: character 26).

233. Sphenoid foramen and postpalatine foramen position: (0) well separated, distinct foramina; (l) foramina located close together in a single depression (Werdelin and Solounias, 1991: character 27).

234. The contribution of the maxilla to the antero-internal rim of the zygomatic arch: (0) small to none; (l) maxillary makes up a substantial portion of the antero-dorsal margin of the zygomatic arch (Werdelin and Solounias, 1991: character 28).

235. Shape of basioccipital in ventral view: (0) flat; (l) lateral ridges and central groove (Werdelin and Solounias, 1991: character 32).

236. Position of premaxillary-maxillary suture on palate: (0) near the middle of the incisive fossa; (l) at the postero-lateral margin of the incisive fossa (Werdelin and Solounias, 1991: character 33).

237. Shape of jugal-maxillary suture in external view: (0) strongly sinusoid; (1) angled downwards posteriorly in a straight or weakly sinusoid manner; (2) horizontally straight; (3) vertical (modified from Werdelin and Solounias, 1991: character 36).

238. Position of external auditory meatus: (0) far forwards of nuchal crest; (l) level with nuchal crest (Werdelin and Solounias, 1991: character 43).

239. Shape of nuchal crest: (0) antero-posteriorly inclined; (1) nearly vertical or vertical (Werdelin and Solounias, 1991: character 44).

240. Size of metacarpal 1: (0) metacarpal 1 has a long, slender diaphysis resembling the other four metacarpals; (1) metacarpal 1 has a blunt and rectangular shape (e.g. felids); (2) vestigial (modified from Werdelin and Solounias, 1991: character 45).

241. Angle of scapular spine in posterior view: (0) angled; (1) straight (Werdelin and Solounias, 1991: character 47).

242. Relative width of p3 (ranked in order by ratio of Wp3 to Lp3): (0) 0.2-0.39; (1) 0.4-0.6; (2) 0.61-0.66; (3) 0.69 and greater (Tseng and Wang, 2007: character 12).

243. Relative width of p4 (ranked in order by ratio of Wp4 to Lp4): (0) 0.38 and less; (1) 0.40-0.54; (2) 0.55-0.68; (3) 0.72 and greater (Tseng and Wang, 2007: character 13).

244. Relative width of P3 (ranked in order by ratio of WP3 to LP3): (0) 0.38 and less; (1) 0.4-0.65; (2) 0.66-0.79; (3) 0.81 and above (Tseng and Wang, 2007: character 14).

245. Labiolingual compression of the C1: (0) very slightly compressed (length/breadth index smaller than 1.5); (1) markedly compressed (index between 1.5 and 1.8); (2) very compressed (index 1.81-3.0); (3) extremely compressed 4.0 and greater (Robles et al., 2013: character 3).

245. C1 vertical grooves: (0) absent; (1) present (Robles et al., 2013: character 4).

247. P3 anterior cingulum cusp: (0) absent; (1) present (Robles et al., 2013: character 7).

248. P4 preparastyle: (0) absent; (1) present (Robles et al., 2013: character 10).

249. p2: (0) present; (1) absent (Robles et al., 2013: character 16).

250. Orbit: (0) open; (1) closed (Robles et al., 2013: character 23).

251. Position of M1. Polarity: (0) distal to P4; (1) medial to P4 (Robles et al., 2013: character 27).

252. c1: (0) larger than i3; (1) same size (Robles et al., 2013: character 31).

253. Ratio P4 length /p4 length: (0) 0.93 and less; (1) 1.0-1.87; (2) 1.95-2.1; (3) 2.2 and higher (modified from Robles et al., 2013: character 32).

254. Masseteric fossa on the lateral surface of the maxilla and jugal: (0) shallow or absent; (1) deep with distinct dorsal margin (Barrett, 2016: character 3).

255. Fossa on the medial face of the zygomatic arch, below the postorbital process: (0) no fossa; (1) presence of a marked fossa (Peigné, 2003: character 12).

256. Zygomata shape in dorsal view: (0) broadly circular; (1) triangular (Barrett, 2016: character 5).

257. Shape of the glenoid socket of the craniomandibular joint: (0) anterior lip is missing; (1) posterior lip of the glenoid socket projects more ventrally than anterior lip; (2) anterior lip and posterior lip project equally ventrally (Barrett, 2016: character 10).

258. Anterior mandible position: (0) in line with the tooth row, mandibular border of cheek tooth row is in the same plane as the mandibular border of the incisors and canines; (1) elevated above tooth row; (2) cheek teeth and anterior teeth brought again into same plane by elevation of cheek teeth on pedestal (Barrett, 2016: character 13).

259. Development and orientation of the coronoid process of the dentary: (0) posteriorly

orientated posterior border without surpassing the level of the mandibular condyle; (1) surpassing the level of the mandibular condyle; (2) vertically orientated posterior border; (3) anteriorly orientated posterior border (Barrett, 2016: character 20).

260. Size of the genial flange of the dentary in adult taxa. Measured as the height of the genial flange from the anterior portion of the postcanine diastema to the ventral apex of the genial flange/length of dentary from the posterior articular surface to the most anterior aspect: (0) no flange, the ventral rim of the chin is regularly curved; (1) no flange, but the ventral rim of the chin is distinctly angulate; (2) short flange, between 22 and 31% of the total length of mandible; (3) deep flange, 32-50% of the total length of the mandible; (4) extremely deep flange, 54% or more of the total mandibular length (Barrett, 2016: character 15).

261. Mental fossa. Fossa on the ventral-internal face of the chin: (0) no fossa; (1) fossa present and marked (Barrett, 2016: character 16).

262. Incisors: (0) spatulate; (1) mostly spatulate, I3 caniform; (2) all caniform (Barrett, 2016: character 17).

263. C1 length. Mesial-distal length of C1 measured at the dentine/enamel boundary: (0) less than that of P4; (1) greater than that of P4 (Barrett, 2016: character 18).

264. Serration density of permanent upper canines per millimeter. Measured over an average of 5 mm: (0) none; (1) 0.7-2.7; (2) 2.8-5.0; (3) $\geq$ 5.5 (modified from Barrett, 2016: character 19).

265. Size of P3 vs. size of P4. Measured as a ratio of crown height (base of cingulum to apex of tooth) on adult minimally worn teeth: (0) 0.69-1.1; (1) 1.2 and greater; (2) 0.48-0.69; (3) 0.45 and lower (modified from Barrett, 2016: character 20).

266. p3 crown height compared to p4: (0) 0.6-0.98; (1) 1.0 and greater; (2) less than 0.58; (3) p3 absent (modified from Barrett, 2016: character 26).

267. Cheek tooth serrations. Serrations on adult minimally worn cheek teeth: (0) absent; (1) present (Barrett, 2016: character 31).

268. Articulation between the calcaneum and navicular : (0) absent; (1) present (Barrett, 2016: character 33).

269. Anterior palatine canal opening location: (0) level with P3; (1) between P2 and P3; (2) P4; (3) M1; (4) P2 or anterior (modified from Bryant, 1996: character 4).

270. Position of nasals relative to maxilla-frontal suture: (0) nasals extend beyond the maxillofrontal suture; (1) nasals shortened, the posterior border lies across or anterior to the maxillofrontal suture (Peigné, 2003: character 9).

271. P4, orientation of the protocone: (0) anterolingually projected; (1) lingually projected (modified from Peigné, 2003: character 23).

272: Processus muscularis on malleus: (0) short, cone-shaped and with tapering apex; (1) distinctly enlarged and cylindrical; (2) absent (modified from Christiansen, 2008: character 2).

273: Lambdoidal-squamous sutures: (0) converging along lamboid crest; (1) separate (modified from Christiansen, 2008: character 12).

274. Dorsal part of frontoparietal (coronal) suture: (0) smooth, lacking a parietal process; (1) suture irregular with a distinct, often very large, medio-dorsally directed parietal process (Christiansen, 2008: character 13).

275. Dorsal Jugal-squamosal suture in zygomatic arch: (0) abuts the postorbital process; (1) does not abut the postorbital process (modified from Christiansen, 2008: character 19).

276. Paroccipital process: (0) ventrally directed; (1) posteriorly directed (modified from Christiansen, 2008: character 22).

277. Angle of long axis of bulla to long axis of skull: (0) Less than or equal to 19°; (1) 20°-27°; (2) 28°-37° (modified from Christiansen, 2008: character 29).

278: Entotympanic process: (0) narrow and raised; (1) wide and flattened; (2) absent (modified from Christiansen, 2008: character 30).

279. Upper incisor arcade: (0) strongly parabolic; (1) slightly parabolic such that the anterior edge of I3 does not contact a straight edge held across the anterior of the arcade; (2) straight (modified from Christiansen, 2013: character 1).

280. P4 anterior cingulum: (0) indistinct; (1) distinct and often forming a ridge; (2) forming a distinct ectoparastyle (Christiansen, 2013: character 11).

281. Mediolateral width of P3 across the metacone relative to width across the paracone: (0) 56 and less; (1) 58- 68; (2) narrow (~70–93%); (3) wide (~95–130%) (modified from Christiansen, 2013: character 17).

282. Relative height of the m1 major cusps, measured from tip of cusp to base of cingulum: (0) 61% and lower; (1) height of paraconid low compared with height of protoconid (65–93%); (2) height of paraconid tall compared with height of protoconid (95–130%). (modified from Christiansen, 2013: character 24).

283. Relative length of p4: (0) 7% and lower; (1) small relative to mandible length (~7.5–9%); (2) large relative to mandible length (~10–15%) (modified from Christiansen, 2013: character 26).

284. Snout area elevation compared with braincase: (0) snout area low, line from dorsal narial aperture to juncture of occipital/sagittal crest lies below frontal postorbital process; (1) snout area elevated, line passes above frontal postorbital process (modified from Christiansen, 2013: character 34).

285. Size of the jugal postorbital process: (0) small, rounded, often almost absent; (1) tall, triangular and tapering (Christiansen, 2013: character 39).

286. Relative width across the upper incisor arcade compared to cranial basilar length (CBL): (0) 11% and less; (1) narrow (12–15% of CBL); (2) wide (16–19% of CBL); (3) extremely wide (21–25% of CBL) (modified from Christiansen, 2013: character 42).

287. Palatal region relative width compared to CBL: (0) 14% and lower; (1) 16-22%; (2) ~23–25%; (3) palatal region across center of P3 relatively wide (~27–34% of CBL); (4) palatal region across center of P3 extremely wide (~36–43% of CBL) (modified from Christiansen, 2013: character 43).

288. Mandibular fossa termination: (0) posterior to the carnassial; (1) terminating below talonid or before carnassial notch: (2) well anterior of the posterior edge of the carnassial, frequently terminating around carnassial saddle or even at the M1/P4 junction (modified from Christiansen, 2013: character 49).

289. Height of horizontal dentary ramus (below m1) relative to ramus length (articular to symphysis between i1s): (0) 14 and less; (1) slender (~15–17%); (2) robust (~18–25%) (modified from Christiansen, 2013: character 50).

290. Lower canines, buccal vertical groove/ridge: (0) present; (1) absent (modified from Salesa et al., 2012: character 22).

291. C1 lingual ridge: (0) absent; (1) present (Salles, 1992: character 11).

292. Relative position of p3 and p4: (0) aligned; (1) not aligned (Salesa et al., 2010: character 24).

293. Palatal ridge/groove: (0) no visibly obvious groove or ridge (but may be felt by touch); (1) visibly obvious but shallow groove with ridges; (2) deep groove with distinctive ridges; (3) extreme medial ridges displacing medial palate ventrally from the main plane of the palate (Sakamoto and Ruta, 2012: character 39).

294. Stylomastoid groove: (0) groove originating from the stylomastoid foramen; (1) groove originating from the tympanohyal pit (Sakamoto and Ruta, 2012: character 41).

295. Metatarsal 1: (0) functional metatarsal, articulating with a phalanx; (1) vestigial metatarsal 1 (Rothwell, 2003: character 20).

296. Orientation of premaxillary-maxillary suture relative to upper tooth row: (0) 50 and less; (1) 52-70°; (2) moderately steep, 70-80°; (3) very steep, greater than 80° (modified from Van Valkenburgh et al., 1990: character 3).

297. Shape of sphenopalatine foramen: (0) oval with long axis oriented anteroposteriorly; (1) round/oval with long axis oriented dorsoventrally (Van Valkenburgh et al., 1990: character 12).

298. Teres major fossa: (0) absent; (1) small, triangular; (2) long (modified from Van Valkenburgh et al., 1990: character 20).

299. Radius, orientation of distal ulnar facet: (0) horizontal; (1) vertical (Van Valkenburgh et al., 1990: character 23).

300. Tibia, cnemial crest in lateral view: (0) straight; (1) concave (Van Valkenburgh et al., 1990: character 27).

301. Fibula, shape of proximal end: (0) without anterior projection; (1) expanded anteriorly with bony process (Van Valkenburgh et al., 1990: character 29).

302. Patella, ridge separating articular facets: (0) absent; (1) present (Van Valkenburgh et al., 1990: character 30).

303. Scapholunar, articular surface for trapezoid: (0) convex and concave; (1) concave only (Van Valkenburgh et al., 1990: character 37).

304. Pisiform, shape of cuneiform facet: (0) oval; (1) triangular (Van Valkenburgh et al., 1990: character 41).

305. Astragalus and calcaneum articulation: (0) astragalus reaches distal end of calcaneum; (1) astragalus does not reach distal end of calcaneum (Van Valkenburgh et al., 1990: character 42).

306. Seventh lumbar vertebra, shape of transverse processes: (0) similar to preceding vertebrae; (1) shorter and angled anteriorly (Van Valkenburgh et al., 1990: character 43).

307. m1 anterolingual cingulum: (0) absent; (1) present.

308. Buccal cingulum, lower molars: (0) absent; (1) present.

309. P2 parastyle: (0) absent or vestigial; (1) present-cuspidate (Morales et al., 2019: character 2).

310. P2 metastyle (posterior cusp): (0) absent or vestigial; (1) strong (Morales et al., 2019: character 3).

311. P3 metastyle (blade on P3): (0) absent or vestigial; (1) strong (Morales et al., 2019: character 8).

312. P3 mesostyle: (0) absent or weak; (1) strong (Morales et al., 2019: character 12).

313. P3 Paracone-Metastyle disposition: (0) aligned with the antero-posterior axis; (1) inclined as in the P4 (Morales et al., 2019: character 14).

314. P4 mesostyle: (0) absent or weak; (1) strong (Morales et al., 2019: character 23).

315. P4 alignment of protocone with paracone and metastylar blade: (0) absent; (1) present (modified from Morales et al., 2019: character 16).

316. M1 paracone-metacone shape: (0) coniform; (1) crestiform (Morales et al., 2019: character 26).

317. M1 protocone shape: (0) coniform with cristas; (1) crestiform with undifferentiated cristas (Morales et al., 2019: character 27).

318. p2 molarization: (0) metaconid absent; (1) metaconid present (Morales et al., 2019: character 38).

319. p3 molarization: (0) no metaconid; (1) with metaconid (Morales et al., 2019: character 40).

320. Masseteric fossa on maxilla below orbit: (0) absent; (1) present.

321. Auriform process of basioccipital: (0) absent; (1) present, large wing-like projection.

322. Frontal sinus, caudal extension: (0) terminates antero-dorsally to the brain cavity; (1) terminates dorsally above brain cavity, >50% of its length; (2) expands caudally over the complete length of the brain cavity.

323. dp4 metaconid alignment: (0) non-linear, triangular alignment with paraconid and protoconid, separated from talonid by transverse deep valley; (1) linear alignment with paraconid and protoconid; (2) no metaconid.

324. Petrobasilar foramen: (0) open vacuity; (1) closed foramen in basioccipital (Barrett, 2021: character 223).

325. Crenulations on the anterior face of the paracone of P4 and occlusal face of the protocone: (0) absent; (1) present (Barrett, 2021: character 225).

References

Barrett, P. Z. 2016. Taxonomic and systematic revisions to the North American Nimravidae (Mammalia, Carnivora). PeerJ 4:e1658.

Barrett, P. Z. 2021. The largest hoplophonine and a complex new hypothesis of nimravid evolution. Scientific Reports 11:1–9.

Barrett, P. Z., S. S. B. Hopkins, and S. A. Price. 2021. How many sabretooths? Reevaluating the number of carnivoran sabretooth lineages with total-evidence Bayesian techniques and a novel origin of the Miocene Nimravidae. Journal of Vertebrate Paleontology e1923523.

Bryant, H. N. 1991. Phylogenetic relationships and systematics of the Nimravidae (Carnivora). Journal of Mammalogy 72:56–78.

Bryant, H. N. 1996. Nimravidae; pp. 453–475 in D. R. Prothero and R. J. Emry (eds.), The Terrestrial Eocene-Oligocene Transition in North America. Cambridge University Press, Cambridge [England]; New York.

Christiansen, P. 2008. Phylogeny of the great cats (Felidae: Pantherinae), and the influence of fossil taxa and missing characters. Cladistics 24:977–992.

Christiansen, P. 2013. Phylogeny of the sabertoothed felids (Carnivora: Felidae: Machairodontinae). Cladistics 29:543–559.

Flynn, J. J., and H. Galiano. 1982. Phylogeny of early Tertiary Carnivora, with a description of a new species of Protictis from the middle Eocene of northwestern Wyoming. American Museum Novitates 2725:1–64.

Gaubert, P., W. C. Wozencraft, P. Cordeiro-Estrela, and G. Veron. 2005. Mosaics of Convergences and Noise in Morphological Phylogenies: What's in a Viverrid-Like Carnivoran? Systematic Biology 56:865–894.

Heinrich, R. E., and K. D. Rose. 1997. Postcranial morphology and locomotor behaviour of two early Eocene miacoidcarnivorans, Vulpavus and Didymictis. Palaeontolgy 40:279–305.

Matthew, W. D. 1909. The Carnivora and the Insectivora of the Bridger Basin, middle Eocene. Memoirs of the American Museum of Natural History 9:291–576.

Morales, J., S. Mayda, A. Valenciano, D. DeMiguel, and T. Kaya. 2019. A new lophocyonid, Izmirictis cani gen. et sp. nov. (Carnivora: Mammalia), from the lower Miocene of Turkey. Journal of Systematic Palaeontology 17:1127–1138.

Peigné, S. 2003. Systematic review of European Nimravinae (Mammalia, Carnivora, Nimravidae) and the phylogenetic relationships of Palaeogene Nimravidae. Zoologica Scripta 32:199–229.

Robles, J. M., D. M. Alba, J. Fortuny, S. De Esteban-Trivigno, C. Rotgers, J. Balaguer, R. Carmona, J. Galindo, S. Almecija, J. V Berto, and S. Moya-Sola. 2013. New craniodental remains of the barbourofelid Albanosmilus jourdani (Filhol, 1883) from the Miocene of the Valles-Penedes Basin (NE Iberian Peninsula) and the phylogeny of the Barbourofelini. Journal of Systematic Palaeontology 11:993–1022.

Rothwell, T. P. 2003. Phylogenetic systematics of North American Pseudaelurus (Carnivora, Felidae). American Museum Novitates 3403.

Sakamoto, M., and M. Ruta. 2012. Convergence and Divergence in the Evolution of Cat Skulls: Temporal and Spatial Patterns of Morphological Diversity. PLoS ONE 7:e39752.

Salesa, M. J., M. Antón, J. Morales, and S. Peigné. 2012. Systematics and phylogeny of the small felines (Carnivora, Felidae) from the Late Miocene of Europe: a new species of Felinae from the Vallesian of Batallones (MN 10, Madrid, Spain). Journal of Systematic Palaeontology 10:87–102.

Salesa, M. J., M. Antón, A. Turner, L. Alcalá, P. Montoya, and J. Morales. 2010. Systematic revision of the late Miocene sabre-toothed felid Paramachaerodus in Spain. Palaeontolgy 53:1369–1391.

Salles, L. O. 1992. Felid Phylogenetics: Extant Taxa and Skull Morphology (Felidae, Aeluroidea). American Museum Novitates 3047:67.

Spaulding, M., and J. J. Flynn. 2012. Phylogeny of the Carnivoramorpha: The impact of postcranial characters. Journal of Systematic Palaeontology 10:653–677.

Taylor, M. E. 1974. The functional anatomy of the forelimb of some African Viverridae (Carnivora). Journal of Morphology 143:307–336.

Tseng, Z. J., and X. Wang. 2007. The first record of the late Miocene Hyaenictitherium hyaenoides Zdansky (Carnivora: Hyaenidae) in Inner Mongolia and an evaluation of the genus. Journal of Vertebrate Paleontology 27:699–708.

Van Valkenburgh, B., F. Grady, and B. Kurtén. 1990. The Plio-Pleistocene cheetah-like cat Miracinonyx inexpectatus of North America. Journal of Vertebrate Paleontology 10:434–454.

Werdelin, L., and N. Solounias. 1991. The Hyaenidae : taxonomy, systematics and evolution. Fossils and Strata 30:104.

Wesley-Hunt, G. D., and J. J. Flynn. 2005. Phylogeny of the Carnivora: basal relationships among the carnivoramorphans, and assessment of the position of "Miacoidea" relative to Carnivora. Journal of Systematic Palaeontology 3:1–28.

Yalden, D. W. 1970. The functional morphology of the carpal bones in carnivores. Acta Anatomica 77:481–500.

Appendix E

Nexus formatted morphological character matrix

#NEXUS

[written Fri Oct 01 13:40:37 PDT 2021 by Mesquite version 3.61 (build 927) at LAPTOP-CRLI5NPQ/128.223.221.117]

BEGIN TAXA;

    TITLE Taxa;

    DIMENSIONS NTAX=129;

    TAXLABELS

        Tungurictis_spocki Ictitherium_viverrinum Hyaenotherium_wongii Hyaenictitherium_hyaenoides Lycyaena_chaeretis Chasmaporthetes_lunensis Chasmaporthetes_ossifragus Palinhyaena_reperta Adcrocuta_eximia Pachycrocuta_brevirostris Crocuta_crocuta Crocuta_crocuta_spelaea Hyaena_hyaena Proteles_cristata Plioviverrops_orbignyi Protictitherium_crassum Belbus_beaumonti Tongxinictis_primordialis Allohyaena_kadici Dinocrocuta_gigantea Percrocuta_carnifex Percrocuta_algeriensis Percrocuta_tobieni Proailurus_lemanensis Pseudaelurus_validus Metailurus_major Nimravides_pedionomus Machairodus_catocopis Megantereon_cultridens Amphimachairodus_giganteus Amphimachairodus_coloradoensis Dinofelis_diastemata Homotherium_ischyrus Homotherium_serum Homotherium_latidens Promegantereon_ogygia Smilodon_fatalis Smilodon_populator Xenosmilus_hodsonae Neofelis_nebulosa Panthera_pardus Panthera_leo Panthera_leo_spelaea Panthera_atrox Caracal_caracal Lynx_canadensis Felis_lybica Leopardus_pardalis Acinonyx_jubatus Miracinonyx_trumani Puma_concolor Otocolobus_manul Prionailurus_planiceps Catopuma_temminckii Profelis_aurata Prionodon_linsang Arctictis_binturong Civettictis_civetta Paradoxurus_hermaphroditus Hemigalus_derbyanus Viverra_tangalunga Genetta_maculata Paguma_larvata Cynogale_bennettii Poiana_richardsonii Viverricula_indica Bdeogale_nigripes Mungos_mungo Suricata_suricata Herpestes_edwardsii Ichneumia_albicauda Crossarchus_obscurus Atilax_paludinosus Rhynchogale_melleri Galerella_sanguinea Helogale_parvula Fossa_fossana Cryptoprocta_ferox Eupleres_goudotii Salanoia_concolor Kichechia_zamanae Kanuites_lewisae Izmirictis_cani Euboictis_aliverensis Sivanasua_viverroides Nandinia_binotata Palaeoprionodon_lamandini Stenogale_julieni Herpestides_antiquus Ginsburgsmilus_napakensis Prosansanosmilus_eggeri Prosansanosmilus_peregrinus Afrosmilus_hispanicus Afrosmilus_turkanae Afrosmilus_africanus Albanosmilus_jourdani Maofelis_cantonensis Eofelis_edwardsii Dinailurictis_bonali

195

Quercylurus_major Dinaelurus_crassus Hoplophoneus_oharrai 'MA-PHQ 348'
Hoplophoneus_dakotensis Hoplophoneus_sicarius Hoplophoneus_adelos
Hoplophoneus_bidentatus Hoplophoneus_villebramarensis Barbourofelis_morrisi
Oriensmilus_liupanensis Sansanosmilus_palmidens Barbourofelis_fricki
Barbourofelis_loveorum Albanosmilus_whitfordi Hoplophoneus_cerebralis
Hoplophoneus_primaevus Hoplophoneus_occidentalis Nimravus_brachyops
Pogonodon_platycopis Pogonodon_davisi Dinictis_felina Nanosmilus_kurteni
Nimravus_intermedius Tapocyon_robustus Procynodictis_vulpiceps Hesperocyon_gregarius
Canis_latrans_frustror Vulpes_vulpes Taxidea_taxus

;

END;

BEGIN CHARACTERS;

TITLE Character_Matrix;

DIMENSIONS NCHAR=325;

FORMAT DATATYPE = STANDARD RESPECTCASE GAP = - MISSING = ?
SYMBOLS = " 0 1 2 3 4 5 6";

MATRIX

Tungurictis_spocki
201020000?113210102??0??2?0?1?211020011?12011001???1?1?110???0000101?????????????
???1?0110011021101011011?1
111???????????????1100???0101000100210001000031??0410000311000111???001?00??111??
?0001?10000?0???0???00000??00122103??10010???001?2????????0?1{0 1}000000001??0000?-
0

Ictitherium_viverrinum   201020002011021 0?0???0??????12211??101101202100{0
1}?0?{0
1}21111????0000101??
???100000101020130002100010003112231 00
2021{1 2}000{1
2}11001000?00??111101000101?00000000000000?101?10?122102220?111100000?1?????????
1100000000100002?-0

Hyaenotherium_wongii
201020002?113210002??01??20?122110?1011012021000?0?0211110???0000101???1????????
?02111?01110211101111001 1?0111?1101001?1???0???00001?001000110111110010 21101001

196

0011????0????????????????100000201020100021000{0 1}0004{0 1}122310020211000210 0?0000000??111100000101001000000000000101?10?1121022210111 11000??1???0??1?0?1100000000100002?-0

Hyaenictitherium_hyaenoides
200020002?103210?????0??????12211??1011012021001?0?121111???0000101????????????? ?? ?????????????????100000201020000002100010014112231002021100121 1???0?0?00??11100{0 1}00010100000?00000000?101?101122102220111121000 0?1??????????1100000000100002?-0

Lycyaena_chaeretis
200020?02?113210?1???0??????12211??0011?12021001?0?021111???000{0 1}1?1??? ????????????????????????????????100000101020000003{1 2}00010?3{5 6}112{2 3}410010111001110??0?00000??11100100010100100000000000?401??0?022102220?1212100 00?21?????????1100000000100002?-0

Chasmaporthetes_lunensis   201020102?113210?2????1?2???12211??0011?{0 1}20{1 2}10{0 1}{0 1}?0?021111????{0 1}0011?1?? ???????????????????????????????10?0?020003000000{3 4}2011{0 1}0?3601234000202{0 1}2001{1 2}1{0 1}??0?01000??11{1 2}00{0 1}0001010?100000100000?401?100022101220023121000??1{0 1}?????????110000?0001??0022-0

Chasmaporthetes_ossifragus
??10?????????????????????????????????110??????????????000?1?1???1?????????????? ?0????????00?0??????????????0?1????0??01???10??0?00??0?11???????????????????????????? ?????????????????????000300002042011000?36?121??001?2120011??????????????111000000101 0???000??00?00???1???????1012????22?00??11??10??????1?0000000??001???-0

Palinhyaena_reperta
30102?002?113210?2???0??????12211??0011?12021001?11121111????01001?1????????????? ??????0????????01?? ?????????????????100000221020000003100010?15112341001011011111001101010??2220010 00101001000000000000?401?111112201220112121000?21?????????1100000000100001?-0

Adcrocuta_eximia
300022002?100210?2???0??2???12211??0011?12021100?1?021111???00011?1??11????11?0? 010110011102101110?0???1???1??1???????1011?110?0???????????1?0110001121101001?1? ?11?10????0??????????10000020203?000003200{0 1}00?360123410010212001110001 10?110{1 2}?32{1 2}000000101001000000000000401???1122201220?{2 3}3121000011?0??????0?11000000001000022-0

Pachycrocuta_brevirostris   300021{0
1}02??13??????????????????????0011?12021000?1???1111????00011?1?????????????????????
???
?????????000?02020300100032000 10?360122410010211100121???1?110{0
1}??3220010001010?100?00000000?400???10??2112?00??0?1000??11?????????11000000001
00??20-0

Crocuta_crocuta   301021002?113210022?00122?001221103?????????10010{0
1}11211110?1?00011?10111???01110102011?011110101011100111011111101001110011 00
110001?0010001111111000112110100111111111011100111001010101000102010300102042 0
1100?360101410010212110020000111100212220 00000?0100101100000110040 1?1010221032
20113121010112001000010000000000 0??000022-0

Crocuta_crocuta_spelaea
30002200200132101 22?00121?001221103?????2?0?10010101211110??? 00011?1?1?1?1???0011?
?02110011110101011010011101111111 011?1???0?????00?01100011111110010121101001
1111?????111?0101001110101000002010300101042011 00?36?10141001021211001 00001111
00?132200100010100100000?00110?400?100022102?201230210101?21210??1?0?110000000?
?00002{0 2}-0

Hyaena_hyaena
300021002?113210022?00122200122211030011?020110000{0
1}11211110110000 11?10001111011101020 11?0111101010110001?11011111101001110001 00
110000?0010001111111000112110100 111111011011100111101 0101{0
1}100010201020010103100100?36010141001021111002101 111011020221001000101001 1110
00000000401?0{0 1}10201122201120210101120110 00010?110000000?1000020-0

Proteles_cristata
211022012?113210122?001212001221102 02???2?001120000121111 0???1001??10001???0111
0002011?011010101011101?11011111101001?11?01?0110000?00100011 11111000012110 10
0101111111011100111101 1000200011?12002??1{1
2}25211100?36002?2102?0?0?0??30100 100111020??20000100 0?0010100001 01?0040??00101
210??001130110?0?11{0 1}010000?0?00??00000??000001-?

Plioviverrops_orbignyi   2?1022{0
1}120113210?0???01?1???12211??0011?1?011001?00121011????0000101?????????????????????
???
??????????110000?{0
2}10101310120000 00001110130000031 10?00210??00?010??12100100010100000000000000?
400??00022103110011 00?010??10?????????0100000000100000?-0

Protictitherium_crassum
20002?002?11300000???012?200122110?0010112011001?0?0210110??? 0000101??01???0110
001201100011020 0?011010??110111101010 11???????011?00?00100010?101?10?012110110
1?1111111001110111101???10110010?0101013100010001000311013000203 12001111???100

110011111000001010000120000000?000??00020121200111110101 10?0?00???0?110000000
01000000-0

Belbus_beaumonti
??01?1???????????????????
??
??????????????0??????00??03100000??5?101????2??1??11??????1???????11????0??0?????1
000????00??????????????22????121?0??????????????11????????00????-?

Tongxinictis_primordialis
???022112001?210?0??0?122?0?1?211?3?0???????1001???021011????0001??????????????????
??
??????????????1100???0?02?010??????????3??1?3310010312001021????00100??2210010001?
10000??0?100000??00??0??22102??0012????00???????????????0000000??00100?-0

Allohyaena_kadici
??????????????????????????????????????100???????????????10011?1???????????????????
??
??????????????2102000??03101100?35???3??001?212?00???????????221??110???1???
???00???000???1?????????22?????0??0???????????110000000??00???0-0

Dinocrocuta_gigantea
200022102?100110?02?00122?0011211040210??2011100?0?0211110??01011?1????????????
??
??????????????0000100020320001032000 00?36012341001011 2101010???00001??222001
0001010?101000100000?401??01132102220022121 1001?1??????????11000000001001121-0

Percrocuta_carnifex
???????????????????????????????????1??220?110???????????????011?1???????????????????
??
?????????????????{0
2}0030000104200000?36???3??001?112?0???????????222??100?1?1??????00??0??0???1?
???????0?2?????1???0??????????????11??00000??00???1-0

Percrocuta_algeriensis
???0??????????????????????????????0010?22011101????????????00011?1???????????????????
??
??????????????02030010103200000?36???1??001?212101?????????????323?010001101?
???1000?00?10???1???????102?????0???1??????????????1100000000100???1-0

Percrocuta_tobieni
??????????????????????????????????001??220111????????????????0011?1???????????????????
??
??????????????02?3001?103201000?36?1?1??000?2?2?10???????????22???100??01???
?1000????00??0???????0??2????021?0??????????????10000000??00???1-0

Proailurus_lemanensis
?00?1??010013110002100122210122110300110?120110100?00001?1?????????????

???

??????????????????10?10?202011000004101100?3501220000202020011????001200??1110000

0000111010200?00000?2???1??12?200121?01120000??2?????????000000000000000001-0

Pseudaelurus_validus
201010002?100110102??0122201122110?0011?12011011?000310110??00011?1??01???0??0?

?1101111101020000010110111000101101001111111?01211111?001{0

1}0010?10110001001101011111000?100?????????????101000?02011000103201100?360122

000{0 1}2010200111020000110010111000000010101101000?001000?0101202{0

1}3220?02120?0{0 1}1010?000??00?0000000000000000?-0

Metailurus_major
201010001?10121012???01?0???122110?0211?22011011?00031011????10011?1??01???001?1

?10?110101?02?????1??0????0??1??1?10?????????1????10??010001???01?0??1??????0?1?1??

???100?110??0001???101000002020310001042011000?36012300022010210121020000110011??

11110101010100110110100000000010??00101031200111110011110?00????0?00??0000000?000

0?-0

Nimravides_pedionomus
?00?1?????1?????1?2??012?20?1????0?0211?22011011?????0110???10011?1???1?????????11

0111101102001001010011101010111100100??00???????00?0010011011011000101110101111

0?????????????10001?????1??0?02000320001042011000?360123??012?10{1

2}00121????0?10???11110101?10101?1011010100010?0??????203{1 2}2????1{1

2}100???2??000???0?000000000??00???-0

Machairodus_catocopis
?00012001?121210?22??012?20?12211?????????10?1?0?131011????10011?1?001???001000

11011110110200100101001110101011110011111110101011101?00100010110110001011101001

11100011001110110001010101000102?0??3200010{3

4}201100?36012300022010200120??????0111001111?20101010101110010101?011000???01201

1?22002?121001?11?00000000?0{0 1}??00000???0000?-0

Megantereon_cultridens
201010010012121012???012??0?10211?????????1111?0?131011????10011?1???1???010?00

110011001112??1011011011?0111011010010111110121100?0000001?1101?001112110?11?

01100??100111011010101110100010200032000105201100?3601210102101111012?10???00?1

00???112000100?1001{1 2}123010020000001??011201{0

1}32201231210031?1?????????01??00000??00000?-0

Amphimachairodus_giganteus
200012001?121210?????012????12211??0211?220111{0

1}1?00031011????10011?1???1???

00??0??0010??0?0???????????01?1110????????????????????10001020103200010420110 0?360

200

1230101101111012002000012l0??110201010{0 1}010011102020120l?000??001200232210221{0 1}10121?11?????????00??00000???0000?-0

Amphimachairodus_coloradoensis
?0?????01?????????????????????????0211?2201111????????????????10011?1???1?????????????????????????????100111???101111001?1??10?1111110?001001101101100010211010010110????0?????????????????????0201030000105201100?360123??01??10310?2??????????????11201010101???110202012011??1???????023121???12100??????000?000?010000000????0?0?-0

Dinofelis_diastemata
201011001?101210?1???01????12211??0211?11011111?0?131011????10011?1??01??0???0?11111100110210101111001110011001010l1?11?11?10111111??0?10110?011?0?000211010010110?0110??????????01???010000020003200010510110 0?360121000210102001110200?011001?11110101010l0?11101010120000 00??000301032200{1 2}3121001?1{1 2}1??0??0?0?00??00000???0000?-0

Homotherium_ischyrus
101111011?121210112??012??0110211???211?22011101?0?0310110???10011?1??11???010000110100001102101011010??110111011110 01?1??11?1???101?0?10?1?111110010021101000{0 1}11000?10000?0?111?10101?1000102010320002052011 00?3601230102001?3001200??01?2001121120001010100101??02013011011?1001200022?1033???0??111??100000?001??00000???0000?-0

Homotherium_serum
100011001?121210?2???0?2000010211??????????1101?0?0310110???10011?1??11???001?00110111001102101001010 0111??111111100??1{0 1}?11?111?010?00?0011?1011?0?????110??00???10?101?1?0111111010?010001021?0320102052011 00?36012200021011200130000 0?1?2001?31220?01010200101{0 2}2{0 1}20??011201??001000032{1 2}103312100211000 0?0???0000????00???0000?-0

Homotherium_latidens   2{0 1}10{1 2}{1 2}001?121210?2???0?????10211??0211?22011101?00131011????10011?1???100010201032000205201100?360123010210112101300200010100??31120101010{1 3}00111{0 2}2{0 1}201321?011?1001{1 2}000{2 3}?{1 2}10{0 3}31{1 2}10021?{0 1}0?????????01??00000???0000?-0

Promegantereon_ogygia
200011101?101210?2???0??0?00122110?0011?22011011?0?03?011????1001101??01?2?01000001011?001?02??1?01?11011101010110101 1?11?11?121?100?00?001101101100{0 1}{0 1}0{0 2}1101001111001110011?0110001?101010000202032000104101100?360102000220102001110??0?01100111111000{0 1}010110111010100200020 1?000010{1 2}13220011111010111?00000001?00??000000?00000?-0

Smilodon_fatalis   2000{0 1}0{0
1}10?131210122?021?020010211030211?220111{0 1}100{0
1}0310110???10011?10111???00100111111010110200101101001110011011110011111110
11101?001000110101100001{0
1}010110101101011000110110101100101000102020320001 05{1
2}01100?3601220102?011200?2101{0 1}001110111?11200010101001212212012{2 3}{0
1}1211000010222322002{3 4}1{1 2}10?3112{0 1}00000000000??0000000?00001-0

Smilodon_populator
2?0??1?10??31210?????0??????11211??021??2201111??00031011????10011?1??11?????????
10?1??1??2??1??1?100111001101111011???????1?1?111?00?1000??1011???01011011010110
?????021?01????01????00010202032000105201100?3601020102001 1210?210??00??101??31
120101010100121321 2112{2
3}01?11??011??1222201241210131?20?????????00??0000000?0000?-0

Xenosmilus_hodsonae   2000{1 2}0111?12121012???0?20???1{2
3}211???2???2?0?11?1?0?031011????10011?1?111???00100111011000110210101101101111 0
1101110000?1??11?11?1?10?00100100110110000121101100111 00??10?????????00?0??1000
1020??31010?05201100?36?1210002?000200?300????1?11011?1320?010?1100111220201?31
1211??000300012210331210?2??1?000000?0?00??0000000??000?-0

Neofelis_nebulosa
201010101?101210122?00120?0011211030211?22011111010131011 0???10011?10101???0110
001111111010021010110111?11000101101001101111 01211101?01100011110110011001 1010
1101100111001110110001111101000002020320002 04101100?360123000120102001 02000000
1110111110000101011001100000000002010000121203220112110110012 10000?00000000000
00??00000?-0

Panthera_pardus
201011002?101210122?00120?00122110?0211?220110110001310110???10011?10101???0110
001{1 2}01100100210100111101110111011{0
1}1001?1??11?1110100?001100111101101101211011011110101100011011000111010100000
20203201010{4
5}201100?360123000010101000210000001000111110010101010001100010000002011100021
2022201121101010111000000000000000000?00001-0

Panthera_leo
200010102?101210122?00120?0011211030211?220111110000310110 11?10011?10001?1?011
000110111101102101001110011101110010100111 01101111101?0010001111011000111 1101
011011000110001101100001111010001020203 2000205201100?3601230012010100120 02000
010001111100101010100011100000020020111100212131201121{1
2}000101110000?0000000000000000000001-0

Panthera_leo_spelaea
201012102?101210122?00120?0011211103?????2???1111 00003101 10???10011?1???1?????????
1111110010021010110100111011101111011?1??11?1?1?101?001000111111 100101111 01011

0110????000110100001???1?10001020203200010520110 0?36?12300012011100120021000010 01?111001010101000110001000000200?1100212022201231200000?20?00??0?0?0000000000 000000?-0

Panthera_atrox   2010{0 1}{1 2}{0 1}02?10121012???01200001{1 2}211030211?22011111100003101 10???10011?100?1???0010001111111110210101101001110 11101111001111111010101 01?0011011111011000111110001101100011000110110000111101 000100{0 2}2032000105201100?360123000 11010{1 2}001{2 3}001{0 1}00013{0 1}0{0 1}111100101010100111100100000030{0 1}?1{0 1}{0 1}0{2 3}{0 1}2{0 1}3220112120{0 1}01011020000000000000000000???00001-0

Caracal_caracal
201011012?101210122?00120?0012211030211?22011111100013101 10???10011?10101???0100 0011011000002101011011011101010111100111111101111100?001000101101100001211010 110110011100011011000101110100000202032000205201100?3601230002201010011200000 0 111011111001010101010011000000000201000002020222011202110001210000000000??000 0000?0000?-0

Lynx_canadensis
201011012?101110122?00120?0012211030211?22011111100013101 10???10011?10011???0110 0011011110110210100111111?110101011110011111110 1111100?011000111101100110211010 1101100111000110110001111101010102000320002052011 00?360122000220101001120000000 111011111000010101010110000000000201000002020212011 31100000121000000010000??000 0000?00001-0

Felis_lybica
201010012?101210122?00120?0012211030211?22011011000 13101 10???10011?10001???0100 00110111001102101011111 1?110111011110011111110111110 1?001000111101100110111010 110111001100011011000101110101010200012000205201100?3601 2200012010100102000000 111011111000010101010110000000002000000020202120113110 0000120000000000000000000 0000?00001-0

Leopardus_pardalis
201011012?101210122?001202001221103 0211?22021011010 13101 10???10011?10101???0010 001011110{0 1}100210000101100110101011110011110110 1011100?001000111111100110011010110110 01100011011000111110100 0?02020220001052011 00?36012300000010100112010000 12101111 10000101010001000000000002000000020202120 1121100100130000 0?0000000000000000000 01-0

Acinonyx_jubatus
2010121020100210122?001202001221101 0011?22011110000031011 0???10011?10001???0110 1011011100110210101111101110111111 0100111 1110111000 10?001100111101100110211010 01?11?011100010011000 0111010001020203200 0205201100?361123000120102001210??010 100011111001010101000001000000 00?211?0{0 1}002020312012 3121010001310110111110000000000??000001-0

203

Miracinonyx_trumani　　　{2 3}01012{0 1}120001210?2??????0???12211??0211?220111110{0 1}?0?1011????10011?1??01???0?10??1??1111?1?02???011??0???11???1?1?100??1?1110111?0????01?001???01000?10211010011110????0??101??????1?101000102020{2 3}2000105201100?360123000{0 2}20101000020??00011001?111001010{0 1}0100000{0 1}0?1000001200?1?003220312013301?000012?00010000100000000000?0000?-0

Puma_concolor
20101001201012101 22?0012020012211030211?220111110{0 1}0131011011010011?10001110011000111111011021010110101?1101010110100110111101111100?0010001111011 0010?21101001011101 1100{0 1}1101100011111010001020203200020520 1100?360123000120201001110100001100111 1100101010101011100000000020100{0 1}00202032201231111100120000100000000000000??00000?-0

Otocolobus_manul
201011012?102210122?00120 2001221101?21??2?011111000031 0110???10011?10101???0110 00100110101102001001111011 1011101111001?1??11?1110100?00 10001111011001100110 10110110001100011011000110110100000202 03200010{4 5}201100?36?123000210 10100102000000111011111000010 10101011000000000201?1000102 022201131101000131 0000?010000??0000000?0000?-0

Prionailurus_planiceps
201011012?10121012???0??0?00 121110?0211?2201111100001310110???10011?1?4??????????
??
?????????????????10000020003200010520 1100?36012200002010200002000100121 0??111000 0111010001100000001 0?201?10102020212011 111101000?20?????????00000000000?0000?-0

Catopuma_temminckii
201011012?101110122??0120?00 1221101 0211?2201111100001310110???10011?10101???0110 00100110101102001001011011 101110111100111011?01010101?00100111101100 10?001010 11011?0011000100110001 110101000102020 32000105201100?36010 3000220201000120200 00110011111000010101010112 001000000201?0000202031201 021 20000?12100010?0000 000000 0000?0000?-0

Profelis_aurata
201011012?101210 12???0120?0012?110?00 11?22011111000013101 10???10011?10??1???????? ?1001110010021010011110111 10111011{0 1}100111111110111 0100?0011001011011 0010??1101111011?001 10???????????????1000?020 203200010520 1100?36012300012010 00012020000110 01?111000010101010111 00000000020 0?000032203120113210000?130?000??01?00000000000?0000?-0

Prionodon_linsang
201020112?113110002?0012200122110310110020110110001210110???00001?1???????????
??

204

?????????????????2010100000100000031 01000?34010110002010100102020100 1110??001001 0000010001000000000?400?00001020 312000100100000020?????????00000 000000000000-0

Arctictis_binturong
1110221020113210102??22?2??012211 ?320?21020010210001310110???00011 010101???0001 0010111110111200010101100011010001 1100110011101 2?1?11?0010010001011001002110110111 10010100101001101001110112011000000 131012101000224012210000000000120 100100 010001222100000000000110000100100001 2100021?0011001101100010112000000000 0000000 0001000000-0

Civettictis_civetta
211022102?113210002?0012221012201 02101101101100100013101100000000010 1000011100110012011101010200101100 001110101001010011110110011000 0?0011001111111000112110001111110111 011100111111101010201001001010111002 0000100030101100020101001110001001 210011210000000010000100000000001 00?00001011211001100100 0?0200000000 000000000000001000000-0

Paradoxurus_hermaphroditus
211022102?113210002?0012220012201 020011?112110210001310110???0000111 01 01???0101 001011111010120011000110101100101101 011101111002110 10?00001111001100000211001 111110011100 1110011101010101010010 210001210000000010004110210000020101 121{0 1}001000210012220000000001000100000 00001004 01?1000121101100010001 01?0100 000000000 000000000000000-0

Hemigalus_derbyanus   2110221020113{1 2}10{0
1}021001222001220102101100212101100 0131 0110??01101110101???010000121111101 111 001001010011110110110100100111100011 010?0110001110011000012110111111110 01100011 1011111101010201001021010131000000001 00031101100020101000211001001100010 1210100 000000000{0 1}0000001 00401200000201102001 10010000000000 0?00000100000000100000 0-0

Viverra_tangalunga
2010211020113210002?001222001220102 101100111100100013101 10??000011 10101???011 00000211111011100001011 0001?1101011110 10011111111011 111110?001000111111100011111101 0111110011100111011111101111111100100 10101300020000110031011000201010101 100010 001000111110000000010000000000001004 00?1000221101200110010 00?0100000?0? 00110000 00001000000-0

Genetta_maculata
201021002?113210002?0012220012201 02101100101101100013101 10??01001010 101???011 0001011111001020010101100101010101 1010111111110 0???10?00100000100110011 121101 011111101110011101111010011021100000 02010100002101000013010210002010200 01212010 01210011110010000010001020000001004 00010000220111000100 0000?0100000?00 00110000 0000010000 0?-0

Paguma_larvata
2100221020013210102?00122??012211020010?02011021000131111 0??00001010?01???????
??1011101001020010?111000011111?0101011101??10?011110?001001110101100111111011
1101100111??????????????????0110100221011310120000102240101100010200010211001001
1000?33200000000100010001000010040021010121011100110110 00?021?0000000?00000000
00100000?-0

Cynogale_bennettii
2010221??00?????11??0?1?22??1??1?021002011001011001131111 0??000011?0?0?0??????? ??
?? ??
????????????????1110?120101003101100001100311011 0002?00101130020?0?11????0110000
00000000000000000110?4012?01???2122200??001000??0??????????11000000001000000-0

Poiana_richardsonii
2010211120013210102?0012220012211020011?12011001000131011????01001010?0?????????
?? ??
???????????????????11100?022000000003101000?35012110002030200002020000 0210??00100
000000100010200?00000?400?10000210012000000 1100?020????????0100000010100000?-0

Viverricula_indica
2010211120013210122?00122200122110210110010110110001310110??00001010101???101
0001211100011020010001000111011101101010111?111101????01?001000101101 1001??01101
011?11?111110111111111101010111000021010130002100010004110210002020200 00212100
0020001110000000010000020000001 0?40020010021011200010010 00?02000000??00010000
00101000000-0

Bdeogale_nigripes
210021012?113210002?001222001220123001 1?0102100100012111 10??011010100 01???0111
0012011101110200100100001111101101010111101010010 0000?00100010010110000 0211010
11111?011100111011110101110211011221110131011000000002111200020211010100001 00
1?10211230010000010001200000000040101000121000{1
2}01110110 00?1210?0000000000000000000100000?-0

Mungos_mungo
200022012?113110002?001222001220123001 0?020110010 0012111 10??11011010 001???0111
101211110001120000000000 1?11010111101011111001001?1?00?00100011110 1100000211011
11111011110011101011010111021 1010221012131001000010003010120001010000002010100
1210011220000000 000000000000110040101010221000211110110 00?0200000?00100000000
000100100?-0

Suricata_suricata
1010220 12?113210?02?001222?012211230010?020110010001211111????11011010101??? 0111
1011011101110200100100001111111010100111000000101001?0010000100110001 0211011
11010001110010101011 00?111111101022201213100100100000301012000100010011 1100100
1100211221000010 010011000000001014010101032100220111011101?13101000?0110000000
000100000?-0

Herpestes_edwardsii
200022012?113210002?001222001220 1230010?020110010{0 1}01211110???01001010001111011110120101000102101001 0001?110101011010111111?11?000000?001000111101100011211000110100011100111011110100010211010 2200121310020010000030101200020101001020201001210??1121010000010000020000000 0?400?101012200 121101011000??21????????0000000000100000?-0

Ichneumia_albicauda   211022012{0 1}113210002?001222?01220123101100201100 10{0 1}0121111????010010100 01???011010120110001102001011 0001?11010110101001????0??01?1?00?0010001011111000 10{0 1}1101??1????? ??0011001011010101021101022201213100000001000 2011220002010100021 0201001210?11120010000010000020010001 0?400?10002210012011100 1001??100000????00000000001000000-0

Crossarchus_obscurus
210022012?113210002?001222?012201230010?020110 0100001211 11????1101101?4???????? ?????? ?? ???????????????????????????? ????????????????211011 22201213100100101000301012000 101020011001010012?0??122101 0000010001000000000?400?1010121011201{0 1}1001000??30?????????0000000000100000?-0

Atilax_paludinosus   200022012?113210?0??00122??0122 1123{0 1}0100020110010001211 11????100110101 01???0111100201100 0010210?1011010111111101 101001?10011?1000001?0?1?01111?1100000??1101011011?0111001100102001011102110102 210101310020000100130101200020201001120 201001110011231000000001000002000000 0014 00?1110221001201110110 10?020000??0?1?01000000001000 00?-0

Rhynchogale_melleri
201022012?11311010??00122?0012211230011?01021001000 1211110???0110101??0?????????? ??? ????????????????21101112201013100100 00?0003000120002011000110 200001200??233001 001001000002000001 00?400?101012100?10111 001000??20?????????0000000000100100?-0

Galerella_sanguinea
200021012?113210 10??00122?0012211230011?120110010 0?1211110???010110100 01???0110 1012011000110210001100001011111101010 1111011?0100000 0?001000101101100110211010 11011000?1001100101101011 1021101022201213000200010100130101200 0102010010202 0000 12100111210100100 1000102000000100400?1010122010201010010 00?02000000?0000100000 000100100?-0

Helogale_parvula
210021012?113210?0??00122??0122112300 11?0201100100012111 1????1101101000 1???0111 1012111 01011021010010000111 11110010101 1???1???????????01?001000 11110?????????? ?????? ?????????????????????????????211010222012130000001010 00301012000102110010210000 01200?

207

1123100000001000000001000107400710100210012011101100077100100777770100000010100
0007-0

Fossa_fossana
100022112?113210002?0012?200132112310100020110010001210110??00001010101???0111
0012111100110210001101001110101101010011111110111100070010001111111100101011010
1101110110011111100101010211011000010130002000000002010120002010100111020100
1110011110010000010000000000000004000000012002021000001000001001000000000000000
000100100?-0

Cryptoprocta_ferox
201022012011321010270012720013211230011712011001000121011077700011710101???0101
0010111110111200001111001111101001110011011070101111170010001011011000002110111
1101100111001010111010101011201022202201000320110073601011000101010001200110
0010001221000000001000000010000001007000000211120011011000112000000770000000000
0001000001-0

Eupleres_goudotii
010021112011321000270012220012201230110702011000000121011177770000010{0 1}0{0
1}???011{0 1}0012011000110210101110{0 1}00111111111010011111{0 1}0{0 1}10{0
1}0{0 1}{0 1}70010000{0 1}01101{0 1}000{0 1}1000{0 1}10101111100111001110110{0 1}10{0
1}010111021011002012101002001000000011320002000100130101001110010001010000110
0000000000000040000000120022000000001000?0000{0 1}00010000000000000001000000-0

Salanoia_concolor
201021012?113210?2??00122??012211230010?02011001000121111?????00011010101???0101
101201101010001000111010111111100111001111111017????017001000100111000101211011
110110011100111010100011110211010200012130002001000002010120001021200021020100
0110011210010000010001000000010040070101210112001101100070200000070000000000
010100000?-0

Kichechia_zamanae
?1?02?????????????????????????1110002011001???1????????0010101????????????????
??
??????????????2010101310021000100031171?7700172010000272??7712?????1231000000?
1????????000010?0?0???????1021?????????000????????????010000000010007?-0

Kanuites_lewisae
210022012?113210?0???0??????12211?2101101201100170012101177770000707?????????????
??
??????????????1120??201010??1002100010077110710007030107712070170170077774100000
00077000000700070740070071021031707017770707771078?????????01000000001770000-0

Izmirictis_cani
????????????????????????????????????111001202100???????????????10?1??????????????????????
??

??????????????????0212013?01200001000?1??1??0???3?200????????????????11??100?0?0??
?????????0?0???0???????031??????????????????????01??10001110?????-0

Euboictis_aliverensis
???????????????????????????????????111100201?01??????????????0100????????????????????
???
????????????????????111013?0??????????1??2??002?3?2000??????????????333??100?001???
?????0???00??0????????11????????1?0????????????????111011111111????-0

Sivanasua_viverroides
???????????????????????????????????111000201?00??????????????0100001??????????????10??
???00?12?????1??0?000??00?111010110???????
????????????????????20111013?0020000100001??3??002?312001??????????????12210100?00
0????????000020???0????????101?????0?110??????????????1111111111111????-0

Nandinia_binotata   20102{1 2}00101130100020001112001120002 0{0 1}110{0
1}2011{0 1}{0 1}{0 1}0001300000000000001010{0 1}01110111{0 1}001{0
1}0100100012011000101 1?00{0
1}10101010001001111000111 11?00010110110110101121100111 10110111001010 1111010011
010210{0 1}20{0 2}002121002101{0 1}00224{0 1}12310000010{1 2}0{0 1}1{1 2}{1 2}{0
1}{1 2}0100{0 1}{1 2}1001{1 2}21000000001000{0 1}00000000100{1 4}00010{0 1}{0
1}021{0 1}{0 1}110001010100002000000000000000000001000000-0

Palaeoprionodon_lamandini
2011211?1011311000110012121012 10002?????????1???000?300??0???0000101??0??????????
???
???????????????????1021???0?00?000003101100?34?1?11000202000100 20????0?000????110000
0001??010000000000?000??0?00210?121??1011?001?1??????????100000000??00000?-0

Stenogale_julieni
2?1020101??1311000210012221012210030111012011 12??00?300??0???0000101??0??????????
???
???????????????????10210??2?01?000103101100?35?1?11000102010000 2?????0?100??113??00
000?1??0?0?00?0?000?0?0?11?002?011?1???0?1?00??1??????????00000000001000000?-0

Herpestides_antiquus
20102000201131100020011212101221102211 1012011?0??0012101 10???0100101??0??????????
???
???????????????????111000?0001000100210000001311?1100020311001121????00200??11100
00000010001000??00000?000??0?102103110???011?01??1??????????11000000001000000-0

Ginsburgsmilus_napakensis   ?--?????????-
???????????????????????0011?1202101???????????????1001101?????????????-????-???????-
?????????-???????????????????1????1??????????-??????????????-
??????????????????????????????????20-0010000?????????36-

??3??102?2010000?????????????11111000?0?1????1?11?02000???0????????0-??-???0-?0--???-?????0????-0000000?00?????-0

Prosansanosmilus_eggeri   ?--?????????-
???????????????????????0011?1202101??????????????1001101?????????????-????-???????-??????????-?????????????????????????????????-???????????????-???????????????????????????????0?2-002000104101100?36-122??101?1120001?????????????010??011?001????0??1???001???0????????0-1?-???0-1?--???-?????????0-0000000?0?0????-0

Prosansanosmilus_peregrinus   ?--?????????-
????????????????????????????0?????????????????011?1?????????????-????-???????-??????????-?????????????????????????????????-???????????????-??????0??????????????????????02?-?0200??04101100??6-122??1?2?111?00??????????????10?2??11??01????1231??2?2????0????????0-12-???1-10--???-?????????0-??00000???0???1-0

Afrosmilus_hispanicus   ?--?????????-
??????????????????????????????01?????????????100?????????????????-????-???????-??????????-?????????????????????????????????-???????????????-???????????????????????????????0-002??0?04101100???-?????12??1?10????????????????2??1??????????????0?2????0????????0-1?-????-??--???-?????????0-??00000????????-0

Afrosmilus_turkanae   ?--?????????-
??????????????????????????0??0??????????????0011?1?????????????-????-???????-??????????-?????????????????????????????????-???????????????-????????????????????????????0-?02??0004101100?36-1????1?2?2110?00?????????????1?????00?00?1???0?11?????0???0????????0-12-???1-??--???-?????????0-??00000??00????-0

Afrosmilus_africanus   ?--1??0?????-
??????????????????????????101?????????????1001?????????????????-????-???????-??????????-?????????????????????????????????-???????????????-???????????????????????????0?0-0020001?????????3?-1?3??122?112000120?????11????1112?10000011???1?1??0?20???0????????10-??-????-??--???-??????????-??00000???0????-0

Albanosmilus_jourdani   ?--12?013??2-
200?0????0?????10211??0211?22021111???0110?????10011?1?????????????-????-???????-??????????-?????????????????????????????????-???????????????-???????????????????????1000?020-002000105201100?36-12251121001210010?????11?01??211211111{0 1}121?11233120?221???1??0011200-22-1341-10--??1-?????????0-??00000??0000?-0

Maofelis_cantonensis   1--12??01??0-
010?0?????10????01????0011?12021001?0?0?????????000???????????????-????-???????-
??????????-????????????????????????????????-???????????????-
??????????????????????????1??10?22-002??01?????????3?-
????000?11?10??020????0?100????20000?00??0?00????1010???0?0?1?010?10-??-001?-?0--
??2-??????????-??0000000??000?00

Eofelis_edwardsii   ?--?????????-
???????????????????????011??202100??????????????{0 1}00{0 1}1?1??????????????-????-
???????-??????????-??????????????????????????????????-???????????????-
??????????????????????????????????22-00?010103201100?3{5 6}-
121??001?1010001?????????????11110000?001????101010200????0???????10-12-???1-10--
???-?????????0-0000000?000?????1

Dinailurictis_bonali   ?--12???????-
???????????????????????0011?22021001???????????????00?1?1?????????????-01??-???????-
0??1??????-??????????????????????????1????????-???????????????-
??????????????????????????????????22-001010103201100?36-
121??0?1?1010001??2?0????????11110000?0?1????1?10?02?0??0?0????????0-1?-???0-?0--
???-?????????0-??00000?0?00?0??1

Quercylurus_major   ?--?2???????-
???????????????????????2?0?100??????????????100????????????????-????-???????-
??????????-??????????????????????????????????-???????????????-
??????????????????????????????????2-001??01?????????3?-
?????00??1?10??20?????????????1??00??0??????????????0?0?0?0????????0-??-????-??--???-
??????????-0000000?????????1

Dinaelurus_crassus   ?--122101000-
010?0??????????10211??0211?22021001????01000????100????????????????-????-???????-
??????????-??????????????????????????????????-???????????????-
??????????????????????????10?1??20-002??11?????????3?-
???5002?11?10??020????00?00????10000?00??1111????0000?0?000???012210-??-013?-?0--
??2-??????????-??00000????000?10

Hoplophoneus_oharrai   1--120000002-
01010???0010?0110211????11?22021101?00001000????10011?1??00???0?1?00-0100-
0001020-0101110000-11010011?0?1?0???1????1?1100100011-110????????????-
???????????010?10111???????10?100?0-0??010004101100?36-
12050?01110?00?110?00?00100?1?1?20?010001001112302 1??2??100??0?11200-?1-?231-10--
??1-??0??1???0-0000000?0?0000?00

'MA-PHQ 348'   ?--1??01?000-
010?00???0201011021110?????????10?????01?00???00?????????????????-????-???????-
??????????-??????????????????????????????????-???????????????-
??????????????????????????10?1??22-?????1????????????-

????0?0?11??0??0?????0??00????200???00???0?????0?????00?????2?1?-??-?12?-?0--??2-??????????-????????????00?0?

Hoplophoneus_dakotensis   2--1?0010?12-
????????0??????10211??0211?2202110??0?0?1000????10011?1?????????????-????-???????-??????????-????????????????????????????????-??????????????-?????????????????????????0?1?020-002010104201100?36-12150?2?110?00?200???0??200???11200?100110012223021?231?101?1001??00-11-0??1-?0---??1-?????????0-??00000????0?0?00

Hoplophoneus_sicarius   2--122010?12-
11011???00?0??110211??0211?2202110??00001000????10011?1?????????????-????-???????-??????????-????????????????????????????????-??????????????-?????????????????????????10?10020-002010104201100?36-1215012?110100?110200011111???103000100110012234021?231?101?10011?00-11-0131-10--??1-?????????0-??00000????000?00

Hoplophoneus_adelos   2--122010012-
10010???00?0?01?0211??0210?22021100?00001000????100?1?1???????????0?-0?0?-?00?02?-???0?1?010-???0?0011?1??????????????????????-??????????????-?????????????????10?01100??10?1??20-002??01?????????36-?2?501{1 2}?11?10??110??0011201?1?01?000?00?10012????2132?1?111?10110?00-??-0231-?0--??1-??????????-00000000???000?00

Hoplophoneus_bidentatus   2--122010?12-
210112?100202011021101?21??1?0?1100?001010000???10011?1???0???000000-0?01-000??2?-????1?0???-0???000??00?????????21?11???0?0011-??????????????-0??????????0?0?????0?????1010?10020-00?010004{1 2}01100?36-1215012?10{0 1}200?110200?10?0111?{0 1}1{1 2}00010011???22340203331?101?10?12210-12-?230-10--?02-????????00-??00000????000?00

Hoplophoneus_villebramarensis   2--12?010?12-
000?0??1001020110211?10211?22021101?0??01000????10011?1?????????????-????-???????-??????????-????????????????????????????????-??????????????-?????????????????????????10?1??20-002010004{1 2}01100?36-1225012?100200?110????10201???102000100?1???213?0?1?33??1?1????11200-?2-?230-?0--???-?????????0-??00000????000?00

Barbourofelis_morrisi   3--120010?12-{0 2}00002??1020?0010211??0211?220?1111?1?0110??0???10011?1???0?????????-0111-0011021-1011010011-101101111001??1????1????11000?0001-10?????????????-1?0110?????00?1???????????10001020-002000105201100?36-1225112?001{2 3}10?21000001?101??31121111111310122331202321?001?10012200-22-1241-?0--1?1-?00??????0-??00000???00?0?-0

Oriensmilus_liupanensis   3--120000?12-00010???0020001102110?0211?2202111{0 1}?0?111000????10011?1?????????????-????-???????-?????????-?????????????????????????????????-??????????????-??????????????????????????10?0?020-00200010520110?0?36-123501210{0 1}12101210???00?100??111211110{0 1}0100101221202?21?00{0 1}?10012200-22-0??0-10--???-?????????0-??00000???000?-0

Sansanosmilus_palmidens   2--120010012-210102?00020001102110?0211?22021111?1?0110??????10011?1???0??0?????-0111-001102?-1011?11011-1111001110?1????1??1?11110100?00?1-1101?0000011101-11?110???10?00?1????0?????010001020-002000105201100?36-??35112101121012?0???001011?1112111100110121?3120222?0000?10012200-2?-0240-?0--1?2-?0?????0?0-??00000???0000?-0

Barbourofelis_fricki   3--122013012-210012??00020001102110??2???2???1101????110??0???10011?1???0?????????-0111-0011011-1011010010-1011?1111001?1??11??????1100110000-100????????????-0?0110?????100?11111???????10001021-002000205?0110??36-12351121001?101200???011101??31331111111310122341202?2??011?10011200-?2-1240-10--1?1-?00??0???0-??00000???0001?-0

Barbourofelis_loveorum   3--122013?12-200102??00020001102110??2???1?0?1100?1?0110??????10011?1?0?0???001000-0111-0011{0 1}11-10110100{0 1}1-1011011111001?1111101211111000000?1-1101100?0011101-11011000?100???1??1????????1000?021-002000205201100?36-12351120001310120?????1??011?111?111111131?11233120232100?1??0?12200-22-1241-10--?1?-000??0?0?0-??00000???0000?-0

Albanosmilus_whitfordi   3--12?013?12-200?12??002??0?102110?0211?220?1111?0??110?????10011?1???0?????????-0111-0011011-10110?????-????????1?0??????????????1100?00000-??????????????-1?0110??????????????????10000020-002000105201100?36-12351122001210121 0???011100??2112111{0 1}?1121012{1 2}231202321?0?1?1?012200-22-1241-10--??1-?????????0-??00000???0000?-0

Hoplophoneus_cerebralis   2--1220100{0 1}2-210112?00010201102110302 11?22021100?0?1010000???10011?1???0???0?00?-0101-0001011-1101111??0-1??????11001???????????110000000?-?1010?00?00110?-1?1110??????00?1?100011101000?10020-00201010{4 5}201100?36-1215012?100110?110200{0 1}10201???112010100120012234020333310111?10111210-11-?1?1-10--??2-??0??????0-??000000???000?00

Hoplophoneus_primaevus   2--121010002-010102??00102011102110?0211?22021101?0?0010000???10011?1?100??000000-0100-0001020-1101111000-110100111011?00?111211111100000010-100100001021101-111110001100101111{0 1}1?11101000?1?020-00201010{3 4}101100?36-121501{0

1}1110200021020001110011111110{0 1}010011001112{2 3}02022210100?10011200-12-0231-10--?01-100000?000-00000000??0000?00

Hoplophoneus_occidentalis   2--120010012-010112?100102011021100021 1?220211?1?000010000???10011?1??00???0??0??-0100-0001020-1101111000-11010111100110011?1121111100000011-110100000021101-111110001100101111101010??10?1?020-???01010{3 4}101100?36-1225012111020002000 00?1110011111200?100110011123020222210100?1?01020?-11-0230-10--??1-?00?0?000{0 1}-??000000??0000?00

Nimravus_brachyops   2--122101000-{0 1}0010210{0 1}02000110211000211?22021001?000010000???{0 1}0011?1??00?????????-0101-0011021-1101011010-111100111001?11?110121111100010001-110110000011101-01011000110010111100011101?10?11020-00201010{3 4}201100?35-12350{0 1}0111020001102?00001001?1111000000011101101100101010000 11012210-12-0120-10--?12-?00??0?0?0-00000000?00000110

Pogonodon_platycopis   2--12?101000-000102??002010110211??0011?12021001???101000????10011?1???0?????????-????-???????-??????????-??????????????????????1100010001-???????????????-?????????????????????????00?11020-002010003201100?36-1215000 11101001200??0000100??1211000000010010112 0211001?000?1??10?10-11-?220-10--??1-?????????0-00000000000000?10

Pogonodon_davisi   2--122101000-00000???002010110211?00011?12021000?0?1010000???10011?1???0???0??0??-0101-?001020-0101111??0-1100?0111?0????????????111???00??-???110000010100-110110?01?0010?11????1?????10?1?020-00201 0003201100?36-121500{0 1 2}11101000200??001100??121200000001001011{2 3}01020011100?1?010?10-1{1 2}-0220-10--??1-????0??0?0-00000000000000?10

Dinictis_felina   2--122101000-0{0 1}0102?002010110211000011?12021001?001010000???10011?1?100??000000-0101-0001020-0101111000-110100111011?10?110121111100010001-100100000010101-110110001?0?10?111{0 1}0011101000?1102{0 2}-00201 0003101100?3{4 5}-12{1 2}5000111010001102000 0110011{0 1}1{0 1}10000000100{0 1}100201020010000?10012210-12-0{1 2}21-10--10{2 3}-100?00?000-00000000000000?10

Nanosmilus_kurteni   2--122?00002-000102?100102011021100021 1?22021101?0?0010000???10011?1?????????????-????-???????-??????????-?????????????????????????????-???????????????-??????????????????????????00?1?020-00201 0104201100?36-12150111110200021 0????01?00??111?00010011???1123020?221?101??0?112?0-12-?121-1?--??1-?????????0-00000000??0000?00

214

Nimravus_intermedius 2--1?{1 2}?01000-0001?2??0020001102110?0211?{1 2}2021001?0??010000??00001?1????????????-{0 1}101-?01102{0 1}-1??10?????-????????1?1?????1??1??1???????????-??????????????-0?0110????????????????????10?11?20-002010104201100?35-??3500011101000110???00100??11110000001110110110010 1010?0?11012210-12-?1?0-10--??1-?????????0-00000000?00000110

Tapocyon_robustus 10101?0000010010112010010100000010?201101102000????0000??0???0000100??0????0100??1100010000020010100010111100101?11111??0?1??1?1?11?0001001100000?0??1?100111?1??1?0??10????????????????1??1?0?2?00000000210100001311 03?0002010100011000?000??00??1111000000011100100000000 0?200????1??201110100010000??1?????????01000000101000 00?-0

Procynodictis_vulpiceps 1?1??0000001111011??1100010010100001011111010 0{0 1}??00?000??0???00001?0???????0110?011111101002001 0?001101110101?1111111????????0010101010001000011010112 101110111?001110?1????110010?0200003?0020000 00??10?20??002?1010?10????????????111000000??1????0?0 ??00000??0????????021???????00??????????????00000000000100?0??-0

Hesperocyon_gregarius 10111?110001211000201121030011200112011111201010?001010010??0000100??00???1?1??012011?0000020000000110100010101111011??????? 000000?1010101011011111101101011 1111??111?0101111??0000000000?0002000000021000000030121?000201010111 10????01100??1111000000010?000000000200?200????1121 1212001101100 1??1??1?????????00000000001000000-0

Canis_latrans_frustror 10011110000101110122?2{0 1}2103001120111101111201100100101001000100001101001000011101 02011?0111001010110{0 1}001110111110101111100000100001?101101111011110112010 1001011110?11101001000010010110001020200000000210000000301 20?000201010?1100101000010011101000000010100000000 02000200?1001200021100110010001110010000?000000000000000000-0

Vulpes_vulpes 2001110000010111012?20210300112011110111102010001001010010001000011010010000111010201 1?01110010101100001101111110101111100000100001?101101110111101121101 001011110?1110100100001001011000102020000000021000100030120?000201010?1100201000010010 10{0 1}00000011100000000000000200?{0 1}00120103110001001000112001100000000000000000000000-0

Taxidea_taxus 2000111000000001022?0221030011201111111110211001100121100001101 11?11001001001110001110100102000011010000110001011101111010000200001?00110011110100001120001 111111111?1001010 0?????101102000102000100010020000 11?340020?100001010?121020100

1000011120000000001000102001000000301??010221002101210210200000001 01?000??000000000?000000000-0

;

END;

Appendix F

## *Custom Evolutionary Models (Rate Matrices)*

Beast 2.6.3 does not include a method to order characters from the BEAUti graphic user interface, thus only non-ordered characters are available for an analysis that does not manually edit the xml file. Below are schematic depictions of the rate matrices used in this analysis, with diagonal elements removed. The xml versions of these models are visible in the provided xml code.

3-state Characters

Ordered

Feliformia_trim_2_3_ordc_ratematrix
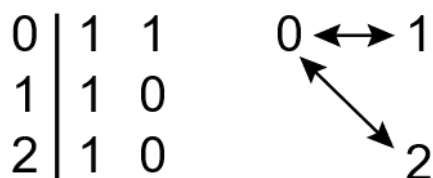
Characters: 5, 6, 14, 18, 19, 22, 24, 31, 37, 41, 42, 83, 185, 196, 200, 203, 219, 220, 229, 257, 258, 262, 279, 280, 282, 283, 288, 289, 322, 323

```
0 | 1 0       0 ←→ 1
1 | 1 1            ↕
2 | 0 1            2
```
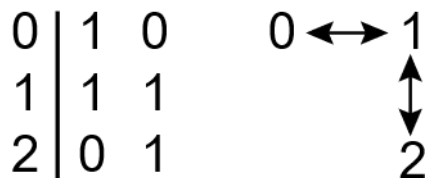
Ordered, multipath

Feliformia_trim_2_3m_ordc_ratematrix

Characters: 47, 127, 192, 193, 231

```
0 | 1 1       0 ←→ 1
1 | 1 0          ↙
2 | 1 0          2
```

4-state Characters

Ordered

Feliformia_trim_2_4c_ord_ratematrix

Characters: 1, 195, 210, 215, 222, 224, 228, 242, 243, 244, 245, 253, 264, 277, 281, 286, 293, 296

```
0 | 1 0 0        0 ←→ 1
1 | 1 1 0             ↕
2 | 0 1 1             
3 | 0 0 1        3 ←→ 2
```
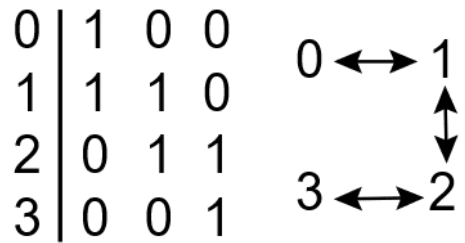
Ordered, multipath 1, irreversible

Feliformia_trim_2_4mi_1ord_ratematrix

Characters: 266

```
0 | 1 1 0        0 ←→ 1
1 | 1 0 0           ↖  ↘
2 | 1 0 1             
3 | 0 0 0        3 ←— 2
```
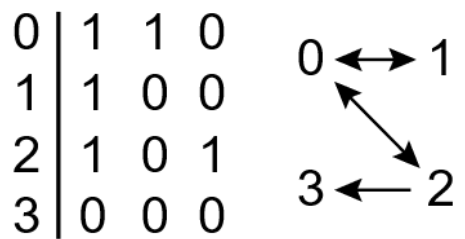
Ordered, multipath 2

Feliformia_trim_2_4m_2ord_ratematrix

Characters: 198

```
0 | 1 0 1      0 ←——→ 1
1 | 1 1 0      ↕        ↕
2 | 0 1 0      3        2
3 | 1 0 0
```

Ordered, multipath 3

Feliformia_trim_2_4m_3ord_ratematrix

Characters: 12, 259, 265

```
0 | 1 1 0      0 ←——→ 1
1 | 1 0 0          ↘
2 | 1 0 1             ↘
3 | 0 0 1      3 ←——→ 2
```

Ordered, multipath 4

Feliformia_trim_2_4m_4ordered_ratematrix

Characters: 53

```
0 | 1 0 1      0 ←——→ 1
1 | 1 1 0      ↕        ↕
2 | 0 1 1      3 ←——→ 2
3 | 1 0 1
```

5-state Characters

Ordered

Feliformia_trim_2_5c_ord_ratematrix

Characters: 260, 287

```
0 | 1 0 0 0        0 ←→ 1
1 | 1 1 0 0               ↕
2 | 0 1 1 0      4        2
3 | 0 0 1 1         ↘   ↗
4 | 0 0 0 1           3
```
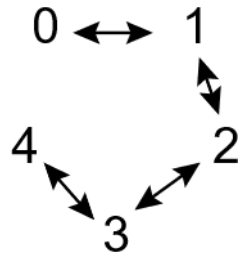
Ordered, multipath

Feliformia_trim_2_5m_ordered_ratematrix

Characters: 35

```
0 | 1 1 0 1        0 ←→ 1
1 | 1 1 0 1
2 | 1 1 1 1      4        2
3 | 0 0 1 1
4 | 1 1 1 1           3
```
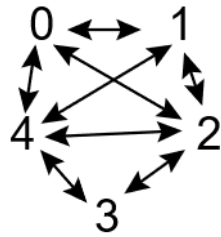
Ordered, multipath 2

Feliformia_trim_2_5m_2ordered_ratematrix

Characters: 269

```
0 | 1 1 0 0        0 ←→ 1
1 | 1 0 0 1
2 | 1 0 1 0      4        2
3 | 0 0 1 0
4 | 0 1 0 0           3
```
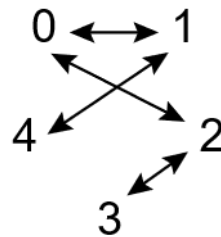
6-state Characters

Ordered

Feliformia_trim_2_6_ordered_ratematrix

Characters: 202

```
0 | 1 0 0 0 0
1 | 1 1 0 0 0
2 | 0 1 1 0 0
3 | 0 0 1 1 0
4 | 0 0 0 1 1
5 | 0 0 0 0 1
```
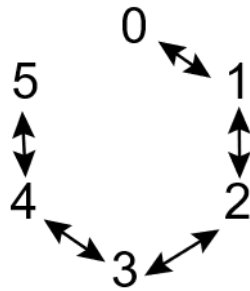

Ordered, multipath

Feliformia_trim_2_6m_ordered_ratematrix

Characters: 216

```
0 | 1 1 0 0 1
1 | 1 1 0 0 1
2 | 1 1 1 0 1
3 | 0 0 1 1 0
4 | 0 0 0 1 0
5 | 1 1 1 0 0
```
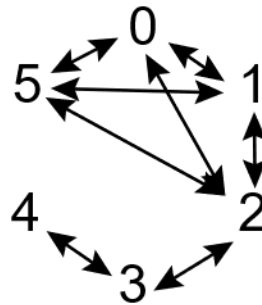
7-state Characters

Ordered

Feliformia_trim_2_7_ordered_ratematrix

Characters: 211

```
0 | 1 0 0 0 0 0
1 | 1 1 0 0 0 0
2 | 0 1 1 0 0 0
3 | 0 0 1 1 0 0
4 | 0 0 0 1 1 0
5 | 0 0 0 0 1 1
6 | 0 0 0 0 0 1
```
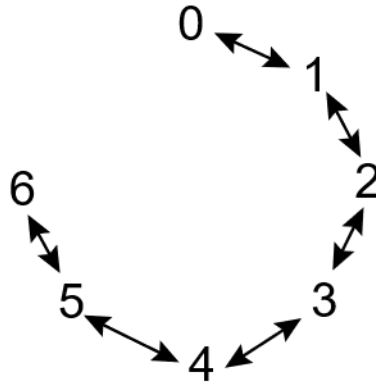
Appendix G

Stratigraphic Ranges and Tip Date Priors

Extant Taxa

Due to the preponderance of molecular data, compared to morphological data, for extant taxa in this analysis, tip dates were fixed to zero for these taxa (n=45). All remaining taxa were given uniform distributions of equal probability between their FAD and LAD, unless otherwise stated.

Caniformia

Hesperocyon gregarious. **Locality***:* Numerous across North America, see Wang (1994).

Absolute age estimate: 41.4-29.75 Ma. A relatively ubiquitous taxon of the Chadronian through Whitneyan, the earliest records extend into possibly the earliest Duchesnean (Wang, 1994). These earliest specimens come from the Lac Pelletier Lower Fauna of Saskatchewan, but precise age constraints for this fauna is still debated (Bryant, 1992). Thus, the age range chosen for this taxon was the entirety of the Duchesnean through Whitneyan (as defined by Kelly et al., 2012; Ogg et al., 2016) pending more precise dating.

Procynodictis vulpiceps. **Locality***:* Wyoming, USA. **Absolute age estimate**: 45.15-41.4 Ma. The stratigraphic range of this taxon appears to encompass the entire Uintan (Robinson et al., 2004), though the latest occurrence is in some doubt (Spaulding et al., 2010; Solé et al., 2016). For this study the entire Uintan NALMA was used (as defined by Kelly et al., 2012; Ogg et al., 2016).

Feliformia

Tapocyon robustus. **Locality**: California, Montana, Wyoming, Utah, USA. Stratigraphy: All Uintan. **Absolute age estimate**: 46.5 - 39.7 Ma (Robinson et al., 2004). *Tapocyon* has typically been placed as the immediate sister taxon to crown Carnivora based on parsimony analysis of morphological data (Wesley-Hunt and Flynn, 2005). However, Barrett et al (2021) recovered it as a stem feliform, as did Tomiya and Tseng (2016).

Feloidea

Stem Feloids

Proailurus lemanensis. **Localites:** Quercy Fissures, Laugnac, Paulhiac, Bassin de St-Gérand, France. **Absolute age estimate**: 27.82-20.44 Ma (Slater and Friscia, 2019).

Stenogale julieni **Locality**: Quercy Fissures, France. **Absolute age estimate**: 27.82 - 23.03 Ma (Slater and Friscia, 2019).

Palaeoprionodon lamandini **Locality**: Quercy Fissures, France. **Absolute age estimate**: 27.82-23.03 Ma (Slater and Friscia, 2019).

Herpestides antiquus **Locality**: France, Germany. **Absolute age estimate**: 23.03-20.44 Ma. Following the revision of Wolsan and Morlo (1997), this taxon is known from the Aquitanian/Agenian (Hunt, 1991). The absolute dates of the former were taken from Ogg et al. (2016).

Felidae

Pseudaelurus validus **Localities**: Various in New Mexico, Nebraska, USA (see Rothwell, 2001, 2003) **Absolute age estimate**: 17.0-14.5 Ma (Slater and Friscia, 2019).

Promeganterereon ogygia **Localities**: Eppelsheim, Germany; Batallones-1 and Crevillente-2, Spain. **Absolute age estimate**: 11.1-7.75 Ma (Slater and Friscia, 2019).

Metailurus major **Locality:** Bulgaria, Greece, China. **Absolute age estimate**: 7.6-5.7 Ma. The referred AMNH material is from the Mahui Formation, 6.7-5.8 Ma (Qiu et al., 2013). The oldest dated specimen of this taxon is from the MN11/12 boundary of Bulgaria (Kovatchev, 2001). Roussiakis (2001) lists further European occurrences from MN12-13. However, the taxonomic revision of *Metailurus* by Spassov and Geraads (2015) casts doubt on the diagnosis of many of these specimens. Confidently referred material comes from Pikermi, Greece (7.37-7.11 Ma; Roussiakis, 2001; Böhme et al., 2017), the type skull from Loc. 30, Tay-Chia-Kou (5.7 Ma; Kaakinen et al., 2013), and intermediate aged dates from Greece and China (Spassov and Geraads, 2015). Thus, the absolute date of this taxon follows the material that was examined for this study and referable to *Metailurus major* by Spassov and Geraads (2015). Absolute age dates given for MN zones follow Hilgen et al. (2012).

Dinofelis diastemata **Locality:** France, China. **Absolute age estimate**: 5.3-1.0 Ma. Referred specimens F:AM 50445, 50446 differ in osteometrics from published values of *Dinofelis diastemata*, namely in smaller values of absolute C1 and P3 size (length, width) (Werdelin and Lewis, 2001). Furthermore, they are substantially smaller than that of Asian *D. cristata*, though a

geographically more-likely taxon, than the French *D. diastemata* (Werdelin and Lewis, 2001). Another possibility is the same species to which the Georgian Melaani skull belongs (Gabunia and Vekua, 1998; Werdelin and Lewis, 2001). The Melaani skull also differs from the above named species by having smaller osteometrics, but more compressed canines, and is stated by Werdelin and Lewis (2001) to be most-similar in dimensions to South African *D. barlowi*. However, barring a more in-depth taxonomic review of additional Eurasian *Dinofelis* specimens, I chose to diagnose F:AM 50445, 50446 to *D. diastemata* based upon similar length of the P4, unreduced P3 and shape of the sagittal crest. *Dinofelis diastemata* is attributed to MN 14 in Europe (Werdelin and Lewis, 2001). The referred Chinese material has an attributed date of Ruscinian-Villafranchian, thus overlapping absolute age dates are given above based on Rook and Martínez-Navarro (2010) and Hilgen et al. (2012).

Nimravides pedionomus **Locality:** Nebraska, USA. **Absolute age estimate**: 13.55-9.95 Ma. Referred material to this taxon has been collected from the Nenzel quarry, Valentine Formation, Crookston Bridge Member; Xmas quarry, channel fills within the Ash Hollow Formation, Cap Rock Member and UCMP locality V-3327 (Antón et al., 2013). The Crookston Bridge Member lies above the Hurlbut Ash, dated at 13.55 ±0.09 Ma (Tedford et al., 2004), while the Xmas quarry was viewed as stratigraphically correlative with the *Machairodus* quarry by Skinner and Johnson (1984), which is capped by a dated ash at 9.95 ±0.8 Ma. UCMP locality V-3327 is where the holotype of *Nimravides pedionomus* comes, also Cap Rock Member of the Ash Hollow Formation, and is thought to be intermediate in age of the previously listed sites (Tedford et al., 2004).

Machairodus catocopis **Locality:** Kansas, USA. **Absolute age estimate**: 7.5-6.6 Ma. This taxon is well known from the Jack Swayze Quarry and Sebastian Ranch fossil localities (Antón et al., 2013). Both of these localities are viewed to be Hh2 in age (Martin, 1998). Absolute dates for this Hemphillian subunit follows Hilgen et al. (2012).

Amphimachairodus coloradoensis **Locality:** USA. **Absolute age estimate**: 6.6-4.9 Ma. This taxon is known from various late Hemphillian sites in the American west (Antón et al., 2013), while material assigned to this taxon from Arroyo Tepalcates, Mexico has since been removed to a new species (Ruiz-Ramoni et al., 2020). Hh3-Hh4 were chosen as the time range for this taxon given imprecise dates for many of these localities. Absolute dates for the Hemphillian subunits follow Hilgen et al. (2012).

Amphimachairodus giganteus **Locality:** Various, Europe, Asia. **Absolute age estimate**: 8.7-5.3 Ma (Slater and Friscia, 2019).

Xenosmilus hodsonae **Locality:** Florida, USA. **Absolute age estimate**: 2.5-1.0 Ma. Specimens from University of Florida localities span the latest Blancan to early Irvingtonian. The Santa Fe River locality is likely the oldest at approximately 2.5 Ma, while the youngest locality is likely Haile 21A, site of the holotype, inferred to be slightly younger than the dated Leisy Shell Pit at 1.1-1.55 Ma (Bell et al., 2004).

Homotherium ischyrus **Locality:** North America. **Absolute age estimate**: 4.9-2.0 Ma. Following the findings of Antón et al. (2014), I limited the biostratigraphic age of this species to the

Blancan, compared to the later, morphologically diverse *Homotherium latidens* (Paijmans et al., 2017). Dates follow Hilgen et al. (2012).

Homotherium latidens **Locality**: Europe. **Absolute age estimate**: 0.033049-0.031674 Ma. The date for this species is tied to the radiocarbon date of the specimen sampled for DNA, Natuurmuseum Rotterdam catalogue number 02-011, GenBank: MF871701. Six total radiocarbon dates have been collected on this specimen (Reumer et al., 2003). The last two of these dates were considered most reliable, with inferred contamination in the first four. Of these two dates I chose the date obtained from the tooth (28,100 ± 220 ^{14}C age yr. BP), as it is the one primarily reported by Reumer et al. (2003) for the age of this specimen. This date in two sigma calibrated years (using CalPal Rev 8.1.0) is the range reported above. A normal distribution spanning this range (2 sigma confidence interval, mean=0.03236, sigma = 0.0004) was used as the tip prior in the phylogenetic analysis.

Homotherium serum **Locality**: North America. **Absolute age estimate**: > 0.0565 Ma. The date for this species is tied to the radiocarbon date of the specimen sampled for DNA, Canadian Museum of Nature, Ottawa, CMN46442; GenBank: MF871703. The provided radiocarbon date (>56,500 ^{14}C age yr. BP; Paijmans et al., 2017) is beyond the 45–50 ka resolution limit of radiocarbon dating and thus provides a minimum age of the specimen. I chose an exponential distribution (mean 0.0511, 95% quantile 0.2 Ma, offset 0.0565) such that the 95% quantile extended to the start of the Rancholabrean, the first occurrence of this species in North America (Slater and Friscia, 2019).

Megantereon cultridens **Locality**: Various, Africa, Eurasia, ?North America. **Absolute age estimate**: 3.5-0.4 Ma (Slater and Friscia, 2019).

Smilodon fatalis **Localities**: North America (USA, Mexico) and possibly western South America. **Absolute age estimate**: 0.6-0.0095 Ma (Slater and Friscia, 2019).

Smilodon populator **Localities**: Various, Venezuela, Ecuador, Bolivia, Argentina, Brazil. **Absolute age estimate**: 0.013372-0.013235 Ma. The date for this species is tied to the radiocarbon date of the specimen sampled for DNA, an uncatalogued left tibia from the Kruimel collection, Naturalis, Leiden, GenBank: MF871700 ($11,335 \pm 30$ ^{14}C age yr. BP; Paijmans et al., 2017). This date in two sigma calibrated years (using CalPal Rev 8.1.0) is the range reported above. A normal distribution spanning this range (2 sigma confidence interval, mean=0.0133035, sigma = 0.00004) was used as the tip prior in the phylogenetic analysis.

Panthera leo spelaea **Localities**: Various, Europe, Asia, North America (Barnett et al., 2009). **Absolute age estimate**: > 0.061Ma. The date for this species is tied to the radiocarbon date of the specimen sampled for DNA, hair bolus, sample F-2678/70, GenBank: KX258452 (Barnett et al., 2016). However, there is a discrepancy in the radiocarbon dates for the hair sample and that of associated skeletal material (Kirillova et al., 2015). This discrepancy the authors attributed to contamination of the hair sample, while not of the skeletal material. Thus, I chose to use the radiocarbon date for the skeletal material, but given its extent beyond the resolution limit of radiocarbon dates I applied an exponential distribution (mean 0.61, 95% quantile 1.89 Ma, offset

0.061) such that the 95% quantile extended to inferred split between *Panthera leo* and *Panthera leo spelaea* (Barnett et al., 2016).

Panthera atrox **Localites**: Various, North America. **Absolute age estimate**: 0.013401-0.013226 Ma. The date for this species is tied to the radiocarbon date of the specimen sampled for DNA, Metatarsal II, Royal Alberta Museum EDM P89, GenBank: DQ899945.1 (11,355 $\pm$ 55 ^{14}C age yr. BP; Barnett et al., 2009). This date in two sigma calibrated years (using CalPal Rev 8.1.0) is the range reported above. A normal distribution spanning this range (2 sigma confidence interval, mean = 0.0133135, sigma = 0.00004) was used as the tip prior in the phylogenetic analysis.

Miracinonyx trumani **Localites**: Various, North America. **Absolute age estimate**: 0.024037-0.023781 Ma. The date for this species is tied to the radiocarbon date of the specimen sampled for DNA, University of Kansas, KS28 NTC43093, GenBank: DQ097168.1, DQ097175.1, DQ097170.1 (19,765 $\pm$ 80 ^{14}C age yr. BP; Barnett et al., 2005). This date in two sigma calibrated years (using CalPal Rev 8.1.0) is the range reported above. A normal distribution spanning this range (2 sigma confidence interval, mean=0.023909, sigma = 0.0001) was used as the tip prior in the phylogenetic analysis.

Lophocyonidae

Izmirictis cani **Localites**: Sabuncubeli, Turkey. **Absolute age estimate**: 19.5-17.2 Ma. This taxon comes from the lower part of the Soma Formation of western Turkey (Morales et al., 2019). No absolute dates are available for this locality, but biostratigraphy suggests an early MN

3 fauna (Morales et al., 2019). However, barring more-detailed temporal placement, I chose to use the entire MN 3 zone for this phylogeny, following Hilgen et al. (2012).

Euboictis aliverensis **Localites**: Aliveri, Greece. **Absolute age estimate**: 18.01-17.5 Ma. Hoek Ostende et al. (2015) place the only known fossil locality of this taxon at the above absolute age.

Sivanasua viverroides **Localites**: France, Germany. **Absolute age estimate**: 17.2-11.2 Ma. This taxon is known from MN4-MN7/8 (Morales et al., 2019), with absolute ages following Hilgen et al. (2012).

Herpestidae

Kichechia zamanae **Localites**: Rusinga, Kenya. **Absolute age estimate**: 20.0-17.0 Ma. A recent revision has split this taxon between at least two species, with *Kichechia zamanae* now only explicitly known from Rusinga and Songhor (Adrian et al., 2018). Additional eastern African localities report this taxon (e.g. *Kichechia sp.* from Napak; Werdelin and Peigné, 2010), but barring additional taxonomic study at these sites I chose to only use the temporal age associated with Rusinga and Songhor (Werdelin and Peigné, 2010; Adrian et al., 2018).

Kanuites lewisae **Localites**: Fort Ternan, Kenya. **Absolute age estimate**: 14.0-13.4 Ma. All material attributable to this taxon is known from Fort Ternan (Werdelin, 2019). The age of this locality is well known from whole-rock K/Ar and single-crystal ^{40}Ar/^{39}Ar at 13.7 ± 0.3 Ma (Pickford et al., 2006). This date in two sigma years is the range reported above. A normal

distribution spanning this range (2 sigma confidence interval, mean=13.7, sigma = 0.2) was used as the tip prior in the phylogenetic analysis.

Hyaenidae

Tongxinictis primordialis **Locality**: Tongxin, China. **Absolute age estimate**: 13.8-12.5 Ma. As described by Qiu et al. (1988), this taxon is known from the earliest Tungurian, roughly equivalent to MN6. The absolute dates follow Agustí et al. (2001).

Allohyaena kadici **Locality**: Hungary, Germany. **Absolute age estimate**: 8.7-7.5 Ma. The described temporal age (MN 11) and geographic range of this taxon follow Turner et al. (2008), while the absolute dates follow Agustí et al. (2001).

Plioviverrops orbignyi **Locality** Greece, Spain: **Absolute age estimate**: 9.7-6.8 Ma. The described temporal age (MN 10-12) and geographic range of this taxon follow Turner et al. (2008), while the absolute dates follow Agustí et al. (2001).

Protictitherium crassum **Locality**: France, Germany, Greece, Spain, Turkey. **Absolute age estimate**: 17.1-5.1 Ma. Following the in-depth study of this species (particularly at Cerro de los Batallones, Spain) by Gracia (2015), the temporal range now extends from the end of MN 4 to MN 13.

Tungurictis spocki **Locality**: Tung Gur, China. **Absolute age estimate**: 12.75-11.1 Ma (Slater and Friscia, 2019).

Ictitherium viverrinum **Locality**: Various Europe, Asia. **Absolute age estimate**: 11.5-4.9 Ma. The described temporal age and geographic range of this taxon follow Turner et al. (2008), while the absolute dates follow Agustí et al. (2001).

Hyaenictitherium wongii **Locality**: Germany, Greece, Ukraine, Turkey, Iran, Kazakhstan, China. **Absolute age estimate**: 11.5-4.2 Ma. This cosmopolitan species ranges from MN 9-14 (Tseng and Wang, 2007). However, there is debate as to the generic assignment of this and other *Hyaenictitherium* taxa (see Semenov, 2008). Here, I followed the taxonomy of Tseng and Wang (2007) and Turner et al. (2008).

Hyaenictitherium hyaenoides **Locality**: China, Ukraine, Iran, Turkey, Kazakhstan, Mongolia. **Absolute age estimate**: 7.5-4.2 Ma. Temporal (MN 11-14) and geographic ranges follow Tseng and Wang (2007).

Lycyaena chaeretis **Locality**: Greece, Spain, Ukraine. **Absolute age estimate**: 8.7-6.8 Ma. The described temporal age (MN 11-12) and geographic range of this taxon follow Turner et al. (2008), while the absolute dates follow Agustí et al. (2001).

Palinhyaena reperta **Locality**: China. **Absolute age estimate**: 7.5-6.8 Ma. The described temporal age (MN 12) and geographic range of this taxon follow Werdelin and Solounias (1991), while the absolute dates follow Agustí et al. (2001).

Belbus beaumonti **Locality**: Greece, Turkey. **Absolute age estimate**: 8.7-6.8 Ma. The described temporal age (MN 11-12) and geographic range of this taxon follow Turner et al. (2008), while the absolute dates follow Agustí et al. (2001).

Adcrocuta eximia **Locality**: Various China, Kyrgyzstan, Europe. **Absolute age estimate**: 8.7-4.9 Ma (Slater and Friscia, 2019; Miller et al., 2020).

Pachycrocuta brevirostris **Locality**: Various South and East Africa, China, Europe and South Asia. **Absolute age estimate**: 3.0 (Asia, Africa) - 0.5 (Europe) Ma (Slater and Friscia, 2019).

Chasmaporthetes lunensis **Locality**: Various China, Europe, Asia. Absolute age estimate: 5.332-2.0 Ma (Slater and Friscia, 2019).

Chasmaporthetes ossifragus **Locality**: Various; USA, Mexico, China? Absolute age estimate: 5.332-0.85 Ma. Werdelin and Solounias (1991) recognized most North American hyaenid material as *C. ossifragus*, expect for the Florida specimens, which were distinguished by a longer m1 relative to the p4. However, Tseng et al. (2013) found this value to be on a continuum of other *Chasmaporthetes* specimens, and thus cast doubt on the validity of this specific character.

Thus, until more clear specific diagnostic criteria for a purported Florida species of *Chasmaporthete* is determined, I chose to include this material into *C. ossifragus*. *Chasmaporthetes* is a Blancan index taxon and thus was used as the first appearance datum (Bell et al., 2004; Tseng et al., 2013). The latest described specimens appear to come from the Mexican El Golfo Fauna, thought to be Irvingtonian in age, but with no associated radiometric or paleomagnetic dates (Bell et al., 2004). For this study an Irvingtonian 1 latest occurrence was used, given the preponderance of Blancan dates for this taxon, and lack of other known Irvingtonian occurrences.

Crocuta crocuta spelaea **Localites**: Various, Europe, Asia. **Absolute age estimate**: 0.021889-0.126 Ma. The date for this species is tied to the age of the specimen sampled for DNA, petrous bone, GenBank: MN320462.1 (Westbury et al., 2020). Unfortunately, there is no connection between GenBank accession numbers and the radiocarbon dates of the three German cave hyena specimens in Westbury et al. (2020). Thus, I chose to use a uniform prior to encompass the dates of all three German cave hyena specimens to be assured of sampling the most likely date. The youngest specimen, Ccsp043, has a reported date of 18,030±50 ^{14}C age yr. BP, while the oldest specimen, Ccsp040, as "Late Pleistocene" (Westbury et al., 2020). The Late Pleistocecne is an informal unit, but has been defined by the Subcomission on Quaternary Stratigraphy (http://quaternary.stratigraphy.org/definitions/pleistocene-subdivision/ accessed on 12/22/2020) at the base of the Eemian, or 0.126 Ma. The youngest date in two sigma calibrated years (using CalPal Rev 8.1.0) returns 0.021889-0.022191 Ma. A uniform distribution spanning the minimum 2 sigma confidence interval to the base of the Late Pleistocene was used as the tip prior in the phylogenetic analysis.

Dinocrocuta gigantea **Localites**: Bulgaria, Mongolia, China. **Absolute age estimate**: 11.5-8.0

Ma. The precise geologic age of this taxon has long been unclear (Zhang, 2005). However,

European remains attributed to this taxon are thought to be Vallesian in age (Spassov and

Koufos, 2002), with a slightly later appearance at approximately Chron 5n.2n in China (Zhang,

2005). The youngest dated record is at approximately 8.0 Ma from the Red Clays of Fugu, China

(Zhang, 2005).

Percrocuta carnifex **Localites**: Pakistan. **Absolute age estimate**: 14.2-9.5 Ma. Recent work has

reviewed the occurrence of this taxon in the Middle Siwalik (Ghaffar et al., 2019). *Percrocuta*

carnifex is known from the Chinji and Nagaro Formations, with referrals to the younger Dhok

Pathan Formation as unlikely (Ghaffar et al., 2019).

Percrocuta algeriensis **Localites**: Algeria. **Absolute age estimate**: 12.18-7.0 Ma. Howell and

Petter (1985) give localities at Bou Hanifia (12.18-9.7 Ma.; Bernor et al., 1980) and Menacer.

The latter locality is viewed as Middle Turolian by Howell and Petter (1985), and approximately

7 Ma by Benefit et al. (2008).

Percrocuta tobieni **Localites**: Kenya, Tunisia. **Absolute age estimate**: 13.8-11.0 Ma. Recent

finds of this taxon at Fort Ternan extend the temporal range of this taxon to 13.8 Ma (Werdelin,

2019), while the youngest occurrences span the Ngorora Formation (12.5-11.0 Ma; Morales and

Pickford, 2005; Werdelin, 2019).

Nimravidae

Oriensmilus liupanensis. **Locality**: Tongxin area of Ningxia Hui Autonomous Region, northern China (Wang et al., 2020). **Absolute age estimate**: 16.0-15.0 Ma (Qiu et al., 2013). The holotype and additionally referred material is from an informal middle member of the Zhang'enbao Formation, from which emanates the Ma'erzhuizi Gou Fauna (Wang et al., 2016), that the authors included within the Dingjia'ergou Fauna. The latter fauna is the date to which I applied the age estimate of this taxon, as did Wang et al. (2020).

Sansanosmilus palmidens. **Locality***:* France. **Absolute age estimate**: 16.0-13.0 Ma. The majority of *S. palmidens* material comes from southern France at the locality of Sansan, MN 6 (Peigné, 2012). However, additional fragmentary material has been described from Savigné-sur-Lathan (MN5) of western France (Ginsburg, 2001).

Barbourofelis fricki **Locality***:* Kansas, Nebraska, Texas, Nevada, USA. **Absolute age estimate:** 9.0–7.0 Ma (Tseng et al., 2010).

Barbourofelis loveorum **Locality***:* Florida, USA. **Absolute age estimate:** 9.5–8.0 Ma (Tseng et al., 2010).

Barbourofelis morrisi **Locality***:* Nevada, South Dakota, Texas, USA. **Absolute age estimate:** 12.0–9.5 Ma (Tseng et al., 2010).

Albanosmilus whitfordi **Locality***:* California, Colorado, Nebraska, Texas, Florida, USA.

Absolute age estimate: 12.0–7.0 Ma (Tseng et al., 2010).

Albanosmilus jourdani **Locality**: Spain, France, Turkey. **Absolute age estimate**:11.9-9.7 Ma (Robles et al., 2013).

Hoplophoneus cerebralis. **Locality***:* South Dakota, California, Oregon, Wyoming, USA. **Absolute age estimate**: 34.7-29.586 Ma. The earliest specimen referable to this taxon is an edentulous dentary from the Crazy Johnson Member of the Chadron Formation (Barrett, 2016). The latest well-documented occurrence is from below the "Blue Basin Tuff" of the Turtle Cove Member of the John Day Formation (29.586 Ma; Famoso et al., 2015).

Hoplophoneus primaevus. **Locality***:* Nebraska, South Dakota, Wyoming, Colorado, Oregon, USA. **Absolute age estimate**: 35.7-30.58 Ma. Following the taxonomy of Barrett (2016), the oldest occurrence of this taxon is from Flagstaff Rim Wyoming (Bryant, 1996; Prothero and Emry, 2004). The youngest specimens attributed to this taxon are found just below the "Upper Whitney Ash" in Nebraska and the basal *Leptauchenia* beds of the Poleslide Member of the Brule in South Dakota (Bryant, 1996; Prothero and Emry, 2004).

Hoplophoneus occidentalis. **Locality***:* Nebraska, North Dakota, South Dakota, Wyoming, USA. **Absolute age estimate**: 33.4-31.4 Ma. The earliest stratigraphically constrained specimens of this taxon come from the "lower nodules" of the Scenic Member of the Brule Formation, correlated to 33.4-33.1 Ma (Bryant, 1996; Prothero and Emry, 2004). The latest occurring

specimens emanate from the *Protoceros* channel sandstones of the Poleslide Member of the Brule Formation (Bryant, 1996; Barrett, 2016).

Nimravus brachyops. **Locality***:* Nebraska, South Dakota, California, Oregon, Wyoming (USA); Saskatchewan (Canada)*.* **Absolute age estimate**: 31.4- 27.14 Ma. This is a geographically wide-ranging taxon in North America with its first occurrence in the *Protoceros* channel sandstones of the Poleslide Member of the Brule Formation, South Dakota (Bryant, 1996; Prothero and Emry, 2004). The last reported occurrence of this taxon is from the K1 unit of the Turtle Cove Member of the John Day Formation (Famoso et al., 2015). The K1 unit is capped by the "Biotite Tuff" and forms the LAD for this study.

Pogonodon platycopis. **Locality***:* South Dakota, Nebraska, Oregon, USA. **Absolute age estimate**: 32.0-29.586 Ma. Numerous specimens of Whitneyan age are referred to this taxon, with none being clearly older (Bryant, 1996; Barrett, 2016). The youngest age comes from Unit E of the Turtle Cove Member of the John Day Formation, below the "Blue Basin Tuff" (Famoso et al., 2015).

Pogonodon davisi. **Locality***:* Wyoming, Nebraska, South Dakota, Oregon, USA. **Absolute age estimate**: 32.0-25.9 Ma. Like *P. platycopis*, the earliest record of this taxon is Whitneyan in age (Bryant, 1996; Barrett, 2016). The youngest specimen (JODA 5841) attributable to this taxon comes from the K2 unit of the Turtle Cove Member of the John Day Formation. This specimen was referred to as a possible new species of *Pogonodon* by Bryant and Fremd (1998) and Albright et al. (2008), but is included in this taxon following the diagnosis of Barrett (2016).

Dinictis felina. **Locality***:* South Dakota, North Dakota, Nebraska, Oregon, Montana, Wyoming (USA); Saskatchewan (Canada). **Absolute age estimate**: 35.7- 29.586 Ma. The oldest record known is at Flagstaff Rim, at just over 35.5 Ma, though several slightly older occurrences are possible from fragmentary remains and provisional dates (Bryant, 1996). For example, *Dinictis sp.* has been collected from the Medicine Poles local fauna of southwestern North Dakota, thought to be Ch2 in age (Boyd and Webster, 2018). This latter occurrence is used as the FAD of this taxon. The LAD includes the occurrence of *Dinictis cyclops* (= *D. felina*; Barrett, 2016) below the Blue Basin Tuff (29.586 Ma; Famoso et al., 2015).

Nanosmilus kurteni. **Locality***:* Nebraska, USA. **Absolute age estimate**: 33.89-32.0 Ma. The holotype and only known specimen is from the Orella Member of the Brule Formation (Martin, 1992). Absolute radiometrically dated boundaries for the Orella Member are not known, but bracketed to 34.6-31.5 Ma (Zanazzi et al., 2009) based on stratigraphically and geographically, nearest dated ash layers. However, dates for the Orellan NALMA are better known and what is used for the range applied to this taxon (Prothero and Emry, 2004; Zanazzi et al., 2009).

Nimravus intermedius. **Locality***:* France, Germany, Mongolia. **Absolute age estimate**: 35.37-27.24 Ma. Numerous fragmentary remains are known from the old Quercy collections, as well as the new stratigraphically documented ones (MP 22 to 25; Peigné, 2003; Peigné et al., 2014). Additional French material comes from Villebramar, MP 22 (Peigné, 2003). Of similar age in Southern Germany are attributed dentition at Möhren 13 (MP 22) and Liptingen (MP 22 or MP 23; Peigné, 2003). Mongolian *Nimravus* material, of Ergilian age, was separated into its own

species, *Nimravus mongoliensis*, for much of the 20th century (Gromova, 1959; Dashzeveg, 1996), but was synonymized to *N. intermedius* by Peigné (2003). Most recently this material was re-established as a valid species by Egi et al. (2016) based upon depth of the horizontal ramus and relative size of p1 and p2. However, the variability in anterior premolars for *Nimravus* has been well documented in the literature (Toohey, 1959; Peigné, 2003; Barrett, 2016). Thus, until more complete material of this purported species is described I chose to follow the assement of Peigné (2003) in its synonymy. The Thai, '*Nimravus*' material described by Peigné et al. (2000) lacks the apomorphy of p4 morphology for this genus, and may be more closely related to *Maofelis* for which no lower dentognathic remains are known.

Ginsburgsmilus napakensis. **Locality**: Langental, Fiskus, Grillental-6, Sperrgebiet, Namibia; Songhor, Kenya; Napak, Uganda. **Absolute age estimate**: 20.0-19.0 Ma. An updated occurrence list can be found in Morales and Pickford (2018), while Werdelin (2010) describes all of the above sites to be correlative to 20-19 Ma.

Prosansanosmilus eggeri. **Locality**: Bavaria, Germany. **Absolute age estimate**: 16.7-15.97 Ma. Thus far, the only known specimens of this taxon come from Sandelzhausen (MN 5) of Bavaria (Morlo et al., 2004). Sandelzhausen is constrained in age to about 16 Ma based on magnetochronological events and biostratigraphy; see Moser et al. (2009) for a detailed overview.

Prosansanosmilus peregrinus. **Locality**: Germany, France. **Absolute age estimate**: 18.0-16.0 Ma. In their original description, Heizmann et al. (1980) named three localities for the

occurrence of this taxon: Langenau 1 of Germany; and Bézian and Artenay of France. To this list, Petersbuch 2 of Germany was added by Morlo (2006). Petersbuch 2 and Artenay are MN 4a in age while Langenau 1 and Bézian are MN 4b. The age of MN 4 is skewed slightly older in the depositional basins of Switzerland and Southern Germany (see Reichenbacher et al., 2013) than the European "standard" (compare to Agustí et al., 2001). Furthermore, the exact age of the above fossil localities within their respective subzones is unequally known, save with Langenau 1 at slightly less than 17.2 Ma (Reichenbacher et al., 2013). Thus conservatively, the base of the South German MN 4a was used as the FAD of this taxon, while the LAD the "standard" top of MN 4.

Afrosmilus africanus. **Locality**: Locherangan, Rusinga, and Karungu (Kenya); Buñol, Spain. **Absolute age estimate**: 17.8-16.0 Ma. *A. africanus* is known from the African sites of Locherangan, Rusinga, and Karungu (Kenya), as well as the Spanish locality of Buñol. The Kenyan locality Locherangan (c. 17.5 Ma; Anyonge, 1991) is located west of Lake Turkana, while Rusinga (c. 17.8 Ma; Werdelin, 2010) and Karungu (c. 17.7-17.5 Ma; Drake et al., 1988), though likely contemporaneous with Rusinga (Werdelin, 2010) or slightly older (Morales and Pickford, 2018) based on biostratigraphy, are localities along the northwestern shore of Lake Victoria. The Spanish locality of Buñol (MN4, 16.6-16.0 Ma; Agustí et al., 2001) is located in the east of Spain in the province of Valencia.

Afrosmilus turkanae. **Locality**: Moruorot Hill and Rusinga, Kenya. **Absolute age estimate**: 17.8-16.8 Ma. *A. turkanae* is known from the African localities of Moruorot Hill and Rusinga (Kenya). Moruorot Hill (c. 17.5-16.8 Ma; Boschetto et al., 1992) is located west of Lake

Turkana, while Rusinga is the same locality (and chronology) as mentioned above for *A. africanus*.

Afrosmilus hispanicus. **Locality***:* Artesilla*,* Spain. **Absolute age estimate**: 16.7-16.0 Ma. *A. hispanicus* is the only non-African originating species of *Afrosmilus*, known only from the Spanish locality of Artesilla (c. 16.7 Ma; Azanza et al., 1993; Morales et al., 2001), in the northeast of the country in the province of Saragossa. *A. hispanicus* is typically correlated to the MN 4 zone (Morlo, 2006; Morales and Pickford, 2018), thus the younger date of 16.0 Ma is applied to its range, being the boundary between MN 4 and 5 (Agustí et al., 2001).

Maofelis cantonensis. **Locality***:* Maoming Basin, Guangdong Province, China. **Absolute age estimate**: 41.03-33.9 Ma. The holotype, and only known specimen, is from the Youganwo Formation, middle-upper Eocene (Averianov et al., 2016). The vertebrate fauna is only known from the upper portion of the formation containing dark oil shales and alternating mudstones (Averianov et al., 2016). The precise stratigraphic horizon of the holotype is unknown, but based on magnetostratigraphy and biostratigraphy it has been correlated to the Bartonian through Priabonian (Li et al., 2016; Averianov et al., 2019).

Eofelis edwardsii. **Locality**: France, Mongolia. **Absolute age estimate**: 35.37-30.83 Ma. The vast majority of material referred to *Eofelis edwardsii* comes from the old collections of the phosphorites of Quercy with no precise age (Peigné, 2000). However, material questionably referred to this taxon has been described from Villebramar, France, MP 22 (Peigné, 2000). Egi et al. (2016) described *Eofelis sp.* from the Ergilin Dzo Formation, Mongolia, which based on their

measurements most closely resembles *Eofelis edwardsii* compared to the larger *E. giganteus* (Peigné, 2000). The Mongolian specimens are dated to the Ergilian ALMA (Egi et al., 2016) and thus forms the oldest occurrence of this taxon while MP 22 the youngest for this study.

Dinailurictis bonali. **Locality**: France, Spain. **Absolute age estimate**: 32.63-27.24 Ma
Most material attributed to this taxon comes from the Quercy fissures, dated MP 22 to 25, and Villebramar, MP 22 (Peigné, 2003; Peigné et al., 2014). The Spanish material, canine fragments, comes from Carrascosa del Campo, approximately MP 25 (Peigné, 2003). Thus, the range of this taxon was chosen as MP 22-25, with absolute dates for these zones following Ogg et al. (2016).

Quercylurus major. **Locality**: France, Spain. **Absolute age estimate**: 28.82-27.24 Ma
The French material, including the holotype, come from the old collections of Quercy which have no precise age (Peigné, 2003). The Spanish material from Carrascosa del Campo has an estimated age of MP 25 and thus the only reliably dated material (Peigné, 2003). Absolute dates follow Ogg et al. (2016).

Dinaelurus crassus. **Locality**: Oregon, USA. **Absolute age estimate**: 29.5-28.5 Ma. The precise stratigraphic context for the holotype, and only known specimen of this taxon, were unknown when Eaton (1922) initially described it. However, a provisional Early Arikareean (Upper John Day Formation) was attributed to the specimen based on preservation and associated matrix (Eaton, 1922; Bryant, 1996). Albright et al. (2008) suggest the origin to be the E unit of the Turtle Cove Member of the John Day Formation. This assessment is given without evidence, but is one of most fossiliferous units of the Turtle Cove Member. The associated absolute dates for

the E unit were used for this study pending additional justification for the provenience of this taxon.

Hoplophoneus oharrai. **Locality**: South Dakota, USA. **Absolute age estimate**: 35.7-34.7 Ma. The type and only specimen comes from the Crazy Johnson Member of the Chadron Formation in southwest South Dakota (Barrett, 2016). Absolute dates are not available for the Crazy Johnson member, though it contains a middle Chadronian fauna (Ch3: 34.7-35.7 Ma: Janis et al., 2008) which is used for its range here.

MA-PHQ 348. **Locality**: Phosphorites of Quercy, south-western France. **Absolute age estimate**: 47.4-23.03 Ma. This plesiomorphic nimravid specimen comes from the old collections of Quercy and thus has little to no stratigraphic context. The Phosphorites have a total extent from the base of MP 11 to the early Miocene (Sigé et al., 1991; Legendre et al., 1992). Given the poor understanding of this specimen's stratigraphic context a broad prior from the base of MP 11 to the end of the Oligocene was chosen.

Eusmilus dakotensis. **Locality**: South Dakota, USA. **Absolute age estimate**: 30.5-29.75 Ma. Three referable specimens come from the Brule Fm., Poleslide Member of South Dakota (Barrett, 2016). Bryant (1996) limits the first appearance to the latter Whitneyan, during Chron C12n or C11r. This leads to the FAD as stated with the LAD being the end of the Whitneyan.

Eusmilus sicarius. **Locality**: South Dakota, USA. **Absolute age estimate**: 33.4-33.1 Ma. Following the results of this study, the only known specimen belonging to this species is the

holotype, which comes from the lower nodule zone of the Scenic Member of the Brule Formation. This stratum is roughly correlative to Chron C13n (Prothero and Emry, 2004).

Eusmilus adelos. **Locality**: Niobrara County, Wyoming, USA. **Absolute age estimate**: 33.7-32.0 Ma. The holotype specimen (Barrett, 2021) comes from the Northwest corner of Seaman Hills, Niobrara County, Wyoming. The additional referred specimen was collected about one mile North of Whitman, Wyoming. Both of these specimens come from the Seaman Hills which spans the entirety of the Orellan in typical outcrops (Prothero and Whittlesey, 1998; Prothero and Emry, 2004). Unfortunately, with no greater stratigraphic or geographic resolution, the entirety of the Orellan was used as the occurrence for this taxon.

Eusmilus bidentatus. **Locality**: France, Germany. **Absolute age estimate**: 33.77-32.63 Ma. This taxon is well known in the Phosphorites of Quercy, but also Soumailles (Ringeade and Michel, 1994; Peigné and Brunet, 2001). Additional material is known from southern Germany, but all of it (along with the French material) has been correlated to MP 21 (Peigné and Brunet, 2001).

Eusmilus villebramarensis. **Locality**: France, Switzerland, Germany. **Absolute age estimate**: 32.63-30.83 Ma. Most material for this taxon comes from France in the old collections of Quercy, but also Villebramar (Peigné and Brunet, 2001). However, occurrences in Switzerland and Germany are also known, which with the Villebramar material also has a MP 22 date (Peigné and Brunet, 2001).

References

Adrian, B., L. Werdelin, and A. Grossman. 2018. New Miocene Carnivora (Mammalia) from Moruorot and Kalodirr, Kenya. Palaeontologia Electronica 21.

Agustí, J., L. Cabrera, M. Garcés, W. Krijgsman, O. Oms, and J. M. Parés. 2001. A calibrated mammal scale for the Neogene of Western Europe. State of the art. Earth Science Reviews 52:247–260.

Albright, L. B., M. O. Woodburne, T. J. Fremd, C. C. Swisher, B. J. MacFadden, and G. R. Scott. 2008. Revised chronostratigraphy and biostratigraphy of the John Day formation (Turtle Cove and Kimberly Members), Oregon, with implications for updated calibration of the Arikareean North American land mammal age. Journal of Geology 116:211–237.

Antón, A. M., M. J. Salesa, and G. Siliceo. 2013. Machairodont Adaptations and Affinities of the Holarctic Late Miocene Homotherin Machairodus (Mammalia, Carnivora, Felidae): The Case of Machairodus Catocopis Cope, 1887. Journal of Vertebrate Paleontology 33:1202–1213.

Antón, M., M. J. Salesa, A. Galobart, and Z. J. Tseng. 2014. The Plio-Pleistocene scimitar-toothed felid genus Homotherium Fabrini, 1890 (Machairodontinae, Homotherini): Diversity, palaeogeography and taxonomic implications. Quaternary Science Reviews 96:259–268.

Anyonge, W. 1991. Fauna from a New Lower Miocene Locality West of Lake Turkana, Kenya. Journal of Vertebrate Paleontology 11:378–390.

Averianov, A., E. Obraztsova, I. Danilov, and J. Jin. 2019. Anthracotheriid artiodactyl Anthracokeryx and an upper Eocene age for the Youganwo Formation of southern China. Historical Biology 31:1115–1122.

Averianov, A., E. Obraztsova, I. Danilov, P. Skutschas, and J. Jin. 2016. First nimravid skull from Asia. Scientific Reports 6:1–8.

Azanza, B., E. Cerdeno, L. Ginsburg, J. Van Der Made, J. Morales, and P. Tassy. 1993. Les grands mammifères du Miocène inférieur d'Artesilla, bassin de Calatayud-Teruel (province de Saragosse, Espagne). Bulletin Du Museum National d'Histoire Naturelle Section C Sciences de La Terre Paleontologie Geologie Mineralogie 15:105–153.

Barnett, R., M. L. Z. Mendoza, A. E. R. Soares, S. Y. W. Ho, G. Zazula, N. Yamaguchi, B. Shapiro, I. V. Kirillova, G. Larson, and M. T. P. Gilbert. 2016. Mitogenomics of the extinct cave lion, Panthera spelaea (Goldfuss, 1810), resolve its position within the panthera cats. Open Quaternary 2:1–11.

Barnett, R., B. Shapiro, I. Barnes, S. Y. Ho, J. Burger, N. Yamaguchi, T. F. Higham, H. T. Wheeler, W. Rosendahl, A. V Sher, M. Sotnikova, T. Kuznetsova, G. F. Baryshnikov, L. D. Martin, C. R. Harington, J. A. Burns, and A. Cooper. 2009. Phylogeography of lions (Panthera leo ssp.) reveals three distinct taxa and a late Pleistocene reduction in genetic diversity. Molecular Ecology 18:1668–1677.

Barnett, R., I. Barnes, M. J. Phillips, L. D. Martin, C. R. Harrington, J. A. Leonard, and A. Cooper. 2005. Evolution of the extinct Sabretooths and the American cheetah-like cat. Current Biology 15:R589–R590.

Barrett, P. Z. 2016. Taxonomic and systematic revisions to the North American Nimravidae (Mammalia, Carnivora). PeerJ 4:e1658.

Barrett, P. Z. 2021. The largest hoplophonine and a complex new hypothesis of nimravid evolution. Scientific Reports 11:1–9.

Barrett, P. Z., S. S. B. Hopkins, and S. A. Price. 2021. How many sabretooths? Reevaluating the number of carnivoran sabretooth lineages with total-evidence Bayesian techniques and a novel origin of the Miocene Nimravidae. Journal of Vertebrate Paleontology e1923523.

Bell, C. J., E. L. Lundelius Jr., A. D. Barnosky, R. W. Graham, E. H. Lindsay, D. R. Ruez Jr., H. A. Semken Jr., S. D. Webb, and R. J. Zakrzewski. 2004. The Blancan, Irvingtonian, and Rancholabrean Mammal Ages; pp. 232–314 in M. O. Woodburne (ed.), Late Cretaceous and Cenozoic Mammals of North American. Columbia University Press, New York.

Benefit, B. R., M. McCrossin, N. T. Boaz, and P. Pavlakis. 2008. New Fossil Cercopithecoids from the Late Miocene of As Sahabi, Libya. Garyounis Scientific Bulletin 5:265–282.

Bernor, R. L., M. O. Woodburne, and J. A. Van Couvering. 1980. A contribution to the chronology of some Old World miocene faunas based on hipparionine horses. Geobios 13:705–739.

Böhme, M., N. Spassov, M. Ebner, D. Geraads, L. Hristova, U. Kirscher, S. Kötter, U. Linnemann, J. Prieto, S. Roussiakis, G. Theodorou, G. Uhlig, and M. Winklhofer. 2017. Messinian age and savannah environment of the possible hominin Graecopithecus from Europe. PLoS ONE 12:e0177347.

Boschetto, H. B., F. H. Brown, and I. M. McDougall. 1992. Stratigraphy of the Lothidok Range, northern Kenya, and K/Ar ages of its Miocene primates. Journal of Human Evolution 22:47–71.

Boyd, C. A., and J. R. Webster. 2018. Depositional History of the Chadron Formation in North Dakota. North Dakota Geological Survey Report of Investigation 120:107.

Bryant, H. N. 1992. The Carnivora of the Lac Pelletier Lower Fauna (Eocene: Duchesnean), Cypress Hills Formation, Saskatchewan. Journal of Paleontology 66:847–855.

Bryant, H. N. 1996. Nimravidae; pp. 453–475 in D. R. Prothero and R. J. Emry (eds.), The Terrestrial Eocene-Oligocene Transition in North America. Cambridge University Press, Cambridge [England]; New York.

Bryant, H. N., and T. J. Fremd. 1998. Revised Biostratigraphy of the Nimravidae (Carnivora) from the John Day Basin of Oregon. Journal of Vertebrate Paleontology 18:30A.

Dashzeveg, D. 1996. Some Carnivorous Mammals from the Paleogene of the Eastern Gobi Desert , Mongolia , and the Application of Oligocene Carnivores to Stratigraphic Correlation. American Museum Novitates 3179:1–14.

Drake, R. E., J. A. Van Couvering, M. H. Pickford, G. H. Curtis, and J. A. Harris. 1988. New chronology for the Early Miocene mammalian faunas of Kisingiri, Western Kenya. Journal of the Geological Society, London 145:479–491.

Eaton, G. F. 1922. John Day Felidae in the Marsh Collection. American Journal of Science 4:425–452.

Egi, N., T. Tsubamoto, M. Saneyoshi, K. Tsogtbaatar, M. Watabe, B. Mainbayar, T. Chinzorig, and P. Khatanbaatar. 2016. Taxonomic revisions on nimravids and small feliforms (Mammalia, Carnivora) from the Upper Eocene of Mongolia. Historical Biology 28:105–119.

Famoso, N. A., J. X. Samuels, S. S. B. Hopkins, M. M. Emery, and E. B. Davis. 2015. Updated Biostratigraphy of the Turtle Cove Member (John Day Formation) in the John Day Basin, Oregon; pp. 6 in Western association of vertebrate Paleontology annual Meeting: Program with abstracts. PaleoBios 32(1). vol. 32.

Gabunia, L., and A. Vekua. 1998. The find of Dinofelis in the Pliocene of Georgia. Bulletin of the Georgian Academy of Sciences 157:335–338.

Ghaffar, A., M. Akhtar, M. A. Khan, and M. A. Babar. 2019. Comments on percrocuta carnifex (carnivora, percrocutidae) based on new fossil material from the nagri formation (middle siwaliks) of hasnot, pakistan. Geologica Acta 17:1–9.

Ginsburg, L. 2001. Les faunes de mammifères terrestres du Miocène moyen des Faluns du bassin de Savigné-sur-Lathan (France). Geodiversitas 23:381–394.

Gracia, S. F. 2015. Estudio de Protictitherium crassum del Cerro de los Batallones (Torrejón de Velasco, Madrid): aportación a la filogenia y evolución de la familia hyaenidae. Universidad Complutense de Madrid, 365 pp.

Gromova, V. 1959. Premiere decoverte d'un chat primitif au Paleogene d'Asie Centrale. Vertebrata PalAsiatica 3:59–72.

Heizmann, E. P. J., L. Ginsburg, and C. Bulot. 1980. Prosansanosmilus peregrinus, ein neuer machairodontider Felide aus dem Miocän Deutschlands und Frankreichs. Stuttgarter Beiträge Zur Naturkunde B 58:1–27.

Hilgen, F. J., L. J. Lourens, J. A. Van Dam, A. G. Beu, A. F. Boyes, R. A. Cooper, W. Krijgsman, J. G. Ogg, W. E. Piller, and D. S. Wilson. 2012. The Neogene Period; pp. 923–978 in F. M. Gradstein, J. G. Ogg, M. D. Schmitz, and G. M. Ogg (eds.), The geologic time scale. Elsevier, Amsterdam.

Hoek Ostende, L. W. van den, S. Mayda, A. Oliver, A. Madern, V. Hernández-Ballarín, and P. Peláez-Campomanes. 2015. Aliveri revisited, a biogeographical appraisal of the early Miocene mammals from the eastern Mediterranean. Palaeobiodiversity and Palaeoenvironments 95:271–284.

Howell, F. C., and G. Petter. 1985. Comparative observations on some middle and upper Miocene hyaenids. Genera: Percrocuta Kretzoi, Allohyaena Kretzoi, Adcrocuta Kretzoi (Mammalia, Carnivora, Hyaenidae). Geobios 18:419–476.

Hunt, R. M. 1991. Evolution of the aeluroid Carnivora: viverrid affinities of the Miocene carnivoran Herpestides. American Museum Novitates 3023:1–34.

Janis, C. M., G. F. Gunnell, and M. D. Uhen. 2008. Evolution of Tertiary Mammals of North America. Volume 2: Small Mammals, Xenarthrans, and Marine Mammals. Cambridge University Press, Cambridge, 795 pp.

Kaakinen, A., B. H. Passey, Z.-Q. Zhang, L.-P. Liu, L. J. Pesonen, and M. Fortelius. 2013. Stratigraphy and Paleoecology of the Classical Dragon Bone Localities of Baode County, Shanxi Province; pp. 203–217 in Fossil mammals of Asia: Neogene biostratigraphy and chronology. Columbia University Press, New York.

Kelly, T. S., P. C. Murphey, and S. L. Walsh. 2012. New Records of Small Mammals From the Middle Eocene Duchesne River Formation, Utah, and Their Implications for the Uintan-Duchesnean North American Land Mammal Age Transition. Paludicola 8:208–251.

Kirillova, I. V., A. V. Tiunov, V. A. Levchenko, O. F. Chernova, V. G. Yudin, F. Bertuch, and F. K. Shidlovskiy. 2015. On the discovery of a cave lion from the Malyi Anyui River (Chukotka, Russia). Quaternary Science Reviews 117:135–151.

Kovatchev, D. 2001. Description d'un squelette complet de Metailurus (Felidae, Carnivora, Mammalia) du Miocène supérieur de Bulgarie. Geologica Balcanica 31:71–88.

Legendre, S., B. Marandat, B. Sigé, J. Crochet, M. Godinot, J. L. Hartenberger, J. Sudre, and M. Vianey-Liaud. 1992. La faune de mammifères de Vielase (phosphorites du Quercy, Sud de la France): Preuve paléontologique d'une karstification du Quercy dès l'Eocène inférieur Par Montpellier ; Toulouse Débutées en 1965 , l ' exploration et l ' exploitation paléontologique no. Neues Jahrbuch Für Geologie Und Paläontologie 7:414–428.

Li, Y. X., W. J. Jiao, Z. H. Liu, J. H. Jin, D. H. Wang, Y. X. He, and C. Quan. 2016. Terrestrial responses of low-latitude Asia to the Eocene-Oligocene climate transition revealed by integrated chronostratigraphy. Climate of the Past 12:255–272.

Martin, L. D. 1992. A new miniature saber-tooth nimravid from the Oligocene of Nebraska. Annales Zoologici Fennici 28:341–348.

Martin, L. D. 1998. Nimravidae; pp. 228–235 in C. M. Janis, K. M. Scott, and L. L. Jacobs (eds.), Evolution of Tertiary Mammals of North America: Volume 1. Cambridge University Press, Cambridge, UK.

Miller, S. A., P. Z. Barrett, W. N. F. McLaughlin, and S. S. B. Hopkins. 2020. Endemism and migration in the Kochkor Basin? Identification and description of Adcrocuta eximia (Mammalia: Carnivora: Hyaenidae) and C.F. Paramachaerodus (Mammalia: Carnivora: Felidae) fossils at the Miocene locality of Ortok, Kyrgyzstan. Palaeontologia Electronica 23:a45.

Morales, J., and M. Pickford. 2005. Carnivores from the middle miocene ngorora formation (13-12 MA), Kenya. Estudios Geologicos 61:271–284.

Morales, J., and M. Pickford. 2018. A new barbourofelid mandible (Carnivora, Mammalia) from the Early Miocene of Grillental-6, Sperrgebiet, Namibia. Communications of the Geological Survey of Namibia 18:113–123.

Morales, J., M. J. Salesa, M. Pickford, and D. Soria. 2001. A new tribe, new genus and two new species of Barbourofelinae (Felidae, Carnivora, Mammalia) from the early Miocene of East Africa and Spain. Transactions of the Royal Society of Edinburgh: Earth Sciences 92:97–102.

Morales, J., S. Mayda, A. Valenciano, D. DeMiguel, and T. Kaya. 2019. A new lophocyonid, Izmirictis cani gen. et sp. nov. (Carnivora: Mammalia), from the lower Miocene of Turkey. Journal of Systematic Palaeontology 17:1127–1138.

Morlo, M. 2006. New remains of Barbourofelidae (Mammalia, Carnivora) from the Miocene of Southern Germany: implications for the history of barbourofelid migrations. Beiträge Zur Paläontologie 30:339–349.

Morlo, M., S. Peigné, and D. Nagel. 2004. A new species of Prosansanosmilus: implications for the systematic relationships of the family Barbourofelidae new rank (Carnivora, Mammalia). Zoological Journal of the Linnean Society 140:43–61.

Moser, M., G. E. Rössner, U. B. Göhlich, M. Böhme, and V. Fahlbusch. 2009. The fossil lagerstätte Sandelzhausen (Miocene; southern Germany): History of investigation, geology, fauna, and age. Palaontologische Zeitschrift 83:7–23.

Ogg, J. G., G. Ogg, and F. M. Gradstein. 2016. A Concise Geologic Time Scale. Elsevier, 240 pp.

Paijmans, J. L. A., R. Barnett, M. T. P. Gilbert, M. L. Zepeda-mendoza, J. W. F. Reumer, J. de Vos, G. Zazula, D. Nagel, G. F. Baryshnikov, J. A. Leonard, N. Rohland, M. V Westbury, A. Barlow, and M. Hofreiter. 2017. Evolutionary History of Saber-Toothed Cats Based on Ancient Mitogenomics. Current Biology 27:3330–3336.

Peigné, S. 2000. A new species of Eofelis (Carnivora: Nimravidae) from the Phosphorites of Quercy, France. Comptes Rendus de l'Académie Des Sciences, Paris 330:653–658.

Peigné, S. 2003. Systematic review of European Nimravinae (Mammalia, Carnivora, Nimravidae) and the phylogenetic relationships of Palaeogene Nimravidae. Zoologica Scripta 32:199–229.

Peigné, S. 2012. Les Carnivora de Sansan; pp. 559–660 in S. E. N. S. (ed.), Mammifères de Sansan. Muséum national d'Histoire naturelle, Paris.

Peigné, S., and M. Brunet. 2001. Une Nouvelle Espèce Du Genre Eusmilus (Carnivora: Nimravidae) De L'Oligocène (MP 22) D'Europe. Geobios 34:657–672.

Peigné, S., M. Vianey-Liaud, T. Pélissié, and B. Sigé. 2014. Valbro: A new site of vertebrates from the early Oligocene (MP22) of France (Quercy). I – Geological context; Mammalia: Rodentia, Hyaenodontida, Carnivora. Annales de Paleontologie 100:1–45.

Peigné, S., Y. Chaimanee, J.-J. Jaeger, V. Suteethorn, and S. Ducrocq. 2000. Eocene nimravid carnivorans from Thailand. Journal of Vertebrate Paleontology 20:157–163.

Pickford, M., Y. Sawada, R. Tayama, Y. ko Matsuda, T. Itaya, H. Hyodo, and B. Senut. 2006. Refinement of the age of the Middle Miocene Fort Ternan Beds, Western Kenya, and its implications for Old World biochronology. Comptes Rendus - Geoscience 338:545–555.

Prothero, D. R., and K. E. Whittlesey. 1998. Magnetic stratigraphy and biostratigraphy of the Orellan and Whitneyan land-mammal "ages" in the White River Group. Geological Society of America Special Paper 325:39–61.

Prothero, D. R., and R. J. Emry. 2004. The Chadronian, Orellan, and Whitneyan North American land mammal ages; pp. 156–168 in M. O. Woodburne (ed.), Late Cretaceous and Cenozoic Mammals of North America: Biostratigraphy and Geochronology. Columbia University Press, New York City.

Qiu, Z.-X., Z.-D. Qiu, T. Deng, C.-K. Li, Z.-Q. Zhang, B.-Y. Wang, and X. Wang. 2013. Neogene land mammal stages/ages of China – toward the goal to establish an Asian land mammal stage/age scheme; pp. 29–90 in X. Wang, L. J. Flynn, and M. Fortelius (eds.), Fossil mammals of Asia: Neogene biostratigraphy and chronology. Columbia University Press, New York.

Qiu, Z., J. Ye, and J. Cao. 1988. A new species of Percrocuta from Tongxin, Ningxia. Vertebrata Palasiatica 26:116–127.

Reichenbacher, B., W. Krijgsman, Y. Lataster, M. Pippèrr, C. G. C. Van Baak, G. Doppler, L. Chang, D. Kälin, J. Jost, D. Jung, J. Prieto, H. A. A. Bohme, M. Böhme, J. Garnish, U. Kirscher, and V. Bachtadse. 2013. A new magnetostratigraphic framework for the Lower Miocene A new magnetostratigraphic framework for the Lower Miocene (Burdigalian / Ottnangian , Karpatian) in the North Alpine Foreland Basin. Swiss Journal of Geosciences 106:309–334.

Reumer, J. W. F., L. Rook, K. Van Der Borg, K. Post, D. Mol, and J. De Vos. 2003. Late pleistocene survival of the saber-toothed cat Homotherium in Northwestern Europe. Journal of Vertebrate Paleontology 23:260–262.

Ringeade, M., and P. Michel. 1994. A propos de l'Eusmilus (Eusmilus bidentatus ringeadei Ringeade et Michel, 1994) de Soumailles, lieu-dit de la commune de Pardaillan, Canton de Duras (Lot et Garonne, France) : étude descriptive. Paléo 6:5–37.

Robinson, P., G. F. Gunnell, S. L. Walsh, W. C. Clyde, J. E. Storer, R. K. Stucky, D. J. Froehlich, I. Ferrusquia-Villafranca, M. C. McKenna, and M. Woodburne. 2004. Wasatchian through duchesnean biochronology.; pp. 106–155 in M. Woodburne (ed.), Late Cretaceous and Cenozoic mammals of North America: Biostratigraphy and Geochronology. Columbia University Press, New York.

Robles, J. M., D. M. Alba, J. Fortuny, S. De Esteban-Trivigno, C. Rotgers, J. Balaguer, R. Carmona, J. Galindo, S. Almecija, J. V Berto, and S. Moya-Sola. 2013. New craniodental remains of the barbourofelid Albanosmilus jourdani (Filhol, 1883) from the Miocene of the Valles-Penedes Basin (NE Iberian Peninsula) and the phylogeny of the Barbourofelini. Journal of Systematic Palaeontology 11:993–1022.

Rook, L., and B. Martínez-Navarro. 2010. Villafranchian: The long story of a Plio-Pleistocene European large mammal biochronologic unit. Quaternary International 219:134–144.

Rothwell, T. P. 2001. Phylogenetic systematics of North American Pseudaelurus (Carnivora: Felidae). Columbia University, 358 pp.

Rothwell, T. P. 2003. Phylogenetic systematics of North American Pseudaelurus (Carnivora, Felidae). American Museum Novitates 3403.

Roussiakis, S. J. 2001. Metailurus major Zdansky, 1924 (Carnivora, Mammalia) from the classical locality of Pikermi (Attica, Greece). Annales de Paleontologie 87:119–132.

Ruiz-Ramoni, D., A. D. Rincón, and M. Montellano-Ballesteros. 2020. Taxonomic revision of a Machairodontinae (Felidae) from the Late Hemphillian of México. Historical Biology 32:1312–1319.

Semenov, Y. 2008. Taxonomical reappraisal of "ictitheres" (Mammalia, Carnivora) from the Late Miocene of Kenya. Comptes Rendus Palevol 7:529–539.

Sigé, B., J. P. Aguilar, J. G. Astruc, and B. Marandat. 1991. Extension au Miocène inférieur des remplissages phosphatés du Quercy. La faune de Vertébrés de Crémat (Lot, France). Geobios 24:497–502.

Skinner, M. F., F. W. Johnson, and C. Frick. 1984. Tertiary stratigraphy and the Frick Collection of fossil vertebrates from north-central Nebraska. Bulletin of the American Museum of Natural History 178:368.

Slater, G. J., and A. R. Friscia. 2019. Hierarchy in adaptive radiation: A case study using the Carnivora (Mammalia). Evolution 73:524–539.

Solé, F., T. Smith, E. de Bast, V. Codrea, and E. Gheerbrant. 2016. New carnivoraforms from the latest Paleocene of Europe and their bearing on the origin and radiation of Carnivoraformes (Carnivoramorpha, Mammalia). Journal of Vertebrate Paleontology 36:e1082480.

Spassov, N., and G. D. Koufos. 2002. The first appearance of Dinocrocuta gigantea and Macbairodus aphanistus (Mammalia: Carnivora) in the Miocene of Bulgaria. Mitteilungen Der Bayerischen Staatssammlung Fur Palaontologie Und Historische Geologie 42:83–101.

Spassov, N., and D. Geraads. 2015. A New Felid from the Late Miocene of the Balkans and the Contents of the Genus Metailurus Zdansky, 1924 (Carnivora, Felidae). Journal of Mammalian Evolution 22:45–56.

Spaulding, M., J. J. Flynn, and R. K. Stucky. 2010. A new basal carnivoramorphan (Mammalia) from the "Bridger B" (Black's fork member, bridger formation, bridgerian nalma, middle eocene) of wyoming, USA. Palaeontology 53:815–832.

Tedford, R. H., L. B. I. Albright, A. D. Barnosky, I. Ferrusquia−Villafranca, R. M. J. Hunt, J. E. Storer, C. C. I. Swisher, M. R. Voorhies, S. D. Webb, and D. . Whistler. 2004. Mammalian biochronology of the Arikareean through Hemphillian interval (late Oligocene through early Pliocene epochs); pp. 169–231 in M.O. Woodburne (ed.), Late Cretaceous and Cenozoic Mammals of North America. Columbia University Press, New York.

Tomiya, S., and Z. J. Tseng. 2016. Whence the beardogs? Reappraisal of the middle to late eocene 'miacis' from Texas, USA, and the origin of amphicyonidae (mammalia, carnivora). Royal Society Open Science 3.

Toohey, L. 1959. The Species of Nimravus (Carnivora, Felidae). Princeton University, New York, 130 pp.

Tseng, Z. J., and X. Wang. 2007. The first record of the late Miocene Hyaenictitherium hyaenoides Zdansky (Carnivora: Hyaenidae) in Inner Mongolia and an evaluation of the genus. Journal of Vertebrate Paleontology 27:699–708.

Tseng, Z. J., G. T. Takeuchi, and X. Wang. 2010. Discovery of the upper dentition of Barbourofelis whitfordi (Nimravidae, Carnivora) and an evaluation of the genus in California. Journal of Vertebrate Paleontology 30:244–254.

Tseng, Z. J., Q. Li, and X. Wang. 2013. A new cursorial hyena from Tibet, and analysis of biostratigraphy, paleozoogeography, and dental morphology of Chasmaporthetes (Mammalia, Carnivora). Journal of Vertebrate Paleontology 33:1457–1471.

Turner, A., M. Antón, and L. Werdelin. 2008. Taxonomy and evolutionary patterns in the fossil Hyaenidae of Europe. Geobios 41:677–687.

Wang, S.-Q., L.-Y. Zong, Q. Yang, B.-Y. Sun, Y. Li, Q.-Q. Shi, X.-W. Yang, J. Ye, and W.-Y. Wu. 2016. Biostratigraphic subdividing of the Neogene Dingjia'ergou mammalian fauna, Tongxin County, Ningxia Province, and its background for the uplift of the Tibetan Plateau36. Quaternary Sciences 36:789–809.

Wang, X. 1994. Phylogenetic systematics of the Hesperocyoninae (Carnivora, Canidae). Bulletin of the American Museum of Natural History 221.

Wang, X., S. C. White, and J. Guan. 2020. A new genus and species of sabretooth , Oriensmilus liupanensis (Barbourofelinae, Nimravidae, Carnivora), from the middle Miocene of China suggests barbourofelines are nimravids, not felids. Journal of Systematic Palaeontology 18:783–803.

Werdelin, L. 2010. Chronology of Neogene Mammal Localities; pp. 27–43 in L. Werdelin and W. J. Sanders (eds.), Cenozoic Mammals of Africa. University of California Press, Berkeley, Los Angeles, London.

Werdelin, L. 2019. Middle miocene carnivora and hyaenodonta from fort Ternan, Western Kenya. Geodiversitas 41:267–283.

Werdelin, L., and N. Solounias. 1991. The Hyaenidae : taxonomy, systematics and evolution. Fossils and Strata 30:104.

Werdelin, L., and M. E. Lewis. 2001. A revision of the genus Dinofelis (Mammalia, Felidae). Zoological Journal of the Linnean Society 132:147–258.

Werdelin, L., and S. Peigné. 2010. Carnivora; pp. 603–657 in L. Werdelin and W. J. Sanders (eds.), Cenozoic Mammals of Africa. University of California Press, Berkeley, Los Angeles, London.

Wesley-Hunt, G. D., and J. J. Flynn. 2005. Phylogeny of the Carnivora: basal relationships among the carnivoramorphans, and assessment of the position of "Miacoidea" relative to Carnivora. Journal of Systematic Palaeontology 3:1–28.

Westbury, M. V., S. Hartmann, A. Barlow, M. Preick, B. Ridush, D. Nagel, T. Rathgeber, R. Ziegler, G. Baryshnikov, G. Sheng, A. Ludwig, I. Wiesel, L. Dalen, F. Bibi, L. Werdelin, R. Heller, and M. Hofreiter. 2020. Hyena paleogenomes reveal a complex evolutionary history of cross-continental gene flow between spotted and cave hyena. Science Advances 6:1–11.

Wolsan, M., and M. Morlo. 1997. The status of "Plesictis" croizeti, "Plesictis" gracilis and "Lutra" minor: synonyms of the early Miocene viverrid Herpestides antiquus (Mammalia, Carnivora). Bulletin of the Natural History Museum London (Geol) 53:1–9.

Zanazzi, A., M. J. Kohn, and D. O. Terry. 2009. Biostratigraphy and paleoclimatology of the Eocene-Oligocene boundary section at Toadstool Park (northwestern Nebraska). Geological Society of America Special Paper 452:197–214.

Zhang, Z. 2005. New materials of Dinocrocuta (Percrocutidae, Carnivora) from Lantian, Shaanxi Province, China, and remarks on Chinese Late Miocene biochronology. Geobios 38:685–689.

Appendix H

Dietary Classification and Ecological Data Tables

Table 1. Extant taxa and associated data used for CVA training set. Dentognathic metrics are averages per species taken from Slater and Friscia (2019). C1 = compression of the upper C1, P4S = ratio of width to length of fourth lower premolar, RBL = relative blade length of the trigonid of m1, M1BS = blade length of the m1 relative to total dentary length. Degree of carnivory is calculated by percent of diet belonging to the Diet-Vend (vertebrate endotherm), Diet-Vect (vertebrate ectotherm), Diet-Vfish (vertebrate fish), Diet-Vunk (vertebrate unknown), Diet-Scav (scavenge) categories of the Elton Traits dataset (Wilman et al., 2014). Diet reflects the following categories: 1 = hypocarnivore, 2 = mesocarnivore, 3 = hypercarnivore.

	C1	P4S	RBL	M1BS	degree of carnivory	diet	clade
Acinonyx jubatus	0.772054	0.401632	1	0.151394	100	3	Felidae
Ailurus fulgens	0.669263	0.634786	0.626106	0.095325	10	1	Ailuridae
Arctictis binturong	0.610208	0.721644	0.5939	0.051077	50	2	Viverridae
Arctogalidia trivirgata	0.727818	0.646774	0.593267	0.056879	60	2	Viverridae

Atelocynus microtis	0.66531	0.475924	0.644595	0.083972	80	3	Canidae
Atilax paludinosus	0.729671	0.682345	0.725312	0.098091	60	2	Herpestidae
Bassaricyon alleni	0.808707	0.791157	0.456011	0.047452	10	1	Procyonidae
Bassaricyon gabbii	0.783069	0.852102	0.492788	0.050596	10	1	Procyonidae
Bassariscus astutus	0.703323	0.501747	0.611853	0.088033	10	1	Procyonidae
Bassariscus sumichrasti	0.697784	0.608978	0.614527	0.077651	10	1	Procyonidae
Bdeogale crassicauda	0.728875	0.588034	0.564133	0.054213	20	1	Herpestidae
Bdeogale nigripes	0.68366	0.623578	0.477484	0.047619	40	1	Herpestidae
Canis adustus	0.638405	0.453178	0.628036	0.084939	50	2	Canidae
Canis aureus	0.616181	0.458079	0.682657	0.109874	80	3	Canidae
Canis latrans	0.576676	0.447496	0.696411	0.109583	100	3	Canidae
Canis lupus	0.62145	0.52157	0.70792	0.11052	100	3	Canidae

260

	5	4	7	8			
Canis mesomelas	0.617045	0.449724	0.658142	0.108242	60	2	Canidae
Canis simensis	0.637207	0.454293	0.684652	0.089647	100	3	Canidae
Caracal caracal	0.759856	0.460379	1	0.148737	100	3	Felidae
Caracal serval	0.743404	0.426307	1	0.140571	100	3	Felidae
Cerdocyon thous	0.65387	0.469945	0.626431	0.089526	50	2	Canidae
Chrotogale owstoni	0.599323	0.396075	0.424473	0.037641	10	1	Viverridae
Chrysocyon brachyurus	0.624258	0.502515	0.641143	0.08739	70	3	Canidae
Civettictis civetta	0.807867	0.59631	0.615087	0.082207	50	2	Viverridae
Crocuta crocuta	0.728864	0.559832	0.916777	0.148063	100	3	Hyaenidae
Crossarchus alexandri	0.64787	0.594871	0.543751	0.057828	20	1	Herpestidae
Crossarchus obscurus	1.113036	0.566672	0.484472	0.053964	20	1	Herpestidae

Crossarchus platycephalus	0.592798	0.541152	0.516441	0.056809	50	2	Herpestidae
Cryptoprocta ferox	0.752583	0.562673	0.804789	0.117678	90	3	Eupleridae
Cuon alpinus	0.605381	0.495661	0.726179	0.123776	100	3	Canidae
Cynictis penicillata	0.686733	0.518147	0.708522	0.086665	10	1	Herpestidae
Cynogale bennettii	0.702797	0.45827	0.480858	0.053386	50	2	Viverridae
Diplogale hosei	0.686275	0.525847	0.477886	0.049218	40	1	Viverridae
Dusicyon australis	0.634636	0.480114	0.712566	0.104221	100	3	Canidae
Eupleres goudotii	0.699804	0.350627	0.585666	0.050524	10	1	Eupleridae
Felis chaus	0.785909	0.384944	1	0.140508	100	3	Felidae
Felis margarita	0.784314	0.432551	1	0.142585	100	3	Felidae
Felis nigripes	0.725768	0.467014	1	0.140991	100	3	Felidae
Felis silvestris	0.77786	0.43040	1	0.14629	90	3	Felidae

		3		4			
Fossa fossana	0.655107	0.450107	0.592517	0.070584	20	1	Eupleridae
Galerella pulverulenta	0.684845	0.480161	0.63871	0.089809	20	1	Herpestidae
Galerella sanguinea	0.662636	0.481126	0.745567	0.104478	20	1	Herpestidae
Galidia elegans	0.691149	0.502992	0.65632	0.109116	80	3	Eupleridae
Galidictis fasciata	0.670525	0.570479	0.627182	0.083729	70	3	Eupleridae
Genetta angolensis	0.743209	0.443671	0.738723	0.090105	90	3	Viverridae
Genetta genetta	0.715939	0.41667	0.743561	0.0892	90	3	Viverridae
Genetta maculata	0.736103	0.418334	0.721206	0.087547	90	3	Viverridae
Genetta pardina	0.68675	0.365353	0.675361	0.082884	70	3	Viverridae
Genetta servalina	0.703367	0.394119	0.73857	0.085909	90	3	Viverridae
Genetta thierryi	0.749218	0.373859	0.650378	0.078706	90	3	Viverridae

Genetta tigrina	0.779945	0.402952	0.695057	0.08791	90	3	Viverridae
Helogale hirtula	0.629818	0.645464	0.824316	0.094996	20	1	Herpestidae
Helogale parvula	0.609528	0.614138	0.784298	0.087415	20	1	Herpestidae
Hemigalus derbyanus	0.654918	0.483404	0.437407	0.046839	0	1	Viverridae
Herpestes brachyurus	0.713763	0.560419	0.616362	0.085122	60	2	Herpestidae
Herpestes edwardsii	0.723072	0.507598	0.634889	0.091266	70	3	Herpestidae
Herpestes fuscus	0.699791	0.498108	0.610047	0.078518	60	2	Herpestidae
Herpestes ichneumon	0.691495	0.498195	0.722738	0.096557	60	2	Herpestidae
Herpestes javanicus	0.700096	0.494911	0.620579	0.084652	60	2	Herpestidae
Herpestes naso	0.71421	0.527384	0.622672	0.082362	60	2	Herpestidae
Herpestes urva	0.704382	0.562407	0.641428	0.090241	60	2	Herpestidae
Herpestes	0.65284	0.54782	0.58815	0.06880	60	2	Herpestidae

vitticollis	9	7	1	3			
Hyaena hyaena	0.683064	0.553721	0.788502	0.103934	80	3	Hyaenidae
Ichneumia albicauda	0.721937	0.509919	0.640764	0.071463	20	1	Herpestidae
Leopardus colocolo	0.697357	0.50534	1	0.152163	100	3	Felidae
Leopardus geoffroyi	0.713502	0.445561	1	0.150046	100	3	Felidae
Leopardus guigna	0.791097	0.459773	1	0.12585	100	3	Felidae
Leopardus pardalis	0.755549	0.448254	1	0.13775	100	3	Felidae
Leopardus tigrinus	0.746228	0.40528	1	0.137453	100	3	Felidae
Leopardus wiedii	0.714396	0.435182	1	0.141586	80	3	Felidae
Liberiictis kuhni	0.626191	0.479691	0.526704	0.049327	20	1	Herpestidae
Lycaon pictus	0.649288	0.492523	0.710661	0.119698	100	3	Canidae
Lynx canadensis	0.788981	0.446342	1	0.159412	100	3	Felidae

Lynx lynx	0.790834	0.500012	1	0.147583	100	3	Felidae
Lynx pardinus	0.81483	0.483928	1	0.152103	100	3	Felidae
Lynx rufus	0.807115	0.491182	1	0.145469	100	3	Felidae
Mungos mungo	0.653983	0.65529	0.754509	0.076472	20	1	Herpestidae
Mungotictis decemlineata	0.733361	0.542626	0.600884	0.089173	20	1	Eupleridae
Nandinia binotata	0.698252	0.650496	0.664097	0.068674	10	1	Nandiniidae
Nasua narica	0.560906	0.647583	0.543559	0.052864	20	1	Procyonidae
Nasua nasua	0.52934	0.578901	0.500482	0.047328	20	1	Procyonidae
Nasuella olivacea	0.439116	0.563084	0.45791	0.035554	20	1	Procyonidae
Neofelis nebulosa	0.735108	0.462399	1	0.134382	100	3	Felidae
Nyctereutes procyonoides	0.67459	0.442697	0.620483	0.093772	40	1	Canidae
Otocolobus manul	0.76252	0.46755	1	0.16595	100	3	Felidae

	7	8		1			
Paguma larvata	0.675643	0.757794	0.564977	0.066331	60	2	Viverridae
Panthera uncia	0.821559	0.480661	1	0.147341	100	3	Felidae
Panthera leo	0.699092	0.477208	1	0.122192	100	3	Felidae
Panthera onca	0.803703	0.45631	1	0.126544	100	3	Felidae
Panthera pardus	0.774586	0.49165	1	0.131715	100	3	Felidae
Panthera tigris	0.745519	0.475593	1	0.126875	100	3	Felidae
Paracynictis selousi	0.655679	0.503312	0.688501	0.079147	40	1	Herpestidae
Paradoxurus hermaphroditus	0.719236	0.6925	0.596092	0.074653	40	1	Viverridae
Paradoxurus zeylonensis	0.695754	0.653212	0.60528	0.07331	40	1	Viverridae
Parahyaena brunnea	0.763287	0.604518	0.820325	0.114841	80	3	Hyaenidae
Pardofelis badia	0.769135	0.455212	1	0.154921	100	3	Felidae

267

Pardofelis marmorata	0.675607	0.478411	1	0.160313	100	3	Felidae
Pardofelis temminckii	0.776404	0.41433	1	0.147842	100	3	Felidae
Potos flavus	0.704178	0.725586	0.440982	0.04392	10	1	Procyonidae
Prionailurus bengalensis	0.75377	0.438902	1	0.134469	100	3	Felidae
Prionailurus planiceps	0.751932	0.349815	1	0.128425	100	3	Felidae
Prionailurus rubiginosus	0.774433	0.449236	1	0.144329	100	3	Felidae
Prionailurus viverrinus	0.768863	0.461598	1	0.135661	80	3	Felidae
Prionodon linsang	0.6281	0.354002	0.739471	0.102925	70	3	Prionodontidae
Prionodon pardicolor	0.705365	0.393119	0.772661	0.106063	70	3	Prionodontidae
Procyon cancrivorus	0.816279	0.755974	0.568805	0.075885	30	1	Procyonidae
Procyon lotor	0.731234	0.679243	0.577085	0.074384	20	1	Procyonidae
Pseudalopex	0.66431	0.40767	0.67306	0.09345	80	3	Canidae

culpaeus	6	5	5				
Pseudalopex fulvipes	0.604072	0.448548	0.629693	0.095011	60	2	Canidae
Pseudalopex griseus	0.662913	0.391039	0.641653	0.100071	60	2	Canidae
Pseudalopex gymnocercus	0.638805	0.406922	0.634599	0.096491	50	2	Canidae
Pseudalopex sechurae	0.657262	0.470373	0.620182	0.083933	60	2	Canidae
Pseudalopex vetulus	0.712788	0.507645	0.632813	0.084573	60	2	Canidae
Puma concolor	0.823543	0.487468	1	0.135203	100	3	Felidae
Puma yaguarondi	0.773825	0.476494	1	0.147145	80	3	Felidae
Rhynchogale melleri	0.87628	0.588574	0.534785	0.051184	30	1	Herpestidae
Salanoia concolor	0.663196	0.513006	0.57352	0.081245	30	1	Eupleridae
Speothos venaticus	0.704419	0.520943	0.74695	0.106851	100	3	Canidae
Suricata suricatta	0.702863	0.639879	0.701842	0.080385	20	1	Herpestidae

Urocyon cinereoargenteus	0.657782	0.477459	0.631509	0.088307	30	1	Canidae
Urocyon littoralis	0.652701	0.468111	0.628086	0.095304	30	1	Canidae
Viverra megaspila	0.668663	0.424138	0.608892	0.086154	70	3	Viverridae
Viverra tangalunga	0.673648	0.450581	0.598886	0.080933	70	3	Viverridae
Viverra zibetha	0.707957	0.49263	0.567746	0.081492	80	3	Viverridae
Viverricula indica	0.780349	0.417961	0.571797	0.071498	60	2	Viverridae
Vulpes chama	0.688799	0.451268	0.623931	0.088382	70	3	Canidae
Vulpes ferrilata	0.693651	0.459236	0.694622	0.105085	100	3	Canidae
Vulpes lagopus	0.635244	0.44493	0.701449	0.105418	90	3	Canidae
Vulpes rueppelli	0.637669	0.420883	0.657205	0.098942	60	2	Canidae
Vulpes velox	0.662934	0.37019	0.678807	0.096551	90	3	Canidae
Vulpes vulpes	0.64426	0.40331	0.67798	0.09955	70	3	Canidae

	5	8	3	3			
Vulpes zerda	0.677148	0.394847	0.609088	0.09014	50	2	Canidae

Table 2. Extinct taxa with associated averages of ecomorphological metrics.

Species	C1	P4S	RBL	M1BS
Adcrocuta eximia	0.747188	0.588566	0.835985	0.112602
Afrosmilus africanus	0.406736	0.489209	NA	NA
Afrosmilus hispanicus	0.513333	NA	0.983271	NA
Afrosmilus turkanae	NA	NA	0.969421	NA
Albanosmilus jourdani	0.373684	0.433526	1	0.167953
Albanosmilus whitfordi	0.386364	0.444976	1	0.171829
Allohyaena kadici	NA	0.571292	0.830248	NA
Amphimachairodus giganteus	0.396489	0.461898	0.935223	0.113028
Barbourofelis fricki	0.157042	0.497861	1	0.133913
Barbourofelis loveorum	NA	0.427078	1	0.176374
Barbourofelis morrisi	0.355795	0.447192	1	0.167111
Belbus beaumonti	NA	0.525	0.75261	0.118533
Chasmaporthetes lunensis	0.750759	0.492451	0.83533	0.10658
Chasmaporthetes ossifragus	0.897561	0.399386	0.899157	0.126683

Crocuta crocuta spelaea	0.724907	0.618027	0.910248	0.134365
Dinaelurus crassus	0.709677	NA	NA	NA
Dinailurictis bonali	0.563907	0.428571	0.812039	NA
Dinictis felina	0.551178	0.455047	0.826374	0.120949
Dinocrocuta gigantea	0.842105	0.56474	0.860564	0.120973
Dinofelis diastemata	0.650263	0.470874	0.955863	0.14701
Eofelis edwardsii	0.666667	0.443872	0.820345	0.143968
Euboictis aliverensis	NA	0.772059	NA	NA
Ginsburgsmilus napakensis	0.583333	0.59434	1	NA
Herpestides antiquus	0.767521	0.458333	0.678161	0.073861
Homotherium ischyrus	0.366998	0.44666	0.966745	NA
Homotherium latidens	0.416956	0.458315	1	0.1394
Homotherium serum	0.460004	0.432468	1	0.14193
Hoplophoneus adelos	NA	0.33574	NA	NA
Hoplophoneus bidentatus	0.487805	0.424895	0.914269	0.145238
Hoplophoneus cerebralis	0.477814	0.500697	0.926823	0.151966
Hoplophoneus dakotensis	0.443933	0.53125	0.929063	0.123486
Hoplophoneus occidentalis	0.440957	0.491782	0.950486	0.125868
Hoplophoneus oharrai	0.465559	0.44174	0.907312	0.122276
Hoplophoneus primaevus	0.537219	0.49914	0.906273	0.147058
Hoplophoneus sicarius	0.240255	0.420154	0.955703	0.11689
Hoplophoneus	0.327681	0.436975	0.921053	0.146346

villebramarensis			
Ictitherium viverrinum	0.636882	0.510467	0.673976	0.089825
Izmirictis cani	NA	0.514256	0.617248	NA
Kanuites lewisae	0.729167	NA	0.606173	NA
Kichechia zamanae	0.682927	0.619048	0.63871	NA
Lycyaena chaeretis	0.756263	0.523179	0.769853	0.107619
Machairodus catocopis	0.415963	0.431696	0.904503	0.126069
Machairodus coloradoensis	0.363719	0.401679	0.958988	0.131272
Maofelis cantonensis	0.76506	NA	NA	NA
MA-PHQ 348	0.725038	NA	NA	NA
Megantereon cultridens	0.497118	0.462991	0.974003	0.134235
Metailurus major	0.57248	0.434636	0.904655	0.098354
Miracinonyx trumani	0.816667	0.48125	0.95892	0.125692
Nanosmilus kurteni	0.404018	0.474055	0.881467	0.155248
Nimravides pedionomus	0.572538	0.457513	0.938835	0.141835
Nimravus brachyops	0.56505	0.445368	0.830725	0.143222
Nimravus intermedius	0.610619	0.416926	0.848941	NA
Oriensmilus liupanensis	0.445055	0.405316	1	0.191014
Pachycrocuta brevirostris	0.704545	0.651515	0.840678	NA
Palaeoprionodon lamandini	0.658436	NA	0.783824	0.085664
Palhyaena reperta	0.74669	0.633072	0.778208	0.114786

Panthera atrox	0.733222	0.491752	1	0.115471
Panthera leo spelaea	0.719254	0.477838	1	0.116486
Percrocuta algeriensis	NA	0.57193	0.831716	NA
Percrocuta carnifex	NA	0.573709	0.89735	NA
Percrocuta tobieni	NA	0.574713	0.838384	0.119752
Plioviverrops orbignyi	0.669246	0.472991	0.674444	0.076506
Pogonodon davisi	0.569334	0.599482	0.840437	0.119177
Pogonodon platycopis	0.556972	0.617188	0.838545	0.114899
Proailurus lemanensis	0.671711	0.458333	0.887452	0.122739
Promegantereon ogygia	0.59299	0.447216	0.930521	0.128398
Prosansanosmilus eggeri	NA	0.522124	0.96875	NA
Prosansanosmilus peregrinus	0.467199	0.375	0.95241	0.114234
Protictitherium crassum	0.591837	0.468531	0.419863	0.059764
Pseudaelurus validus	0.704031	0.491611	0.858555	0.119611
Quercylurus major	NA	NA	NA	NA
Sansanosmilus palmidens	0.460606	0.412776	1	0.180789
Sivanasua viverroides	0.655518	0.680128	0.693564	NA
Smilodon fatalis	0.4905	0.483591	1	0.136957
Smilodon populator	0.463153	0.451665	1	0.136113
Stenogale julieni	NA	0.471074	0.831325	NA
Tapocyon robustus	0.598083	0.47106	0.695688	0.065691
Thalassictis hyaenoides	0.741935	0.502005	0.737882	0.101481

Thalassictis wongii	0.601575	0.484962	0.727808	0.102206
Tongxinictis primordialis	0.683761	0.552486	NA	NA
Tungurictis spocki	0.454198	0.463883	0.707547	NA
Xenosmilus hodsonae	0.525	0.510823	1	0.160784

Table 3. Dietary classification of *Percrocuta* species using the canonical variates analysis of Coca-Ortega and Pérez-Claros (2019). Diet category 3 = Fully developed bone cracker.

	Diet	Civet-like	cursorial_meat	Full_bone	Jackal/wolf-like	Mongoose-like	Trans_bone
Percrocuta carnifex	3	3.62E-07	3.34E-09	0.924457	1.23E-05	2.82E-06	0.075528
Percrocuta algeriensis	3	7.68E-24	0.045511	0.954489	1.96E-14	1.79E-30	1.08E-08
Percrocuta tobieni	3	0.000797	1.88E-10	0.993324	0.001611	8.33E-11	0.004268

Table 4. Dietary classification of extinct non-durophagous and questionable sabertooth taxa based on dentognathic variables in canonical variates analysis. Diet: 1 = hypocarnivorous; 2 = mesocarnivorous; 3 = hypercarnivorous.

	diet	P.hypo	P.meso	P.hyper	P.saber
Belbus beaumonti	3	0.070803	0.244877	0.531351	0.152969
Chasmaporthetes lunensis	3	0.058428	0.065953	0.87559	2.93E-05
Chasmaporthetes ossifragus	3	0.001783	0.008813	0.989404	3.78E-08
Dinaelurus crassus	3	0.312037	0.187957	0.497663	0.002343
Dinofelis diastemata	3	0.001254	0.012282	0.915439	0.071025
Euboictis aliverensis	1	0.922125	0.059729	0.010637	0.007509
Herpestides antiquus	1	0.426162	0.221477	0.352361	2.29E-07
Ictitherium viverrinum	2	0.340978	0.404937	0.253603	0.000481
Izmirictis cani	1	0.477878	0.406266	0.105721	0.010136
Kanuites lewisae	1	0.580569	0.326893	0.092534	4.08E-06
Kichechia zamanae	1	0.72625	0.238773	0.03492	5.75E-05
Lycyaena chaeretis	3	0.132535	0.193906	0.673541	1.86E-05
Maofelis cantonensis	3	0.276446	0.155494	0.567772	0.000289
MA-PHQ 348	3	0.302467	0.178764	0.517454	0.001314
Metailurus major	3	0.022531	0.01939	0.869325	0.088753
Miracinonyx trumani	3	0.004811	0.007994	0.987188	6.45E-06
Palaeoprionodon lamandini	3	0.122438	0.145578	0.72617	0.005814
Panthera atrox	3	0.008033	0.005211	0.986459	0.000297
Panthera leo spelaea	3	0.006048	0.00484	0.988571	0.000542
Plioviverrops orbignyi	1	0.434927	0.281416	0.283625	3.23E-05
Proailurus lemanensis	3	0.008773	0.030235	0.957263	0.003729
Promegantereon ogygia	3	0.002953	0.013493	0.760499	0.223055
Protictitherium crassum	2	0.392143	0.599815	0.008037	4.23E-06
Pseudaelurus validus	3	0.022985	0.056354	0.919908	0.000754
Sivanasua viverroides	1	0.795004	0.171522	0.032811	0.000662

Stenogale julieni	3	0.02149	0.050873	0.675502	0.252136
Tapocyon robustus	1	0.588692	0.180363	0.230443	0.000503
Thalassictis hyaenoides	3	0.162663	0.244622	0.5927	1.56E-05
Thalassictis wongii	3	0.133929	0.324479	0.529699	0.011893
Tungurictis spocki	3	0.155341	0.280326	0.513479	0.050853

Table 5. Ecological data used in Chapter III analyses. Diet refers to dietary category, 1 = hypocarnivorous; 2 = mesocarnivorous; 3 = hypercarnivorous; 4 = durophagous; 5 = sabertooth; RBL = relative blade length of the lower m1; g = body mass in grams.

	diet	RBL	log_cuberoot_mass	g
Acinonyx_jubatus	3	1	3.610417	50577
Adcrocuta_eximia	4	0.835985	3.616675	51535.48
Afrosmilus_africanus	5	NA	NA	NA
Afrosmilus_hispanicus	5	0.983271	3.480055	34206.27
Afrosmilus_turkanae	5	0.969421	3.187158	14206.77
Albanosmilus_jourdani	5	1	3.85289	104680.8
Albanosmilus_whitfordi	5	1	3.8472	102908.8
Allohyaena_kadici	4	0.830248	3.588347	47336.72
Amphimachairodus_coloradoensis	5	0.935223	4.121573	234384.7
Amphimachairodus_giganteus	5	0.958988	4.150483	255620.7
Arctictis_binturong	2	0.5939	3.157543	12999
Atilax_paludinosus	2	0.725312	2.729563	3600
Barbourofelis_fricki	5	1	4.233938	328342.7
Barbourofelis_loveorum	5	1	4.179069	278509.7
Barbourofelis_morrisi	5	1	3.977234	152009.9
Bdeogale_nigripes	1	0.477484	2.624025	2623
Belbus_beaumonti	3	0.75261	3.461368	32341.43
Caracal_caracal	3	1	3.129886	11964

Catopuma_temminckii	3	1	2.984116	7726
Chasmaporthetes_lunensis	3	0.83533	3.454764	31706.94
Chasmaporthetes_ossifragus	3	0.899157	3.540839	41048.8
Civettictis_civetta	2	0.615087	3.132964	12075
Crocuta_crocuta	4	0.916777	3.685577	63369
Crocuta_crocuta_spelaea	4	0.910248	3.686889	63618.99
Crossarchus_obscurus	1	0.484472	2.41355	1395
Cryptoprocta_ferox	3	0.804789	3.053016	9500
Cynogale_bennettii	2	0.480858	2.784578	4246
Dinaelurus_crassus	3	NA	3.521503	38735.41
Dinailurictis_bonali	5	0.812039	3.954974	142190.5
Dinictis_felina	5	0.826374	3.589415	47488.67
Dinocrocuta_gigantea	4	0.860564	4.067907	199530
Dinofelis_diastemata	3	0.955863	3.814638	93331.72
Eofelis_edwardsii	5	0.820345	3.194692	14531.53
Euboictis_aliverensis	1	NA	NA	NA
Eupleres_goudotii	1	0.585666	2.641357	2763
Felis_lybica	3	1	2.809308	4573
Fossa_fossana	1	0.592517	2.508187	1853
Galerella_sanguinea	1	0.745567	2.099036	543
Genetta_maculata	2	0.721206	2.525195	1950
Ginsburgsmilus_napakensis	5	1	3.260098	17681.83
Helogale_parvula	1	0.442353	1.879452	281
Hemigalus_derbyanus	1	0.437407	2.380151	1262
Herpestes_edwardsii	3	0.634889	2.391064	1304
Herpestides_antiquus	1	0.678161	2.836014	4954.46
Homotherium_ischyrus	5	1	4.102459	221322.4
Homotherium_latidens	5	1	4.141736	249000
Homotherium_serum	5	1	4.050205	189210.5
Hoplophoneus_adelos	5	NA	3.87149	110687.8

Hoplophoneus_bidentatus	5	0.914269	3.513513	37817.95
Hoplophoneus_cerebralis	5	0.926823	3.286854	19159.63
Hoplophoneus_dakotensis	5	0.929063	3.85158	104270.1
Hoplophoneus_occidentalis	5	0.950486	3.800259	89391.28
Hoplophoneus_oharrai	5	0.907312	3.668141	60139.55
Hoplophoneus_primaevus	5	0.906273	3.59462	48235.91
Hoplophoneus_sicarius	5	0.955703	3.634071	54296.46
Hoplophoneus_villebramarensis	5	0.921053	3.645912	56259.84
Hyaena_hyaena	4	0.788502	3.488367	35070
Hyaenictitherium_hyaenoides	3	0.737882	3.39525	26522.56
Hyaenotherium_wongii	3	0.727808	3.317363	20996.01
Ichneumia_albicauda	1	0.491228	2.732146	3628
Ictitherium_viverrinum	2	0.673976	3.245832	16941.06
Izmirictis_cani	1	0.617248	2.937566	6719.02
Kanuites_lewisae	1	0.606173	2.793518	4361.422
Kichechia_zamanae	1	0.63871	2.634546	2707.111
Leopardus_pardalis	3	1	3.127537	11880
Lycyaena_chaeretis	3	0.769853	3.426575	29135.83
Lynx_canadensis	3	1	3.059341	9682
MA_PHQ_348	3	NA	2.894135	5898.212
Machairodus_catocopis	5	0.904503	4.120902	233913.7
Maofelis_cantonensis	3	NA	3.576047	45621.75
Megantereon_cultridens	5	0.974003	3.688356	63899.53
Metailurus_major	3	0.904655	3.581296	46345.93
Miracinonyx_trumani	3	0.95892	3.535222	40362.89
Mungos_mungo	1	0.516129	2.379622	1260
Nandinia_binotata	1	0.664097	2.560366	2167
Nanosmilus_kurteni	5	0.881467	3.410991	27805.08
Neofelis_nebulosa	3	1	3.204044	14945
Nimravides_pedionomus	5	0.938835	3.877899	112836.6

Nimravus_brachyops	5	0.830725	3.896134	119181.3
Nimravus_intermedius	5	0.848941	3.759695	79148.88
Oriensmilus_liupanensis	5	0.936422	3.616048	51438.58
Otocolobus_manul	3	1	2.06081	6324.129
Pachycrocuta_brevirostris	4	0.840678	3.869412	110000
Paguma_larvata	1	0.564977	2.78879	4300
Palaeoprionodon_lamandini	3	0.783824	2.68948	3192.12
Palinhyaena_reperta	4	0.778208	3.203014	14898.91
Panthera_atrox	3	1	4.088114	212000
Panthera_leo	3	1	3.991429	158623
Panthera_leo_spelaea	3	1	4.141736	249000
Panthera_pardus	3	1	3.622214	52399
Paradoxurus_hermaphroditus	1	0.596092	2.690302	3200
Percrocuta_algeriensis	4	0.831716	3.627596	53251.82
Percrocuta_carnifex	4	0.89735	3.492805	35540.07
Percrocuta_tobieni	4	0.838384	3.407761	27536.88
Plioviverrops_orbignyi	1	0.674444	2.699183	3286.407
Pogonodon_davisi	5	0.840437	3.84183	101264.3
Pogonodon_platycopis	5	0.838545	3.905489	122573.8
Poiana_richardsonii	1	0.779359	2.115212	570
Prionailurus_planiceps	3	1	2.723301	3533
Prionodon_linsang	3	0.739471	2.175986	684
Proailurus_lemanensis	3	0.887452	3.271761	18311.48
Profelis_aurata	3	1	3.110174	11277
Promegantereon_ogygia	3	0.930521	3.585968	47000
Prosansanosmilus_eggeri	5	0.96875	3.198023	14677.45
Prosansanosmilus_peregrinus	5	0.95241	3.508625	37267.45
Proteles_cristata	1	NA	3.001474	8139
Protictitherium_crassum	2	0.419863	2.93761	6719.9
Pseudaelurus_validus	3	0.858555	3.483199	34530.5

Puma_concolor	3	1	3.631962	53954
Quercylurus_major	5	NA	NA	NA
Rhynchogale_melleri	1	0.534785	2.57141	2240
Salanoia_concolor	1	0.730315	2.188891	711
Sansanosmilus_palmidens	5	1	3.593764	48112.23
Sivanasua_viverroides	1	0.693564	2.94273	6823.919
Smilodon_fatalis	5	1	4.098942	219000
Smilodon_populator	5	1	4.197112	294000
Stenogale_julieni	3	0.831325	2.67532	3059.356
Suricata_suricata	1	0.701842	2.197225	729
Tapocyon_robustus	1	0.695688	3.030226	8872.208
Tongxinictis_primordialis	4	NA	3.125784	11817.68
Tungurictis_spocki	3	0.707547	2.798452	4426.461
Viverra_tangalunga	1	0.598886	2.96744	7349
Viverricula_indica	1	0.571797	2.659551	2918
Xenosmilus_hodsonae	5	1	4.201001	297450.9

Table 6. Standard error of the mean in continuous variables listed in Table 3.

	RBL	log_cuberoot_mass
Acinonyx_jubatus	0	0.0345
Adcrocuta_eximia	0.0345	0.0345
Afrosmilus_africanus	NA	NA
Afrosmilus_hispanicus	0.0345	0.0345
Afrosmilus_turkanae	0.0345	0.0345
Albanosmilus_jourdani	0	0.0345
Albanosmilus_whitfordi	0	0.0345
Allohyaena_kadici	0.0345	0.0345
Amphimachairodus_coloradoensis	0.0345	0.0345
Amphimachairodus_giganteus	0.0345	0.0345

Arctictis_binturong	0.013861	0.0345
Atilax_paludinosus	0.009469	0.0345
Barbourofelis_fricki	0	0.0345
Barbourofelis_loveorum	0	0.0345
Barbourofelis_morrisi	0	0.0345
Bdeogale_nigripes	0.025931	0.0345
Belbus_beaumonti	0.0345	0.0345
Caracal_caracal	0	0.0345
Catopuma_temminckii	0	0.0345
Chasmaporthetes_lunensis	0.0345	0.0345
Chasmaporthetes_ossifragus	0.0345	0.0345
Civettictis_civetta	0.010171	0.0345
Crocuta_crocuta	0.011597	0.0345
Crocuta_crocuta_spelaea	0.0345	0.0345
Crossarchus_obscurus	0.012224	0.0345
Cryptoprocta_ferox	0.011597	0.0345
Cynogale_bennettii	0.012966	0.0345
Dinaelurus_crassus	NA	0.0345
Dinailurictis_bonali	0.0345	0.0345
Dinictis_felina	0.004529	0.0345
Dinocrocuta_gigantea	0.005321	0.0345
Dinofelis_diastemata	0.0345	0.0345
Eofelis_edwardsii	0.0345	0.0345
Euboictis_aliverensis	NA	NA
Eupleres_goudotii	0.013861	0.0345
Felis_lybica	0	0.0345
Fossa_fossana	0.010586	0.0345
Galerella_sanguinea	0.009469	0.0345
Genetta_maculata	0.007486	0.0345
Ginsburgsmilus_napakensis	0	0.0345

Helogale_parvula	0.014971	0.0345
Hemigalus_derbyanus	0.010171	0.0345
Herpestes_edwardsii	0.025931	0.0345
Herpestides_antiquus	0.0345	0.0345
Homotherium_ischyrus	0	0.0345
Homotherium_latidens	0	0.0345
Homotherium_serum	0	0.0345
Hoplophoneus_adelos	NA	0.0345
Hoplophoneus_bidentatus	0.0345	0.0345
Hoplophoneus_cerebralis	0.013624	0.0345
Hoplophoneus_dakotensis	0.0345	0.0345
Hoplophoneus_occidentalis	0.028924	0.0345
Hoplophoneus_oharrai	0.0345	0.0345
Hoplophoneus_primaevus	0.00555	0.0345
Hoplophoneus_sicarius	0.0345	0.0345
Hoplophoneus_villebramarensis	0.0345	0.0345
Hyaena_hyaena	0.011597	0.0345
Hyaenictitherium_hyaenoides	0.0345	0.0345
Hyaenotherium_wongii	0.0345	0.0345
Ichneumia_albicauda	0.009469	0.0345
Ictitherium_viverrinum	0.0345	0.0345
Izmirictis_cani	0.0345	0.0345
Kanuites_lewisae	0.0345	0.0345
Kichechia_zamanae	0.0345	0.0345
Leopardus_pardalis	0	0.0345
Lycyaena_chaeretis	0.0345	0.0345
Lynx_canadensis	0	0.0345
MA_PHQ_348	NA	0.0345
Machairodus_catocopis	0.0345	0.0345
Maofelis_cantonensis	NA	0.0345

Megantereon_cultridens	0.0345	0.0345
Metailurus_major	0.0345	0.0345
Miracinonyx_trumani	0.0345	0.0345
Mungos_mungo	0.009469	0.0345
Nandinia_binotata	0.010586	0.0345
Nanosmilus_kurteni	0.0345	0.0345
Neofelis_nebulosa	0	0.0345
Nimravides_pedionomus	0.0345	0.0345
Nimravus_brachyops	0.008036	0.0345
Nimravus_intermedius	0.0345	0.0345
Oriensmilus_liupanensis	0.0345	0.0345
Otocolobus_manul	0	0.0345
Pachycrocuta_brevirostris	0.0345	0.0345
Paguma_larvata	0.010171	0.0345
Palaeoprionodon_lamandini	0.0345	0.0345
Palinhyaena_reperta	0.0345	0.0345
Panthera_atrox	0	0.0345
Panthera_leo	0	0.0345
Panthera_leo_spelaea	0	0.0345
Panthera_pardus	0	0.0345
Paradoxurus_hermaphroditus	0.014971	0.0345
Percrocuta_algeriensis	0.0345	0.0345
Percrocuta_carnifex	0.008929	0.0345
Percrocuta_tobieni	0.0345	0.0345
Plioviverrops_orbignyi	0.0345	0.0345
Pogonodon_davisi	0.011505	0.0345
Pogonodon_platycopis	0.0345	0.0345
Poiana_richardsonii	0.0345	0.0345
Prionailurus_planiceps	0	0.0345
Prionodon_linsang	0.014971	0.0345

Proailurus_lemanensis	0.0345	0.0345
Profelis_aurata	0	0.0345
Promegantereon_ogygia	0.0345	0.0345
Prosansanosmilus_eggeri	0.0345	0.0345
Prosansanosmilus_peregrinus	0.0345	0.0345
Proteles_cristata	NA	0.0345
Protictitherium_crassum	0.0345	0.0345
Pseudaelurus_validus	0.0345	0.0345
Puma_concolor	0	0.0345
Quercylurus_major	NA	NA
Rhynchogale_melleri	0.018336	0.0345
Salanoia_concolor	0.012224	0.0345
Sansanosmilus_palmidens	0	0.0345
Sivanasua_viverroides	0.0345	0.0345
Smilodon_fatalis	0	0.0345
Smilodon_populator	0	0.0345
Stenogale_julieni	0.0345	0.0345
Suricata_suricata	0.012966	0.0345
Tapocyon_robustus	0.0345	0.0345
Tongxinictis_primordialis	NA	0.0345
Tungurictis_spocki	0.0345	0.0345
Viverra_tangalunga	0.0164	0.0345
Viverricula_indica	0.0164	0.0345
Xenosmilus_hodsonae	0	0.0345

References

Coca-Ortega, C., and J. A. Pérez-Claros. 2019. Characterizing ecomorphological patterns in hyenids: A multivariate approach using postcanine dentition. PeerJ 6:e6238.

Slater, G. J., and A. R. Friscia. 2019. Hierarchy in adaptive radiation: A case study using the Carnivora (Mammalia). Evolution 73:524–539.

Wilman, H., B. J., S. J., de L. R. C., R. M., and J. W. 2014. EltonTraits 1.0 : Species-level foraging attributes of the world's birds and mammals. Ecology 95:2027.

Appendix I

Digitized Specimen List - Subsample

Sample of crania used in the three-dimensional geometric morphometric analyses of Chapter IV. Unless otherwise specified, specimens were digitized via Microscribe with the methodology described in Chapter IV. Specimen number institutional codes are the same as in Appendix C, save CB = Bone Clones, Inc. 9200 Eton Ave. Chatsworth, CA 91311 USA.

Clade	Genus	Species	Specimen #	Male (n)	Female (n)	Unknown sex (n)	Source
Eupleridae	*Cryptoprocta*	*ferox*	FMNH 161793, 33950			2	
Eupleridae	*Eupleres*	*goudotii*	FMNH 30492; MNHN CG 1962-2105	2			
Eupleridae	*Fossa*	*fossana*	FMNH 156648, 85196	1	1		
Eupleridae	*Salanoia*	*concolor*	MNHN CG 1866-233, 1962-2111	1	1		
Felidae	*Pseudaelurus*	*validus*	FAM 61834, 61847; FM			3	

			61835				
Felinae	*Acinonyx*	*jubatus*	FM 45071; FMNH 29635, 34589	1		2	
Felinae	*Caracal*	*caracal*	FMNH 135042, 32945	1		1	
Felinae	*Catopuma*	*temminckii*	MNHN 1939-2152, 1941-293	1	1		
Felinae	*Felis*	*lybica*	FMNH 104579, 97861	1	1		
Felinae	*Leopardus*	*pardalis*	FMNH 85503, 88887, 93174	2	1		
Felinae	*Lynx*	*canadensis*	FMNH 138821, 145822	1	1		
Felinae	*Otocolobus*	*manul*	MNHN CG 2009-251, 2010-646	1	1		
Felinae	*Prionailurus*	*planiceps*	MNHN CG 1873-228			1	
Felinae	*Profelis*	*aurata*	MNHN CG 1917-8, 1939-687	1	1		

Felinae	*Puma*	*concolor*	FMNH 28334, 51875	1	1		
Herpestidae	*Atilax*	*paludinosus*	MNHN CG 1950-266, 1995-426	1	1		
Herpestidae	*Bdeogale*	*nigripes*	FMNH 8383, 85974	1	1		
Herpestidae	*Crossarchus*	*obscurus*	FMNH 4374, 54410	1	1		
Herpestidae	*Galerella*	*sanguinea*	MNHN CG 2000-1054, 2000-1072			2	
Herpestidae	*Helogale*	*parvula*	MNHN CG 1969-72, 1987-176	1	1		
Herpestidae	*Herpestes*	*edwardsii*	FMNH 83094, 97856	1	1		
Herpestidae	*Ichneumia*	*albicauda*	FMNH 73024, 85970	1	1		
Herpestidae	*Mungos*	*mungo*	FMNH 149365, 177229	1	1		
Herpestidae	*Rhynchogale*	*melleri*	MNHN CG	2			

			1962-1577, 1962-992				
Herpestidae	*Suricata*	*suricata*	FMNH 38348, 38349	2			
Hyaenidae	*Adcrocuta*	*eximia*	AMNH 22880; China 32-L-255, 41L-339, C-L-6, 80-L613			5	
Hyaenidae	*Chasmaporthetes*	*lunensis*	MNCN 67100			1	CT scan (Tseng et al., 2011)
Hyaenidae	*Crocuta*	*crocuta*	FMNH 34582, 98952	1	1		
Hyaenidae	*Crocuta*	*crocuta spelaea*	MFN MB. Ma 44381, 49139			2	
Hyaenidae	*Dinocrocuta*	*gigantea*	IVPP V15649			1	CT scan (Tseng, 2009)
Hyaenidae	*Hyaena*	*hyaena*	FMNH 101982, 27008	1	1		
Hyaenidae	*Hyaenotherium*	*wongii*	Bx. 71-L665; China (G) L-49, 42-l331, 89-L 746, 95-L789			5	

Hyaenidae	*Ictitherium*	*viverrinum*	China 51-L437; FAM 19665			2	
Hyaenidae	*Palinhyaena*	*reperta*	FAM 129667, 144897			2	
Hyaenidae	*Tungurictis*	*spocki*	AMNH 26600			1	
Machairodontinae	*Amphimachairodus*	*giganteus*	FAM 50476			1	
Machairodontinae	*Dinofelis*	*diastemata*	FAM 50446			1	
Machairodontinae	*Homotherium*	*ischyrus*	AMNH 95297			1	
Machairodontinae	*Homotherium*	*latidens*	AMNH 104641 (cast); FAM 50462			2	
Machairodontinae	*Homotherium*	*serum*	TMM 933-3444			1	CT scan, DigiMorph
Machairodontinae	*Megantereon*	*cultridens*	AMNH 105446 (cast)			1	
Machairodontinae	*Metailurus*	*major*	AMNH 131854 (cast)			1	
Machairodontinae	*Smilodon*	*fatalis*	LACMHC 2001-42, 2001-44, 2001-50, 2001-58, 2001-59, 2001-63, 2001-82, 2001-83;			10	

291

			LACMHC R-10688, R-10864				
Nimravidae	*Barbourofelis*	*fricki*	AMNH 108193 (cast)			1	
Nimravidae	*Barbourofelis*	*morrisi*	AMNH 61870, 79999			2	
Nimravidae	*Dinictis*	*felina*	AMNH 38805, 6937, 8777			3	
Nimravidae	*Eusmilus*	*cerebralis*	AMNH 6941; JODA 7047			2	Microscribe and photogrammetry
Nimravidae	*Eusmilus*	*dakotensis*	CB 15			1	Photogrammetry, courtesy of D. Tamagnini
Nimravidae	*Eusmilus*	*sicarius*	CB 07			1	Photogrammetry, courtesy of D. Tamagnini
Nimravidae	*Hoplophoneus*	*occidentalis*	RAM 10356			1	CT scan, courtesy of A. Farke
Nimravidae	*Hoplophoneus*	*primaevus*	AMNH 38981, 38982, 9764; FAM 125662			4	

Nimravidae	*Nanosmilus*	*kurteni*	AMNH 140559.001 (cast)			1	
Nimravidae	*Nimravus*	*brachyops*	AMNH 6930, 6933			2	
Nimravidae	*Pogonodon*	*davisi*	AMNH 102156 (cast)			1	
Nimravidae	*Pogonodon*	*platycopis*	AMNH 6938			1	
Pantherinae	*Neofelis*	*nebulosa*	FMNH 75830, 75831	1		1	
Pantherinae	*Panthera*	*atrox*	AMNH 14397; LACMHC 2900-10, 2900-7, 2900-8, 2900-9; UCMP 14001, 20049			7	
Pantherinae	*Panthera*	*leo*	FMNH 20757, 23970 (cast), 35739	3			
Pantherinae	*Panthera*	*leo spelaea*	MFN MB. Ma. 48115.1, 50947, 50948			3	

Pantherinae	*Panthera*	*pardus*	MNHN 1962-2884; MNHN CG 1996-521	1	1		
Prionodontidae	*Prionodon*	*linsang*	FMNH 8371, 88606	1	1		
Stenoplesictidae	*Proailurus*	*lemanensis*	AMNH 101931 (cast)			1	
Stenoplesictidae	*Nandinia*	*binotata*	AMNH 2409 C.A; FMNH 55758, 73804	1	1	1	
Viverridae	*Arctictis*	*binturong*	AMNH C.A. 1182; FMNH 53744, 53747	1	1	1	
Viverridae	*Civettictis*	*Civetta*	FMNH 108174, 27278	1	1		
Viverridae	*Cynogale*	*bennettii*	MNHN A-2094; MNHN CG 1962-170			2	
Viverridae	*Genetta*	*maculata*	FMNH 17525, 85984	1	1		
Viverridae	*Hemigalus*	*derbyanus*	AMNH 9 C.A; FMNH 33465,	1	1	1	

			68717				
Viverridae	*Paguma*	*larvata*	MNHN CG 1962-1588, 1988-163	1	1		
Viverridae	*Paradoxurus*	*hermaphroditus*	FMNH 338000, 39345	1	1		
Viverridae	*Poiana*	*richardsonii*	MNHN CG 1976-389			1	
Viverridae	*Viverra*	*tangalunga*	FMNH 68704, 85116	1	1		
Viverridae	*Viverricula*	*indica*	MNHN CG 1932-3552	1			

References

Tseng, Z. J. 2009. Cranial function in a late Miocene Dinocrocuta gigantea (Mammalia: Carnivora) revealed by comparative finite element analysis. Biological Journal of the Linnean Society 96:51–67.

Tseng, Z. J., M. Antón, and M. J. Salesa. 2011. The evolution of the bone-cracking model in carnivorans: cranial functional morphology of the Plio-Pleistocene cursorial hyaenid Chasmaporthetes lunensis (Mammalia: Carnivora). Paleobiology 37:140–1.

References

Adams, D. C. 2014a. A method for assessing phylogenetic least squares models for shape and other high-dimensional multivariate data. Evolution 68:2675–2688.

Adams, D. C. 2014b. A generalized K statistic for estimating phylogenetic signal from shape and other high-dimensional multivariate data. Systematic Biology 63:685–697.

Adams, D. C. 2014c. Quantifying and comparing phylogenetic evolutionary rates for shape and other high-dimensional phenotypic data. Systematic Biology 63:166–177.

Adams, D. C., and M. L. Collyer. 2015. Permutation tests for phylogenetic comparative analyses of high-dimensional shape data: What you shuffle matters. Evolution 69:823–829.

Adams, D. C., M. L. Collyer, A. Kaliontzopoulou, and E. K. Baken. 2021. Geomorph: Software for geometric morphometric analyses. R package version 4.0. Https://Cran.r-Project.Org/Package=geomorph.

Alroy, J. 1992. Conjunction among taxonomic distributions and the Miocene mammalian biochronology of the Great Plains. Paleobiology 18:326–343.

Andersson, K. 2005. Were there pack-hunting canids in the Tertiary, and how can we know? Paleobiology 31:56–72.

Antoine, P. O., J. L. Welcomme, L. Marivaux, I. Baloch, M. Benammi, and P. Tassy. 2003. First record of Paleogene Elephantoidea (Mammalia, Proboscidea) from the Bugti Hills of Pakistan. Journal of Vertebrate Paleontology 23:977–980.

Antón, A. M., M. J. Salesa, and G. Siliceo. 2013. Machairodont Adaptations and Affinities of the Holarctic Late Miocene Homotherin Machairodus (Mammalia, Carnivora, Felidae): The Case of Machairodus Catocopis Cope, 1887. Journal of Vertebrate Paleontology 33:1202–1213.

Antón, M., M. J. Salesa, A. Galobart, and Z. J. Tseng. 2014. The Plio-Pleistocene scimitar-toothed felid genus Homotherium Fabrini, 1890 (Machairodontinae, Homotherini): Diversity, palaeogeography and taxonomic implications. Quaternary Science Reviews 96:259–268.

Averianov, A., E. Obraztsova, I. Danilov, P. Skutschas, and J. Jin. 2016. First nimravid skull from Asia. Scientific Reports 6:1–8.

Averyanov, A. O., and G. F. Baryshnikov. 1996. Origin and systematic position of aardwolf proteles cristatus (mammalia, carnivora). Zoologicheskii Zhurnal 75:1256–1258.

Baken, E. K., M. L. Collyer, A. Kaliontzopoulou, and D. C. Adams. 2021. geomorph v4.0 and gmShiny: Enhanced analytics and a new graphical interface for a comprehensive morphometric experience. Methods in Ecology and Evolution 12:2355–2363.

Bapst, D. W. 2012. Paleotree: an R Package for Paleontological and Phylogenetic Analyses of Evolution. Methods in Ecology and Evolution 3:803–807.

Barnett, R., M. L. Z. Mendoza, A. E. R. Soares, S. Y. W. Ho, G. Zazula, N. Yamaguchi, B. Shapiro, I. V. Kirillova, G. Larson, and M. T. P. Gilbert. 2016. Mitogenomics of the extinct cave lion, Panthera spelaea (Goldfuss, 1810), resolve its position within the panthera cats. Open Quaternary 2:1–11.

Barnett, R., B. Shapiro, I. Barnes, S. Y. Ho, J. Burger, N. Yamaguchi, T. F. Higham, H. T. Wheeler, W. Rosendahl, A. V Sher, M. Sotnikova, T. Kuznetsova, G. F. Baryshnikov, L. D. Martin, C. R. Harington, J. A. Burns, and A. Cooper. 2009. Phylogeography of lions (Panthera leo ssp.) reveals three distinct taxa and a late Pleistocene reduction in genetic diversity. Molecular Ecology 18:1668–1677.

Barnett, R., M. V. Westbury, M. Sandoval-Velasco, F. G. Vieira, S. Jeon, G. Zazula, M. D. Martin, S. Y. W. Ho, N. Mather, S. Gopalakrishnan, J. Ramos-Madrigal, M. de Manuel, M. L. Zepeda-Mendoza, A. Antunes, A. C. Baez, B. De Cahsan, G. Larson, S. J. O'Brien, E. Eizirik, W. E. Johnson, K.-P. Koepfli, A. Wilting, J. Fickel, L. Dalén, E. D. Lorenzen, T. Marques-Bonet, A. J. Hansen, G. Zhang, J. Bhak, N. Yamaguchi, and M. T. P. Gilbert. 2020. Genomic Adaptations and Evolutionary History of the Extinct Scimitar-Toothed Cat, Homotherium latidens. Current Biology 30:1–8.

Barnett, R., I. Barnes, M. J. Phillips, L. D. Martin, C. R. Harrington, J. A. Leonard, and A. Cooper. 2005. Evolution of the extinct Sabretooths and the American cheetah-like cat. Current Biology 15:R589–R590.

Barrett, P. Z. 2016. Taxonomic and systematic revisions to the North American Nimravidae (Mammalia, Carnivora). PeerJ 4:e1658.

Barrett, P. Z. 2021. The largest hoplophonine and a complex new hypothesis of nimravid evolution. Scientific Reports 11:1–9.

Barrett, P. Z., S. S. B. Hopkins, and S. A. Price. 2021. How many sabretooths? Reevaluating the number of carnivoran sabretooth lineages with total-evidence Bayesian techniques and a novel origin of the Miocene Nimravidae. Journal of Vertebrate Paleontology e1923523.

Baryshnikov, G. F., and A. O. Averianov. 1993. Deciduous teeth of carnivorous mammals (Order Carnivora) Part V. Families Protelidae and Hyaenidae. Russian Academy of Sciences Proceedings of the Zoological Institute St. Petersburg 263:46–84.

Beaulieu, J. M., D. C. Jhwueng, C. Boettiger, and B. C. O'Meara. 2012. Modeling stabilizing selection: Expanding the Ornstein-Uhlenbeck model of adaptive evolution. Evolution 66:2369–2383.

Bell, M. A., and G. T. Lloyd. 2014. Strap: Stratigraphic Tree Analysis for Palaeontology. R package version 1.4. https://CRAN.R-project.org/package=strap.

Bergsten, J. 2005. A review of long-branch attraction. Cladistics 21:163–193.

Blomberg, S. P., T. Garland, and A. R. Ives. 2003. Testing for phylogenetic signal in comparative data: behavioral traits are more labile. Evolution 57:717–745.

Bobe, R., A. K. Behrensmeyer, and R. E. Chapman. 2002. Faunal change, environmental variability and late Pliocene hominin evolution. Journal of Human Evolution 42:475–497.

Böhme, M., M. Aiglstorfer, P. O. Antoine, E. Appel, P. Havlik, G. Métais, L. T. Phuc, S. Schneider, F. Setzer, R. Tappert, D. N. Tran, D. Uhl, and J. Prieto. 2013. Na Duong (northern Vietnam) - An exceptional window into Eocene ecosystems from Southeast Asia. Zitteliana Reihe A: Mitteilungen Der Bayerischen Staatssammlung Fur Palaontologie Und Geologie 53:121–167.

Bonferroni, C. E. 1936. Teoria statistica delle classi e calcolo delle probabilità. Pubblicazioni Del R Istituto Superiore Di Scienze Economiche e Commerciali Di Firenze 8:1–62.

de Bonis, L., S. Peigné, H. T. Mackaye, A. Likius, P. Vignaud, and M. Brunet. 2018. New sabre toothed felidae (Carnivora, mammalia) in the hominid-bearing sites of toros menalla (late miocene, Chad). Geodiversitas 40:69–86.

Bookstein, F. L., P. Gunz, P. Mittercker, H. Prossinger, K. Schæfer, and H. Seidler. 2003. Cranial integration in Homo: Singular warps analysis of the midsagittal plane in ontogeny and evolution. Journal of Human Evolution 44:167–187.

Borths, M. R., P. A. Holroyd, and E. R. Seiffert. 2016. Hyainailourine and teratodontine cranial material from the late Eocene of Egypt and the application of parsimony and Bayesian methods to the phylogeny and biogeography of Hyaenodonta (Placentalia, Mammalia). PeerJ 4:e2639.

Bouckaert, R., J. Heled, D. Kühnert, T. Vaughan, C. H. Wu, D. Xie, M. A. Suchard, A. Rambaut, and A. J. Drummond. 2014. BEAST 2: A Software Platform for Bayesian Evolutionary Analysis. PLoS Computational Biology 10:e1003537.

Boyer, D. M. 2008. Relief index of second mandibular molars is a correlate of diet among prosimian primates and other euarchontan mammals. Journal of Human Evolution 55:1118–1137.

Bright, J. A., J. Marugán-Lobón, S. N. Cobb, and E. J. Rayfield. 2016. The shapes of bird beaks are highly controlled by nondietary factors. Proceedings of the National Academy of Sciences of the United States of America 113:5352–5357.

Brocklehurst, N. 2019. Morphological evolution in therocephalians breaks the hypercarnivore ratchet. Proceedings of the Royal Society B: Biological Sciences 286.

Browne, I., and R. E. Reynolds. 2015. Nimravides marshi (Felidae): an early scimitar-cat from the upper Barstovian section of the Mud Hills, Mojave Desert, California. Mojave Miocene 136–144.

Bryant, H. N. 1996. Nimravidae; pp. 453–475 in D. R. Prothero and R. J. Emry (eds.), The Terrestrial Eocene-Oligocene Transition in North America. Cambridge University Press, Cambridge [England]; New York.

Cantalapiedra, J. L., R. G. FitzJohn, T. S. Kuhn, M. H. Fernández, D. DeMiguel, B. Azanza, J. Morales, and A. Mooers. 2013. Dietary innovations spurred the diversification of ruminants during the Caenozoic. Proceedings of the Royal Society B: Biological Sciences 281.

Carbone, C., A. Teacher, and J. M. Rowcliffe. 2007. The costs of carnivory. PLoS Biology 5:0363–0368.

Carbone, C., G. M. Mace, S. C. Roberts, and D. W. Macdonald. 1999. Energetic constraints on the diet of terrestrial carnivores. Nature 402:286–288.

Chamoli, U., and S. Wroe. 2011. Allometry in the distribution of material properties and geometry of the felid skull: Why larger species may need to change and how they may achieve it. Journal of Theoretical Biology 283:217–226.

Chen, G. F., and N. Schmidt-Kittler. 1983. The deciduous dentition of Percrocuta Kretzoi and the diphyletic origin of the hyaenas (Carnivora, Mammalia). Paläontologische Zeitschrift 57:159–169.

Chow, M. M. 1958. A record of the earliest sabre-toothed cats from the Eocene of Lushih, Honan. Science Record 2:347–349.

Christensen, H. B. 2014. Similar associations of tooth microwear and morphology indicate similar diet across marsupial and placental mammals. PLoS ONE 9:e102789.

Christiansen, P. 2006. Sabertooth characters in the clouded leopard (Neofelis nebulosa Griffiths 1821). Journal of Morphology 267:1186–1198.

Christiansen, P. 2008a. Phylogeny of the great cats (Felidae: Pantherinae), and the influence of fossil taxa and missing characters. Cladistics 24:977–992.

Christiansen, P. 2008b. Evolution of skull and mandible shape in cats (Carnivora: Felidae). PLoS ONE 3:e2807.

Christiansen, P. 2008c. Evolutionary convergence of primitive sabertooth craniomandibular morphology: the clouded leopard (Neofelis nebulosa) and Paramachairodus ogygia compared. Journal of Mammalian Evolution 15:155–179.

Christiansen, P. 2012. The making of a monster: Postnatal ontogenetic changes in craniomandibular shape in the great sabercat Smilodon. PLoS ONE 7:19–21.

Christiansen, P. 2013. Phylogeny of the sabertoothed felids (Carnivora: Felidae: Machairodontinae). Cladistics 29:543–559.

Christiansen, P., and J. M. Harris. 2005. Body size of Smilodon (Mammalia: Felidae). Journal of Morphology 266:369–384.

Clavel, J., G. Escarguel, and G. Merceron. 2015. mvMORPH: An R package for fitting multivariate evolutionary models to morphometric data. Methods in Ecology and Evolution 6:1311–1319.

Coca-Ortega, C., and J. A. Pérez-Claros. 2019. Characterizing ecomorphological patterns in hyenids: A multivariate approach using postcanine dentition. PeerJ 6:e6238.

Collard, M., and P. O'Higgins. 2001. Ontogeny and homoplasy in the papionin monkey face. Evolution and Development 3:322–331.

Collyer, M. L., and D. C. Adams. 2018. RRPP: An R package for fitting linear models to high-dimensional data using residual randomization. Methods in Ecology and Evolution 9:1772–1779.

Collyer, M. L., and D. C. Adams. 2019. RRPP: linear model evaluation with randomized residuals in a permutation procedure. R package version 1.1.2. Available at https://cran.r-project.org/packagepRRPP.

Collyer, M. L., D. J. Sekora, and D. C. Adams. 2015. A method for analysis of phenotypic change for phenotypes described by high-dimensional data. Heredity 115:357–365.

Costa, E., M. Garcés, A. Sáez, L. Cabrera, and M. López-blanco. 2011. The age of the "Grande Coupure" mammal turnover : New constraints from the Eocene – Oligocene record of the Eastern Ebro Basin (NE Spain). Palaeogeography, Palaeoclimatology, Palaeoecology 301:97–107.

Dashzeveg, D. 1996. Some Carnivorous Mammals from the Paleogene of the Eastern Gobi Desert , Mongolia , and the Application of Oligocene Carnivores to Stratigraphic Correlation. American Museum Novitates 3179:1–14.

Desantis, L. R. G., B. W. Schubert, E. Schmitt-linville, P. S. Ungar, S. L. Donohue, and R. J. Haupt. 2015. Dental microwear textures of carnivorans from the La Brea tar pits, California, and potential extinction implications. Natural History Museum of Los Angeles County, Science Series 42:37–52.

DeSantis, L. R. G., R. S. Feranec, M. Antón, and E. L. Lundelius. 2021. Dietary ecology of the scimitar-toothed cat Homotherium serum. Current Biology 31:2674-2681.e3.

Ding, S., J. Zhen, Y. Zhang, and Y. Tong. 1977. The age and characteristic of the Liuniu and the Dongjun faunas, Bose Basin of Guangxi. Vertebrata Palasiatica 15:35–45.

Dobzhansky, T. 1951. Genetics and the Origin of Species, 3rd ed. Columbia University Press, New York, 364 pp.

Drake, A. G., and C. P. Klingenberg. 2008. The pace of morphological change: Historical transformation of skull shape in St Bernard dogs. Proceedings of the Royal Society B: Biological Sciences 275:71–76.

Ducrocq, S., Y. Chaimanee, V. Suteethorn, and J. J. Jaeger. 1995. Mammalian faunas and the ages of the continental Tertiary fossiliferous localities from Thailand. Journal of Southeast Asian Earth Sciences 12:65–78.

Eimer, G. H. T. 1890. Organic Evolution as the Result of the Inheritance of Acquired Characters According to the Laws of Organic Growth. Macmillan, London, UK, 435 pp.

Eldredge, N., and S. J. Gould. 1972. Punctuated equilibria: an alternative to phyletic gradualism; pp. 82–115 in T. J. M. Schopf (ed.), Moddels in Paleobiology. Freeman, Cooper and Co., San Francisco.

Evans, A. R., G. P. Wilson, M. Fortelius, and J. Jernvall. 2007. High-level similarity of dentitions in carnivorans and rodents. Nature 445:78–81.

Evans, R. A., and S. Pineda-Munoz. 2018. Inferring mammal dietary ecology from dental morphology; pp. 37–51 in D. A. Croft, D. F. Su, and S. W. Simpson (eds.), Methods in Paleoecology: Reconstructing Cenozoic terrestrial environments and ecological communities, 1st ed. Springer.

Ewer, R. F. 1973. The Carnivores. Weidenfeld and Nicolson, London, England, 494 pp.

Faith, J. T., and A. K. Behrensmeyer. 2013. Climate change and faunal turnover: testing the mechanics of the turnover-pulse hypothesis with South African fossil data. Paleobiology 39:609–627.

Famoso, N. A., and J. D. Orcutt. 2022. First occurrences of Palaeogale von Meyer, 1846 in the Pacific Northwest, United States. Geodiversitas 41:427–436.

Fan, Y., R. Wu, M. H. Chen, L. Kuo, and P. O. Lewis. 2011. Choosing among partition models in Bayesian phylogenetics. Molecular Biology and Evolution 28:523–532.

Feranec, R. S. 2004. Isotopic evidence of saber-tooth development, growth rate, and diet from the adult canine of Smilodon fatalis from Rancho La Brea. Palaeogeography, Palaeoclimatology, Palaeoecology 206:303–310.

Ferguson, J. W., and R. P. Atit. 2019. A tale of two cities: The genetic mechanisms governing calvarial bone development. Genesis 57:e23248.

Figueirido, B., Z. J. Tseng, and A. Martín-Serra. 2013. Skull shape evolution in durophagous carnivorans. Evolution 67:1975–1993.

Figueirido, B., A. Martín-Serra, Z. J. Tseng, and C. M. Janis. 2015. Habitat changes and changing predatory habits in North American fossil canids. Nature Communications 6.

Figueirido, B., N. MacLeod, J. Krieger, M. De Renzi, J. A. Pérez-Claros, and P. Palmqvist. 2011. Constraint and adaptation in the evolution of carnivoran skull shape. Paleobiology 37:490–518.

Flynn, J. J., J. A. Finarelli, S. Zehr, J. Hsu, and M. A. Nedbal. 2005. Molecular phylogeny of the Carnivora (Mammalia): assessing the impact of increased sampling on resolving enigmatic relationships. Systematic Biology 54:317–337.

Forasiepi, A. M., and M. R. Sánchez-Villagra. 2014. Heterochrony, dental ontogenetic diversity, and the circumvention of constraints in marsupial mammals and extinct relatives. Paleobiology 40:222–237.

Friscia, A. R., B. Van Valkenburgh, and A. R. Biknevicius. 2007. An ecomorphological analysis of extant small carnivorans. Journal of Zoology 272:82–100.

Friscia, A. R., M. Macharwas, S. Muteti, F. Ndiritu, and D. Tab Rasmussen. 2020. A Transitional Mammalian Carnivore Community from the Paleogene–Neogene Boundary in Northern Kenya. Journal of Vertebrate Paleontology 40.

Frost, S. R. 2007. African Pliocene and Pleistocene cercopithecid evolution and global climate change; pp. 51–76 in R. Bobe, Z. Alemseged, and A. K. Behrensmeyer (eds.), Hominin environments in the East African Pliocene: an assessment of the faunal evidence. Springer, Dordrecht.

Galton, F. 1869. Hereditary Genius: An Inquiry into Its Laws and Consequences. Macmillan, London, 390 pp.

Gaubert, P., and G. Veron. 2003. Exhaustive sample set among Viverridae reveals the sister-group of felids: The linsangs as a case of extreme morphological convergence within Feliformia. Proceedings of the Royal Society B: Biological Sciences 270:2523–2530.

Gaubert, P., W. C. Wozencraft, P. Cordeiro-Estrela, and G. Veron. 2005. Mosaics of Convergences and Noise in Morphological Phylogenies: What's in a Viverrid-Like Carnivoran? Systematic Biology 56:865–894.

Gavryushkina, A., D. Welch, T. Stadler, and A. J. Drummond. 2014. Bayesian inference of sampled ancestor trees for epidemiology and fossil calibration. PLoS Computational Biology 10:e1003919.

Gehring, W. J. 1996. The master control gene for morphogenesis and evolution of the eye. Genes Cells 1:11–15.

Goldschmidt, R. B. 1940. The Material Basis of Evolution. Yale University Press, New Haven, CT, 438 pp.

Goloboff, P. A., and S. A. Catalano. 2016. TNT version 1.5, including a full implementation of phylogenetic morphometrics. Cladistics 32:221–238.

Goodall, C. 1991. Procrustes Methods in the Statistical Analysis of Shape. Journal of the Royal Statistical Society: Series B (Methodological) 53:285–321.

Goswami, A. 2006. Morphological Integration in the Carnivoran Skull. Evolution 60:169–183.

Goswami, A., and P. D. Polly. 2010a. The Influence of Modularity on Cranial Morphological Disparity in Carnivora and Primates (Mammalia). PLoS ONE 5:e9517.

Goswami, A., and P. D. Polly. 2010b. Methods for Studying Morphological Integration and Modularity. The Paleontological Society Papers 16:213–243.

Goswami, A., N. Milne, and S. Wroe. 2011. Biting through constraints: cranial morphology, disparity and convergence across living and fossil carnivorous mammals. Proceedings of the Royal Society B 278:1831–1839.

Goswami, A., J. B. Smaers, C. Soligo, and P. D. Polly. 2014. The macroevolutionary consequences of phenotypic integration: from development to deep time. Philosophical Transactions of the Royal Society B 369:20130254.

Goswami, A., W. J. Binder, J. Meachen, and F. R. O'Keefe. 2015. The fossil record of phenotypic integration and modularity: A deep-time perspective on developmental and evolutionary dynamics. Proceedings of the National Academy of Sciences of the United States of America 112:4891–4896.

Gould, S. J. 1989. Wonderful Life: The Burgess Shale and the Nature of History. W. W. Norton & Company, New York City, 352 pp.

Gould, S. J. 2002. The Structure of Evolutionary Theory. Belknap Press of Harvard University Press, Cambridge, Mass., 1433 pp.

Gracia, S. F. 2015. Estudio de Protictitherium crassum del Cerro de los Batallones (Torrejón de Velasco, Madrid): aportación a la filogenia y evolución de la familia hyaenidae. Universidad Complutense de Madrid, 365 pp.

Grohé, C., L. De Bonis, Y. Chaimanee, O. Chavasseau, M. Rugbumrung, C. Yamee, K. Suraprasit, C. Gibert, J. Surault, C. Blondel, and J. J. Jaeger. 2020. The Late Middle Miocene Mae Moh Basin of Northern Thailand: The Richest Neogene Assemblage of Carnivora from Southeast Asia and a Paleobiogeographic Analysis of Miocene Asian Carnivorans. American Museum Novitates 2020:1–57.

Grossnickle, D. M. 2020. Feeding ecology has a stronger evolutionary influence on functional morphology than on body mass in mammals. Evolution 74:610–628.

Guillerme, T., N. Cooper, S. L. Brusatte, K. E. Davis, A. L. Jackson, S. Gerber, A. Goswami, K. Healy, M. J. Hopkins, M. E. H. Jones, G. T. Lloyd, J. E. O'Reilly, A. Pate, M. N. Puttick, E. J. Rayfield, E. E. Saupe, E. Sherratt, G. J. Slater, V. Weisbecker, G. H. Thomas, and P. C. J. Donoghue. 2020. Disparities in the analysis of morphological disparity: Analysis of morphological disparity. Biology Letters 16.

Haeckel, E. 1866. Generelle Morphologie Der Organismen: Allgemeine Grundzüge Der Organischen Formen-Wissenschaft, Mechanisch Begründet Durch Die von Charles Darwin Reformirte Decendenz-Theorie. Georg Reimer, Berlin, 574 pp.

Hans-Volker, K., E. Gröning, and C. Brauckmann. 2007. Comment on a fossil civet skull from the Lower Oligocene of the Weisselster Basin (Saxonia, Germany). Studia Geologica Salmanticensia 43:215–225.

Hansen, T. F. 1997. Stabilizing selection and the comparative analysis of adaptation. Evolution 51:1341–1351.

Hanson, C. B. 1996. Stratigraphy and vertebrate faunas of the Bridgerian-Duchesnean Clarno Formation, north-central Oregon; pp. 206–239 in D. R. Prothero and R. J. Emry (eds.), The Terrestrial Eocene-Oligocene Transition in North America. Cambridge University Press.

Harjunmaa, E., K. Seidel, T. Häkkinen, E. Renvoisé, I. J. Corfe, A. Kallonen, Z. Q. Zhang, A. R. Evans, M. L. Mikkola, I. Salazar-Ciudad, O. D. Klein, and J. Jernvall. 2014. Replaying evolutionary transitions from the dental fossil record. Nature 512:44–48.

Harmon, L. J., J. B. Losos, T. Jonathan Davies, R. G. Gillespie, J. L. Gittleman, W. Bryan Jennings, K. H. Kozak, M. A. McPeek, F. Moreno-Roark, T. J. Near, A. Purvis, R. E. Ricklefs, D. Schluter, J. A. Schulte, O. Seehausen, B. L. Sidlauskas, O. Torres-Carvajal, J. T. Weir, and A. T. Mooers. 2010. Early bursts of body size and shape evolution are rare in comparative data. Evolution 64:2385–2396.

Hassanin, A., G. Veron, A. Ropiquet, B. J. van Vuuren, A. Lécu, S. M. Goodman, J. Haider, and T. T. Nguyen. 2021. Evolutionary history of Carnivora (Mammalia, Laurasiatheria) inferred from mitochondrial genomes. PLoS ONE 16:1–28.

Holliday, J. A., and S. J. Steppan. 2004. Evolution of hypercarnivory: the effect of specialization on morphological and taxonomic diversity. Paleobiology 30:108–128.

Hopkins, S. S. B., S. A. Price, and A. J. Chiono. 2021. Influence of phylogeny on the estimation of diet from dental morphology in the Carnivora. Paleobiology 1–16.

Humphreys, A. M., and T. G. Barraclough. 2014. The evolutionary reality of higher taxa in mammals. Proceedings of the Royal Society B: Biological Sciences 281.

Hunt, G. 2007. The relative importance of directional change, random walks, and stasis in the evolution of fossil lineages. Proceedings of the National Academy of Sciences of the United States of America 104:18404–18408.

Hunt Jr., R. M., and N. Solounias. 1991. Evolution of the aeluroid Carnivora: hyaenid affinities of the Miocene carnivoran Tungurictis spocki from Inner Mongolia. American Museum Novitates 1–25.

Hunt, R. M. 1987. Evolution of the aeluroid Carnivora: significance of auditory structure in the nimravid cat Dinictis. American Museum Novitates 2886:1–74.

Hunt, R. M. 1989. Evolution of the Aeluroid Carnivora: Significance of the Ventral Promontorial Process of the Petrosal, and the Origin of Basicranial Patterns in the Living Families. American Museum Novitates 2930:1–32.

Hunt, R. M. 1991. Evolution of the aeluroid Carnivora: viverrid affinities of the Miocene carnivoran Herpestides. American Museum Novitates 3023:1–34.

Hunt, R. M. 1996. Biogeography of the order Carnivora; pp. 485–541 in J. L. Gittleman (ed.), Carnivore Behavior, Ecology, and Evolution. Cornell University Press, New York.

Hunt, R. M. 1998a. Evolution of the aeluroid Carnivora. Diversity of the earliest aeluroids from Eurasia (Quercy, Hsanda-Gol) and the origin of felids. American Museum Novitates 3252.

Hunt, R. M. 1998b. Amphicyonidae; pp. 196–227 in C. M. Janis, K. Scott, and L. L. Jacobs (eds.), Evolution of Tertiary Mammals of North America, Volume 1: Terrestrial Carnivores, Ungulates, and Ungulatelike Mammals. Cambridge University Press, Cambridge.

Hunt, R. M. 2001a. Basicranial anatomy of the living linsangs Prionodon and Poiana (Mammalia, Carnivora, Viverridae), with comments on the early evolution of aeluroid carnivorans. American Museum Novitates 3330.

Hunt, R. M. 2001b. Small Oligocene amphicyonids from North America (Paradaphoenus, Mammalia, Carnivora). American Museum Novitates 3331:1–20.

Hunter, J. P., and J. Jernvall. 1995. The hypocone as a key innovation in mammalian evolution. Proceedings of the National Academy of Sciences of the United States of America 92:10718–10722.

Hutchinson, G. E. 1959. Homage to Santa Rosalia or why are there so many kinds of animals? American Naturalist 93:145–159.

Hyatt, A. 1897. Cycle in the life of the individual (ontogeny) and in the evolution of its own group (phylogeny). Proceedings of the American Academy of Arts and Sciences 32:209–224.

Janis, C. M., and P. B. Wilhelm. 1993. Were there mammalian pursuit predators in the Tertiary? Dances with wolf avatars. Journal of Mammalian Evolution 1:103–125.

Jernvall, J., and H. Jung. 2000. Genotype, phenotype, and developmental biology of molar tooth characters. American Journal of Physical Anthropology 113:171–190.

Jones, K. E., J. Bielby, M. Cardillo, S. A. Fritz, J. O'Dell, C. D. L. Orme, K. Safi, W. Sechrest, E. H. Boakes, C. Carbone, C. Connolly, M. J. Cutts, J. K. Foster, R. Grenyer, M. Habib, C. A. Plaster, S. A. Price, E. A. Rigby, J. Rist, A. Teacher, O. R. P. Bininda-Emonds, J. L. Gittleman, G. M. Mace, and A. Purvis. 2009. PanTHERIA: a species-level database of life history, ecology, and geography of extant and recently extinct mammals. Ecology 90:2648–2648.

Jones, K. E., J. B. Smaers, and A. Goswami. 2015. Impact of the terrestrial-aquatic transition on disparity and rates of evolution in the carnivoran skull. BMC Evolutionary Biology 15.

Kangas, A. T., A. R. Evans, I. Thesleff, and J. Jernvall. 2004. Nonindependence of mammalian dental characters. Nature 432:211–214.

Katoh, K., J. Rozewicki, and K. D. Yamada. 2019. MAFFT online service: Multiple sequence alignment, interactive sequence choice and visualization. Briefings in Bioinformatics 20:1160–1166.

Kavanagh, K. D., A. R. Evans, and J. Jernvall. 2007. Predicting evolutionary patterns of mammalian teeth from development. Nature 449:427–432.

Koepfli, K. P., S. M. Jenks, E. Eizirik, T. Zahirpour, B. Van Valkenburgh, and R. K. Wayne. 2006. Molecular systematics of the Hyaenidae: Relationships of a relictual lineage resolved by a molecular supermatrix. Molecular Phylogenetics and Evolution 38:603–620.

Koufos, G. D., L. de Bonis, and S. Sen. 1995. Lophocyon paraskevaidisi, a new viverrid (Carnivora, Mammalia) from the middle Miocene of Chios island, Greece. Geobios 28:511–523.

Kretzoi, N. 1929. Materialien zur phylogenetischen Klassifikation der Aeluroïdeen . Congrès International de Zoologie 10 8:1293–1355.

Lanfear, R., P. B. Frandsen, A. M. Wright, T. Senfeld, and B. Calcott. 2016. PartitionFinder 2: new methods for selecting partitioned models of evolution for molecular and morphological phylogenetic analyses . Molecular Biology and Evolution 34:772–773.

Lautenschlager, S., B. Figueirido, D. D. Cashmore, E. M. Bendel, and T. L. Stubbs. 2020. Morphological convergence obscures functional diversity in sabre-toothed carnivores: Sabre-tooth functional morphology. Proceedings of the Royal Society B: Biological Sciences 287.

Law, C. J. 2021. Ecological drivers of carnivoran body shape evolution. American Naturalist 198:406–420.

Law, C. J., G. J. Slater, and R. S. Mehta. 2018a. Lineage Diversity and Size Disparity in Musteloidea: Testing Patterns of Adaptive Radiation Using Molecular and Fossil-Based Methods. Systematic Biology 67:127–144.

Law, C. J., E. Duran, N. Hung, E. Richards, I. Santillan, and R. S. Mehta. 2018b. Effects of diet on cranial morphology and biting ability in musteloid mammals. Journal of Evolutionary Biology 31:1918–1931.

Lee, M., P. Oliver, and M. Hutchinson. 2009. Phylogenetic uncertainty and molecular clock calibrations: a case study of legless lizards (Pygopodidae, Gekkota). Molecular Phylogenetics and Evolution 50:661–666.

Li, Y., and N. Spassov. 2017. A new species of Paramachaerodus (Mammalia, Carnivora, Felidae) from the late Miocene of China and Bulgaria, and revision of Promegantereon Kretzoi, 1938 and Paramachaerodus Pilgrim, 1913. Paläontologische Zeitschrift 91:409–426.

Liow, L. H., and J. A. Finarelli. 2014. A dynamic global equilibrium in carnivoran diversification over 20 million years. Proceedings of the Royal Society B: Biological Sciences 281.

Liu, J., J. Liu, H. Zhang, J. Wagner, Q. Jiangzuo, Y. Song, S. Liu, Y. Wang, and C. Jin. 2021. The giant short-faced hyena Pachycrocuta brevirostris (Mammalia, Carnivora, Hyaenidae) from Northeast Asia: A reinterpretation of subspecies differentiation and intercontinental dispersal. Quaternary International.

Lucas, S. G., and O. G. Bendukidze. 1997. Proboscidea (Mammalia) from the Early Miocene of Kazakhstan. Neues Jahrbuch Fur Geologie Und Palaontologie - Monatshefte 4:659–673.

Lucas, T., and A. Goswami. 2017. paleomorph: Geometric Morphometric Tools for Paleobiology. R package version 0.1.4. Https://CRAN.R-Project.Org/Package=paleomorph.

Maestri, R., B. D. Patterson, R. Fornel, L. R. Monteiro, and T. R. O. de Freitas. 2016. Diet, bite force and skull morphology in the generalist rodent morphotype. Journal of Evolutionary Biology 29:2191–2204.

Marcy, A. E., T. Guillerme, E. Sherratt, K. C. Rowe, M. J. Phillips, and V. Weisbecker. 2020. Australian rodents reveal conserved cranial evolutionary allometry across 10 million years of murid evolution. American Naturalist 196:755–768.

Marroig, G., and J. M. Cheverud. 2005. Size as a line of least evolutionary resistance: Diet and adaptive morphological radiation in New World monkeys. Evolution 59:1128–1142.

Martin, L. D. 1989. Fossil History of the Terrestrial Carnivora; pp. 536–568 in J. L. Gittleman (ed.), Carnivore Behavior, Ecology, and Evolution. Cornell University Press, Ithaca, New York.

Marugán-Lobón, J., S. M. Nebreda, G. Navalón, and R. B. J. Benson. 2022. Beyond the beak: Brain size and allometry in avian craniofacial evolution. Journal of Anatomy 240:197–209.

Matthew, W. D. 1926. The evolution of the horse: a record and its interpretation. The Quarterly Review of Biology 1:139–185.

McBratney-Owen, B., S. Iseki, S. D. Bamforth, B. R. Olsen, and G. M. Morriss-Kay. 2008. Development and Tissue Origins of the Mammalian Cranial Base. Developmental Biology 322:121–132.

McHorse, B. K., A. A. Biewener, and S. E. Pierce. 2019. The Evolution of a Single Toe in Horses: Causes, Consequences, and the Way Forward. Integrative and Comparative Biology 59:638–655.

McNab, B. K. 1986. The Influence of Food Habits on the Energetics of Eutherian Mammals. Ecological Monographs 56:1–19.

Meachen-Samuels, J., and B. Van Valkenburgh. 2009. Craniodental indicators of prey size preference in the Felidae. Biological Journal of the Linnean Society 96:784–799.

Meloro, C., M. Clauss, and P. Raia. 2015. Ecomorphology of Carnivora challenges convergent evolution. Organisms Diversity and Evolution 15:711–720.

Michaud, M., G. Veron, and A. C. Fabre. 2020. Phenotypic integration in feliform carnivores: Covariation patterns and disparity in hypercarnivores versus generalists. Evolution 74:2681–2702.

Michaud, M., G. Veron, S. Peigné, A. Blin, and A. C. Fabre. 2018. Are phenotypic disparity and rate of morphological evolution correlated with ecological diversity in Carnivora? Biological Journal of the Linnean Society 124:294–307.

Miller, M. A., W. Pfeiffer, and T. Schwartz. 2011. The CIPRES science gateway: a community resource for phylogenetic analyses. TG '11: Proceedings of the 2011 TeraGrid Conference: Extreme Digital Discovery 1–8.

Mishina, Y., and T. N. Snider. 2014. Neural crest cell signaling pathways critical to cranial bone development and pathology. Experimental Cell Research 325:138–147.

Mitteroecker, P., P. Gunz, M. Bernhard, K. Schaefer, and F. L. Bookstein. 2004. Comparison of cranial ontogenetic trajectories among great apes and humans. Journal of Human Evolution 46:679–698.

Morales, J., and M. Pickford. 2011. A new paradoxurine carnivore from the Late Miocene Siwaliks of India and a review of the bunodont viverrids of Africa. Geobios 44:271–277.

Morales, J., and M. Pickford. 2021. Taxonomic revision of the genus Leptoplesictis (Viverridae, Mammalia) with description of new fossils from Grillental VI (Namibia) and Moratilla 2 (Spain). Communications of the Geological Survey of Namibia 23:161–176.

Morales, J., S. Mayda, A. Valenciano, D. DeMiguel, and T. Kaya. 2019. A new lophocyonid, Izmirictis cani gen. et sp. nov. (Carnivora: Mammalia), from the lower Miocene of Turkey. Journal of Systematic Palaeontology 17:1127–1138.

Navalón, G., S. M. Nebreda, J. A. Bright, M. Fabbri, R. B. J. Benson, B. A. Bhullar, J. Marugán-Lobón, and E. J. Rayfield. 2021. Craniofacial development illuminates the evolution of nightbirds (Strisores). Proceedings of the Royal Society B: Biological Sciences 288.

Nyakatura, K., and O. Bininda-Emonds. 2012. Updating the evolutionary history of Carnivora (Mammalia): a new species-level supertree complete with divergence time estimates. BMC Biology 10:1–31.

O'Brien, C. L., M. Huber, E. Thomas, M. Pagani, J. R. Super, L. E. Elder, and P. M. Hull. 2020. The enigma of Oligocene climate and global surface temperature evolution. Proceedings of the National Academy of Sciences of the United States of America 117:25302–25309.

O'Meara, B. C., C. Ané, M. J. Sanderson, and P. C. Wainwright. 2006. Testing for Different Rates of Continuous Trait Evolution Using Likelihood. Evolution 60:922.

Okonechnikov, K., O. Golosova, M. Fursov, A. Varlamov, Y. Vaskin, I. Efremov, O. G. German Grehov, D. Kandrov, K. Rasputin, M. Syabro, and T. Tleukenov. 2012. Unipro UGENE: A unified bioinformatics toolkit. Bioinformatics 28:1166–1167.

Olsen, A. M., and M. W. Westneat. 2015. StereoMorph: An R package for the collection of 3D landmarks and curves using a stereo camera set-up. Methods in Ecology and Evolution 6:351–356.

Olson, E. C., and R. L. Miller. 1958. Morphological Integration. University of Chicago Press, Chicago, Il., 376 pp.

Osborn, H. F. 1902. The Law of Adaptive Radiation. The American Naturalist 36:353–363.

Paijmans, J. L. A., R. Barnett, M. T. P. Gilbert, M. L. Zepeda-mendoza, J. W. F. Reumer, J. de Vos, G. Zazula, D. Nagel, G. F. Baryshnikov, J. A. Leonard, N. Rohland, M. V Westbury, A. Barlow, and M. Hofreiter. 2017. Evolutionary History of Saber-Toothed Cats Based on Ancient Mitogenomics. Current Biology 27:3330–3336.

Palmqvist, P., B. Martínez-Navarro, J. A. Pérez-Claros, V. Torregrosa, B. Figueirido, J. M. Jiménez-Arenas, M. Patrocinio Espigares, S. Ros-Montoya, and M. De Renzi. 2011. The giant hyena Pachycrocuta brevirostris: Modelling the bone-cracking behavior of an extinct carnivore. Quaternary International 243:61–79.

Paterson, R. S., N. Rybczynski, N. Kohno, and H. C. Maddin. 2020. A Total Evidence Phylogenetic Analysis of Pinniped Phylogeny and the Possibility of Parallel Evolution Within a Monophyletic Framework. Frontiers in Ecology and Evolution 7:1–16.

Peigné, S. 1999. Proailurus, l' un des plus anciens Felidae (Carnivora) d'Eurasie: systématique et évolution. Bulletin de La Société d'histoire Naturelle de Toulouse 135:125–134.

Peigné, S. 2003. Systematic review of European Nimravinae (Mammalia, Carnivora, Nimravidae) and the phylogenetic relationships of Palaeogene Nimravidae. Zoologica Scripta 32:199–229.

Peigné, S., and L. De Bonis. 1999. The genus Stenoplesictis Filhol (Mammalia, Carnivora) from the Oligocene deposits of the Phosphorites of Quercy, France. Journal of Vertebrate Paleontology 19:566–575.

Peigné, S., M. J. Salesa, M. Antón, and J. Morales. 2008. A new amphicyonine (Carnivora: Amphicyonidae) from the upper miocene of batallones-1 Madrid, Spain. Palaeontology 51:943–965.

Peigné, S., Y. Chaimanee, J.-J. Jaeger, V. Suteethorn, and S. Ducrocq. 2000. Eocene nimravid carnivorans from Thailand. Journal of Vertebrate Paleontology 20:157–163.

Pennell, M. W., J. M. Eastman, G. J. Slater, J. W. Brown, J. C. Uyeda, R. G. Fitzjohn, M. E. Alfaro, and L. J. Harmon. 2014. Geiger v2.0: An expanded suite of methods for fitting macroevolutionary models to phylogenetic trees. Bioinformatics 30:2216–2218.

Pickford, M., and J. Morales. 1994. Biostratigraphy and palaeobiogeography of East Africa and the Iberian peninsula. Palaeogeography, Palaeoclimatology, Palaeoecology 112:297–322.

Pineda-Munoz, S., A. R. Evans, and J. Alroy. 2016. The relationship between diet and body mass in terrestrial mammals. Paleobiology 42:659–669.

Piras, P., D. Silvestro, F. Carotenuto, S. Castiglione, A. Kotsakis, L. Maiorino, M. Melchionna, A. Mondanaro, G. Sansalone, C. Serio, V. A. Vero, and P. Raia. 2018. Evolution of the sabertooth mandible: A deadly ecomorphological specialization. Palaeogeography, Palaeoclimatology, Palaeoecology 496:166–174.

Pires, M. M., D. Silvestro, and T. B. Quental. 2017. Interactions within and between clades shaped the diversification of terrestrial carnivores. Evolution 71:1855–1864.

Plessis, L. du. 2016. BDSKY Tools. R package version 0.0.1.0. Https://Github.Com/Laduplessis/Bdskytools/.

Prevosti, F. J., A. M. Forasiepi, M. D. Ercoli, and G. F. Turazzini. 2012. Paleoecology of the mammalian carnivores (Metatheria, Sparassodonta) of the Santa Cruz Formation (late Early Miocene); pp. 173–193 in S. F. Vizcaíno, R. F. Kay, and M. S. Bargo (eds.), Early Miocene Paleobiology in Patagonia. Cambridge University Press, Cambridge, UK.

Price, S. A., S. S. B. Hopkins, K. K. Smith, and V. L. Roth. 2012. Tempo of trophic evolution and its impact on mammalian diversification. Proceedings of the National Academy of Sciences of the United States of America 109:7008–7012.

Pyron, R. A. 2011. Divergence time estimation using fossils as terminal taxa and the origins of Lissamphibia. Systematic Biology 60:466–481.

R Core Team. 2020. R: A language and environment for statistical computing. R Foundation for Statistical Computing, Vienna, Austria. URL https://www.R-project.org/.

Radinsky, L. B. 1981a. Evolution of skull shape in carnivores: 1. Representative modern carnivores. Biological Journal of the Linnean Society 15:369–388.

Radinsky, L. B. 1981b. Evolution of the skull shape in carnivores 2. Additional modern carnivores. Biological Journal of the Linnean Society 16:337–355.

Radinsky, L. B. 1982. Evolution of Skull Shape in Carnivores. 3. The Origin and Early Radiation of the Modern Carnivore Families. Paleobiology 8:177–195.

Rambaut, A., A. J. Drummond, D. Xie, G. Baele, and M. A. Suchard. 2018. Posterior summarisation in Bayesian phylogenetics using Tracer 1.7. Systematic Biology syy032.

Randau, M., D. Sanfelice, and A. Goswami. 2019. Shifts in cranial integration associated with ecological specialization in pinnipeds (Mammalia, Carnivora). Royal Society Open Science 6.

Raup, D. M. 1966. Geometric Analysis of Shell Coiling: General Problems. Journal of Paleontology 40:1178–1190.

Raup, D. M., and S. J. ay Gould. 1974. Stochastic Simulation and Evolution of Morphology-Towards a Nomothetic Paleontology. Systematic Zoology 23:305–322.

Renard, A., M. Lavoie, J. A. Pitt, and S. Larivière. 2015. Felis nigripes (Carnivora: Felidae). Mammalian Species 47:78–83.

Reuter, D. M. 2021. Trophic structure evolution in Oregon Oligo-Miocene terrestrial communities. University of Oregon, 163 pp.

Revell, L. J. 2012. phytools: An R package for phylogenetic comparative biology (and other things). Methods Ecol. Evol. 3 217–223.

Robles, J. M., D. M. Alba, J. Fortuny, S. De Esteban-Trivigno, C. Rotgers, J. Balaguer, R. Carmona, J. Galindo, S. Almecija, J. V Berto, and S. Moya-Sola. 2013a. New craniodental remains of the barbourofelid Albanosmilus jourdani (Filhol, 1883) from the Miocene of the Valles-Penedes Basin (NE Iberian Peninsula) and the phylogeny of the Barbourofelini. Journal of Systematic Palaeontology 11:993–1022.

Robles, J. M., J. Madurell-Malapeira, J. Abella, C. Rotgers, R. Carmona, S. Almécija, J. Balaguer, and D. M. Alba. 2013b. New Pseudaelurus and Styriofelis remains (Carnivora: Felidae) from the Middle Miocene of Abocador de Can Mata (Vallès-Penedès Basin). Comptes Rendus - Palevol 12:101–113.

Rohlf, F. J., and M. Corti. 2000. Use of two-block partial least-squares to study covariation in shape. Systematic Biology 49:740–753.

Ronquist, F., S. Klopfstein, L. Vilhelmsen, S. Schulmeister, D. L. Murray, and A. P. Rasnitsyn. 2012. A total-evidence approach to dating with fossils, applied to the early radiation of the Hymenoptera. Systematic Biology 61:973–999.

Rothwell, T. P. 2001. A Partial Skeleton of Pseudaelurus (Carnivora: Felidae) from the Nambé Member of the Tesuque Formation, Española Basin, New Mexico. American Museum Novitates 3342:1–31.

Rothwell, T. P. 2003. Phylogenetic systematics of North American Pseudaelurus (Carnivora, Felidae). American Museum Novitates 3403.

Rovinsky, D. S., A. R. Evans, and J. W. Adams. 2021. Functional ecological convergence between the thylacine and small prey-focused canids. BMC Ecology and Evolution 21.

Sacco, T., and B. Van Valkenburgh. 2004. Ecomorphological indicators of feeding behaviour in the bears (Carnivora: Ursidae). Journal of Zoology 263:41–54.

Sakamoto, M., and M. Ruta. 2012. Convergence and Divergence in the Evolution of Cat Skulls: Temporal and Spatial Patterns of Morphological Diversity. PLoS ONE 7:e39752.

Salesa, M. J., M. Antón, J. Morales, and S. Peigné. 2012. Systematics and phylogeny of the small felines (Carnivora, Felidae) from the Late Miocene of Europe: a new species of Felinae from the Vallesian of Batallones (MN 10, Madrid, Spain). Journal of Systematic Palaeontology 10:87–102.

Salesa, M. J., M. Antón, A. Turner, L. Alcalá, P. Montoya, and J. Morales. 2010. Systematic revision of the late Miocene sabre-toothed felid Paramachaerodus in Spain. Palaeontolgy 53:1369–1391.

Salles, L. O. 1992. Felid Phylogenetics: Extant Taxa and Skull Morphology (Felidae, Aeluroidea). American Museum Novitates 3047:67.

Sanderson, M. J., and M. J. Donoghue. 1994. Shifts in Diversification Rate with the Origin of Angiosperms. Science 264:1590–1593.

Santana, S. E., and E. Cheung. 2016. Go big or go fish: Morphological specializations in carnivorous bats. Proceedings of the Royal Society B: Biological Sciences 283:20160615.

Schaefer, K., P. Mitteroecker, P. Gunz, M. Bernhard, and F. L. Bookstein. 2004. Craniofacial sexual dimorphism patterns and allometry among extant hominids. Annals of Anatomy 186:471–478.

Schaeffer, B. 1948. The Origin of a Mammalian Ordinal Character. Evolution 2:164–175.

Schlager, S. 2017. Morpho and Rvcg – Shape Analysis in R; pp. 217–256 in Z. G, L. S, and S. G (eds.), Statistical Shape and Deformation Analysis. Academic Press.

Schluter, D. 2000. The Ecology of Adaptive Radiation. Oxford University Press, Oxford, 296 pp.

Schmidt-Kittler, N. 1976. Raubtiere aus dem Jungtertiär Kleinasiens. Palaeontographica Abteilung A 155:1–131.

Semenov, Y. 1989. Ictitheres and Morphologically Similar Hyaenas from the Neogene of the USSR. Naukova dumka, Kiev, 180 pp.

Semenov, Y. 2008. Taxonomical reappraisal of "ictitheres" (Mammalia, Carnivora) from the Late Miocene of Kenya. Comptes Rendus Palevol 7:529–539.

Sen, S. 2013. Dispersal of African mammals in Eurasia during the Cenozoic: Ways and whys. Geobios 46:159–172.

Shubin, N., C. Tabin, and S. Carroll. 1997. Fossils, genes and the evolution of animal limbs. Nature 388:639–648.

Simons, E. A., S. R. Frost, K. Harvati, K. McNulty, and M. Singleton. 2020. Comparing Rates of Linage Diversification with Rates of Size and Shape Evolution in Catarrhine Crania. Evolutionary Biology 47:152–163.

Simpson, G. G. 1944. Tempo and Mode in Evolution. Columbia University Press, New York, 237 pp.

Simpson, G. G. 1953. Major Features of Evolution. Columbia University Press, New York, 434 pp.

Singleton, M. 2002. Patterns of cranial shape variation in the Papionini (Primates: Cercopithecinae). Journal of Human Evolution 42:547–578.

Slater, G. J. 2013. Phylogenetic evidence for a shift in the mode of mammalian body size evolution at the Cretaceous-Paleogene boundary. Methods in Ecology and Evolution 4:734–744.

Slater, G. J. 2015. Iterative adaptive radiations of fossil canids show no evidence for diversity-dependent trait evolution. Proceedings of the National Academy of Sciences of the United States of America 112:4897–4902.

Slater, G. J., and B. Van Valkenburgh. 2008. Long in the tooth: evolution of sabertooth cat cranial shape. Paleobiology 34:403–419.

Slater, G. J., and B. Van Valkenburgh. 2009. Allometry and performance: The evolution of skull form and function in felids. Journal of Evolutionary Biology 22:2278–2287.

Slater, G. J., and A. R. Friscia. 2019. Hierarchy in adaptive radiation: A case study using the Carnivora (Mammalia). Evolution 73:524–539.

Solé, F. 2014. New carnivoraforms from the early Eocene of Europe and their bearing on the evolution of the Carnivoraformes. Palaeontology 57:963–978.

Solé, F., and S. Ladevèze. 2017. Evolution of the hypercarnivorous dentition in mammals (Metatheria, Eutheria) and its bearing on the development of tribosphenic molars. Evolution and Development 19:56–68.

Solé, F., R. Smith, T. Coillot, E. de Bast, and T. Smith. 2014. Dental and tarsal anatomy of Miacis latouri and a phylogenetic analysis of the earliest carnivoraforms (Mammalia, Carnivoramorpha). Journal of Vertebrate Paleontology 34:1–21.

Solé, F., T. Smith, E. de Bast, V. Codrea, and E. Gheerbrant. 2016. New carnivoraforms from the latest Paleocene of Europe and their bearing on the origin and radiation of Carnivoraformes (Carnivoramorpha, Mammalia). Journal of Vertebrate Paleontology 36:e1082480.

Soledad Domingo, M., L. Domingo, C. Badgley, O. Sanisidro, and J. Morales. 2013. Resource partitioning among top predators in a Miocene food web. Proceedings of the Royal Society B: Biological Sciences 280.

Spassov, N., and D. Geraads. 2015. A New Felid from the Late Miocene of the Balkans and the Contents of the Genus Metailurus Zdansky, 1924 (Carnivora, Felidae). Journal of Mammalian Evolution 22:45–56.

Spaulding, M., and J. J. Flynn. 2009. Anatomy of the postcranial skeleton of "mlacis" uintensis (Mammalia: Carnivoramorpha). Journal of Vertebrate Paleontology 29:1212–1223.

Spaulding, M., and J. J. Flynn. 2012. Phylogeny of the Carnivoramorpha: The impact of postcranial characters. Journal of Systematic Palaeontology 10:653–677.

Stadler, T., D. Kühnert, S. Bonhoeffer, and A. J. Drummond. 2013. Birth-death skyline plot reveals temporal changes of epidemic spread in HIV and hepatitis C virus (HCV). Proceedings of the National Academy of Sciences of the United States of America 110:228–233.

Tomarev, S. I., P. Callaerts, L. Kos, R. Zinovieva, G. Haider, W. Gehring, and J. Piatigorsky. 1997. Squid Pax-6 and eye development. Proceedings of the National Academy of Sciences of the United States of America 94:2421–2426.

Tomiya, S., and Z. J. Tseng. 2016. Whence the beardogs? Reappraisal of the middle to late eocene 'miacis' from Texas, USA, and the origin of amphicyonidae (mammalia, carnivora). Royal Society Open Science 3.

Tomiya, S., S. P. Zack, M. Spaulding, and J. J. Flynn. 2021. Carnivorous mammals from the middle Eocene Washakie Formation, Wyoming, USA, and their diversity trajectory in a post-warming world. Journal of Paleontology 95:1–115.

Towns, J., T. Cockerill, M. Dahan, I. Foster, K. Gaither, A. Grimshaw, V. Hazlewood, S. Lathrop, D. Lifka, G. D. P. R. Roskies, J. R. Scott, and N. Wilkins-Diehr. 2014. XSEDE: Accelerating Scientific Discovery. Computing in Science & Engineering 16:62–74.

Tseng, J. Z., and J. J. Flynn. 2018. Structure-function covariation with nonfeeding ecological variables influences evolution of feeding specialization in carnivora. Science Advances 4.

Tseng, Z., and X. Wang. 2011. Do convergent ecomorphs evolve through convergent morphological pathways? Cranial shape evolution in fossil hyaenids and borophagine canids (Carnivora, Mammalia). Paleobiology 37:470–489.

Tseng, Z. J. 2009. Cranial function in a late Miocene Dinocrocuta gigantea (Mammalia: Carnivora) revealed by comparative finite element analysis. Biological Journal of the Linnean Society 96:51–67.

Tseng, Z. J. 2012. Connecting Hunter-Schreger Band microstructure to enamel microwear features: New insights from durophagous carnivores. Acta Palaeontologica Polonica 57:473–484.

Tseng, Z. J. 2013. Testing Adaptive Hypotheses of Convergence with Functional Landscapes: A Case Study of Bone-Cracking Hypercarnivores. PLoS ONE 8:e65305.

Tseng, Z. J., and X. Wang. 2007. The first record of the late Miocene Hyaenictitherium hyaenoides Zdansky (Carnivora: Hyaenidae) in Inner Mongolia and an evaluation of the genus. Journal of Vertebrate Paleontology 27:699–708.

Tseng, Z. J., and W. J. Binder. 2010. Mandibular biomechanics of Crocuta crocuta, Canis lupus, and the late Miocene Dinocrocuta gigantea (Carnivora, Mammalia). Zoological Journal of the Linnean Society 158:683–696.

Tsuboi, M., W. van der Bijl, B. T. Kopperud, J. Erritzøe, K. L. Voje, A. Kotrschal, K. E. Yopak, S. P. Collin, A. N. Iwaniuk, and N. Kolm. 2018. Breakdown of brain–body allometry and the encephalization of birds and mammals. Nature Ecology and Evolution 2:1492–1500.

Turner, A., M. Antón, and L. Werdelin. 2008. Taxonomy and evolutionary patterns in the fossil Hyaenidae of Europe. Geobios 41:677–687.

Uyeda, J. C., and L. J. Harmon. 2014. A novel Bayesian method for inferring and interpreting the dynamics of adaptive landscapes from phylogenetic comparative data. Systematic Biology 63:902–918.

Vaidya, G., D. J. Lohman, and R. Meier. 2011. SequenceMatrix: concatenation software for the fast assembly of multi-gene datasets with character set and codon information. Cladistics 27:171–180.

Van Valen, L. 1971. Adaptive zones and the orders of mammals. Evolution 25:420–428.

Van Valkenburgh, B. 1990. Skeletal and dental predictors of body mass in carnivores; pp. 181–205 in J. Damuth and B. J. MacFadden (eds.), Body Size in Mammalian Paleobiology: Estimation and Biological Implications. Cambridge University Press.

Van Valkenburgh, B. 1991. Iterative evolution of hypercarnivory in canids (Mammalia: Carnivora): Evolutionary interactions among sympatric predators. Paleobiology 17:340–362.

Van Valkenburgh, B. 1996. Feeding behavior in free-ranging, large African carnivores. Journal of Mammalogy 77:240–254.

Van Valkenburgh, B. 2007. Déjà vu: the evolution of feeding morphologies in the Carnivora. Integrative and Comparative Biology 47:147–163.

Van Valkenburgh, B., and K.-P. Koepfli. 1993. Cranial and dental adaptations to predation in canids. Symposium Zoological Society of London 65:15–37.

Van Valkenburgh, B., F. Grady, and B. Kurtén. 1990. The Plio-Pleistocene cheetah-like cat Miracinonyx inexpectatus of North America. Journal of Vertebrate Paleontology 10:434–454.

Van Valkenburgh, B., T. Sacco, and X. Wang. 2003. Pack hunting in Miocene borophagine dogs: Evidence from craniodental morphology and body size. Bulletin of the American Museum of Natural History 279:147–162.

Van Valkenburgh, B., X. Wang, and J. Damuth. 2004. Cope's rule, hypercarnivory, and extinction in North American canids. Science 306:101–104.

Venables, W. N., and B. D. Ripley. 2002. Modern Applied Statistics with S, 4th Ed. Springer, New York, 495 pp.

Vermeij, G. J. 1973. Adaptation, versatility, and evolution. Systematic Zoology 22:466–477.

Viranta, S. 1996. European Miocene Amphicyonidae-taxonomy, systematics and ecology. Zoologica Fennica 204:1–61.

Vrba, E. S. . 1992. Mammals as a Key to Evolutionary Theory. Journal of Mammalogy 73:1–28.

Wang, B., M. Zelditch, and C. Badgley. 2021. Geometric morphometrics of mandibles for dietary differentiation of Bovidae (Mammalia: Artiodactyla). Current Zoology 1–13.

Wang, J., and Z.-Q. Zhang. 2015. Phylogenetic analysis on Palaeogale (Palaeogalidae , Carnivora) based on specimens from Oligocene strata of Saint-Jacques , Nei Mongol. Vertebrata PalAsiatica 53:310–334.

Wang, X. 1993. Transformation from plantigrady to digitigrady: functional morphology of locomotion in Hesperocyon (Canidae: Carnivora). American Museum Novitates 1–23.

Wang, X., Z. J. Tseng, W. Y. Wu, J. Ye, J. Meng, and S. Bi. 2020. A new species of Tungurictis Colbert, 1939 (Carnivora, hyaenidae) from the middle miocene of Junggar basin, Northwestern China and the early divergence of basal hyaenids in East Asia. Geodiversitas 42:29–45.

Wang, Y., J. Meng, X. Ni, and C. Li. 2007. Major events of Paleogene mammal radiation in China. Geological Journal 42:415–430.

Welsh, E. 2021. A new species of an enigmatic carnivore Palaeogale (Feliformia: Palaeogalidae) from Badlands National Park, South Dakota. Proceedings of the South Dakota Academy of Science 100:107–120.

Werdelin, L. 1996. Carnivoran ecomorphology: a phylogenetic perspective; pp. 582–624 in J. L. Gittleman (ed.), Carnivore Behavior, Ecology, and Evolution. Cornell University Press, Ithaca, New York.

Werdelin, L. 2019. Middle miocene carnivora and hyaenodonta from fort Ternan, Western Kenya. Geodiversitas 41:267–283.

Werdelin, L. 2021. African Barbourofelinae (Mammalia, Nimravidae): a critical review. Historical Biology 00:1–9.

Werdelin, L., and N. Solounias. 1991. The Hyaenidae : taxonomy, systematics and evolution. Fossils and Strata 30:104.

Werdelin, L., and M. E. Lewis. 2001. A revision of the genus Dinofelis (Mammalia, Felidae). Zoological Journal of the Linnean Society 132:147–258.

Werdelin, L., and M. E. Lewis. 2005. Plio-Pleistocene Carnivora of eastern Africa: Species richness and turnover patterns. Zoological Journal of the Linnean Society 144:121–144.

Werdelin, L., and T. Flink. 2018. The Phylogenetic Context of Smilodon; pp. 14–29 in L. Werdelin, H. G. Mcdonald, and C. A. Shaw (eds.), Smilodon: The Iconic Sabertooth. Johns Hopkins University Press, Baltimore.

Werdelin, L., N. Yamaguchi, W. E. Johnson, and S. J. O'Brien. 2010. Phylogeny and Evolution of Cats (Felidae); pp. 59–82 in D. W. Macdonald and A. J. Loveridge (eds.), Biology and Conservation of Wild Felids. Oxford University Press, New York.

Wesley-Hunt, G. D., and J. J. Flynn. 2005. Phylogeny of the Carnivora: basal relationships among the carnivoramorphans, and assessment of the position of "Miacoidea" relative to Carnivora. Journal of Systematic Palaeontology 3:1–28.

Wesley-Hunt, G. D., R. Dehghani, and L. Werdelin. 2010. Comparative ecomorphology and biogeography of Herpestidae and Viverridae (Carnivora) in Africa and Asia; pp. 246–268 in A. Goswami and A. R. Friscia (eds.), Carnivoran Evolution: New Views on Phylogeny, Form, and Function. Cambridge University Press.

Westbury, M. V., S. Hartmann, A. Barlow, M. Preick, B. Ridush, D. Nagel, T. Rathgeber, R. Ziegler, G. Baryshnikov, G. Sheng, A. Ludwig, I. Wiesel, L. Dalen, F. Bibi, L. Werdelin, R. Heller, and M. Hofreiter. 2020. Hyena paleogenomes reveal a complex evolutionary history of cross-continental gene flow between spotted and cave hyena. Science Advances 6:1–11.

Wheeler, H. T., and G. T. Jefferson. 2009. Panthera atrox: body proportions, size, sexual dimorphism, and behavior of the cursorial lion of the North American plains. Museum of Northern Arizona Bulletin 65:423–444.

Wible, J. R., and M. Spaulding. 2013. On the cranial osteology of the African palm civet, Nandinia Binotata (Gray, 1830) (Mammalia, Carnivora, Feliformia). Annals of Carnegie Museum 82:1–114.

Wilman, H., B. J., S. J., de L. R. C., R. M., and J. W. 2014. EltonTraits 1.0 : Species-level foraging attributes of the world's birds and mammals. Ecology 95:2027.

Wilson, L. A. B., A. Balcarcel, M. Geiger, L. Heck, and M. R. Sánchez-Villagra. 2021. Modularity patterns in mammalian domestication: Assessing developmental hypotheses for diversification. Evolution Letters 5:385–396.

Wroe, S., and N. Milne. 2007. Convergence and remarkably consistent constraint in the evolution of carnivore skull shape. Evolution 61:1251–1260.

Xiong, W.-Y. 2019. Basicranial morphology of Late Miocene Dinocrocuta gigantea (Carnivora: Hyaenidae) from Fugu, Shaanxi. Vertebrata Palasiatica 57:274–307.

Yoder, A. D., M. M. Burns, S. Zehr, T. Delefosse, G. Veron, S. M. Goodman, and J. J. Flynn. 2003. Single origin of Malagasy Carnivora from an African ancestor. Nature 421:734–737.

Zachos, J., H. Pagani, L. Sloan, E. Thomas, and K. Billups. 2001. Trends, rhythms, and aberrations in global climate 65 Ma to present. Science 292:686–693.

Zack, S. P. 2019a. The first North American propterodon (Hyaenodonta: Hyaenodontidae), a new species from the late Uintan of Utah. PeerJ 7:e8136.

Zack, S. P. 2019b. A skeleton of a Uintan machaeroidine 'creodont' and the phylogeny of carnivorous eutherian mammals. Journal of Systematic Palaeontology 17:653–689.

Zack, S. P., A. W. Poust, and H. Wagner. 2022. Diegoaelurus, a new machaeroidine (Oxyaenidae) from the Santiago Formation (late Uintan) of southern California and the relationships of Machaeroidinae, the oldest group of sabertooth mammals. PeerJ 10:e13032.

Zheng, J. [郑家坚], Y. [汤英俊] Tang, R. [翟人杰] Zhai, S. [丁素因] Ding, and X. [黄学诗] Huang. 1978. Early Tertiary strata of Lunan Basin, Yunnan [云南路南盆地的早第三纪地层]. Professional Papers on Stratigraphy and Paleontology, Beijing [地层古生物论文集] 7:22-29 [in Chinese].

Zhou, Y., S.-R. Wang, and J.-Z. Ma. 2017. Comprehensive species set revealing the phylogeny and biogeography of Feliformia (Mammalia, Carnivora) based on mitochondrial DNA. PLoS ONE 12:e0174902.